

H 24/3705

MONASH UNIVERSITY
THESIS ACCEPTED IN SATISFACTION OF THE
REQUIREMENTS FOR THE DEGREE OF
DOCTOR OF PHILOSOPHY

ON..... 1 September 2004.....

.....
Sec. Research Graduate School Committee

Under the Copyright Act 1968, this thesis must be used only under the normal conditions of scholarly fair dealing for the purposes of research, criticism or review. In particular no results or conclusions should be extracted from it, nor should it be copied or closely paraphrased in whole or in part without the written consent of the author. Proper written acknowledgement should be made for any assistance obtained from this thesis.

Errata

➤ The following substitutions should be made for non-standard symbols used throughout this thesis:

- “L” for “ℓ” (litres),
- “h” for “hrs” (hours),
- “20” for “2θ”

Additionally, a space should be placed in between the number and unit in all cases where no space is present.

➤ Replace “density” with “bulk density” in the following locations:

- p.171, paragraph 6.5.3, 5th line
- p.172, Table 6.8: caption, and column heading
- p.172, 1st paragraph: 1st line (delete “full”), 7th line and 10th line
- p.176, paragraph 7.1.1, last sentence
- p.177, Section 7.1.2 heading and 2nd sentence
- p.178, Table 7.1: caption and column heading
- p.201, Table 7.3: column heading

p.52, last paragraph, 2nd line: change reference from (Jin and Guo 2003) to (Jiang, Wang, *et al.* 2003). Details of this reference are given in the Errata for p.229, below.

p.55, Table 3.1 column heading: substitute “pyrophyllite” for “pyrohpyllite”

p.66, Section 3.4.5.2, 2nd paragraph, 2nd line: “1200” for “120”

p.100, last paragraph, 2nd line: “events” for “peaks”

p.102, 1st point: “CaSO₄” for “CaSO4”

p.137, 2nd paragraph, 4th line: “0.10:1” for “1.9:1”

p.144, Equation 6.1 should read:

$$\% \beta = \frac{I\beta_{(101)} + I\beta_{(210)}}{I\beta_{(101)} + I\beta_{(210)} + I\alpha_{(102)} + I\alpha_{(210)}}$$

p.178, Table 7.1: FeSi' for FeSi, and TiN' for TiN

p.217, 2nd point, 2nd last line: “in” for “In”

p.229, replace the reference for Jin and Guo 2003 with: “Jiang, J., Wang, P.-L., Chen, W.-W., Zhuang, H., Cheng, Y.-B., and Yan, D.-S. (2003), Phase Assemblages of (Ca,Mg)- α -Sialon Ceramics Derived from an α -Sialon Powder Prepared by SHS, *J.Eur.Cer.Soc.*, 23(13), pp.2343-2349.”

Addendum

p.54, last paragraph: substitute “the molecular weight, including all components” for “its molecular weight”

p.55, 1st paragraph: “including all components but excluding the loss on ignition” for “excluding the loss on ignition”

p.55, last paragraph: Comment. The particle size reduction was performed at Monash, via wet ball milling for 72 hours using a polyethylene jar filled to 1/3 with sand and 1/2 with isopropanol.

p.59, last paragraph after point v.: “muffle furnace in air at 650°C for 2 hours, heated at 10°C/minute.” for “muffle furnace in air at 650°C for 2 hours”

- p.61, paragraph after point v.: "muffle furnace in air at 650°C for 2 hours, heated at 10°C/minute." for "muffle furnace in air at 650°C for 2 hours"
- p.62, Section 3.3.2 & p.63, Section 3.3.3: Comment: The optical pyrometer calibration was checked several times using the melting of 99.99% pure Fe as a standard, and was found to be $\pm 3^\circ\text{C}$.
- p.65, 1st paragraph: substitute "approximately 10 wt%" for "a small amount"
- p.65, Section 3.4.2: replace "These scans were performed in air." with "These scans were performed using Pt crucibles, in flowing air."
- p.65, paragraph 3.4.3: replace "scans were run in an atmosphere of" with "scans were run using Pt crucibles, in an atmosphere of"
- p.66, Section 3.4.5.2, 2nd paragraph, 2nd line: replace "grinding on successively finer SiC papers down to 120 grade" with "grinding on 180, 360, 800, and 1200 grade SiC papers"
- p.67, 1st paragraph: replace "successively finer grades of SiC papers" with "180, 360, 800, and 1200 grade SiC papers"
- p.67, 1st paragraph: Comment: The dimpler model was a Gatan 656.
- p.67, last paragraph: replace "using a load of 10kg." with "using a load of 10 kg applied for 10s."
- p.68, end of 1st paragraph: add: "This relationship was used because it does not require a known value of elastic modulus (E) for the determination of fracture toughness."
- p.68, below equation 3.5: replace " $\phi=3$ " with " $\phi =$ constraint factor, $= 3$ ", and
- p.68, below equation 3.5: replace " $k = 3.2$ if $c/a > 2$ " with " $k =$ correction factor $= 3.2$ if $c/a > 2$ "
- p.74, 1st paragraph of Section 4.2.2: Comment: The bloating and splaying of the specimens is a result of the movement of N_2 gas into the pellet, and CRN product gases out of the pellet during firing.
- p.82, add to end of paragraph 4.2.3.2: "An Si powder was added to several of these scans as an internal standard to verify that the peak shifts detected were true, and not due to apparatus or sample misalignment".
- p.84, paragraph 4.2.4 replace the last line "This may be due to...after firing" with "This event remains unidentified".
- p.100, paragraph 4.3.1.2 before the last sentence "Note..." insert: "The temperatures given for DTA events are all for the onset of latent heat, not for the peak maxima."
- p.121, 1st paragraph: 2nd line: replace "for 72 hours." with "for 72 hours, as described in Section 3.1.4."
- p.154, after 1st paragraph: Comment: The low heat capacity of N_2 gas and the range of gas flowrates used were found not to have any cooling effect on the sample inside the furnace tube.
- p.176, paragraph 7.1.1: replace "1700°C for 1 hour" with "1700°C, heating at 30°C/min, for 1 hour".
- p.201, paragraph 7.3: comment: The Evans and Charles relationship was used due to it not requiring a value for the elastic modulus of the material. No mechanical property data is available for the E' - or D' -phases, and the inherent softness of E' as seen during polishing (and which is reflected in the following results), indicates that it would significantly lower the modulus of this multiphase material compared to that of pure α -sialon.
- p.271, third bullet point, replace with:
- The theoretical models for erosion were inadequate to describe the erosion behaviour of these materials, with no correlation found between fracture toughness and ΔE . This is due to the very different microstructures present in the four materials. Coincidentally however, the erosion resistance of the four materials did follow the rank order of hardness; with P02 displaying extremely high resistance to erosion at sliding impacts. Intergranular cracking followed by grain ejection was the dominant material removal mechanism in the equiaxed grained materials P02, K06, and P08. Brittle fracture and transgranular cracking dominated material removal in the coarse, plate K33 sample, and in areas of plate-like grains in P08.

**The Production of Low-Cost
 α - Sialons Via
Carbothermal Reduction-
Nitridation of Slag-Based
Mixtures**

Mark Robert Turner

B.A. (Hons) (Japanese Studies)

B.E. (Hons) (Materials Engineering)

Submitted for the Degree of Doctor of Philosophy

December 2003

School of Physics and Materials Engineering

Monash University, Victoria, 3800

Australia

Table of Contents

Table of Contents	i
Table of Figures and Tables	viii
List of Symbols and Nomenclature	xiii
Declaration	xv
Acknowledgements	xvi
Summary	xvii
Chapter One – Introduction	1
1.1 Advanced Ceramics and α-Sialon	2
1.1.1 Processing of Advanced Ceramics	3
1.1.2 Silicon Nitride and the Sialons	5
1.2 Recycling of Wastes Into Ceramics	6
1.2.1 Carbothermal Reduction-Nitridation	7
1.3 Scope and Structure of the Thesis	9
Chapter Two – Literature Review	
2.1 Silicon Nitride and Sialon Ceramics	11
2.1.1 Crystal Chemistry of Silicon Nitride and Sialons	12
2.1.1.1 Si_3N_4	12
2.1.1.2 β -Sialon	12
2.1.1.3 α -Sialon	13
2.1.1.4 Representation of α -Sialons on Behaviour Diagrams	14
2.1.1.5 AlN and AlN-Polytypoids	17
2.1.2 Production of α-Sialon – Reaction Sintering	18
2.1.3 Properties and Applications of Ca-α-Sialons	19
2.1.3.1 Hardness and Fracture Toughness	19
2.1.3.2 High-Temperature Stability	20
2.1.3.3 Solid Particle Erosion Resistance	20

2.1.3.4 Applications of α -Sialons	22
2.1.4 Other Phases in the Ca-Al-Si-O-N System	23
2.1.4.1 Gehlenite ($\text{Ca}_2\text{Al}_2\text{SiO}_7$)	24
2.1.4.2 D-, M-, and E- phases	24
2.2 Carbothermal Reduction-Nitridation (CRN)	26
2.2.1 Si_3N_4 Formation via CRN of SiO_2	26
2.2.2 β -Sialon Production Via CRN of Kaolinite	27
2.2.2.1 Clay Minerals Used for CRN	27
2.2.2.2 Reaction Sequence of CRN	28
2.2.2.3 Parameters Affecting CRN	30
2.2.3 CRN of Other Aluminosilicates	32
2.2.4 CRN of Waste Materials	33
2.3 α-Sialon Production via Carbothermal Reduction-Nitridation	33
2.3.1 Ca- α -Sialon via CRN	34
2.3.1.1 CRN of Fine, High-Purity Powders	34
2.3.1.2 CRN of Standard Laboratory Reagents	36
2.3.1.3 Hollow Ball Formation via CRN of Standard Laboratory Reagents	39
2.3.1.4 CRN of Fly Ash Waste	40
2.3.2 Other α -Sialon Systems	42
2.3.2.1 Y- α -Sialon From Halloysite Clay	42
2.3.2.2 Mg- α -Sialon From Talc and Halloysite Clay	44
2.3.3 Densification and Mechanical Properties of CRN- α -Sialon	46
2.3.3.1 Ca- α -Sialons Derived From Laboratory Chemicals	46
2.3.3.2 Nano-Sized Ca- α -Sialons Derived from Laboratory Chemicals	47
2.3.3.3 Y- α -Sialons Derived from Halloysite Clay and Si/ SiO_2 additions	48
2.3.4 Summary	48
2.4 Slag-Based α-Sialons	50
2.4.1 Preliminary Work on the CRN formation of Ca- α -Sialon from Slag	51
2.4.2 SHS of Slag to Form α -Sialon	52
Chapter Three – Experimental Procedure	54
3.1 Raw Materials	54
3.1.1 Slag	54

3.1.2 Clay-K (Kaolinite)	54
3.1.3 Clay-P (Pyrophyllite)	55
3.1.4 Sand (Quartz)	55
3.1.5 Carbon-Black	56
3.1.6 Silicon Nitride	56
3.1.7 Nitrogen Gas	56
3.2 Composition Selection and Specimen Preparation	56
3.2.1 K-Series: Composition Range Testing	56
3.2.2 K-Series: Intermediate Reaction Product Testing	57
3.2.3 P-Series: Pyrophyllite-Based Compositions	58
3.2.4 S-Series: Sand-Based Compositions	58
3.2.5 Effect of Firing Parameters	59
3.2.5.1 Specimen Density and Geometry	59
3.2.5.2 Seeding	
3.2.6 High-Temperature Phase Behaviour	59
3.2.7 Microstructure and Property Evaluation	60
3.3 Furnaces and Firing Schedules	60
3.3.1 Nitridation Furnaces and CRN	60
3.3.1.1 Standard CRN Firing Schedule	
3.3.1.2 Determination of Intermediate CRN Reaction Products	61
3.3.2 High-Temperature Furnace	62
3.3.3 Hot-pressing	63
3.4 Analytical Techniques	63
3.4.1 XRD	63
3.4.1.1 Phase Content Analysis	64
3.4.1.2 Determination of Ca-content in α -Sialon	64
3.4.2 DTA	65
3.4.3 TGA	65
3.4.4 Optical Microscopy	65
3.4.5 SEM	65
3.4.5.1 Powder Sample Preparation	66
3.4.5.2 Thermal Etching of Densified Pellets	66
3.4.6 TEM	66
3.4.6.1 Sample Preparation	67
3.4.7 Density Measurement	67

3.4.8 Hardness & Fracture Toughness Measurement	67
3.4.9 Erosion Resistance	68
Chapter Four – Fundamental Reaction Processes During CRN of Slag and Clay Mixtures	70
4.1 Analysis of the Raw Materials	70
4.1.1 Slag	70
4.1.2 Clay-K (Kaolinite)	71
4.1.3 Silicon Nitride Seeds	73
4.2 K-series Firings: Slag + Clay-K (kaolinite)	74
4.2.1 Experimental Procedure	74
4.2.2 Appearance of Fired Pellets	74
4.2.3 Phase Analysis of K-series Powders After CRN	75
4.2.3.1 Identification of Minor Phases	81
4.2.3.2 Identification of Solid-solution Phases	82
4.2.4 Carbon Content of Selected Compositions	84
4.2.5 SEM Analysis of Selected CRN Powders	86
4.2.6 Calcium Content of α -sialon	90
4.2.7 Phase Formation in the Slag–Clay-K system	92
4.2.7.1 Low-Slag Compositions K01 and K02	92
4.2.7.2 Medium-Slag Compositions K03 and K05	96
4.2.7.3 High-Slag Compositions K06→K33	96
4.2.8 Summary	98
4.3 Intermediate Phase Formation	99
4.3.1 Low Temperature Mineral Phase Changes During Heating in Air	100
4.3.1.1 Experimental Procedure	100
4.3.1.2 Phase Transformations in Slag	100
4.3.1.3 Phase Transformations in Clay-K	102
4.3.1.4 Phase Transformations in Slag+Clay-K Mixtures	103
4.3.2 CRN Reaction Sequence	106
4.3.2.1 Intermediate Reactions in Composition K06	106
4.3.2.2 Intermediate Reactions in Composition K10	112
4.3.2.3 Intermediate Reactions in Composition K19	112
4.3.2.4 Surface/Core Effect and Influence of Reaction Kinetics	116

4.3.3 Summary	117
4.4 Conclusions for Chapter Four	117
Chapter Five – Effect of Using Concentrated Sources of Silica on the Carbothermal Reduction-Nitridation of Slag	119
5.1 Analysis of the Raw Materials and Experimental Procedure	119
5.1.1 Clay-P (Pyrophyllite)	120
5.1.2 Sand (Quartz)	121
5.1.3 Composition Selection and Firing	122
5.2 P-series Firings: Slag + Clay-P (pyrophyllite)	123
5.2.1 Firings Performed for 12 Hours at 1450°C	123
5.2.2 Firings Performed for 18 and 24 Hours at 1450°C	127
5.2.2.1 Ca-Content of α -Sialon in P-series CRN powders	130
5.2.2.2 SEM Analysis of P02 Powder Fired for 18 Hours	131
5.2.2.3 SEM Analysis of P08 Powder Fired for 18 Hours	133
5.2.3 Discussion of CRN of the P-series Compositions	135
5.3 S-series Firings: Slag + Sand	138
5.4 Conclusions for Chapter 5	141
Chapter Six – Optimisation Of The CRN Process	
6.1 Experimental Outline	143
6.1.1 Composition Selection	143
6.1.2 Quantitation of α -Sialon / E'- phase ratio	143
6.2 Specimen Density & Geometry	145
6.2.1 Powder Packing Density	145
6.2.1.1 Mass Production of α -Sialon (Sample Size and Geometry)	149
6.3 Nitrogen Flow Rate	151
6.4 Seeding	155
6.4.1 Effect of α -Si ₃ N ₄ Seeds	155
6.4.2 Self-Seeding with CRN- α' Powder	157
6.5 Effect of Elevated Temperature on CRN Reactions and Phase Stability	158

6.5.1	Stability of the CRN Powders at 1600°C.	159
6.5.2	Factors Affecting the Conversion of E' to α' in K33	163
6.5.2.1	Effect of Temperature on the CRN Reactions in K33	163
6.5.2.2	Effect of Carbon on the CRN Reactions in K33	166
6.5.2.3	Effect of Compaction Pressure and Packing Powder on the CRN Reactions in K33	167
6.5.3	Pressureless Sintering of CRN Powders at 1800°C	171
6.5.4	Summary of Findings From High-Temperature Heat-treatments	173
6.6	Conclusions for Chapter 6	173
 Chapter Seven – Microstructure And Property Evaluation Of Ca-α-Sialon Bulk Materials		175
7.1	Hot-Pressing	176
7.1.1	Experimental Procedure	176
7.1.1.1	Green-body Fragility	176
7.1.2	Density of Hot-Pressed Pellets	177
7.1.3	Phase Transformations During Hot-Pressing	178
7.1.3.1	Preferential Orientation of α -Sialon	182
7.2	Microstructural Analysis	183
7.2.1	Experimental Conditions	183
7.2.2	K06 Pellet	184
7.2.3	K33 Pellet	189
7.2.3.1	Depth of the E' \rightarrow α' Transformed Layer in K33	194
7.2.4	P02 Pellet	196
7.2.5	P08 Pellet	197
7.2.6	Summary of Microstructural Analysis of Hot-pressed Pellets	200
7.3	Hardness and Fracture Toughness	201
7.4	Erosion Resistance	203
7.4.1	Experimental Conditions	203
7.4.2	Cumulative Mass Loss	205
7.4.2.1	Comparison of CRN- α' to Reaction-Sintered Ca- α'	206
7.4.3	Eroded Surfaces	207
7.4.3.1	K33	207
7.4.3.2	P08	209

7.4.3.3 K06	211
7.4.3.4 P02	212
7.4.4 Discussion of the Erosion Behaviour of CRN Materials	214
7.4.5 Summary of Findings from Erosion Resistance Testing of CRN Materials	216
7.5 Conclusions For Chapter Seven	216
Chapter Eight – Conclusions and Suggestions for Future Work	218
8.1 Conclusions	218
8.2 Suggestions for Future Work	221
List of Publications	224
References	225

Table of Figures and Tables

Chapter Two

Figure 2.2	Schematic representation of α - Si_3N_4 structure	14
Figure 2.3	Sialon behaviour diagrams	15
Figure 2.4	Ca- α -plane	16
Figure 2.5	Cumulative volume loss of various target ceramics as a function of the amount of SiC erodent impinging on the surface at 90° incidence angle	22
Figure 2.6	Phase relations in the Si_3N_4 -AlN-CaO system	24
Figure 2.7	The structure of kaolinite and pyrophyllite	28
Figure 2.8	XRD of CRN-derived Ca- α -sialon powder	35
Figure 2.9	Hollow balls consisting of 85 wt% Ca- α -sialon and 15 wt% AlN	39
Figure 2.10	Phase formation as a function of reaction time at 1500°C during the CRN formation of Ca- α' from fly ash	41
Figure 2.11	Effect of Si_3N_4 seeds on Mg- α' formation via CRN of talc and halloysite	44
Table 2.1	Summary of successful conditions for producing α -sialon via CRN of various raw materials	49

Chapter Three

Figure 3.1	Standard firing schedule.	61
Figure 3.2	Firing schedule for determining the intermediate reaction products	62
Figure 3.3	Schematic of gas blast erosion rig	69
Table 3.1	Chemical composition and approximate cost of minerals used for CRN	55
Table 3.2	Slag:clay-K molar ratio of K-series compositions and seeding content for K - series compositions	57

Chapter Four

Figure 4.1	XRD trace of slag	71
Figure 4.2	SEM micrograph of slag	71
Figure 4.3	XRD trace of clay-K	72
Figure 4.4	SEM micrograph of clay-K	72

Figure 4.5	XRD trace of Si_3N_4 seeds	73
Figure 4.6	SEM micrograph of Si_3N_4 seeds	73
Figure 4.7	XRD traces of slag:clay-K compositions fired for 12 hours at 1450°C	77
Figure 4.7	(cont.)	78
Figure 4.8	XRD traces of the surface and core regions of the K09 pellet	81
Figure 4.9	SEM micrographs of CRN powders formed after 12 hours at 1450°C	87
Figure 4.10	SEM micrographs of K06 α -sialon powders with various morphologies	88
Figure 4.11	EDXS spectra typical of α' grains in K06 powder, E' plates in K19 powder	89
Figure 4.12	Schematic showing phase compatibility region for composition K02 after CRN for 12 hours at 1450°C	95
Figure 4.13	Schematic showing phase compatibility region for compositions K03, K05, and K06 to K33, after CRN for 12 hours at 1450°C	97
Figure 4.14	DTA curve of slag	101
Figure 4.15	DTA curve of clay-K	102
Figure 4.16	DTA curve of 0.62:1 slag:clay-K mixture	104
Figure 4.17	DTA of 1.9:1 slag:clay-K mixture	105
Figure 4.18	XRD traces from samples taken at various intermediate points between 1300-1450°C during firing of composition K06	113
Figure 4.19	XRD traces from samples taken at various intermediate points between 1300-1450°C during firing of composition K19	114
Table 4.1	Phases identified in slag:clay-K compositions fired at 1450°C for 12 hours	76
Table 4.2	Comparison of experimental E-phase XRD peaks to JCPDS PDF	83
Table 4.3	Residual carbon-content of selected K-series compositions	85
Table 4.4	Typical EDXS peak height ratios of particles in K06 and K33	89
Table 4.5	Lattice parameters, m -values, and Ca-content of α -sialon phases	91
Table 4.6	XRD of slag after heating in air at various temperatures	101
Table 4.7	XRD of 0.62:1 slag:clay-K mixture heated in air at various temperatures	104
Table 4.8	XRD of 1.9:1 slag:clay-K mixture heated in air at various temperatures	105
Table 4.9a	XRD traces from samples taken at various intermediate points between 1000-1450°C during firing of composition K06	108
Table 4.9b	XRD traces from samples taken at various intermediate points between 1000-1450°C during firing of composition K10	109
Table 4.9c	XRD traces from samples taken at various intermediate points between 1000-1450°C during firing of composition K19	110

Chapter Five

Figure 5.1	XRD trace of clay-P	120
Figure 5.2	SEM micrographs of pyrophyllite clay-P and milled sand	121
Figure 5.3	XRD trace of sand after milling	121
Figure 5.4	XRD traces of slag:clay-P samples fired at 1450°C for 12 hours	124
Figure 5.5	XRD traces of slag:clay-P samples fired at 1450°C for 18 hours	128
Figure 5.6	XRD traces of surface and core of P20 fired for 24 hours at 1450°C	129
Figure 5.7	SEM micrographs of P02-18 powder fired for 18 hours at 1450°C	132
Figure 5.8	EDXS spectra of particles in P02 powder fired for 18hrs at 1450°C	132
Figure 5.9	SEM micrographs of P08-18 powder fired for 18 hours at 1450°C	133
Figure 5.10	EDXS spectra of P08-18 particles	134
Figure 5.11	Diagram showing the relationship between glass viscosity and temperature for a variety of glass compositions	137
Figure 5.12	XRD traces of S03 sample fired for 12 and 24 hours at 1450°C	139
Table 5.1	Summary of the composition of the SiO ₂ -additives	119
Table 5.2	Molar ratios of K-series and equivalent P- and S-series compositions	122
Table 5.3	XRD analysis of slag:clay-P samples fired for 12, 18, and 24 hours at 1450°C	125
Table 5.4	Calculated lattice parameters, corresponding estimate of m- values and Ca-content of α -sialon from P02 and P08 fired for 18 hours at 1450°C	130
Table 5.5	EDXS peak height ratios of 3 types of particle found in P02 fired for 18hrs at 1450°C	133
Table 5.6	Measured EDXS peak height ratios of particles found in P08-18 fired for 18hrs at 1450°C	135
Table 5.7	XRD phase analysis of slag:sand samples fired for 12 and 24 hours at 1450°C	138

Chapter Six

Figure 6.1	XRD of fired K06 powder compacts of varying compaction density	147
Figure 6.2	XRD traces of K33 powder fired at 1450°C for 12 hours under different N ₂ flowrates	153
Figure 6.3	α' formation as a function of α -Si ₃ N ₄ seeding content for K06 pellets fired at 1450°C for 12 hours under N ₂ flowing at 30ℓ/hr	156

Figure 6.4	XRD of oxidised (C-free) K02 CRN powder heat-treated at 1600°C for 1 hour	161
Figure 6.5	XRD scans of K33 powders heat-treated at various temperatures for 2 hours	164
Figure 6.6	XRD of CRN-K33 pellet after heat-treating in packing powder at 1800°C for 2 hours	170
Table 6.1	α' / E' ratios in fired powder compacts of different compaction density	147
Table 6.2	α' content after firing a full boat of powder at 1450°C for 12 hours	150
Table 6.3	Phase analysis and α' content for samples fired under varying N ₂ flow rates at 1450°C for 12 hours.	152
Table 6.4	Effect of type of seed on α' content of loose K06 powder fired at 1450°C for 12 hours in N ₂ flowing at 30l/hr	157
Table 6.5	Phase analysis of oxidised (C-free) CRN powders heat-treated at 1600°C for 1 hour	160
Table 6.6	Phase analysis of oxidised and as-fired K33 CRN powder heat-treated at various temperatures for 2 hours	164
Table 6.7	Phases present after firing oxidised (C-free) K33 powder and pellets at 1800°C for 2 hours, with and without packing powder	169
Table 6.8	Density of pellets pressureless sintered from CRN powders at 1800°C for 2 hours	172

Chapter Seven

Figure 7.1	Schematic showing orientation of pellets produced by hot pressing	179
Figure 7.2	XRD showing phase transformations on the K33 pellet surface after hot-pressing at 1700°C	180
Figure 7.3	XRD showing D' → α' phase transformation on P08 pellet surface after hot-pressing at 1700°C	181
Figure 7.4	SEM micrograph of K06 pellet hot-pressed at 1700°C	185
Figure 7.5	TEM bright field overviews of K06 pellet hot-pressed at 1700°C	186
Figure 7.6	Typical CBEDP and EDXS spectra of grains in the K06 pellet	187
Figure 7.7	TEM micrograph of glass pocket in K06 pellet hot-pressed at 1700°C	189
Figure 7.8	Optical micrographs of the K33 pellet hot-pressed at 1700°C	191
Figure 7.9	SEM micrographs of the etched K33 pellet hot-pressed at 1700°C	193
Figure 7.10	EDXS spectra from the K33 pellet hot pressed at 1700°C	194
Figure 7.11	SEM micrograph of the etched K33 pellet hot-pressed at 1700°C	195

Figure 7.12 SEM micrographs of the etched P02 pellet hot-pressed at 1700°C	196
Figure 7.13 EDXS spectrum typical of α' in the P02 pellet hot-pressed at 1700°C	197
Figure 7.14 SEM micrographs of the etched P08 pellet hot-pressed at 1700°C	199
Figure 7.15 Cumulative mass loss of the samples vs. mass of SiC erodent for the four materials K06, K33, P02, P08, under impact angles of 30° and 90°	204
Figure 7.16 Eroded surfaces of the K33 pellet	208
Figure 7.17 Eroded surfaces of the P08 pellet	210
Figure 7.18 Partial melting of grain boundary glass in the P08 pellet eroded at 90°	211
Figure 7.19 Eroded surfaces of the the K06 pellet	212
Figure 7.20 Eroded surfaces of the P02 pellet	213
Table 7.1 Density and phases of bulk pellets hot-pressed at 1700°C.	178
Table 7.2 Average EDXS peak height ratios of particles categorised as α' , D', and indeterminate in the P08 pellet hot-pressed at 1700°C	199
Table 7.3 Physical and mechanical property data for K06 K33 P02 & P08 pellets hot pressed at 1700°C.	201
Table 7.4 Table 7.4 Steady-state erosion rates (ΔE) for K06, K33, P02, P08 pellets	205

List of Symbols and Nomenclature

'	indicates solid-solution rather than pure stoichiometric compound
α	alpha silicon nitride (α -Si ₃ N ₄)
α'	alpha-sialon (α -sialon) $\text{Ca}_{m/v}\text{Si}_{12-(m+n)}\text{Al}_{m+n}\text{O}_n\text{N}_{16-n}$
β	beta-silicon nitride (β -Si ₃ N ₄)
β'	beta-sialon (β -sialon Si _{6-x} Al ₂ O _z N _{8-z})
ΔE	erosion rate (target material volume loss per unit mass of erodent)
θ	impact angle between erodent and target surface during erosion testing
2H	SiC polytypoid with 2-layer hexagonal stacking sequence (α -SiC)
3C	SiC polytypoid with 3-layer cubic stacking sequence (β -SiC)
a	unit cell parameter
a_c	activity of carbon
AlN'	AlN solid-solution
atm	atmosphere (pressure)
c	unit cell parameter
CBEDP	convergent beam electron diffraction pattern (from TEM)
CIP	cold isostatic pressing
clay-K	kaolinite clay [K-series compositions]
clay-P	pyrophyllite clay [P-series compositions]
core	central bulk region of samples
CRN	carbothermal reduction-nitridation
CRN- α'	α -sialon powder produced via carbothermal reduction-nitridation
D/D'	D-phase (Ca ₂ Si ₃ O ₂ N ₄)/ D-phase solid-solution
DTA	differential thermal analysis
E / E'	E-phase (CaAlSiN ₃)/ E-phase solid-solution
EDXS	energy dispersive x-ray spectroscopy
exo	exothermic reaction/event
G / G'	gehlenite (Ca ₂ Al ₂ SiO ₇)/ Gehlenite solid-solution
HT	heat treatment
Hv	Vickers hardness
JCPDS	publisher of x-ray Powder Diffraction File <i>see PDF</i>
K _{IC}	fracture toughness
Kxx	K-series compositions using using clay-K (kaolinite), where xx denotes 10x the slag:clay molar ratio rounded to 2 significant figures

K-series	compositions formed from a mixture of slag+clay-K
LOI	loss on ignition
m	α -sialon m-value, from $\text{Ca}_{m/v}\text{Si}_{12-m-n}\text{Al}_{m+n}\text{O}_n\text{N}_{16-n}$
M	metal
M ^{v+}	metal cation with valency = v+
M/M'	M-phase $\text{Ca}_2\text{AlSi}_3\text{O}_2\text{N}_5$ / M-phase solid-solution
n	α -sialon n-value, from $\text{Ca}_{m/v}\text{Si}_{12-m-n}\text{Al}_{m+n}\text{O}_n\text{N}_{16-n}$
p[]	partial pressure
PDF	Powder Diffraction File, as published by JCPDS
Pxx	compositions using clay-P (pyrophyllite-clay) where xx denotes 10x the slag:clay-P molar ratio rounded to 2 significant figures
P-series	compositions formed from a mixture of slag+clay-P
RE	rare-earth element
SEM	scanning electron microscopy
SHS	self-propagating high-temperature synthesis
SPS	spark plasma sintering
surf	surface layer on samples, where distinct
Sxx	S-series compositions using sand, where xx denotes 10x the slag:sand molar ratio rounded to 2 significant figures
S-series	compositions formed from a mixture of slag+sand
TEM	transmission electron microscopy
TGA	thermogravimetric analysis
V	vacancy
x	α -sialon x-value, = m/valency of the stabilising cation. Represents the number of cations per α -sialon unit cell.
XRD	X-ray diffraction
z	β -sialon z-value, from $\text{Si}_{6-z}\text{Al}_2\text{O}_z\text{N}_{8-z}$

Declaration

This thesis contains no material that has been accepted previously for the award of any other degree or diploma in any University or other institution. To the best of my knowledge and belief, it contains no material published previously or written by any other person, except where due reference is made in the text.



Mark R. Turner

December 2003

Acknowledgements

I would like to acknowledge the following people whose contributions have been invaluable to the production of this thesis:

Firstly, my supervisor Dr. Yi-Bing Cheng, for his constant guidance and direction throughout this investigation. Without his unyielding enthusiasm for this project and his confidence in my abilities, the momentum would have been lost many times.

Thanks to all the technical staff, in particular Silvio Mattievich, for helping me in the constant battle to keep 'Charles' and 'Diana' from falling apart and staying that way. Many thanks also Renji Pan for his help with the electron microscope facility.

I would like to thank the other members of our research group, past and present, who were my officemates, colleagues, and friends (and usually all of the above): Steven Swenser, Aaron Seeber, Yu Zhang, Andrew Carman, Wei-Wu Chen, David Menzies and Judy Hart. Thanks for your technical assistance, friendship, support, and maintenance of my coffee habit. Thanks also to the various souls in SPME who have stopped by for a chat over the years, and especially to the inhabitants of the 'coffee office' (Hayley, Scott, Ali, and John) who willingly endured the distractions.

Thanks to Aaron, Peta, Sissi, and Michael for their help at the very end. And thanks also to all my other friends, Big Band'ers, taiko drummers, and my twenty-six past housemates; life outside the thesis would have been much less interesting without you.

Finally, I would like to give special thanks to all of my family, for the love and unending support provided throughout my long education, and especially over the course of this PhD.

"...There is little that can be learned in comfort. Comfort is the warm bed at the end of a long journey. It was never meant to be slept in forever."

Mark Driver, *Where I've Been*,
(www.blindwino.com/driver.html)

Summary

α -Sialon (α') is a nitride ceramic with many desirable engineering properties, such as high hardness and high strength at elevated temperatures, however the relatively high cost of fabrication has been one of the main barriers to it attaining more widespread use by industry. This is partly due to the expensive, high-purity, synthesised reactant powders and complex furnace equipment needed to fabricate α -sialon materials. Carbothermal reduction-nitridation (CRN) is a process that has been successfully used to fabricate other sialon materials such as β -sialon from less-expensive oxide starting materials including clay minerals and industrial waste products. However this process has received much less attention for the production of the more complex α -sialons. Slag is a good candidate raw material for the production of inexpensive α -sialons via CRN; it is an abundant waste product from steelmaking with a composition amenable to α -sialon formation.

This thesis explored the CRN process as a means of producing inexpensive α -sialons from mixtures based on this slag waste. Various mixtures of slag, clay, carbon-black and α - Si_3N_4 'seeds' were reacted at 1450°C for 12 hours under N_2 flowing at 30ℓ/hr. α -Sialon was produced in all compositions tested, however the quantity of α' amongst the final products varied with composition. AlN and a grain boundary glass were secondary phases produced in all compositions, in addition to one of α - Si_3N_4 , gehlenite, or E' -phase, depending on slag content. The Ca- α -sialon formed from these powders was generally equiaxed, sub-micron in size, and relatively rich in Ca. Impurities in the slag and clay formed phases such as FeSi and TiN, with many other impurities taken up by the glass.

The CRN reaction process was investigated and found to occur in three stages: 1) decomposition and phase transformations within the oxide reactants during heating to 1300°C; 2) melting of the oxide phases and early stage CRN between 1300 and 1400°C to produce the first oxynitride phases; and 3) final product formation and elimination of intermediate phases with extended holding time at 1450°C. A low z-value β -sialon and M' -phase were the two main intermediate phases produced during CRN. These phases were converted into α' via a series of solution-precipitation steps. Secondary phases such as E' -phase and gehlenite were also found to be metastable intermediate CRN phases able to form α' under more appropriate CRN conditions.

The effects of various compositional factors and processing parameters on CRN were studied, including slag content, clay composition, seeding, powder compaction, and nitrogen flowrate. It was found that these parameters are inter-dependent, and that the optimum CRN conditions are composition-specific. Generally, CRN was enhanced by higher temperatures, low powder packing density, and a N_2 flowrate lower than 30ℓ/hr. Seeding the mixtures with $\alpha-Si_3N_4$ was not particularly effective in boosting α -sialon formation.

The α -sialon formed via CRN was found to be stable at elevated temperatures, and minor amounts of secondary phases were converted to α' during sintering, however pressureless sintering was unable to produce highly densified materials. Hot-pressing was used to produce fully dense materials which were determined to have hardness and toughness values similar to those of high glass-content Ca- α -sialons produced from conventional laboratory reagents. The solid-particle erosion resistance of the CRN material was also similar, if not better, than that of conventional α -sialons, demonstrating its potential for use as an industrial wear-resistant lining.

Chapter One

Introduction

“Waste is food”... Whatever you can't use in any manufacturing or energy-creating industry has to go back into natural or industrial systems to feed them; otherwise it's proof you're losing part of your investment and causing damage to natural systems.

(Suzuki and Dressel 2002)

Businesses worldwide are under pressure to address the concept of *sustainability*. One method to do this is to adopt the so-called “triple bottom line”, which is a measure of business performance that includes measures of social equity and environmental protection in addition to simple economic growth (Mowat 2002). Most industrial processes have an adverse effect on the environment: mineral and organic resources get depleted, non-renewable energy is consumed, and waste by-products, some toxic, are amassed and must be re-processed or stored. Sustainability requires maximising energy efficiency, minimising raw material use and costs via recycling, and seeking alternative strategies to produce less waste in the first place. This is not only good for the social and physical environment, but in most cases can also significantly improve profits, thereby improving all three areas of the triple bottom line (Roston 2002). One criticism of this focus on sustainability, however, is that it concentrates solely on liability minimisation, ie. just making a business “less bad” (McDonough and Braungart 2002). A more fundamental change in design philosophy is that of ‘cradle to cradle’ espoused by McDonough Braungart Design Chemistry, where, just as in nature the waste from one process is food for another, and the product itself can be fully recycled into an equally valuable new product at the end of its useful life (MBDC 2003). This is a worthy ultimate goal, but as an interim measure, the immediate benefits of making a business “less bad” by better utilisation of wastes should not be underestimated.

Slag is an industrial waste product produced in massive amounts each year from iron and steel foundries. It is generally piled up in ‘slagheaps’ on site, and in addition to being unsightly they require considerable financial investment in land and facilities for storage and handling. Despite advances in storage technology, there is still the possibility that fine particles can be dispersed by wind, or compounds will leach into the soil and groundwater, which can cause

various ill effects to the local environment (Pioro and Pioro 2003). There exists the opportunity to convert steelmaking slag into a considerably higher value-added product – an advanced ceramic material known as α -sialon, using the process of carbothermal reduction-nitridation. Advanced ceramics such as α -sialon are of great interest to industry due to their high-performance properties such as hot-strength, wear resistance, and corrosion resistance. As with other ceramics, the brittle nature of α -sialons can be a hindrance in utilising the material, however one of the main obstacles to broader acceptance by industry is the high cost of fabrication.

This thesis is concerned with the development of the process of carbothermal reduction-nitridation to convert slag, an industrial waste product, into α -sialon (α'), an advanced ceramic material. The potential benefits of such a process, if successfully realised are many: a) the environment benefits by reducing the amount of unused slag that must be safely stored; b) energy may be saved because the currently used raw-materials for α' production are very energy intensive to produce; c) profits may be generated through value adding; and d) new efficiencies in processes down the line may be generated where a cost-competitive sialon replaces inexpensive but less-effective materials. Furthermore, the α -sialon produced by this process may have novel properties that finds new markets.

This chapter introduces some of the general issues and concepts that form the basis of the work presented in this thesis. Firstly, some of the factors that lead to advanced ceramics such as α -sialons being so costly are discussed. This is followed by examples of the recycling of industrial wastes such as slag into useful ceramic products, with a focus on the CRN process.

1.1 Advanced Ceramics and α -Sialon

Ceramics are often differentiated into two categories: 'traditional' or 'classical' ceramics, and 'advanced' or 'engineering' ceramics, though the distinction between the two is often vague. Broadly speaking, traditional ceramics are those popularly associated with the word 'ceramic', based on the clays and silicates located in abundance near the surface of the earth, and which have been in use since at least 5000 B.C. (Grimshaw 1971). Many high-volume commodity objects such as bricks, coffee mugs, porcelain whiteware, and electrical insulators are produced from these materials as they are easy to obtain, easy to make into complex shapes when mixed with water, and easy to densify in relatively low temperature kilns.

Advanced ceramics are usually identified as highly refined, specialised materials used for more 'high-tech' applications, such as electronic components, or high-temperature corrosion

resistant linings. These materials have a more recent history, starting around 60 years ago with the initial development of oxide-based materials such as high-purity alumina (Al_2O_3) and ferroelectric BaTiO_3 materials (Rahaman 2003). Since the 1970s, new non-oxide ceramic materials such as the carbides, nitrides, and borides have been developed with unique chemistries, microstructures and properties specifically tailored for use in severely demanding engineering applications. Some examples include SiC gas burners, TiB_2 crucibles, B_4C body armour, and AlN substrates for integrated circuits (Srinivasan and Rafaniello 1997).

1.1.1 Processing of Advanced Ceramics

The atomic bonding in ceramics is a combination of ionic and covalent bonding, and in non-oxide advanced ceramics covalent bonding is often dominant. For example in Si_3N_4 the bonding is 70% covalent (Komeya 1994). Covalent bonding is very strong and directional in nature, thus these materials have very limited atomic diffusion, even at high temperatures. This imparts many beneficial properties to the material, including: high strength; retention of strength at elevated temperatures; and resistance to plastic deformation. Unfortunately this makes densification of the ceramic precursor powders into solid bodies very difficult due to a lack of diffusive mass transport. To overcome their lack of diffusivity many advanced ceramics are fired at temperatures between 1600°C and 2000°C , but high temperatures alone are often inadequate to achieve full density, so the simultaneous addition of pressure may also be required. It is also often necessary to replace the furnace atmosphere with inert gases to protect the furnace materials and non-oxide ceramics from oxidation. A modern furnace is thus a complicated apparatus, involving costly high-temperature materials, and complicated cooling and mechanical systems such as hydraulic presses and pumps.

Engineering ceramics have specific in-service performance requirements, and are thus very sensitive to the microstructures formed during sintering, so good control over the chemical composition and microstructure of the raw materials is vital to maximising material properties. The optimal characteristics for powder precursors are generally: a fine ($<1\mu\text{m}$) size, narrow particle size dispersion, and a spherical or equiaxed particle shape to assist powder packing and sintering (Rafaniello 1997). The powders should also be high-purity, and single phase, to avoid the formation of secondary phases which can be detrimental to the material as a whole. Such fine, high-purity powders are commonly formed via chemical methods from synthetic or naturally occurring raw materials that have been highly refined. Nowadays a very high degree of control over powder purity and homogeneity is achievable, with purities of 99.99% and particle size down to the nanometre level with narrow particle size distribution routinely produced. Given the amount of energy, sophisticated equipment, and strict process control

required to produce these fine powders, it is not surprising that they come at great cost; a 10,000-fold cost difference exists between refined mineral sand for glassmaking (AUD\$0.01/kg) and silicon nitride powder derived from sand (AUD \$100/kg). In the case of commercial components made from silicon nitride such as an automotive turbo rotor, raw materials costs were estimated to account for up to half of the component's cost (Das and Curlee 1992).

Metals and plastics can be easily formed into complex shapes while in the liquid or semi-solid state, and can be easily modified after solidification. Most ceramics, however, do not melt or may be only partially melted during sintering, and form hard, brittle bodies after firing that resist machining operations. This is a generally desirable trait, but becomes problematic if the fired component does not meet specified tolerances and must be further shaped or ground. Post-firing machining requires expensive diamond tooling and very careful process control to avoid the introduction of surface flaws that may be catastrophic to the component's toughness, and depending on size and geometry of the component this may account for 80-90% of a component's cost (Klocke, Schippers, *et al.* 2001). Therefore, the ceramic green-body before firing must be as densely packed, and as close to the desired final shape, as possible.

Many high-volume, inexpensive forming techniques used for traditional clay products, such as extrusion, injection moulding, slip-casting, or tape-casting, can be used for advanced ceramic production, however, unlike traditional ceramics they generally do not form slips with water. This means that a polymer binder must be added to the ceramic powder, which introduces additional complexity to the manufacturing process and requires careful control over binder burnout so as not to degrade the structure and properties of the final product (Rahaman 2003). The most commonly used green-body forming mechanism is uniaxial pressing, but this allows only simple geometries to be formed; more complex shapes require the use of expensive isostatic presses.

Cost factors alone are not the sole cause of the failure of advanced ceramics to be widely adopted by industry; intrinsic material issues such as poor fracture toughness, difficulty in joining to other components, and the low reliability of manufactured products are fundamental issues that also need to be addressed. However the cost issue cannot be ignored, especially when there is sometimes a 10 to 1000-fold cost differential to currently used materials (McColm 1995). One example is the cost of silicon nitride engine valves, which have been estimated to cost AUD\$48/valve (Schafer 2000). When a minimum of 12 valves are required for a typical 6-cylinder engine, this becomes a major expense compared to metal valves which cost around AUD\$1 each. From the customers' point of view, performance

improvements are somewhat intangible, and cannot easily justify the higher overall cost. This was concisely summarised by the response given by Dr. W. Pollman from Daimler-Chrysler to a question about when ceramic engine and brake components, many of which have already been developed, would actually be found in cars for sale in the showroom. His answer was simply: "When the ceramic parts cost the same as the metal or plastic ones" (Pollmann 2000).

1.1.2 Silicon Nitride and the Sialons

Silicon nitride (Si_3N_4) was thought to be a potential material for the ceramic gas turbine project that originated in 1971, due to properties such as high strength and strength retention at elevated temperatures, good wear resistance, low coefficient of thermal expansion, and good oxidation resistance. Unfortunately, its high covalent bonding and very low diffusivity meant that the required mechanical properties could not be produced without hot pressing, which prevented the necessary complex shapes from being produced. This shaping problem can be overcome by using up to 5% MgO or Y_2O_3 sintering additives in a pressureless sintering process, but the additives result in a residual glassy phase, which is detrimental to the mechanical properties of the material (Hampshire 1994).

The first sialons were identified independently by both Jack and Oyama in the early 1970s after mixtures of Si_3N_4 and Al_2O_3 were fired at high temperatures and a Si-Al-O-N solid solution was formed. This was found to be isostructural with the β -form of Si_3N_4 and designated β' , or β -sialon. Another mixture involving LiSi_2N_3 and Al_2O_3 gave a Li-(Si-Al-O-N) material isostructural with α - Si_3N_4 , designated α' , or α -sialon. The α -sialon structure contains two interstices, which are able to accommodate the extra metal cations within the α' lattice. This provides a mechanism to minimise the amount of detrimental grain boundary glass in these materials, as the metal-oxide sintering additives are required for α' formation and are incorporated into the α' crystal structure. α -Sialons are now commonly formed using Ca, Mg, Y, and rare-earth cations.

The processing of α -sialons is typical of advanced ceramics, requiring costly, high-purity, synthesised powder precursors, and sophisticated high-temperature processing techniques. The powders used for reaction-sintering are fine, pure Si_3N_4 , AlN , SiO_2 , Al_2O_3 powders, and expensive metal oxides such as Y_2O_3 . The materials are fired at 1600-1800°C in a N_2 atmosphere to simultaneously achieve chemical reaction between the powders and densification to form a solid α -sialon body. Often pressure densification techniques such as hot-pressing, hot-isostatic pressing, gas pressure sintering, or more recently, spark plasma sintering, are used. This makes α -sialons one of the more expensive advanced ceramics, hence

α' materials have thus far only found use in specialised applications that specifically require their high-performance characteristics and can justify the high cost, such as lathe inserts for metal cutting tools.

Engineering research into α -sialons and other advanced ceramics is generally focused on attaining the best ultimate material properties to suit the most demanding applications. These materials require very strict control over starting powder characteristics and processing conditions, and are therefore relatively expensive to fabricate. However, if the intended application environment is less severe, it may be possible to sacrifice some degree of performance for easier and/or cheaper fabrication. One method that can reduce the fabrication cost is to utilise cheaper minerals or waste by-products from other processes as the raw materials for ceramic production. For example, silicon oxynitride can be produced via the self-propagating high-temperature synthesis (SHS) of desert sand and silicon reclaimed from zinc smelting (Radwan and Miyamoto 2003).

1.2 Recycling of Wastes Into Ceramics

Traditionally, wastes from industrial processes were simply dumped into landfill. However with growing awareness of environmental concerns and increasingly strict legislative controls being enacted to prevent leaching of toxins into groundwater and soils, new methods for minimising and converting waste into benign and potentially useful forms are receiving greater attention. Particular attention is being paid to wastes from primary and secondary materials production as they often contain heavy metals, organic compounds, and other mineral components that are uneconomical to recover and thus must be rendered inert before dumping (Pelino 2000).

Steelmaking slag is a waste product produced in vast quantities worldwide, with approximately 300kg of slag produced for every ton of steel produced in blast furnaces (ASA 2003). Currently, slag is most commonly used in vitrified form as an additive to concrete where it is not only cheaper than the cement it replaces, but improves the drying properties and chemical durability (Bakhtev, Sanjayan, *et al.* 1999). It is also widely used as a filler and stabiliser in roads and pavements. Steelmaking slags are composed mainly of SiO_2 , Al_2O_3 , CaO , though a wide variety of other impurities are also present.

Vitrification of wastes is a common treatment for slags and fly ashes, whereby heavy metals are trapped in an amorphous matrix via rapid cooling from the molten state. The high temperature removes hazardous organic contaminants, but the process is costly and the

vitrified product has poor mechanical and chemical properties, which limit its potential for industrial application (Ferreira, Ribeiro, *et al.* 2003). Controlled crystallisation of these vitrified wastes into glass-ceramic materials can produce a more durable crystalline product with considerably improved mechanical properties that can be marketed to recover the production cost. Applications of these glass-ceramics include: low-grade use as a filler in road paving; in concrete as aggregate; and in commodity ceramics such as non load-bearing construction bricks, floor paving and wall tiles (Boccaccini, Petitmermet, *et al.* 1997; Dominguez and Ullmann 1996).

The conversion of wastes into advanced ceramics such as sialons, holds potential for even greater value-adding. For example, rice husk waste from rice beneficiation contains significant amounts of silica, and with controlled combustion, a fine amorphous silica can be produced for use in whitewares, cements, or as a source for other ceramic materials such as SiC, Si₃N₄ and β-sialon (Della, Kuhn, *et al.* 2002). Fly ash generated from the combustion of coal in power plants contains all the elements necessary for β-sialon production (and sometimes for α-sialon), and have been produced via the carbothermal reduction-nitridation process to be described in the following section. Sometimes novel processes must be created to utilise non-traditional raw materials, and this may produce novel properties in the final product. For example the process of silicon metal infiltration has been adapted to use pyrolised wood as the carbon preform, which provides a cellular structure that is then converted to form a cellular SiC ceramic (Singh and Salem 2002). Waste cardboard or sawdust could also be used for this process, allowing complex geometries to be formed before siliconisation, and thus expanding the potential of this process to new products.

1.2.1 Carbothermal Reduction-Nitridation

Carbothermal reduction-nitridation (CRN) is a process that produces nitride materials from oxide precursors, such as ZrN from ZrO₂ and AlN from Al₂O₃ minerals. The oxides are mixed with a carbon-based reductant, usually carbon-black, and fired in a nitrogen-containing atmosphere at temperatures ~1300-1500°C. During CRN the metal oxide reacts with the carbon, which allows replacement of oxygen by nitrogen via CO and CO₂ gas formation. This may occur via a series of steps with various intermediate nitrogen-containing phases formed. The CRN process is widely used commercially for the synthesis of Si₃N₄ powder, from both synthesised and refined mineral SiO₂ sources (van Dijen and Vogt 1992; Arik 2003), and various sialon phases such as β-, O-, and X-sialon can be produced via the CRN of aluminosilicate clays (Mazzoni and Aglietti 1998).

The production of β -sialon from clays is one of the most intensively studied CRN processes due to the ability to form a high-purity $z=3$ β -sialon ($\text{Si}_3\text{Al}_3\text{O}_3\text{N}_5$) from kaolinite clay ($2\text{SiO}_2 \cdot \text{Al}_2\text{O}_3 \cdot 2\text{H}_2\text{O}$) alone, and this process is now used to produce β' for commercial components. In addition to mineral oxide raw materials, some waste products have also been investigated as precursors for sialons fabricated via CRN. β -Sialon has been produced from a mixture of carbon-bearing rice husk ash and Al_2O_3 (Rahman and Saleh 1995); from sodium-containing wastes from alumina refining (Cardile 1990); and from fly ashes produced from the combustion of coal in power plants (Gilbert and Mosset 1998).

α -Sialon is chemically more complex than β -sialon as it requires an additional metallic component, therefore its formation via CRN has received considerably less research attention. This is despite some significant potential economic advantages by using CRN, namely, the ability to use considerably cheaper raw materials such as naturally occurring minerals and waste by-products, instead of expensive synthesised powders. A further advantage is that CRN generally requires lower firing temperatures and can therefore use less-expensive furnace equipment. There also exists the potential for the formation of α -sialon powders with unique morphologies and novel properties.

A few research groups have investigated the use of CRN to form α -sialons from various oxide raw materials, including laboratory-grade reagents, clay minerals, and fly ash. However, little detailed information has been obtained regarding the reaction mechanisms occurring during CRN in these systems, and only a cursory description of the densification of CRN- α' powders has been given. The resultant physical and mechanical properties of these materials have also largely been neglected in these studies, offering no method to evaluate the potential of CRN- α -sialon as an engineering material for industrial application. This thesis seeks to address these deficiencies, and is an investigation into using steelmaking slag as the basis for α -sialon production by CRN.

Clearly, it is unlikely that α -sialons prepared from slag and other wastes would attain the same level of excellent high-temperature properties seen in products fabricated from high-purity synthesised powders. However, many low-temperature applications for α -sialon can be conceived in the mining and metallurgical industries, such as wear-resistant linings for ore or slurry transport equipment, or refractory linings for molten metal containers, which may benefit from using an inexpensive α -sialon material. Currently, steel plates and alumina ceramics are widely used in these industries, however their performance is relatively poor they and require constant replacement (Rojan 2002). α -Sialon not only has lower density than these

two materials (3.2 gcm^{-3} , compared to 7.8 and 3.9 gcm^{-3} for steel and alumina, respectively), it has high hardness, wear resistance, and chemical durability. Consequently, if the cost barrier can be overcome, an inexpensive α -sialon may be a viable alternative in large-scale, relatively low technology industrial applications. This thesis will show that the development of such a material is indeed possible.

1.3 Scope and Structure of the Thesis

This thesis is concerned with developing the CRN technology for producing α -sialon ceramics from slag and clay mixtures. Being the first such examination into this particular system, rather than focusing solely on the details of the reaction chemistry, a wide range of features have been investigated to evaluate the feasibility of using this technology to produce useful industrial components. Such a wide scope of investigation prevents a full examination of every possible process parameter or property, and limits the detail in which these features can be investigated. Therefore, selective attention has been paid to the essential features governing this process and the quality of the final product, to provide a thorough overview of the potential of this technology.

The investigation can be divided into three main areas: 1) details of the CRN reaction mechanism and effect of various composition and process parameters on the final product; 2) the high-temperature stability and densification ability of the CRN powder; and 3) evaluation of the physical and mechanical properties of components densified from the CRN powder. The structure of the thesis is as follows:

Chapter Two presents a survey of the literature relevant to the issues to be investigated in this study, relating to the features and properties of α -sialons, and previous work on the CRN process of sialon formation.

Chapter Three outlines the experimental conditions used in this investigation for the firing and analysis of the samples.

Chapter Four is the first of four results chapters, and investigates the CRN reaction process across a range of slag+clay mixtures. The intermediate phase formation is studied to provide insight into the reaction mechanisms occurring during CRN.

Chapter Five investigates the effect of changing the starting composition on the products of CRN.

Chapter Six details the effects of various processing parameters on the CRN reactions of the most successful compositions found in the previous chapters. The main processing parameters investigated are powder packing density, gas flowrate, seeding, and the effect of elevated temperatures on the thermal stability of the CRN product phases.

A study of the mechanical properties such as hardness, fracture toughness and erosion resistance is presented in Chapter Seven, to evaluate the potential of the CRN- α' as a useful engineering material.

Chapter Eight is a summary of the major findings from this investigation, and will provide some suggestions for further work.

Chapter Two

Literature Review

This chapter presents a selective review of the literature to establish the extent of current knowledge regarding the carbothermal reduction-nitridation (CRN) process, particularly as it applies to α -sialon formation. Firstly, an overview of the structure, properties and applications of the target α -sialon material is given in Section 2.1. Section 2.2 presents a discussion of the fundamental carbothermal reduction-nitridation process as used to fabricate α - Si_3N_4 from SiO_2 and β -sialon materials from clays. This is followed by details of α -sialon production via carbothermal reduction-nitridation in Section 2.3. The final Section 2.4 is a brief description of the preliminary study into α' production from slag.

2.1 Silicon Nitride and Sialon Ceramics

The sialons (often referred to as SiAlONs) were discovered in the early 1970s independently by both Jack and Oyama (Jack 1976). It was known in the silicate minerals that similar sized AlO_4^{5-} tetrahedra could replace SiO_4^{4-} tetrahedra in the crystalline network, provided that the extra negative charge in AlO_4^{5-} could be balanced somewhere else in the structure. It was postulated that a similar process could occur in Si_3N_4 , and that new phases could be formed by reacting nitride and oxide powders such as Si_3N_4 , Al_2O_3 , AlN , and LiSi_2N_3 at elevated temperatures. The first sialon phase discovered was formed by hot-pressing Si_3N_4 with Al_2O_3 at 1700°C and identification via x-ray diffraction (XRD) showed it to be a Si-Al-O-N solid solution isostructural to the β -form of Si_3N_4 , hence it was designated β -sialon (β'). Other sialon phases were soon discovered, including: α -sialon (α') based on the α - Si_3N_4 structure; O-sialon based on silicon oxynitride ($\text{Si}_2\text{N}_2\text{O}$); X-phase ($\text{Si}_3\text{Al}_6\text{O}_{12}\text{N}_2$); and a variety of polytypoids based on AlN , but with various levels of Si and O incorporation (Hampshire 1994).

Since the α - and β -sialons are solid solutions of Si_3N_4 , many of their structural and behavioural features are directly related to the parent Si_3N_4 polytypoids from which they are derived. A description of the crystal chemistry of these materials is presented in the following section. Features specific to Ca- α -sialon, which is the target material of the current investigation, will be emphasised in this discussion. O-Sialon and X-phase are outside the scope of the present work and will not be discussed here.

2.1.1 Crystal Chemistry of Silicon Nitride and Sialons

2.1.1.1 Si_3N_4

Silicon nitride (Si_3N_4) has a hexagonal crystal structure comprising of SiN_4 tetrahedra sharing corners to form a 3-dimensional network. The slightly distorted SiN_4 tetrahedra form 'puckered rings' of alternating Si and N atoms at fractional heights of $z=0.25$ and 0.75 as shown in Figure 2.1a, which can be considered to be a 2-layer AB unit (Hampshire 1994). $\beta\text{-Si}_3\text{N}_4$ is formed when multiple unit cells are stacked on top of each other in an ABAB stacking sequence, forming long continuous channels along the c -axis (Figure 2.1b). $\alpha\text{-Si}_3\text{N}_4$ has a 4-layer ABCD stacking sequence, where the CD layers are the same AB layers as in $\beta\text{-Si}_3\text{N}_4$ but rotated through 180° , as shown in Figure 2.2. This results in a closing off of the long channels found in $\beta\text{-Si}_3\text{N}_4$, creating two large interstices or 'cages' centred at $1/3, 2/3, 3/8$, and $2/3, 1/3, 7/8$ in the lattice (Figure 2.2b).

2.1.1.2 β -Sialon

β -Sialon is structurally based on $\beta\text{-Si}_3\text{N}_4$, but differs chemically via alloying with Al and O in an equimolar ratio; i.e. $z[\text{Si-N}]^+$ bonds are replaced by $z[\text{Al-O}]^+$ bonds. Both Al^{3+} and O^{2-} are one charge lower than the Si^{4+} and N^{3-} ions they replace, hence overall charge neutrality is preserved. β -Sialon compositions can be represented by Equation 2.1, where the substitution limit of $z \leq 4.2$ has been determined experimentally (Jack 1976).



The slightly longer bond length of the Al-O bond (1.77\AA) compared to Si-N (1.76\AA) (Hyde, Thompson, *et al.* 1994) enlarges the β -sialon unit cell, which allows for differentiation from $\beta\text{-Si}_3\text{N}_4$ by producing detectable shifts in the β -sialon XRD peaks towards lower 2θ values, as well as changing the relative intensities of the peaks. For very small values of z , these changes may be small and difficult to detect.

Morphologically, $\beta\text{-Si}_3\text{N}_4$ and β -sialon form as acicular grains elongated along the c -axis. Aspect ratios for β -sialon are often in the range of 4 to 7, imparting a relatively high fracture toughness to β -sialon materials, which are found to have the highest fracture toughness of all the sialon phases investigated (Ekstrom and Nygren 1992).

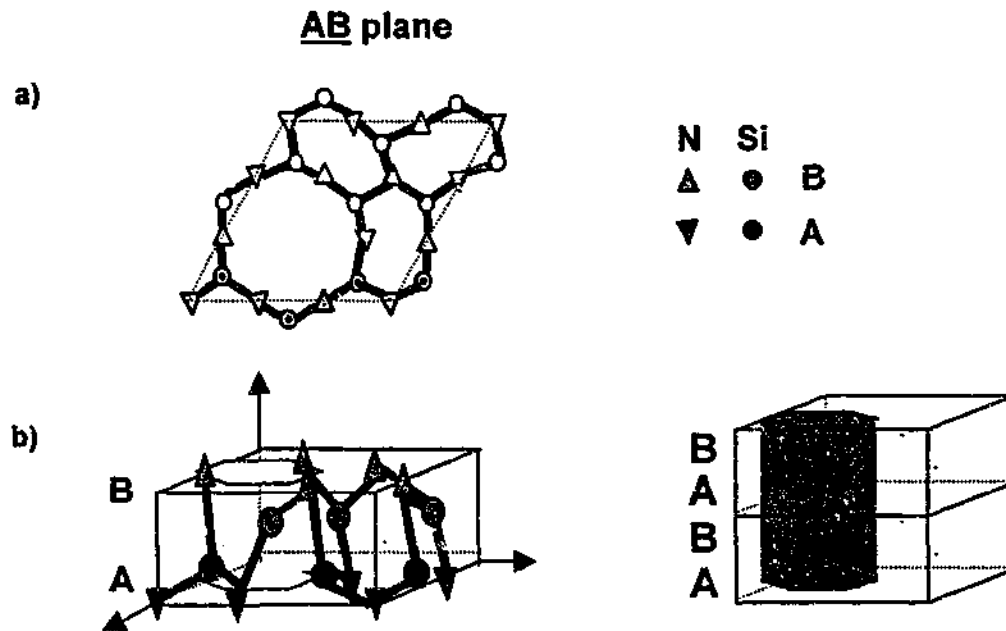


Figure 2.1 Schematic representation of β - Si_3N_4 structure: (a) the (001) projection of the idealised planar SiN_4 network, (b) side view showing AB stacking and formation of hexagonal channels.

2.1.1.3 α -Sialon

Structurally based on α - Si_3N_4 , α -sialon contains an extra substitution of $m[\text{Al-N}]$ bonds for $m[\text{Si-N}]^+$ in addition to the $n[\text{Al-O}]^+$ for $n[\text{Si-N}]^+$ substitutions that occur in β -sialon. This extra substitution of Al^{3+} for Si^{4+} results in a net negative charge, which must be compensated by the addition of metal cations to the system, which are known as 'stabilising cations'. The two interstices provide convenient locations for these cations to be incorporated into the α -sialon structure. The formula representing α -sialon compositions is given in Equation 2.2.

$$M_x \text{Si}_{12-(m+n)} \text{Al}_{m+n} \text{O}_n \text{N}_{16-n} \quad x = m / \text{valency of } M^{n+} \text{ cation} \quad [2.2]$$

The size of the interstices limits the elements able to be used as stabilisers, and the amount of stabilising additive incorporated into the structure will depend on its valency (Izhevskiy, Genova, *et al.* 2000). The most frequently used cations include Y^{3+} , the rare earths (RE) Sm^{3+} , Nd^{3+} , Dy^{3+} , and Yb^{3+} , the alkaline earth metals Ca^{2+} and Mg^{2+} , and Li^+ . The largest RE cation able to enter the α' structure alone is Nd^{3+} , though larger cations such as Ce^{3+} and La^{3+} can be partially incorporated via quenching and/or in combination with smaller cations such as Ca^{2+} and Yb^{3+} , thus forming multi-cation stabilised α -sialons (Mandal and Hoffmann 1999).

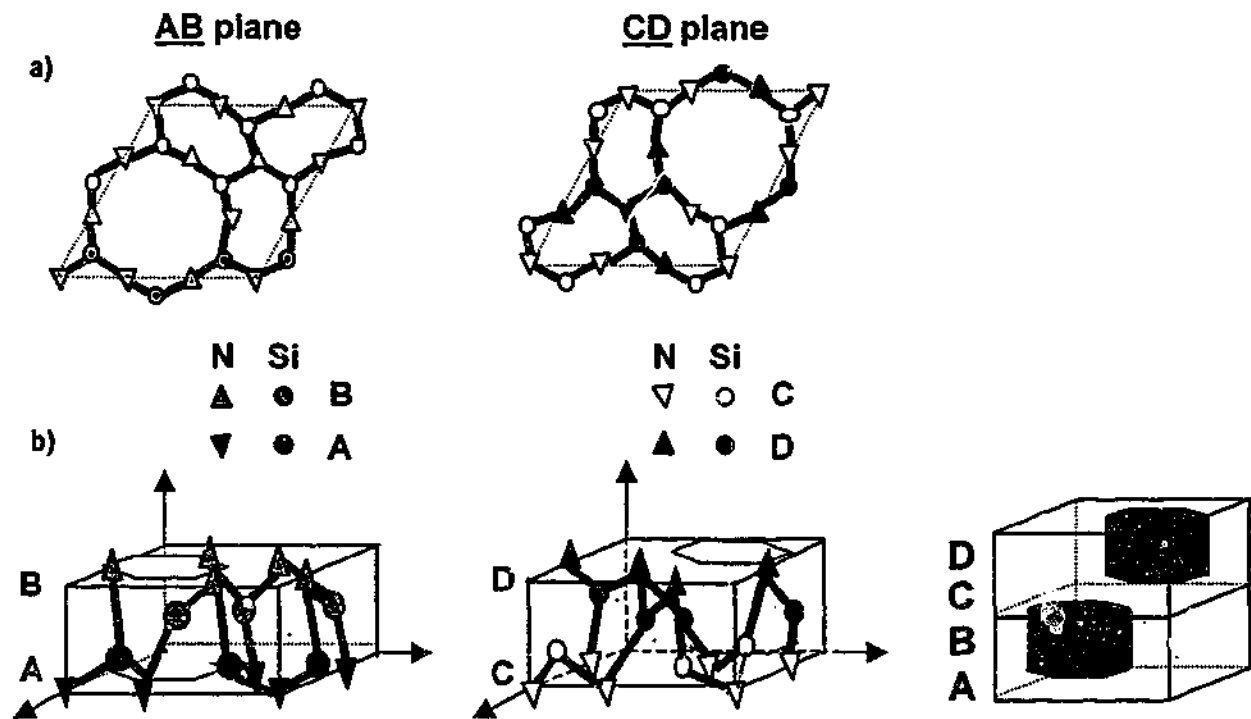


Figure 2.2 Schematic representation of α - Si_3N_4 structure: (a) (001) projection of the idealised AB and CD planes, (b) side view showing the ABCD stacking sequence and formation of interstices.

Compared to the Y- α' and RE- α' materials, the divalent nature of Ca^{2+} allows more of the calcium added to the system to be incorporated into the α' structure. The highest reported m -value is 3.66 ($x=1.83 \text{ Ca}^{2+}/\text{unit-cell}$), which was obtained by using Ca_3N_2 as a Ca source (Jack 1983), however a maximum of only $m=2.8$ ($x=1.4 \text{ Ca}^{2+}/\text{unit-cell}$) has been observed elsewhere, where CaO is used as the Ca source (Huang, Sun, *et al.* 1985). This is much higher than for other cations, where a maximum of $m=1.0$ is reported for the smallest RE cation Yb^{3+} (Wang, Zhang, *et al.* 1999a), and allows 'cleaning' of the grain boundary glass by removing glass-forming Ca^{2+} from the liquid phase. A value of $m=0.6$ ($x=0.3 \text{ Ca}^{2+}/\text{unit cell}$) corresponds to the minimum Ca content required for α' formation, which indicates that a miscibility gap exists between α - Si_3N_4 and α -sialon (Wang, Zhang, *et al.* 1999a).

As with α - Si_3N_4 , α -sialon generally forms with an equiaxed morphology (Wang, Cheng, *et al.* 1996). This gives α -sialon products lower toughness than elongated β -sialon, however the 4-layer stacking sequence increases the Burgers vector in the a -direction, imparting a higher hardness to the α' phase (Cao and Metselaar 1991).

2.1.1.4 Representation of α -Sialons on Behaviour Diagrams

The sialon behaviour diagram is a useful way to plot sialon compositions, and can be used much like a phase diagram in graphically plotting phase boundaries at specific temperatures.

For compositions in the 4-component Si-Al-O-N system, a 2-dimensional behaviour diagram is shown in Figure 2.3a. Assuming all the elements maintain fixed valencies and ignoring gas phase interactions, any sialon compound can be represented by only two variables, ie. Al- and O- content, and these are plotted on perpendicular axes using Si_3N_4 as the origin. The unit of concentration is not mol% or wt%, but 'equivalent concentration' or 'eq%', a unit that accounts for the cation and anion substitutions in $\text{Si}^{4+}/\text{Al}^{3+}$ and $\text{N}^{3-}/\text{O}^{2-}$ pairs. The total valencies of the end points Si_3N_4 , Al_2O_3 , SiO_2 and AlN are scaled up such that each corner of the square has a total of 12+ and 12- valencies (Jack 1978). The β -sialon phase field extends along a narrow compositional range, from the Si_3N_4 corner along a line of constant cation:anion ratio of 3:4, corresponding to the 1:1 substitution of Al and O atoms into Si_3N_4 . The limit of this substitution is at the maximum z-value of 4.2.

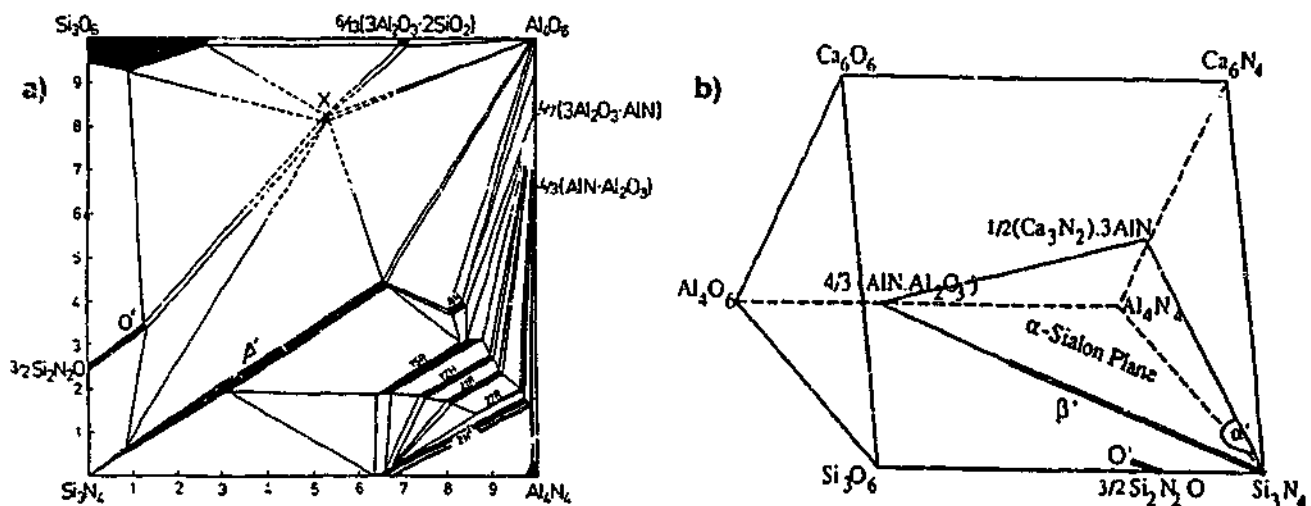


Figure 2.3 (a) Si-Al-O-N behaviour diagram (after Jack 1978), (b) Janecke prism construction for the Ca-Al-Si-O-N system (after Hewett, Cheng, *et al.* 1988).

In the case of α -sialon the additional metal component requires representation via a 3-dimensional construction known as the Janecke prism; the 4-component Si-Al-O-N behaviour diagram (Figure 2.3a) forms the base of a triangular prism with all sides of equal length, and the additional metal component is the top edge (Figure 2.3b). The triangular M-Si-Al-O end is the ternary oxide phase diagram expressed in equivalent concentration, with the other end representing the fully nitrated M-Si-Al-N phases. Partially nitrated oxynitride phases are located within the prism, and lie in a region of compatibility defined by a maximum of four phases which form the corners of a tetrahedron.

It should be noted that these are not technically phase diagrams because they do not represent true thermodynamic equilibrium; it is not kinetically possible to completely remove the intermediate liquid phase which forms the grain boundary glass, and any gas phases and minor impurity phases are ignored (Cao and Metselaar 1991). Hence these are usually referred to as sialon 'behaviour diagrams'.

The α -sialon plane or ' α '-plane' as indicated in Figure 2.3b is presented in detail for the Ca-Si-Al-O-N system in Figure 2.4. It has corners at $4/3(\text{AlN}\cdot\text{Al}_2\text{O}_3)$, $1/2(\text{Ca}_3\text{N}_2)\cdot 3\text{AlN}$ and Si_3N_4 , and shares a bottom edge with the β' phase field. The metal to non-metal atomic ratio on this plane is always 3:4. The single-phase α' field is contained in this two-dimensional plane near the Si_3N_4 corner. The size of the single-phase α' region is largest for the Ca- α' system due to the high solubility of Ca^{2+} , and decreases with temperature (Izhevskiy, Genova, *et al.* 2000).

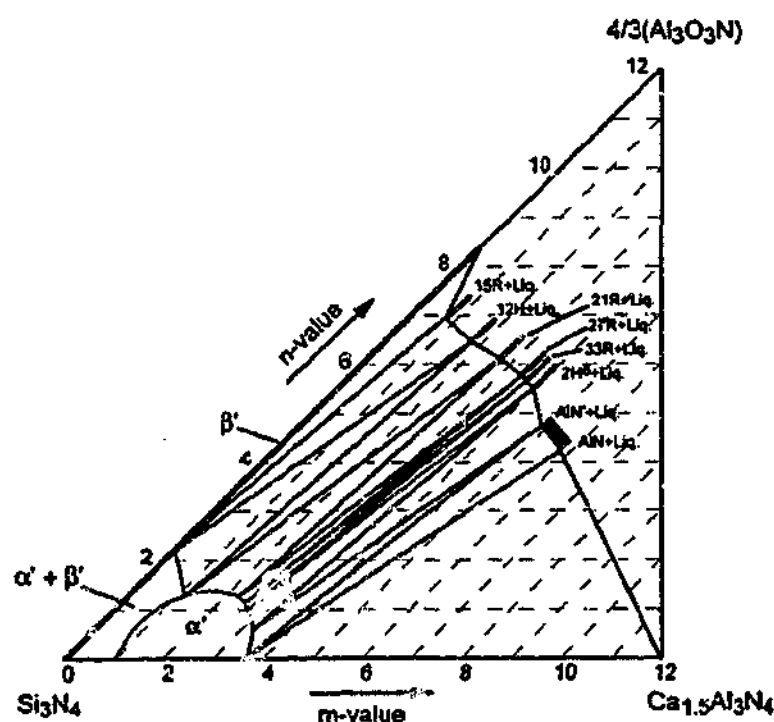


Figure 2.4 Ca- α -plane (after Wood and Cheng 2000).

At low Ca-contents outside of the single-phase region, α' is in equilibrium with β' , and at high Ca-contents α' is found together with various AlN-based polytypoid phases and large amounts of glass. At sintering temperatures, AlN and the AlN-polytypoids coexist with α' along with substantial quantities of liquid phase, thus the AlN-based regions on the α' -plane (Figure 2.4) are the intersections of the polytypoid-liquid tie-lines with this plane. The residual glass is not contained within this plane but is located at the oxide end of the Jancke prism. The

substitution of 17-25 eq% of N for O extends the glass phase field some way into the prism, however the exact shape of the glass field depends greatly on composition (Hampshire 1994).

2.1.1.5 AlN and AlN-Polytypoids

AlN-polytypoid phases, sometimes called 'sialon polytypoids', are AlN defect structures that arise from the incorporation of Si and O into the hexagonal AlN wurtzite unit cell. Each of the polytypoids has a fixed metal (M) to non-metal (X) ratio of the form M_nX_{m+1} where $4 \leq n \leq 11$ (Sorrell 1983). The structures are built up along the *c*-axis from AB and ABC stacking sequences of MX layers, interspersed periodically with MX_2 layers to accommodate the stoichiometry (Wang, Sun, *et al.* 1999). The polytypoids are usually described using Ramsdell notation, which uses numerals to indicate the number of planes in the stacking sequence, and either H or R to signify a hexagonal or rhombohedral unit cell, respectively.

Six AlN-polytypoids are located between AlN and β' as shown in Figure 2.4, with the M/X ratio decreasing from 1/1 to 4/5. The $2H^\delta$ polytypoid is a disordered 2H-AlN structure where the concentration of additional non-metal atoms is too small to create an ordered structure, and has an M/X ratio $>9/10$ but $<1/1$ (Sorrell 1983). Work by Wood and Cheng (2000) on high-Ca-containing α -sialon compositions recently identified a small extent of solid solution of Si and O within the AlN-2H structure, but less than the amount required to form the $2H^\delta$ polytypoid. This solid solution has been designated AlN', and retains the same hexagonal structure and has almost identical lattice parameters as AlN, thus is indistinguishable from AlN using XRD. AlN and AlN' grains in high-glass Ca- α -sialon based compositions were found to have a distinct, elliptical morphology (Wood and Cheng 2000). Mg-containing polytypoid phases have been identified in the Mg-Al-Si-O-N system, however no equivalent Ca-containing polytypoids have been detected in the Ca-Al-Si-O-N system (Thompson 1989).

The polytypoids are structurally and chemically distinct from AlN or AlN', and form elongated fibres or plate-like grains (Wang, Jia, *et al.* 1999). Al-N based ceramics have poorer mechanical properties when compared to Si-N based materials, however AlN has found wide application as a heat-dissipating substrate and packaging material in microelectronics, due to its high thermal conductivity (Rafaniello 1997). The poor mechanical properties and difficulty in controlling polytypoid formation has meant that little attention has been paid to developing these materials for structural applications, however, the fibrous nature of the polytypoid phases appears to produce materials with high flexure strength at elevated temperatures (Wang, Sun, *et al.* 1999).

2.1.2 Production of α -Sialon – Reaction Sintering

The CRN process developed in the current work is an alternative to reaction sintering, which is the process initially used to produce the sialon phases and which remains the most widely used technique for α -sialon production. The main features of this process are briefly outlined in this section.

The reactants for reaction sintering are commonly α - Si_3N_4 , AlN, SiO_2 and/or Al_2O_3 to adjust the oxygen content, and the relevant metal oxide. The nitride powders contain an oxide layer on the surface, which is usually taken into account when designing sialon compositions (Cao and Metselaar 1991). Sintering is performed in an inert atmosphere to avoid oxidation at the sintering temperature, which is usually in the range of 1600-1800°C to achieve the highest possible density and ensure maximum conversion of silicon nitride to sialon. Densification occurs via a eutectic liquid phase formed from reactions between the metal oxide additive and the SiO_2 and Al_2O_3 oxide layers present on the nitride particles. The liquid phase allows for the dissolution of Si_3N_4 into the liquid and the subsequent precipitation of Si-Al-O-N phases from this liquid. The reaction-sintering process can be divided into three overlapping stages (van Rutten, Hintzen, *et al.* 1996):

- 1) primary particle rearrangement, brought about by the formation of the liquid phase whereby capillary forces cause solid particles to slide over each other;
- 2) a solution-precipitation process if the solid particles have sufficient solubility in the liquid (reaction);
- 3) grain growth, coalescence and closed-pore elimination (sintering).

The resultant product is a densified solid body, either single- or multi-phase sialon depending on the starting composition and firing conditions used. The volume of liquid produced during sintering may be too large and too viscous to be absorbed into the α' structure, thus any excess liquid will remain in the system and form a grain boundary glass on cooling. Glass generally has detrimental effect on bulk material properties, especially at temperatures above the glass softening temperature of 900-1100°C (Izhevskiy, Genova, *et al.* 2000).

The demanding performance requirements of engineering ceramics such as α -sialon requires very good control over the final chemical composition and microstructure of the sintered product. This in turn requires high quality starting powders with very high purity, fine size ($\sim < 1\mu\text{m}$), and narrow size distribution, (Rahaman 2003). There are three main methods used

for commercial Si_3N_4 powder synthesis: 1) direct nitridation of Si metal, 2) carbothermal reduction-nitridation of SiO_2 by carbon at 1400-1500°C, 3) decomposition of SiCl_4 gas in ammonia at 1200-1500°C (Komeya 1994). The Si_3N_4 powder formed from these methods varies in purity, particle size, and α/β content, but is generally 99.7 to >99.98% pure and sub-micron in size. The reactants for Si_3N_4 production, such as Si metal, are relatively expensive and involve many stages of refining and high-energy processes such as extractive metallurgy to produce them, which substantially contributes to the cost of α -sialon materials. A recent advance is the production of nanometre scale Si_3N_4 powders using laser heating of SiH_4 or SiCl_4 gases (Rahaman 2003), however this is currently an expensive process that has not yet seen industrial application.

Further details regarding the CRN formation of Si_3N_4 powders from SiO_2 are given in Section 2.2.

2.1.3 Properties and Applications of Ca- α -Sialons

2.1.3.1 Hardness and Fracture Toughness

The defining characteristic of α -sialon is its high hardness, which is often above 15 GPa and as high as 22 GPa in some systems (Ekstrom 1996). This is comparable to alumina, the most widely used ceramic material, and is higher than hot isostatically pressed Si_3N_4 (Mandal and Hoffmann 2000). Although alumina generally has higher room temperature hardness, α -sialons better retain their hardness and strength at high temperatures, experiencing only a 30% decrease in strength at 1000°C compared to 75% for alumina (Hampshire 1994). However, wide scatter in mechanical property data is reported for the α -sialons due to the different microstructure formed, especially the amount of grain boundary glass (Cao and Metselaar 1991). Typically, Ca- α -sialon materials have hardness values ranging from 15.5-19.75 GPa, depending on the amount and type of secondary phases present such as β' , AlN-polytypoids and glass (Wang, Zhang, *et al.* 1999a).

The fracture toughness (K_{1C}) of non-toughened ceramic materials is generally 3-5 $\text{MPam}^{3/2}$ (Kingery, Bowen, *et al.* 1976), and Ca- α -sialon materials with equiaxed microstructures have a reported toughness in the range of 4.4-5.1 (Wang, Zhang, *et al.* 1999a). This is lower than that of β -sialon, which has a fracture toughness as high as 7.7 $\text{MPam}^{3/2}$ due to the presence of in-situ toughening mechanisms such as crack deflection, crack bridging, and grain pullout arising from the elongated β' grain morphology (Cothier 1987). To improve the fracture toughness of monolithic α' materials, elongated α' grain growth has recently been promoted by seeding

with elongated β - Si_3N_4 , or specially prepared Y- α' seeds (Zenotchkine, Shuba, *et al.* 2002); or by controlling sintering parameters such as soak time, and using high-temperature (1800-1900°C) post-sintering heat-treatments without seeding (Chen, Sun, *et al.* 2002). In the Ca- α' system, elongated grains were easily formed during pressureless sintering of AlN- and Al_2O_3 -rich compositions (ie. high m- and n-value), which produce large quantities of liquid at the sintering temperature (Wood, Zhao, *et al.* 1998). This produces self-reinforced materials with significant improvements to fracture toughness previously only seen in hot-pressed systems, giving a K_{IC} greater than 6 $\text{MPam}^{1/2}$ (Wood, Zhao, *et al.* 1998). Similar results have also been observed in the Y- α' system (Kurama, Herrmann, *et al.* 2002).

2.1.3.2 High-Temperature Stability

The α' phases of the rare earth (RE)-sialons, although stable at high temperatures, are unstable and transform to β' and RE-containing melilite or similar phases in the relatively low temperature range of 1300-1600°C (Mandal 1999). Decreasing α' stability is associated with decreasing solubility of the cation in the α' phase, which is in turn related to increasing ionic radius, thus the larger RE cations such as Nd and Sm produce the least stable α' phases (Mandal and Hoffmann 1999). Above 1600°C the β' can back-transform to α' , which shows that the $\alpha' \rightarrow \beta'$ transformation is fully reversible, and depends on temperature and compositional factors such as the amount of grain boundary glass and the presence of β -sialon nucleation sites (Rosenflanz 1999). The $\alpha' \rightarrow \beta'$ transformation has not been observed in Ca- α' -sialons, even after heat-treatment for over 200 hours at 1450°C, indicating that Ca is the most stable α' stabiliser found thus far (Hewett, Cheng, *et al.* 1998). In fact adding a more soluble and stable cation such as Yb^{3+} or Ca^{2+} to less stable RE- α' systems can significantly improve their overall thermal stability. Sm- α' is one of the least stable α' systems and transforms to β' within a few hours at 1450°C, but the addition of 5 wt% Ca into Sm- α' can prevent the $\alpha' \rightarrow \beta'$ transformation from occurring (Seeber and Cheng 2003).

2.1.3.3 Solid Particle Erosion Resistance

The erosion and fracture of brittle materials encompasses a vast field of research, hence only a cursory description of the literature directly relevant to the current investigation is presented here. Studies of the erosion resistance of engineering ceramics have largely been focused on the two most widely used wear materials, alumina (Al_2O_3) and SiC. These materials have considerable microstructural complexity, and no common model has been able to account for the effects of factors such as grain size, impurities, and porosity (Zhang, Cheng, *et al.* 2000). Little work has been performed on the erosion resistance of nitride ceramics, and the only

detailed study of monolithic α -sialon materials was performed by Zhang (Zhang 2002). In this study, the effects of various material and microstructural factors were investigated, including material density, hardness and fracture toughness, grain boundary phases and grain morphology. Contrary to the theoretical models, no simple relationship between fracture toughness or hardness and erosion resistance was found, with microstructural factors strongly influencing erosion behaviour.

Ca- α' materials with a fine, equiaxed grain morphology experienced grain ejection as the major material removal mechanism, whereas the interlocking, elongated grains produced in high m- and n-value compositions experienced combined transgranular and intergranular fracture. It was discovered that an optimum amount of grain boundary glass may improve the erosion resistance by providing a stress cushioning effect. An excessive amount of soft grain boundary glass was detrimental to the erosion resistance, but removal of the glass via devitrification also lowered the erosion resistance, with all heat-treated samples performing worse than the non-heat-treated counterparts. The glass can help to cushion the stresses due to it having similar composition to the α' grains, thus producing good bonding between grains. Devitrification of the glass caused the formation of stresses due to thermal mismatch, weakening the bonding between grains, and thus reducing the cushioning effect.

It was found that the erosion resistance of Ca- α' to a softer erodent was very high. Garnet has a lower hardness (13.8 GPa) than the target α' materials, and undergoes severe deformation and fragmentation when impinging on the target surface, resulting in less energy being transferred to the target and thus low erosion efficiency. When using harder SiC erodent (30.4 GPa) very high rates of material removal were observed. Examination of the effect of impact angle (θ) showed that the erosion rate increased monotonically with θ , with the maximum erosion rate experienced at 90° . This is due to an increase in the normal component of impact velocity ($v \cdot \sin\theta$) with increasing θ .

Figure 2.5 is a graph of the erosion rates of two in-house prepared Ca- α -sialons (CA2613) tested against a range of commercially produced ceramics. The steady-state erosion rate is defined as the linear region of the cumulative volume curve plotted against the mass of erodent, which in this case was SiC impacting at 90° . The CA2613 material had a design composition of $m=2.6$, $n=1.3$, and was the most wear resistant of the Ca- α' materials investigated in Zhang's study. CA2613 was formed by pressureless sintering alone, and CA2613C was produced via pressureless sintering followed by hot-pressing to improve the density.

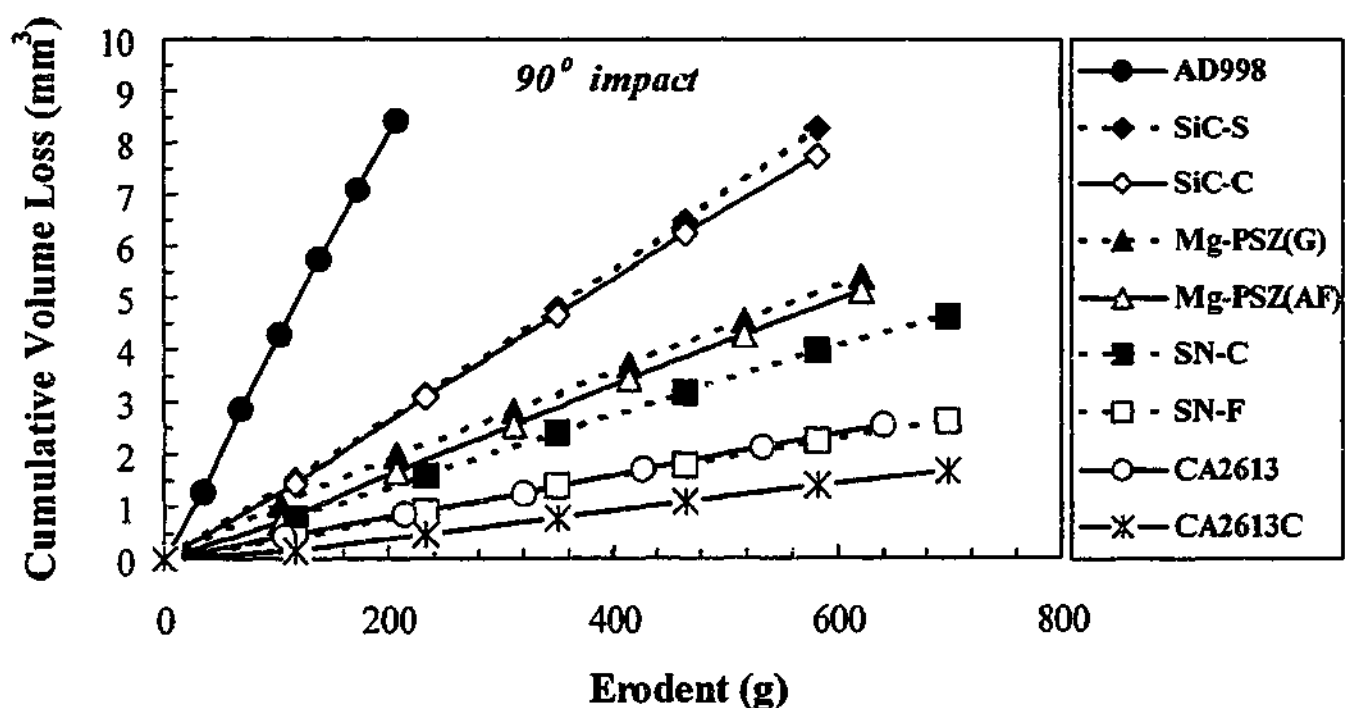


Figure 2.5 Cumulative volume loss of various target ceramics as a function of the amount of SiC erodent impinging on the surface at 90° incidence angle (after Zhang 2002).

Key: AD998 = 99.8% high purity alumina, SiC-S & SiC-C = siliconised silicon carbide from two different suppliers, Mg-PSZ = Mg-partially stabilised zirconia (G=ground surface, AF=as-fired surface), SN = silicon nitride (C=with β - Si_3N_4 seeds, F = without seeds), CA2613 = pressureless sintered Ca- α -sialon, CA2613C = hot-pressed Ca- α -sialon.

It is clear that the Ca- α' materials possess extremely good wear resistance, with the wear rate of the hot-pressed Ca- α' being the lowest of all materials tested. Only the gas-pressure sintered SN-F material, which incorporated 5 wt% β - Si_3N_4 seeds to promote an elongated microstructure, displayed a similarly low wear rate. Decreasing wear resistance was found for the Mg-PSZ ceramics, followed by the siliconised silicon carbides, and the alumina material displayed the worst resistance to erosion. This result clearly demonstrates the potential for Ca- α -sialons to be used as wear resistant materials.

2.1.3.4 Applications of α -Sialons

Single-phase α -sialon materials have not found widespread use in industry. This is mainly due to their low fracture toughness, which can be improved through the formation of a two-phase α/β -sialon material. One of the first successful applications of sialons was as lathe tool inserts for metal cutting. Conditions at the tool tip are severe; temperatures can exceed 1200°C , fluctuate by several hundred degrees, and experience large stresses and thermal gradients (Brandt 1991). Inserts that combine the chemical inertness, hardness and thermal shock resistance of α' with the toughness of β' produced significant performance improvements

over conventional cemented carbide tools, especially for cutting non-ferrous alloys such as Ni-based superalloys and copper-based alloys; α/β -sialons allow higher cutting speeds and depth of cut, and have a significantly longer tool life (Cothier 1987). Sialons can generally not be used for iron-based alloys due to chemical instability.

Metal-working components such as cold drawing dies and extrusion die inserts are being made from sialons for non-ferrous applications (Katz 1993). The non-wetting nature of the sialon-metal interface results in lower friction and higher wear resistance than in traditionally used specialty steel dies, and for copper extrusion improvements in the extrusion speed, surface finish and dimensional tolerances have been reported, with some dies exceeding 30 times the lifetime of traditional materials (Cothier 1987).

Wear parts may provide a huge potential market for sialons, especially α -sialons. According to Ekstrom, ceramic materials held only a 2% share of the USD\$ 6000 million/year market, with most of that share being filled by alumina and silicon carbide (Ekstrom 1993). As discussed previously in Section 2.1.3.3, the tests by Zhang (2002) clearly demonstrated that Ca- α' materials possessed equal or greater wear resistance than these materials, and the lower density of ~ 3.2 g/cm³ vs 3.9 g/cm³ for alumina may be advantageous in lowering the weight of α' components. However, for commercial viability the cost of α -sialons must be reduced; the cost of alumina and SiC powders are $\sim 1/10$ and $1/4$ the cost of conventional Si₃N₄ powder, respectively.

Slag-based α' have also shown excellent resistance to attack by molten slags. A preliminary investigation into the erosion/corrosion resistance of a slag-based α' material produced via self-propagating high-temperature synthesis (SHS – to be discussed in Section 2.4.2) produced very promising results. A tile hot-pressed from this SHS- α' powder at 1750°C for 1 hour was fixed on a steel plate and eroded by 300,000 tons of molten slag flowing perpendicular to the ceramic for over 2 months. It experienced almost no detectable mass loss and maintained its polished surface, unlike the steel substrate which was substantially eroded (Wang 2002).

2.1.4 Other Phases in the Ca-Al-Si-O-N System

Many different phases exist in the Ca-Al-Si-O-N system, and the phases relevant to the work in this investigation are introduced here.

2.1.4.1 Gehlenite ($\text{Ca}_2\text{Al}_2\text{SiO}_7$)

Gehlenite ($\text{Ca}_2\text{Al}_2\text{SiO}_7$) is the end-point of a continuous range of melilite solid-solutions with akermanite ($\text{Ca}_2\text{MgSi}_2\text{O}_7$) at the other end, formed by complete substitution of Mg^{2+} and Si^{4+} for 2Al^{3+} (Grimshaw 1971). Gehlenite has been detected as an intermediate phase produced during the formation of Ca- α -sialon via reaction sintering. Hewett discovered gehlenite to be present only between 1200-1400°C (Hewett 1998), however van Rutten and co-workers detected gehlenite up to higher temperatures of 1600°C (van Rutten, Hintzen, *et al.* 1996). It was also observed that the calculated cell parameters for the gehlenite detected in the Ca- α -sialon deviated from the expected values, and this was attributed to the formation of a nitrogen-containing solid solution of the form $\text{Ca}_2\text{Al}_{2-x}\text{Si}_{1+x}\text{O}_{7-x}\text{N}_x$ (van Rutten, Hintzen, *et al.* 1996). Similar N-containing melilite phases of the form $(\text{M}_2\text{O}_3 \cdot \text{Si}_3\text{N}_4)$, where M = Y or RE, are often found as grain boundary phases in α -sialon systems (Wang and Werner 1997). Gehlenite is also seen as the main devitrification product of the Ca-Al-Si-O-N glass in this system (Hewett, Cheng, *et al.* 1998).

2.1.4.2 D-, M-, and E- phases

Huang and co-workers identified several new phases in the Si_3N_4 -AlN-CaO system: Z-phase ($3\text{CaO} \cdot \text{Si}_2\text{N}_2\text{O}$), D-phase ($2\text{CaO} \cdot \text{Si}_3\text{N}_4$), M-phase ($2\text{CaO} \cdot \text{Si}_3\text{N}_4 \cdot \text{AlN}$), and E-phase (CaAlSiN_3) (Huang, Sun, *et al.* 1985). The subsolidus phase diagram and isothermal section at 1700°C are presented in Figure 2.6.

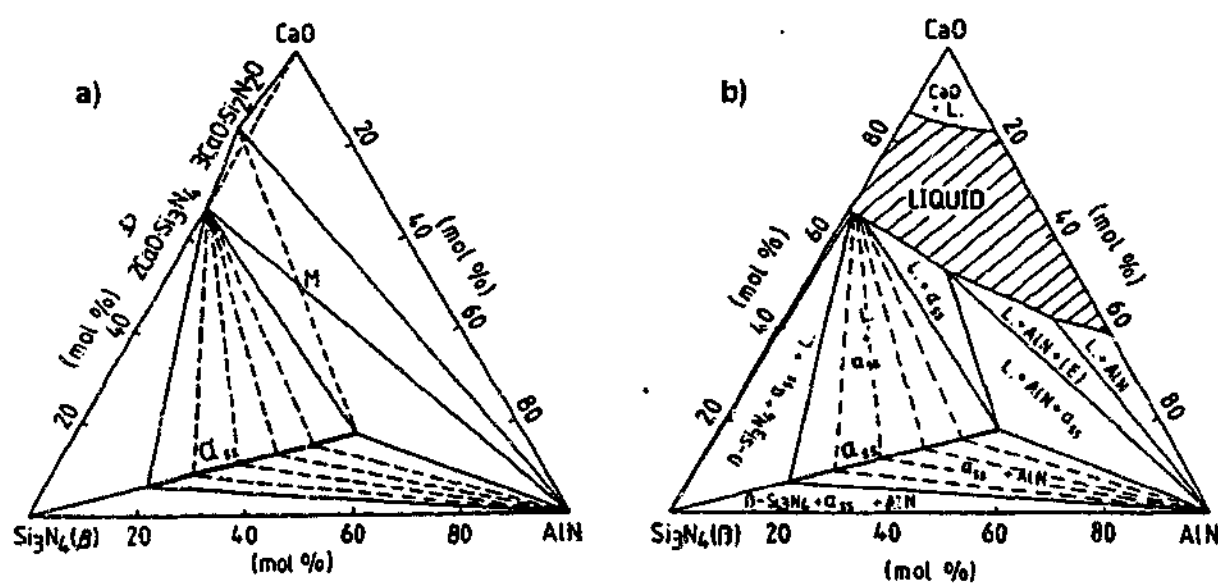


Figure 2.6 Phase relations in the Si_3N_4 -AlN-CaO system: (a) subsolidus diagram, (b) isothermal section at 1700°C (after Huang, Sun, *et al.* 1985).

D-phase ($2\text{CaO}\cdot\text{Si}_3\text{N}_4$) was formed from compositions hot-pressed in the binary $\text{CaO}\text{-Si}_3\text{N}_4$ system above 1400°C , usually accompanied by some Z-phase ($3\text{CaO}\cdot\text{Si}_2\text{N}_2\text{O}$). A single-phase product was difficult to obtain, with a nearly single-phase product formed at 1650°C . The morphology of D-phase as shown in the paper appears to be that of roughly square plates, but no indication of size was given. The XRD peak positions for this phase have been listed, but the crystal structure has not been determined and no further reports of this phase appear in the literature. The subsolidus diagram in Figure 2.6a shows that a binary phase compatibility region exists between D-phase and the full range of α -sialon solid solutions.

M-phase ($2\text{CaO}\cdot\text{Si}_3\text{N}_4\cdot\text{AlN}$) was discovered to be a metastable phase produced only in the composition $2\text{CaO}:\text{Si}_3\text{N}_4:\text{AlN}$. A mixture of M- and D-phases was formed at 1400°C , with single-phase M-phase found to exist only at 1450°C , above which it decomposed to E-phase (CaAlSiN_3), AlN, and a glass. XRD data for the M-phase was provided, however the crystal structure was not determined.

M-phase has also been detected as an intermediate phase during the reaction sintering of Ca- α -sialons, where a small amount ($<10\%$) was formed at 1200°C as a precursor to gehlenite formation, melting at 1350°C (Hewett 1998).

E-phase (CaAlSiN_3) was not only formed via the decomposition of M-phase, but formed simultaneously with AlN above 1500°C in almost all compositions restricted to the $3\text{CaO}\cdot\text{Si}_2\text{N}_2\text{O}\text{-}2\text{CaO}\cdot\text{Si}_3\text{N}_4\text{-AlN}$ subsystem. E-phase is a fully nitrated phase that does not lie within the plane of the oxynitride diagram given in Figure 2.6, and was identified as having an orthorhombic crystal structure with space group $\text{Cmc}2_1$. The XRD peak positions were listed but no morphological features were described.

A further investigation of E-phase revealed that there is some ambiguity regarding its composition (Thompson 1989). Microprobe analysis gave a composition closer to 1:1:2 Ca:Al:Si, rather than the 1:1:1 previously reported by Huang and co-workers. The crystal structure of CaAlSiN_3 is the same as MgAlSiN_3 and LiAlSiN_3 , which are ternary nitrides with wurtzite superlattice structures based on AlN. These nitrides have a 1:1 ratio of metal (M) to nonmetal (N) ions, where both M and N are in 4-fold co-ordination. The Ca^{2+} ion is generally considered to be too large to occupy 4-fold co-ordinated sites, and unlike Mg or Li, does not form other wurtzite superlattice nitrides of the form MgSiN_2 . The presence of Ca in the E-phase structure was thought to be a result of possible enlargement of the site by substitutions of Si for Al. Furthermore, it was stated that nitrides with these structures can form a range of

solid-solutions, such as $\text{MSiN}_2 \rightarrow \text{MAISiN}_3 \rightarrow \text{AlN}$, or $\text{MAISiN}_3 \rightarrow \text{Si}_2\text{N}_2\text{O}$, which may further complicate the determination of the E-phase composition.

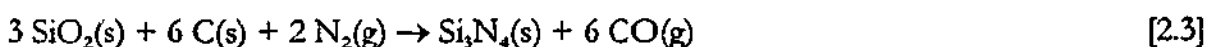
2.2 Carbothermal Reduction-Nitridation (CRN)

Carbothermal reduction alone, without nitridation, is often used to produce various non-oxide ceramics from a variety of oxide-based precursors and carbon sources, often with unique morphologies. Examples include the production of single crystal boron carbide nanowires (Ma and Bando 2002), and ZrC-SiC composite materials (Das, Panneerselvam, *et al.* 2003). If a nitrogen atmosphere is used, nitride ceramics such as TiN, AlN and Si_3N_4 can be produced (Tsukada, Naito, *et al.* 1989). This process, also known as 'carboreduction-nitridation' or 'carbonitriding', was first patented as a method of producing Si_3N_4 from SiO_2 back in 1896, and is now commonly used to economically produce high purity Si_3N_4 powder (Cho and Charles 1991a).

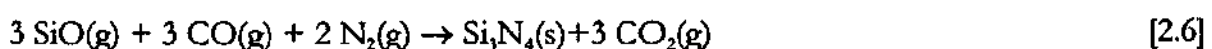
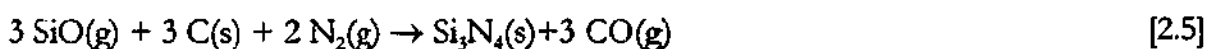
The reaction process that converts SiO_2 to Si_3N_4 during CRN is fundamental to the production of β' from SiO_2 -based minerals via CRN, which in turn provides a basis for understanding the process of α' production. Accordingly, the features of these processes are outlined in this section.

2.2.1 Si_3N_4 Formation via CRN of SiO_2

The overall equation for the CRN of SiO_2 to form Si_3N_4 is given by Equation 2.3 (Weimer, Eisman, *et al.* 1997).



A sequence of reactions occur at the SiO_2 -C interface to produce gaseous SiO (Equation 2.4), which then reacts with nitrogen to produce Si_3N_4 according to Equation 2.5 or 2.6:



The optimum CRN process is one that fully converts the SiO_2 -C mixture to Si_3N_4 with a high α/β ratio and minimal by-products such as SiC. This requires optimising the balance of temperature, carbon content, nitrogen flowrate, and powder characteristics (size, purity and

morphology). Elevating the reaction temperature increases SiO(g) formation, but also increases the likelihood of SiC formation (Cho and Charles 1991a). SiC formation will also be promoted by a high C content, however, since α -Si₃N₄ nucleation occurs at the points of contact between C and SiO₂ particles, Si₃N₄ formation is generally enhanced by a high C/SiO₂ ratio, and ratios of ~4:1 are often used, which is higher than the stoichiometric ratio of 2:1 (Cho and Charles 1991a). CRN can also be promoted by using C sources with a high specific surface area (Weimer 1997). Higher N₂ gas flowrates have been shown to promote Si₃N₄ formation by removing the unwanted CO gases and thus making SiO(g) more stable (Weimer 1997). Seeding the sample with a small amount (≤ 0.2 wt%) of the target α -Si₃N₄ product was shown to both significantly enhance the α/β ratio of the product (from ~75 wt% α to >95 wt%), and refine the particle size to <1 μ m by providing pre-existing sites for α -Si₃N₄ nucleation (Kang, Komeya, *et al.* 1996).

2.2.2 β -Sialon Production Via CRN from Kaolinite

Lee and Cutler first produced β' via CRN, using mixtures of kaolinite clay and carbon-black to avoid the use of the expensive raw materials required for the reaction sintering route (Lee and Cutler 1979). The composition of kaolinite lends itself to the production of a $z=3$ β -sialon without the need for compositional adjustments, hence this is the most intensively studied sialon-forming CRN process and is now used commercially to produce β' components (Fabbri and Dondi 1991).

2.2.2.1 Clay Minerals Used for CRN

Clay is a common term used to encompass various hydrous layered silicates (Brindley and Brown 1984). The basic unit of these minerals is the [SiO₄]⁻⁴ tetrahedron, which can be arranged into 2-dimensional sheets when three of the four oxygen atoms are shared with adjacent tetrahedra. To satisfy bonding requirements, the apical oxygen anion at the top of each tetrahedron may be linked to external cations, or to an apical oxygen of another mineral layer such as the octahedral gibbsite layer, which consists of Al³⁺ ions in 6-fold coordination with O²⁻ ions. Apical oxygen that is not shared between layers will usually link to hydrogen to form a hydroxyl (OH⁻) group. The sheet-like nature of these materials means that the minerals formed are usually plate-like in morphology.

Kaolinite (2SiO₂·Al₂O₃·2H₂O) is the main component of what is commonly termed 'china clay', and is the most important of the clay minerals. Kaolinite is a 1:1 layered mineral where each tetrahedral silicate layer is linked to one octahedral gibbsite layer (Figure 2.7a). Kaolinite is electrically neutral, rarely contains isomorphous substitutions such as Fe for Al, and the

layers are bonded together by relatively weak, long distance hydrogen bonds (Grimshaw 1971). Kaolinitic clays often contain SiO_2 quartz as the main impurity, though mica and feldspar are also common. It finds a very wide range of uses, including as a filler in paper production, and is the main ingredient of porcelain. The phase changes occurring during heating are described in Section 2.2.2.2.

Pyrophyllite is a 2:1 layered mineral, where one octahedral gibbsite layer is sandwiched between two tetrahedral silicate layers (Figure 2.7b). The chemical formula is $4\text{SiO}_2 \cdot \text{Al}_2\text{O}_3 \cdot x\text{H}_2\text{O}$, and it has double the Si content of kaolinite. Like kaolinite, it is electrically neutral and isomorphous substitutions are rare (Grimshaw 1971). The forces binding adjacent layers are thought to be mostly Van der Waals linkages, with a small ionic attraction between layers (Brindley and Brown 1984). Upon heating it dehydroxylises at $\sim 800^\circ\text{C}$ and decomposes above 1100° to form a 'felted mass' of cristobalite and mullite needles. These phase transformations occur with negligible shrinkage, thus pyrophyllite is widely used as a volume stabilising additive in many ceramic products, including electrical porcelains, tile bodies, and refractories (Grimshaw 1971). Both kaolinite and pyrophyllite are used as additions to the slag in the current investigation.

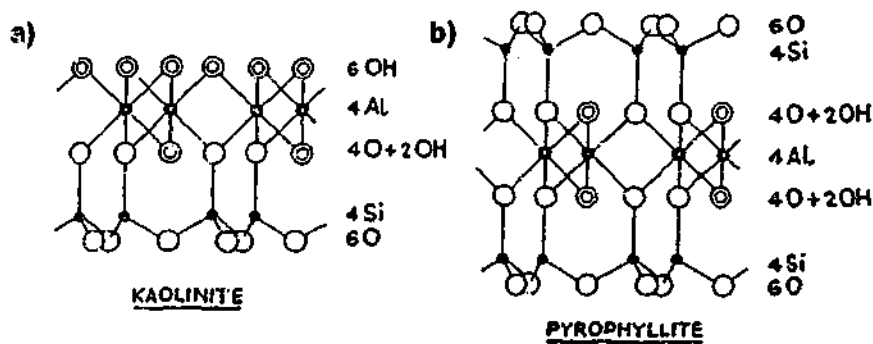
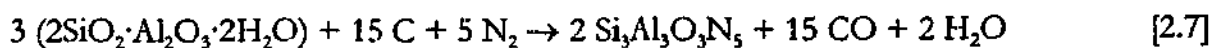


Figure 2.7 The structure of (a) kaolinite, and (b) pyrophyllite (after Grimshaw 1971).

2.2.2.2 Reaction Sequence of CRN

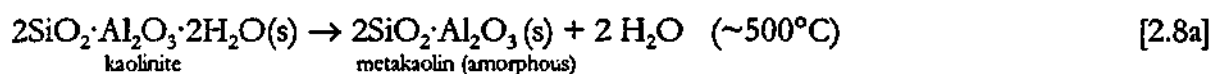
The idealised overall reaction for producing β -sialon ($z=3$) from kaolinite at temperatures around 1400°C is (Higgins and Hendry 1986):



This process was found to occur in several stages (Mazzoni, Aglietti, *et al.* 1992a):

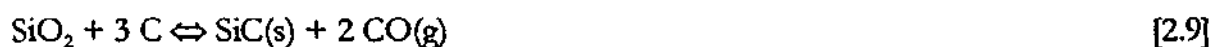
a) *Clay decomposition reactions during heating*

The loss of structural water below 600°C results in a collapse of the kaolinite structure and the formation of amorphous metakaolin, which then decomposes to produce crystalline mullite and amorphous silica at ~1100°C according to reactions 2.8a and b. These decomposition reactions are independent of the furnace atmosphere.



b) *Carbothermal reduction of silica to form SiC at ~1400°C*

The amorphous silica released from decomposition of the kaolinite undergoes carbothermal reduction to form SiC according to Equation 2.9.



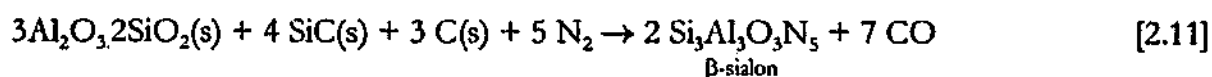
This reaction occurs via an intermediate SiO gas phase, ie:



The extent of CO removal by the flowing gas during this stage of carbothermal reduction was also shown independent of furnace atmosphere (N₂ or Ar), thus nitridation has not yet started (Higgins and Hendry 1986). Mullite does not take part in these SiC-forming reactions, with the concentration remaining constant during this stage of CRN (Mazzoni, Aglietti, *et al.* 1992a).

c) *Nitridation*

In the later stages of CRN, incorporation of nitrogen into the system occurs. At this stage, the mullite reacts with SiC, N₂ from the furnace atmosphere, and a transient liquid phase produced from these reagents to form Si-Al-O-N phases such as X-phase and β' (Thompson and Hendry 1991).



The β' product from CRN tends to be $\sim 1\mu\text{m}$ in size, which is often smaller than the size of the initial mineral reactants (Mazzoni, Aglietti, *et al.* 1993a; Mazzoni and Aglietti 1998).

2.2.2.3 Parameters Affecting CRN

a) Reaction temperature and time

The majority of studies determined the appropriate reaction temperature and time for completion of the CRN reactions by monitoring the CO concentration in the exit gas stream (Higgins and Hendry 1986). Therefore there has been little explicit investigation of the effects of changing these variables on CRN product formation. Successful reaction temperatures ranging from 1250–1500°C have been reported for the CRN of various aluminosilicate minerals (Fabbri and Dondi 1991), with temperatures between 1400–1500°C and a reaction time of 6–8 hours commonly used for the CRN of kaolinite clay (Morrison, Maher, *et al.* 1989; Edrees and Hendry 1995). Occasionally, reaction times as short as 3 hours were seen to be sufficient for final product formation (Mazzoni, Aglietti, *et al.* 1993a), but this is heavily dependent on sample mass and size, with larger masses requiring longer reaction times (Antsiferov, Gilev, *et al.* 2000). Excessively high CRN temperatures or extended reaction times were found to result in the carbothermal reduction of mullite by SiC to form Al_2O_3 , which is much less effective than SiO_2 in forming β' (Barris, Brown, *et al.*).

b) Carbon source and quantity

Various carbon-based reductants have been investigated, including coal dust, carbon-black, and SiC (Higgins and Hendry 1986). It was seen that a high level of contact between the carbonaceous reductant and mineral reagents was the main requirement for effective CRN, thus the higher specific surface area of carbon-black produced a faster reaction rate when compared to both SiC and coal particles (Mazzoni, Aglietti, *et al.* 1993a). Although it was found that carbothermal reduction proceeds more slowly when using the larger SiC particles, the yield of nitride products increased as a result of the intermediate $\text{SiO}(\text{g})$ species having greater opportunity to react with the nitrogen gas (Higgins and Hendry 1987).

It was found that an excess of carbon 10–20% greater than that defined by the stoichiometric reaction equations was required to maximise the yield of β' (Mazzoni, Aglietti, *et al.* 1993a; Higgins and Hendry 1987). This is due to depletion of C via side reactions with impurities in the clay, such as iron.

c) Nitrogen gas flowrate

In addition to providing reactant N for nitridation, the N_2 gas flowrate plays an important role in CRN. The initial carbothermal reduction reactions (Equations 2.9, 2.10a and b) occur via a gas phase, and are reversible equilibrium reactions that produce $CO(g)$. Accordingly, the concentration of $CO(g)$ must be kept low to keep the reactions proceeding in the forward direction, i.e. to the RHS of the equation. Low N_2 flow rates were found to result in a buildup of CO gas that impeded the rate and extent of the CRN reactions, whereas reasonably high gas flow rates were found to increase the reaction rates and nitride formation due to the continual removal of the gaseous by-products (Mazzoni, Aglietti, *et al.* 1993a). The optimum flowrate was determined to be $\sim 30\text{ l/hr}$, but may depend on furnace geometry (Mazzoni, Aglietti, *et al.* 1992a).

It was also found, however, that there was a depletion of Si from the system due to the intermediate $SiO(g)$ being swept away by the N_2 gas flow (Wild 1975). Evidence of this was the formation of SiO_2 whiskers at cooler parts of the tube, and enrichment of the sample in Al. The extent of Si depletion was found to increase with increasing N_2 gas flowrates (Cho and Charles 1991b), and was promoted by low C/clay ratios (Mazzoni and Aglietti 1998). Higher carbon contents provide more opportunity for the Si to remain in the system, forming the $SiC(s)$ intermediate phase from the reaction between $SiO(g)$ and C (Equation 2.10b).

d) Impurities in the starting powders

Clays may contain various impurity elements even after refining, and these impurities can have a significant effect on CRN. SiO_2 quartz is a major impurity in many clay deposits (Grimshaw 1971), and studies of kaolinite clays containing quartz have shown that the quartz does not participate in the early stage reduction process, remaining unchanged in the system until the formation of nitrogenous products starts (Mazzoni, Aglietti, *et al.* 1992a). It is the more reactive, amorphous SiO_2 produced from the dissociation of metakaolin which starts the early stage reduction to form $SiO(g)$. Free quartz is later incorporated into β' formation (Mazzoni, Aglietti, *et al.* 1993a).

Iron is often present as Fe_2O_3 in clay minerals, and has been found to catalyse the nitridation reactions, increasing the formation of nitride products and decreasing the amount of residual intermediate phases after CRN (Mazzoni, Aglietti, *et al.* 1993a). This occurs through the formation of low eutectic temperature Fe-Si liquids at $\sim 1200^\circ\text{C}$, however the exact mechanism by which the Fe-Si liquids enhance nitridation is not known. Iron has been seen to

promote the formation of the SiC intermediate phase that is used during the final stage of CRN to form β' (Mazzoni, Aglietti, *et al.* 1993a). A study of the enhancement of nitridation by Fe during the direct nitridation of Si metal for Si_3N_4 production showed that iron also caused the devitrification of the protective SiO_2 layer on the Si metal at low oxygen partial pressures (Boyer and Moulson 1978). This promoted SiO(g) formation at the Si/ SiO_2 interface, thereby promoting nitridation; a threefold increase in Si nitridation rate was detected with very small iron additions of 55ppm and was associated with the formation of an FeSi_x liquid above 1212°C . The catalytic effect of Fe is small compared to the general enhancement of CRN arising from clay systems that produce significant amounts of liquid from the mineral decomposition reactions, such as bentonites (Mazzoni and Aglietti 1996). The FeSi_x compounds often detected in intermediate stages of the CRN process are found to remain amongst the final products as hard agglomerates which are detrimental to the mechanical behaviour of the materials (Mazzoni and Aglietti 1996).

Potassium impurities have been shown to lead to greater formation of the intermediate X-phase sialon and lower yields of β' (Higgins and Hendry 1987), whereas calcium and magnesium impurities can promote the reduction process via the production of fluid eutectic liquids at the nitriding temperature (Mazzoni and Aglietti 2000). The low vapour pressure of the alkaline earth oxides such as CaO and MgO results in considerable volatilisation at the CRN temperatures, and it has been reported that these oxides were totally evaporated during CRN at temperatures $\sim 1400^\circ\text{C}$ (Mazzoni and Aglietti 2000). Titanium was seen to have no effect on CRN, but was found as TiN in the final products (Fabbri and Dondi 1991).

2.2.3 CRN of Other Aluminosilicates

In addition to kaolinite, various other aluminosilicate materials have also been used for sialon production via CRN, including pyrophyllite, bentonite, andalusite, pyrophyllite, and diatomite (Fabbri and Dondi 1991). The work by Mazzoni and co-workers (1988) has shown that the reaction mechanism described above for the CRN of kaolinite was common to all the aluminosilicate minerals studied (Mazzoni and Aglietti 1998). The first reactions are thermal decomposition of the minerals during heating to produce mullite or glassy phases, depending on composition. This is followed by the formation of intermediate SiC, which then reacts with the mullite or glassy phases to produce nitrogenous phases. The exact nature of the intermediate and final Si-Al-O-N product phases produced from CRN depend on the Al/Si ratio of the starting mineral. Common products include β' and O-sialon from Si-rich minerals, and AlN-polytypoid phases from Al-rich minerals or from other systems where extensive SiO(g) loss occurred. Clay mixtures have also been added to SiC grit and reacted via CRN to

form β' , O', and X-sialon bonding phases to produce reaction bonded SiC refractory materials (Edrees, Holling, *et al.* 1995; White, Ekstrom, *et al.* 1998).

2.2.4 CRN of Waste Materials

Industrial wastes have also been used to produce β -sialons via CRN, such as alumina refining waste (Cardile 1990), and rice husks (Prasad, Maiti, *et al.*). The rice husks (or 'hulls') account for about 23% of the mass of rice before beneficiation and contain significant amounts of silica in the form of a hydrated amorphous gel, which can be processed via chemical digestion and pyrolysis to produce an ash consisting of intimately mixed SiO_2 and carbon, in controlled ratios. By adding Al_2O_3 powder, a single phase β -sialon with $z=1.3$ was prepared after CRN at 1430°C for 16hrs from a composition of 1:0.1: 2.1 $\text{SiO}_2:\text{Al}_2\text{O}_3:\text{C}$ (Rahman and Saleh 1995).

Fly ash is a waste product from electricity generation in coal power plants, though the term is sometimes used for municipal incinerator ashes. It is produced in vast quantities worldwide, with 150 Mtons produced in 1990 (Gilbert and Mosset 1998). Compositions vary with coal source and from plant to plant, but generally consist of a mix of fine crystalline and amorphous particles $<10\mu\text{m}$ diameter containing 10-30 wt% Al_2O_3 , 30-70 wt% SiO_2 , 5-25 wt% carbon, and small amounts of other elements and minerals. This makes them suitable for β -sialon manufacture by CRN without additional processing. β -Sialons with $z= 2.55$ and 2.25 were produced via CRN of 0.5g fly ash pellets at 1500°C after 1hr (Gilbert and Mosset 1998). The production of Ca- α -sialon from Ca-bearing fly ashes is described in the following section.

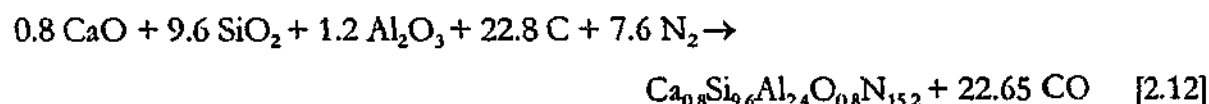
2.3 α -Sialon Production via Carbothermal Reduction-Nitridation

The requirements for α -sialon formation are more complex than for β' , X, or O-sialon due to the additional metal cation that is required to act as the stabilising additive. Therefore investigations into the α -sialon system have been considerably fewer than for the simpler sialon phases, with only six major studies performed. A variety of raw materials and α' systems were investigated, hence this discussion will present each study individually. The slag used in the current investigation is rich in CaO and forms Ca- α -sialon, hence the studies dealing with Ca- α' production are presented first, followed by those dealing with other α' systems. Section 2.3.3 will detail the limited work that has been performed on densifying and evaluating the mechanical properties of the CRN- α' material, which is followed by a summary of experimental findings relevant to the current investigation.

2.3.1 Ca- α -Sialon via CRN

2.3.1.1 CRN of Fine, High-Purity Powders

The very first investigation into using CRN to produce single-phase α -sialon was performed in Japan in 1988 by Mitomo and co-workers (Mitomo, Takeuchi, *et al.* 1988). In this work the cost of the powders was not a concern; rather, it was desired to minimise the defects and microstructural inhomogeneities produced in sintered products that result from inhomogeneities in the nitride starting powders. Fine, high purity, oxide powders with a particle size $\sim 0.1\mu\text{m}$ were fabricated via the hydrolysis of organic alkoxide precursors such as tetraethyl orthosilicate and aluminium isopropoxide. Calcium ethoxide and yttrium nitrate provided stabilising additions for both Ca- and Y- α -sialon formation. The details of the hydrolysis reactions will not be presented here, but it should be noted that the oxides were precipitated directly onto particles of carbon-black, hence the oxide reactants and the carbon reductant were intimately pre-mixed. The stoichiometric design equation for the overall CRN reaction is given in Equation 2.12, which was designed to produce an $m=1.6$, $n=0.8$ Ca- α -sialon. Carbon equivalent to 1.2 times the calculated stoichiometric amount was used.



Ca- α -sialon was formed between 1350-1450°C, with significant amounts of β - Si_3N_4 , a Ca-containing residual glass, and some AlN also produced. The phase assembly changed with reaction time; β - Si_3N_4 dominated the initial products after 0.5 hours at 1450°C, and α' dominated after 1 hour. The small amount of AlN was fully removed after 4 hours of reaction at 1450°C, however β - Si_3N_4 and the Ca-bearing glass remained among the products even after 16 hours of firing at 1450°C. Heat-treating this CRN powder at an elevated temperature (1550°C) for 1 hour removed the β - Si_3N_4 , and produced an essentially single-phase Ca- α' powder (Figure 2.8). This was thought to be due to the higher solubility of Ca in the α' phase at higher temperature, allowing greater α' formation via reaction between the β - Si_3N_4 and Ca-containing glass. However it is also possible that the α' -forming reaction is kinetically unfavourable at the lower temperature.

This is the only study on the production of α' via CRN that identified β - Si_3N_4 rather than a low z-value β -sialon as a precursor to α' formation. This identification was based solely on the XRD results, where it may be difficult to discriminate between β - Si_3N_4 and a very low z-value

β -sialon with a very low level of Al-O substitution. It is therefore possible that the β - Si_3N_4 identified here (Figure 2.8a) was actually a low z-value β -sialon.

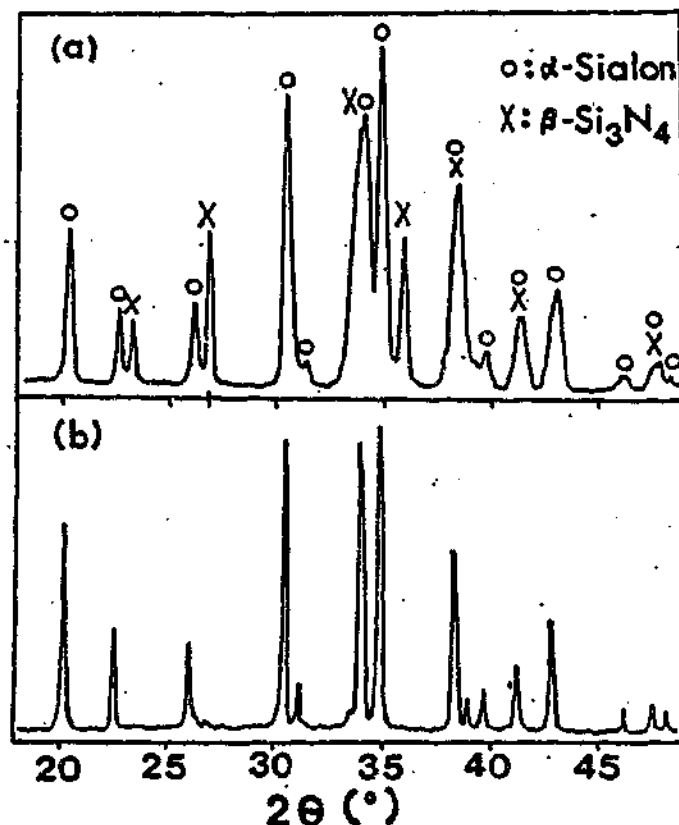
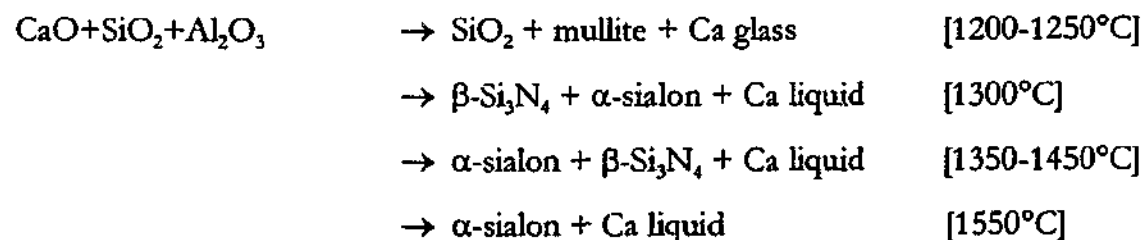


Figure 2.8 XRD of CRN-derived Ca- α -sialon powder: (a) CRN powder as formed after 16 hours at 1450°C, (b) after heat treatment at 1550°C for 1 hour (after Mitomo, Takeuchi, *et.al.* 1988).

At lower temperatures the intermediate phases detected include the oxide phases α -cristobalite (SiO_2) and mullite ($3\text{Al}_2\text{O}_3 \cdot 2\text{SiO}_2$), the oxynitride phase $\text{Si}_2\text{N}_2\text{O}$, and a CaO- Al_2O_3 - SiO_2 liquid. It was thought that α -sialon formation would occur via the solution and reprecipitation of the oxides into the liquid, forming nitrogen-containing phases such as $\text{Si}_2\text{N}_2\text{O}$ and β - Si_3N_4 which are then re-dissolved and precipitated as α' . A greater extent of weight loss was detected than expected from a consideration of the design equation, and this was attributed to evaporative $\text{SiO}(\text{g})$ loss during CRN. The following reaction sequence was proposed:



The Ca- α' was determined to have an m -value of 1.2, indicating that only $\sim 75\%$ of the CaO entered the α' structure, with $\sim 25\%$ remaining in the glass. The α' particles had a grain size of 0.5-2 μm , which was significantly greater than the $\sim 0.1\mu\text{m}$ size of the initial reagent powders, although it was thought that these may be agglomerates of finer particles.

In the same paper, Y- α' formation was shown to be a more complex process than that of Ca- α' . More minor product phases were formed in addition to α' at 1450°C, including $\beta\text{-Si}_3\text{N}_4$ (or β -sialon), 15R sialon-polytypoid, and a crystalline Y-containing solid-solution based on $\text{Y}_4\text{Al}_2\text{O}_9$. Nearly single-phase Y- α' could only be produced by further heating the CRN powder at 1600°C for 1 hour, but a small amount of $\beta\text{-SiC}$ was also formed at this temperature. It was thought that the formation of the Y-containing $\text{Y}_4\text{Al}_2\text{O}_9$ phase depleted the liquid of Y_2O_3 , thus hindering the formation of Y- α' at 1450°C and therefore requiring a higher temperature to decompose the $\text{Y}_4\text{Al}_2\text{O}_9$ and release Y_2O_3 into the liquid for Y- α' formation. The grain size was about the same as that of Ca- α' .

As the first reported use of CRN to produce α -sialons from oxide starting powders, this study shed some light on several aspects of the CRN process as it applies to α' formation, and demonstrated that a single-phase α' material could be produced by this process. The CRN reaction sequence was found to be relatively complex, with several intermediate phases produced prior to α' formation, occurring via a succession of solution-precipitation steps involving the liquid produced by melting of the reactants, and nitrogen from the furnace atmosphere. Ca- α -sialon formation was found to be somewhat easier than Y- α' formation, occurring at lower temperatures (1350-1450°C) and with fewer crystalline secondary phases present, none of which contain the Ca stabilising additive. The final phase assembly is very dependent on thermodynamic factors (ie. reaction temperature), with increased formability of Ca- α' seen at elevated temperatures.

2.3.1.2 CRN of Standard Laboratory Reagents

In contrast to the expensive, in-house fabricated powders used by Mitomo and co-workers, several studies have been performed at the Centre for Technical Ceramics in the Netherlands using cheaper starting powders for Ca- α' production via CRN. The first of these involved using commercial laboratory reagents CaSiO_3 , Al_2O_3 , and SiO_2 mixed in a ratio designed to produce α' with a composition of $m=1.6$ and $n=1.2$ (van Rutten, Terpstra, *et al.* 1995).

Single-phase α' was unable to be produced at 1450°C, where even after 14 hours of firing the products contained significant amounts of β -sialon and a small amount of amorphous glass in

addition to α' . The onset of α -sialon formation occurred after 6 hours of reaction at 1450°C, with shorter reaction times and/or lower temperatures (1350°C) producing higher amounts of β -sialon, SiO_2 , and $\text{Si}_2\text{N}_2\text{O}$ as intermediate phases.

A maximum α'/β' ratio of 0.49 was determined for samples fired at 1450°C for 7.5 hours, as estimated from the XRD peak heights of the α' and β' peaks. Using a higher CRN reaction temperature of 1500°C increased the yield of α' to >95%, demonstrating that a single-stage CRN process can generate single-phase α' . However, this level of α' formation required firing for the very long time of 65 hours, which may be impractical for commercial production.

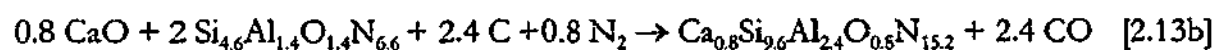
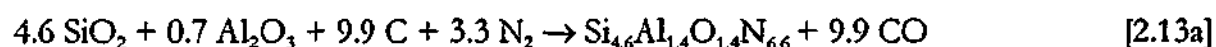
A two-stage firing process similar to that seen in the study by Mitomo and co-workers, was also able to produce an essentially single-phase α' powder by re-firing (ie. heat-treating) the α' -containing CRN powder at higher temperatures. The yield of α' increased with increasing heat-treatment temperature, reaching a maximum of >95% α' at 1700°, but this effect was only produced in CRN powders that were milled and re-pressed into pellets before heat-treatment. No such improvement in the α' content was produced in CRN derived α'/β' powders that were heat-treated without prior milling of the powder; instead a decrease in α' content was experienced, with no explanation given for this behaviour. In experiments where the CRN reactions were incomplete and contained little or no α' formation, the presence of free carbon was seen to produce SiC as the main product phase when heat-treating at temperatures 1650° or higher. This result indicates that there is a maximum temperature for CRN above which the thermodynamics of the system are such that nitride (ie. sialon) formation becomes less favourable than carbide (SiC) formation.

Nitrogen flowrate was also observed to influence the extent of α' formation in this system; 5ℓ/hr through 25mm diameter tube was found to be too low and produced $\text{Si}_2\text{N}_2\text{O}$ rather than the higher N-containing α - or β -sialon phases. A flowrate of 12ℓ/hr was adequate for reaction at 1450°C, however a higher flowrate of 30ℓ/hr was required when firing larger samples (200g pellets) in a furnace fitted with a larger tube of 50mm diameter. This suggests that the flux of N_2 experienced by the sample is an important parameter for CRN, and will depend on both furnace and specimen geometry.

The Ca- α' powder produced from a single-stage CRN reaction at 1500°C had an agglomerate size of ~5-8 μm , and that of the refired powder was larger, ~10-20 μm . The size of individual particles was not determined.

The CRN reaction mechanism was investigated and it was found that a significant amount of amorphous phase (ie. liquid) is present at the start of CRN. Intermediate crystalline products include low z-value β -sialons ($z < 1.2$), $\text{Si}_2\text{N}_2\text{O}$ or the related O-sialon ($\text{Si}_{2-x}\text{Al}_x\text{O}_{1+x}\text{N}_{2-x}$) and SiC; no crystalline Ca-containing intermediate phases were detected. During reaction at 1500°C the first sialon products were formed after only a short time (~ 100 mins), and the composition was dominated by β' , which was converted to a 90 wt% α' , 10 wt% β' product after ~ 240 mins. Quantification of the N-content of the system via a wet chemistry process showed that almost the entire quantity of N as predicted from the stoichiometric reactions (35.0 wt%) was incorporated into the system at early stages of CRN, when the concentration of α' was still low (40 wt%). This shows that most of the nitrogen required for continued Ca- α' formation is already available in the sample.

The following reaction mechanism was proposed by the authors: a liquid phase is produced at the CRN temperature from the molten reactants, and CRN reactions between this liquid and the N_2 gas cause the precipitation of a low z-value β -sialon (Equation 2.13a). The extra Ca and N required for Ca- α -sialon formation is incorporated via a second CRN step, probably involving reactions between the Ca-containing liquid and β -sialon (Equation 2.13b).



The conversion of the α'/β' powder to α' when refired at higher temperatures was thought to occur via a reaction between the Ca-containing liquid and the β -sialon, similar to the process occurring during reaction sintering, and not involving any further N incorporation.

These equations describe the general CRN process, but do not show any details regarding the intermediate solution-precipitation reactions that were observed, nor do they account for deviations from the ideal stoichiometry of the phases formed in the CRN powders. Both the Ca- α' and the β' phases had m- and z-values, respectively, that were lower than those predicted from the ideal reaction equations.

The most significant finding from this paper is that a single-phase α' product could be formed from a single-stage CRN reaction at higher CRN temperatures, though this may require a long reaction time. It was also shown that incorporation of nitrogen into the system occurred very quickly during the early stages of CRN.

2.3.1.3 Hollow Ball Formation via CRN of Standard Laboratory Reagents

A novel result was found in another investigation into the CRN of standard laboratory reagents by Hotta and co-workers at Yokohama University in Japan. Standard laboratory-grade reagents SiO_2 , Al_2O_3 , CaCO_3 , and carbon-black were reacted for just 2 hours at 1450°C under N_2 flowing at $30\ell/\text{hr}$ through an 80mm diameter tube. The composition was designed to produce an $m=2.0$, $n=1$ Ca- α -sialon ($\text{Ca}_{1.0}\text{Si}_{9.0}\text{Al}_{3.0}\text{O}_{1.0}\text{N}_{15.0}$), and 120% of the stoichiometric carbon requirement was used (Hotta, Tatami, *et al.* 2002).

The final product contained 85 wt% Ca- α -sialon and 15 wt% AlN. The powder particles were extremely fine, $\sim 30\text{-}50\text{nm}$ in diameter, and formed agglomerates with the unique morphology of large, hollow balls, $200\text{-}500\mu\text{m}$ diameter (Figure 2.9). These nanoparticles were formed from standard laboratory reagents that were not especially fine; for example the SiO_2 had a mean particle size of $\sim 0.6\mu\text{m}$. Changing the form of the SiO_2 reactant did not alter the morphology of the CRN- α' formed; both ultrafine, $0.005\text{-}0.05\mu\text{m}$ amorphous SiO_2 , and coarse, $>10\mu\text{m}$ crystalline SiO_2 powders produced essentially the same results (Hotta, Tatami, *et al.* 2002).

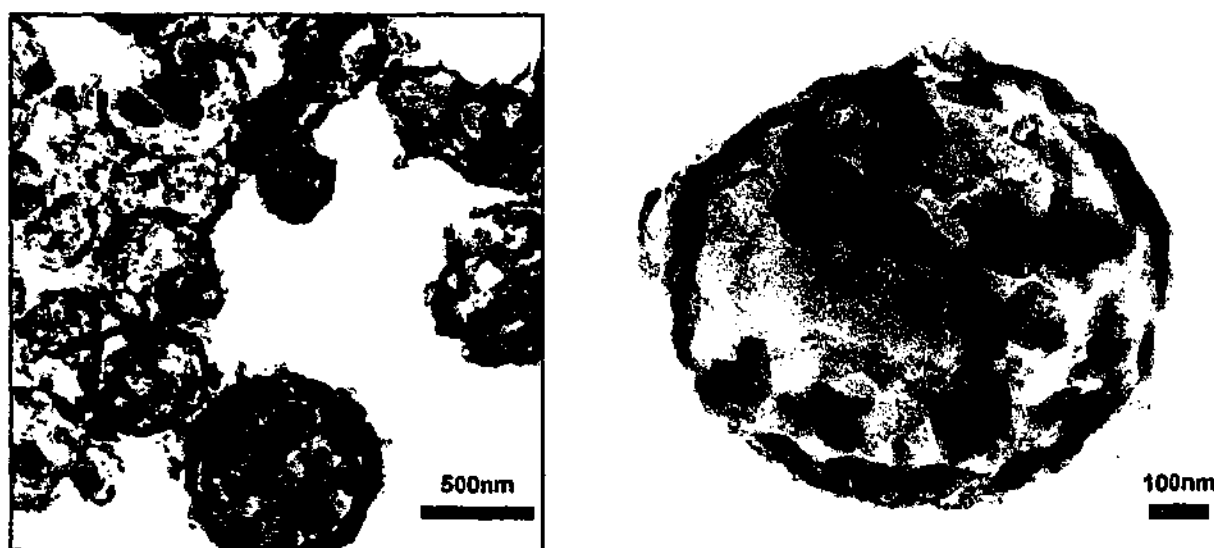


Figure 2.9 Hollow balls of Ca- α -sialon (85 wt%) and AlN (15 wt%) (after Hotta *et al.* 2002).

Further analysis of these powders was performed via TEM in collaboration with this author. It was found that by the time the CRN temperature of 1450°C is reached, the components have melted to form solid balls of amorphous Si-Al-Ca-O-N glass, similar in size to that of the final hollow-balls. The reason for the glass forming with this spherical morphology was attributed to surface tension interactions with the carbon-black particles. CRN was found to operate

from the outside→inwards; the first crystalline products form at the surface of the solid balls in contact with the carbon and nitrogen, and these have a smaller volume (higher density) than the glass, causing shrinkage and cracking which then exposes the interior to further reaction.

This novel morphology may allow for new applications such as filters or catalyst substrates to be developed for α' , or the hollow balls could be broken down to produce nano-sized Ca- α' powder for further sintering. A discussion regarding the sintering of this powder is presented in Section 2.3.3.2.

2.3.1.4 CRN of Fly Ash Waste

In the Netherlands, fly ash waste has been successfully used as an even cheaper starting powder than laboratory reagents for both β' and α' production via CRN. Fly ashes were described previously in Section 2.2.4, and are a by-product of coal combustion for energy production. The first investigation into the CRN of fly ash was performed by Metselaar and co-workers, using a high-carbon grade (8 wt% C) fly ash consisting of 54 wt% SiO₂, 28 wt% Al₂O₃, 5 wt% Fe₂O₃, and 5 wt% CaO. The crystalline phases mullite (3Al₂O₃·2SiO₂) and quartz (SiO₂) were detected in the fly ash via XRD. Additional carbon was added to the fly ash before reaction at 1500°C (Metselaar, Exalto, *et al.* 1996).

CRN process of the fly ash was seen to operate by the same two-stage process identified by Van Rutten and co-workers for the CRN of laboratory reagents (Equations 2.13a and b above); β -sialon was produced in large quantities in the early stages of CRN, and increasing the reaction time increased the α'/β' ratio of the final products (Figure 2.10). After reaction at 1500°C for 25 hours a maximum of 65 wt% Ca- α' was formed, with the remainder comprising of 15 wt% β' , and 10 wt% each of the 12H and 21R polytypoids. The m-value of the α' was m=1.8, and the z-value of the β' was z=1.4.

Kudyba-Jansen and co-workers further expanded on this study and used five different fly ashes to produce α - and β -sialons via CRN (Kudyba-Jansen, Hintzen, *et al.* 2001). Four of the five fly ashes were similar in composition and characteristics to the fly ash first used by Metselaar, described above. Consideration of the quantity of Ca, Al, and Si in these fly ashes placed them outside the single-phase α' region of the phase diagram, thereby predicting the formation of at least one other phase in equilibrium with Ca- α' . The other fly ash was richer in Si and lower in Al, and corresponded to the single-phase α' region of the phase diagram, thus predicting the equilibrium product to be single-phase Ca- α' .

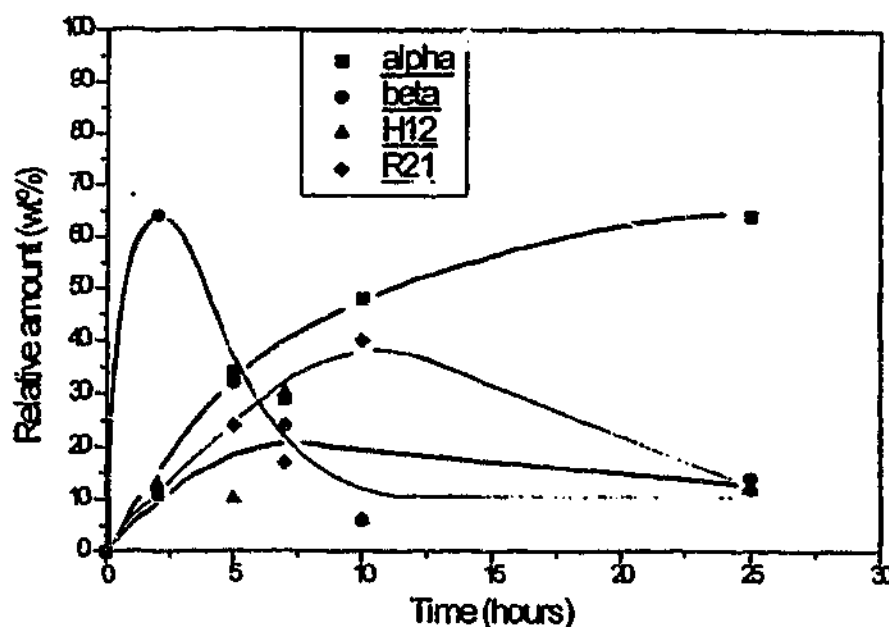


Figure 2.10 Phase formation as a function of reaction time at 1500°C during the CRN formation of Ca- α' from fly ash (after Metselaar, Exalto, *et al.* 1996).

The target Ca- α' compositions were based on the Ca:Al:Si ratios of the individual fly ashes, and stoichiometric equations were developed for each fly ash as per Equations 2.13a and b. The fly ash predicted to form single-phase α' did not, with only 8 wt% α' (estimated from XRD peak height ratios) formed after 25 hours of reaction at 1500°C. The remainder was β' with minor amounts of 12H, 21R, Fe₂Si, and Fe₂O₃ also present. It was postulated that a longer reaction time would be required to increase the yield of α' in this system, but no explanation was given regarding why the rate of α' formation was slower using this fly ash compared to all of the others.

Three of the other fly ashes were fired for 25 hours at 1500°C and produced powders with an α -sialon content between 51 and 64 wt%, with β -sialon being the main secondary phase. The firing time of one of the fly ashes that produced 51 wt% α' was extended to 50 hours, and this significantly increased the α'/β' ratio such that α' was now the dominant phase. This composition lies very close to the border of the single-phase α' region, hence was predicted from a thermodynamic equilibrium viewpoint to form a highly α' product. The dependence on α' yield with reaction time shows that the reaction kinetics have a limiting effect on the ability of the thermodynamic equilibrium phases to be produced. If the reaction rate is too slow, the time required for high levels of α' formation may be too long to be practical.

A process was investigated for the removal of Fe-based impurities from the CRN powder before densification. As discussed in Section 2.2.2.3, Fe₂O₃ impurities in the starting powders

form FeSi_x phases which are detrimental to mechanical properties. A simple magnetic separation process was shown to be 90% effective in removing these impurities, and considerably less environmentally damaging and less complicated than an alternative process involving washing in an 18% hydrochloric acid solution. The other low-level impurities in the fly ash such as oxides of K, Ti, Mg, P, Na and S, were not explicitly investigated in this study, but were assumed to be lost through volatilisation during CRN, or during a 750°C heat-treatment prior to batch mixing.

These studies have shown that it is possible to use an industrial waste by-product (fly ash) to produce α -sialon via CRN. The final phases formed are clearly dependent on initial composition, reaction temperature, and time, with long reaction times up to 50 hours required to obtain a fully α' product with only minor residual amounts of β' and polytypoid phases. Magnetic separation was shown to be effective in removing Fe-based impurities from the CRN powder.

2.3.2 Other α -Sialon Systems

2.3.2.1 Y- α -Sialon From Halloysite Clay

The production of Y- α' sialons via CRN was first performed in the study by Mitomo and co-workers (1988) from very fine, high purity oxide starting powders, and the results were briefly discussed in Section 2.3.1.1. Ekstrom and co-workers have since produced Y- α -sialons via CRN of mixtures of a New Zealand halloysite clay ($\text{Al}_2\text{Si}_2\text{O}_5(\text{OH})_4$), laboratory-grade Y_2O_3 powder, and laboratory-grade SiO_2 or Si metal additions (Ekstrom, Shen, *et al.* 1998).

The Si metal or SiO_2 additions were used to boost the Si content from 1:1 Si:Al in the clay to $\sim 8:1$ Si:Al as needed for sialon formation, and both additives produced the same CRN reaction products after reaction at 1475°C for 8 hours as detected via XRD: β -sialon ($z \approx 0.4$), $\text{Y}_3\text{Si}_6\text{N}_{11}$, α -sialon, and a small amount of amorphous glass. In the absence of any indication of quantities, it is assumed that these phases are listed in decreasing order of intensity; hence this system was not particularly successful at producing α' via CRN. The lack of α' was attributed to the formation of a Y-bearing crystalline phase ($\text{Y}_3\text{Si}_6\text{N}_{11}$), which, as in the study by Mitomo and co-workers, was seen to limit the extent of α' formation due to removal of the Y^{3+} cations needed to stabilise α' .

Although the XRD analysis of the crystalline CRN products showed that the same phase assembly was produced regardless of the type of Si addition (SiO_2 or Si metal), ^{29}Si NMR analysis revealed that amorphous Si-C was present within the amorphous phase of both types

of sample. SiC is produced by the carbothermal reduction of SiO_2 present in the starting composition (Equation 2.9), and the SiO_2 -based compositions therefore had both a much higher glass content, and a higher proportion of Si-C bonds within the glass, relative to Si-N bonds. Si-N bonds represent both α - and β -sialon (it is not possible to discriminate between them using ^{29}Si NMR), and the Si metal based samples which contained only a low level of SiO_2 from the clay contained a much higher proportion of Si-N bonds within the amorphous phase.

Hot-pressing at 1800°C further highlighted the differences between the two types of sample, with XRD detecting crystalline phases that precipitated from the previously invisible amorphous phase. Most notably, nanocrystalline SiC was precipitated in all samples, with the large quantity of amorphous Si-C bonds discovered in the SiO_2 -based compositions resulting in bulk materials dominated by SiC rather than sialon. α -Sialon was the dominant phase produced in the Si-based samples after hot-pressing, with β -sialon and small amounts of polytypoid phases 21R and 12H as secondary phases. The higher extent of sialon formation in the Si metal based samples was a consequence of the higher extent of Si-N bonds present in the amorphous phase.

The higher content of residual glass in the SiO_2 -based samples aided sintering of the CRN powder, and these samples generally had a higher density than the Si metal-based compositions. Increasing the m- and n-value of the design composition (increasing Y_2O_3 and Al_2O_3) also helped improve the hot-pressed density due to the formation of a larger amount of glass, which was aided by the release of additional yttrium via decomposition of $\text{Y}_3\text{Si}_6\text{N}_{11}$.

Although little detailed information was given regarding the CRN reaction process, this study does present some findings that may be relevant to the current investigation. Firstly, if the composition of the oxide must be adjusted to meet the needs for α -sialon production, the type of additive (ie. pure metal or oxide) will have a significant effect on the CRN process and resultant products. In this case, SiO_2 additions were carbothermally reduced to form SiC, which reduced the amount of α -sialon formed. Secondly, amorphous SiC may be formed which is undetectable in the XRD, but which may influence the behaviour of the CRN products during processing and produce crystalline SiC in the final products. Thirdly, further processing of the CRN powder at elevated temperatures may introduce phase changes due to metastability of the CRN-derived phases. However, it should be noted that the phase changes observed here, such as dissolution of $\text{Y}_3\text{Si}_6\text{N}_{11}$, may not accurately reflect the processes during sintering of CRN-derived Ca- α' powders due to the lack of an equivalent Ca-containing

crystalline phase. Some mechanical properties of the densified material are discussed in Section 2.3.3.3.

2.3.2.2. *Mg- α -Sialon From Talc and Halloysite Clay*

Mg- α -sialons have been produced by Zhang and co-workers at Yokohama University, Japan, in collaboration with Monash University, using mixtures of cheap mineral talc ($\text{Mg}_3(\text{Si}_2\text{O}_5)_2(\text{OH})_2$) and halloysite clay ($\text{Al}_2\text{Si}_2\text{O}_5(\text{OH})_4$) (Zhang, Komeya, *et al.* 2000). Mg- α -sialon has a much lower formability than Ca-, Y-, or RE- α' , and pure Mg- α' has not been obtained by conventional sintering methods. CRN was seen as a potential way to overcome this difficulty and use cheap starting materials at the same time.

Various mixtures of talc, halloysite clay, carbon, and 1-5 wt% Si_3N_4 seeds were reacted at 1450°C for 6 hours under flowing N_2 . The initial talc:clay ratio was the main control variable in this study, and it was determined that a 1.5:1 ratio was the optimum composition, producing the highest Mg- α -sialon content of ~35 wt%. β -Sialon was the dominant phase produced in this powder, and minor amounts of 15R polytypoid, and SiC were also present. The α' grains were 1 μm in diameter and generally equiaxed. It was found that the α' content of this composition could be considerably boosted by the addition of ~3 wt% Si_3N_4 seeds, which increased the α' content >90 wt% (Figure 2.11).

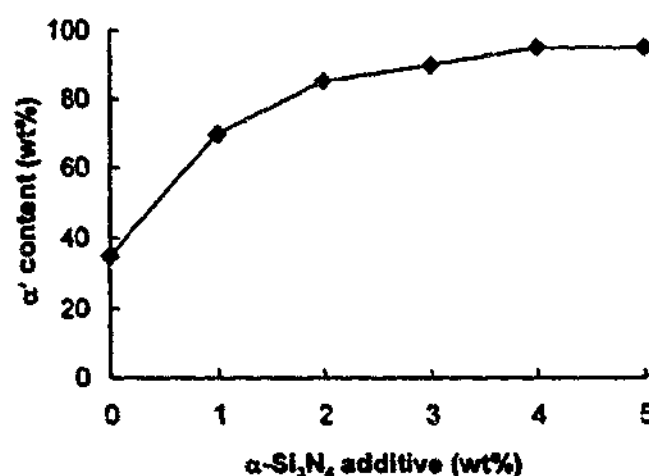


Figure 2.11 Effect of Si_3N_4 seeds on Mg- α' formation via CRN of talc and halloysite clay (after Zhang, Komeya, *et al.* 2000).

α - Si_3N_4 seed particles were seen in Section 2.2.1 to promote the preferential nucleation of α - Si_3N_4 during the CRN of SiO_2 , by reducing the energy required for nucleation and growth

through the provision of pre-existing nuclei. A similar process was thought to occur in this system, despite the slightly larger unit cell of α -sialon compared to α - Si_3N_4 .

The CRN reaction process was found to consist of 4 main stages: 1) low temperature phase transformations in the mineral components, such as decomposition of the talc and clay to silicates and silica; 2) initial incorporation of nitrogen into the system at $\sim 1300^\circ\text{C}$ by reaction of SiO_2 with C and N_2 to form $\text{Si}_2\text{N}_2\text{O}$; 3) melting of the components at 1400°C to form a Mg-Al-Si-O-N liquid and early-stage CRN to form intermediate phases such as SiC, MgSiN_2 , X-phase ($\text{Si}_3\text{Al}_6\text{O}_{12}\text{N}_2$), and $\text{CO}(\text{g})$; and 4) late-stage CRN at 1450°C involving conversion of the liquid and intermediate phases into β -sialon, Mg- α -sialon, and 15R polytypoid.

More work was performed in this system by Qiu and co-workers, who investigated the role of carbon content, composition, and firing temperature (Qiu, Tatani, *et al.* 2002). It was seen here that too much carbon was detrimental to α' production; the highest yield of Mg- α' was obtained from the composition using the exact stoichiometric quantity of carbon. Boosting the carbon content by an additional 50% produced large amounts of SiC whiskers at the expense of Mg- α' , and the Mg- α' formed had very irregular morphologies. This was attributed to the carbon forming a thick layer over the talc and clay particles, which boosted the $\text{CO}(\text{g})$ partial pressure to favour the production of SiC via the carbothermal reduction of $\text{SiO}(\text{g})$ (Equations 2.10a and b), and simultaneously hindered access to the nitrogen gas.

Another significant finding was that a large amount of Mg was lost during CRN, requiring the use of high talc contents 1.5:1 talc:clay (molar ratio) or higher to provide sufficient Mg for Mg- α' formation. The loss of Mg may occur via carbon induced reduction of MgO or MgSiO_3 to $\text{Mg}(\text{g})$, or by the decomposition of the MgSiN_2 intermediate phase above 1400°C . The low boiling point of Mg ($\sim 1170^\circ\text{C}$) allows any $\text{Mg}(\text{g})$ to be easily swept away by the flowing gas stream. Some of the Mg will also be consumed by a small amount of glass phase likely to be present. In fact, this depletion of Mg may be responsible for the previous finding that low carbon levels (100% of the stoichiometric amount) are better for α' formation than when an excess of C is present; extensive Mg loss will enrich the system in Si, thus contributing to preferential SiC formation instead of α' . This was not seen to be a problem in the Ca- or Y-sialon systems discussed above, where no loss of the stabilising cation was detected.

Raising the CRN temperature from 1450°C to 1480°C was seen to improve the yield of α' , however further increasing the reaction temperature to 1500°C produced an increase in β -sialon and AlN content. This was thought to be due to instability of the α' phase when the

liquid becomes oversaturated with nitrogen, decomposing via the $\alpha' \rightarrow \beta'$ transformation into the more nitrogen-rich phases β' and AlN.

The most significant finding from this study is the effectiveness of the incorporation of a few percent α - Si_3N_4 seeds in promoting α' formation in the system. More generally, it is clear that the CRN of natural minerals can be used to produce essentially single-phase Mg- α' via CRN, where such materials cannot be produced via conventional methods.

2.3.3 Densification and Mechanical Properties of CRN- α -Sialon

Most of the studies discussed above were focused on analysing the CRN reaction process and the factors affecting the formation of the final product phases. Only a few of these studies went further and produced bulk materials from the CRN- α' powder and examined their mechanical properties. The work that has been performed in this arena is summarised in this section.

2.3.3.1 Ca- α -Sialons Derived From Laboratory Chemicals

The sintering behaviour of CRN- α' powders produced from laboratory chemicals was investigated by Van Rutten and co-workers (van Rutten, Hintzen, *et al.* 2001). It was found that the CRN- α' powder was unable to be densified without the use of sintering additives, with a maximum density of only 68% of the theoretical density achieved using pressureless sintering. Removal of the residual carbon before sintering and the addition of 15 wt% CaO as a sintering additive was required to produce >95% density. The density could be increased further to ~97% ($3.11\text{g}/\text{cm}^3$) when using hot-pressing and a protective powder bed to prevent sample decomposition.

Dilatometry experiments were performed to determine the shrinkage curves during sintering. The overall shape of the curve was similar to that observed in reaction-sintered systems. It was found that the CRN- α' powder first produced a eutectic liquid at the same temperature (~1350°C) as reaction sintered materials, which is due to the same liquid being produced from the Ca-O and Al-Si-O compounds present on the surface of both types of starting material. However, wetting of the sialon starting material (which induces solution-precipitation) took place in the CRN- α' material at a significantly higher temperature (~1500-1550°C) compared to ~1450°C for Si_3N_4 material. Unidentified events in the dilatometry curves indicate that some unidentified intermediate phase(s) may also dissolve during sintering, a feature also found in reaction sintering systems.

The potential for slip-casting Ca- α -sialon powders prepared by CRN has been investigated in detail by Kudyba-Jansen and co-workers (Kudyba, Almeida, *et al.* 1997; Kudyba-Jansen, Hintzen, *et al.* 2001; Kudyba-Jansen, Almeida, *et al.* 1999). These studies have focused on examining the aqueous suspension characteristics and evaluating various particle and suspension characterisation methods. The best conditions for slip-casting CRN- α' powders (lowest viscosity, lowest sediment volume, largest zeta potential) were found to occur at a pH of 10-11 with a solid loading of 60 wt%. It was seen that the addition of 0.3 wt% deflocculant was beneficial to achieving suspensions of Ca- α' that behaved nearly identically to suspensions of CRN-derived β' (to which deflocculant was also added). However, despite this considerable amount of preparatory work, no experiments detailing the slip-casting and densification of the CRN- α' material have been reported. The single-phase β' powders produced from fly ash have been slip-cast and were shown to produce the same final density after pressureless sintering as pellets cold isostatically pressed (CIP-ed) at 250 MPa (Kudyba-Jansen, Hintzen, *et al.* 2001). This suggests that slip-casting may also be an effective green-body forming mechanism for CRN-derived α' powders.

The fly ash-derived Ca- α' powder has not been densified into Ca- α' bulk materials, perhaps because of the low α' content of these α'/β' powders (51-64 wt%) (Kudyba-Jansen, Hintzen, *et al.* 2001). One sintering experiment designed to produce an α'/β' composite material was performed, but only included a small amount (22.5 wt%) of the α'/β' fly ash-derived CRN powder, with the remainder being Si_3N_4 (67.5 wt%) and CaO (10 wt%). After firing, this sample was largely Ca- α' ; however this α' was formed via reaction between the Si_3N_4 and CaO additives, and therefore does not represent a CRN- α' material. No explanation is given as to why the α'/β' CRN powder was not attempted to be densified on its own.

2.3.3.2 Nano-Sized Ca- α -Sialons Derived from Laboratory Chemicals

Densification of the nano-sized Ca- α' powder was performed by Tatami and co-workers after hand grinding the hollow balls in a mortar and pestle to separate the nano-powder particles (Tatami, Iguchi, *et al.* 2003). Gas pressure sintering (GPS) and spark plasma sintering (SPS) were both performed, however no densification was achieved using GPS at 1800°C, 0.9 MPa N_2 . SPS at 1700°C with a 20 minute soak time produced a material with 99.2% theoretical density and no changes to the phase assembly. Very little grain growth was detected; the calculated particle size was 27nm before SPS and 34nm afterwards. A grain boundary glass is usually present in all α -sialon materials, however no evidence of any grain boundary glass was detected via TEM analysis of this material. The reasons for this were not clearly understood,

but attributed to either the unique properties of the nano-sized particles or the unconventional sintering processes occurring during sintering via the SPS technique.

The nano-sized Ca- α -sialon material densified using SPS at 1700°C was seen to have a Vickers hardness of ~18 GPa, and a fracture toughness of 3.3 MPam^{1/2}. The fracture toughness is a little lower than that commonly seen for Ca- α' materials, but is not outside the lower limit expected for fine-grained, equiaxed ceramics (Cao and Metselaar 1991). The results of 3-point bending tests showed that the mean bending strength of the material was 700 MPa, and with careful control over machining it was thought that this can be significantly improved. The wear rate determined using a ball on disk method showed that the wear rate of the Ca- α -sialon disk was only marginally higher than for a commercial Si₃N₄ wear material. The nano-Ca- α -sialon material also displayed a lower corrosive weight loss when placed in 5 wt% sulfuric acid for 80 hours, than the commercial Si₃N₄ material. The low corrosive weight may be due to the lack of a grain boundary glass, which is more readily corroded than crystalline material. Overall, it can be said that this CRN material displayed very good mechanical properties.

2.3.3.3 Y- α -Sialons Derived from Halloysite Clay and Si/SiO₂ Additions

The hardness and fracture toughness of the highest density materials hot-pressed at 1800°C from the Y- α -containing powders produced via the CRN of halloysite clay were determined to be 17.6-19.9 GPa and ~3.0 MPam^{1/2}, respectively (Ekstrom, Shen, *et al.* 1998). These values are comparable to conventional Y- α -sialon ceramics (Cao and Metselaar 1991).

2.3.4 Summary

α -Sialons have been successfully produced via CRN from a variety of oxide raw materials, both pure and impure. Table 2.1 lists the most successful process conditions for producing α -sialons via CRN from the studies discussed above. The study by Ekstrom and co-workers on the CRN of halloysite clay is not included, because CRN did not directly produce a high yield of Y- α -sialon.

α -Sialon formation has tended to occur at a temperature between 1450 and 1500°C, and has generally required between 4 to 25 hours for reaction. A nitrogen flowrate of 30l/hr or greater was commonly used, though the optimum flowrate may depend on the diameter of the furnace tube and the size of the specimen. Several CRN studies used a slight excess of carbon up to 1.2 times the predicted stoichiometric amount, which was a feature seen to be useful from work on the CRN formation of α -Si₃N₄ and β -sialon powders. Only one study analysed the effects of carbon concentration, and found that in the case of Mg- α' production from talc

and halloysite clay the exact stoichiometric amount was most favourable (Qiu, Tatami, *et al.* 2002).

Table 2.1 Summary of successful conditions for producing α -sialon via CRN of various raw materials

CRN raw material (Study authors)	Sample Size	CRN Temp (°C)	CRN Time (hrs)	N ₂ flowrate & Carbon [Ⓞ]	Main CRN Products	Intermediate CRN Phases
lab reagents (Mitomo <i>et al.</i>)*	0.5g	1450	16	N ₂ = ? C = 120%	Ca- α -sialon (85 wt%), β -Si ₃ N ₄ / (β')	SiO ₂ mullite Si ₂ N ₂ O
laboratory reagents (Van Rutten <i>et al.</i>)	10ml	1500	65	N ₂ = 12.5l/hr C = 100%	Ca- α -sialon (>95%),	SiO ₂ Si ₂ N ₂ O/O' β -sialon 12H, 21R
laboratory reagents (Hotta <i>et al.</i>)	?	1450	2	N ₂ = 30l/hr C = 120%	Ca- α -sialon (85 wt%), AlN	Si ₂ N ₂ O
fly ash waste (Kudyba-Jansen <i>et al.</i>)	30-300g	1500	25 ^Δ	N ₂ = 35l/hr C = 100%	Ca- α -sialon (51-64 wt%), ^Δ β -sialon	β -sialon 12H, 21R
halloysite clay & talc (Qiu <i>et al.</i>)	?	1475	4	N ₂ = 42l/hr C = 100%	Mg- α -sialon (90 wt%), 15R, SiC	Si ₂ N ₂ O SiC MgSiN ₂ X-phase β -sialon

* These results are for the Ca- α -sialon system

? = not specified.

[Ⓞ] Percentage as a function of the stoichiometric amount of carbon defined by the proposed CRN equations.

^Δ Extending the time to 50 hours boosted the α' content to >90%.

Other significant findings include:

- The amount of Ca- α' formed is highly dependent on both thermodynamics (reaction temperature) and reaction kinetics (time). In some systems, increasing the CRN temperature from 1450°C increased the yield of α' , however SiC starts to be a thermodynamically favourable CRN product at ~1500-1550°C. Reaction for longer times, or a two-stage process of CRN at 1450°C followed by heat-treating the CRN powder at a higher temperature, can improve the yield of α' .
- The CRN reaction process is seen to involve a complex series of solution-precipitation steps involving liquid formed from the molten reactants. Oxide and oxynitride phases

such as $\text{Si}_2\text{N}_2\text{O}$ or O-sialon, AlN-polytypoids and β -sialon are the first phases to form, followed by α' . The α' -plane from the phase behaviour diagram (Figure 2.4) shows that β' and AlN/AlN-polytypoid phases can exist in equilibrium with α' , and these phases are commonly seen to be secondary phases remaining in equilibrium with the α' product after CRN.

- Fly ash wastes were not as effective as laboratory-grade reagents in forming single-phase Ca- α -sialon. The yield of α' from fly ash may be increased by heat-treating the powders at temperatures above 1500°C.
- Seeding the sample with a few percent Si_3N_4 seeds may significantly increase the yield of α' produced.
- No real attempt has been made to densify the CRN- α' powders and evaluate their mechanical properties.

2.4 Slag-Based α -Sialons

Steelmaking slag is an inexpensive raw material suitable for α -sialon production via CRN. It generally has a composition rich in CaO, SiO_2 , and Al_2O_3 , which are all Ca- α -sialon forming compounds. Slag is formed during the reduction of iron ore to metallic iron. Limestone (CaCO_3) is added to the blast furnace to act as a flux to combine with impurities in the iron ore; it decomposes above $\sim 850^\circ\text{C}$ to form CaO, which then reacts with impurities such as SiO_2 , Al_2O_3 , and MnO to form slag. The molten iron and slag are tapped off separately, and the slag is quenched and crushed (McTigue 1982). Approximately 300kg of slag is formed for every ton of steel produced in blast furnace in Australia, which presents a significant storage problem (ASA 2003). The slag is generally piled up in 'slagheaps', which are potentially hazardous to the local environment through dispersal of fine particles by wind, or leaching of compounds into the soil and groundwater. Slagheaps also require considerable financial investment in land and facilities for storage and handling.

Currently, vitrified slag is most commonly used in low value-added applications such as an additive in concrete, or as a filler and stabiliser in roads and pavements (ASA 2003). More recently, there has been some research effort aimed at finding more value-added applications, such as glazes for commodity wall and floor tiles for the building industry (Ghosh, Das, *et al.* 2002; Piore and Piore 2003). The potential for converting this slag into an even higher value-added engineering ceramic, may present both economic and environmental advantages.

The following section presents the results of a preliminary study on the production of α -sialon from slag via CRN, followed by a description of a recent development that produces α -sialons from slag via a rapid combustion process.

2.4.1 Preliminary Work on the CRN formation of Ca- α -Sialon from Slag

A preliminary study was performed in 1997 by David Walker, a final year undergraduate student at the School of Physics and Materials Engineering at Monash University (formerly the Department of Materials Engineering) to establish the feasibility of producing α -sialon from slag via CRN. Little detailed information regarding the CRN process was produced from this study, with much of the attention focused on overcoming various difficulties encountered with the operation of the reaction furnaces and specimen preparation techniques. Eventually a predominantly Ca- α -sialon powder was successfully produced, and some basic conditions for success were identified which have informed the current investigation, and are described here (Walker 1997).

Due to the slag being CaO-rich and thus not containing a high enough proportion of Si or Al for α -sialon, a kaolinite clay (54 wt% SiO₂, 45 wt% Al₂O₃) was added to adjust the composition to more closely match that required for α -sialon production. A two-stage process based on Equations 2.13a and b, was assumed to occur, and balanced stoichiometric equations were developed to produce a Ca- α -sialon with a predicted $m=3.6$, $n=1.8$. Firing was performed at 1450°C for 12 hours under various N₂ flowrates. The main findings from this study were:

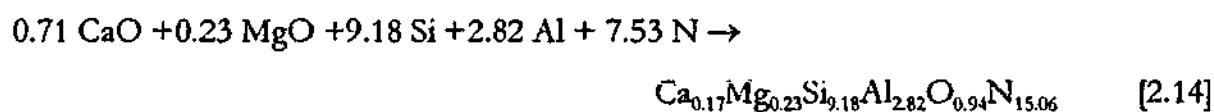
- α -Sialon containing powders could be produced from the slag and clay mixtures, however large amounts of secondary phases remained in the products. These were designated \star -phase (erroneously identified as CaAlSi₃N₄) and Δ -phase, which remained unidentified.
- Carbon in excess of that required to balance the assumed reaction stoichiometry was required to increase the yield of α -sialon, with 25 wt% of the overall batch mix deemed optimum.
- Nitrogen penetration of the pellets was important. High flow-rates of 30 l/hr were most favourable to α -sialon formation, and reducing the density of the powder compact by not using polymeric binder appeared to increase the yield of α -sialon.

- The addition of ~10 wt% Si₃N₄ powder to seed the samples increased the proportion of α-sialon at the expense of the ★ and Δ impurity phases.

The preliminary study proved that the production of α' from slag is feasible, however only one composition was investigated, and no detailed information regarding the reaction process was obtained.

2.4.2 SHS of Slag to Form α-Sialon

A recent advance while undertaking this project has been the use of self-propagating high-temperature synthesis (SHS) to form α-sialon from slag. This work was performed by Chen and co-workers at the Shanghai Institute of Ceramics, in collaboration with Monash University (Chen, Wang, *et al.* 2002). For the SHS process, slag was mixed with pure Al and Si metal powders to both adjust the composition and provide fuel for the reaction. The mixture was placed in a graphite crucible with a layer of Ti metal powder placed on the top, which was then placed in a sealed vessel under a high pressure (50 MPa) of N₂. A tungsten coil was used to ignite the Ti powder and induce the Al and Si metal powders to violently combust, starting an exothermic, self-sustaining reaction that reached over 2000°C and proceeded through the powder compact in seconds. The overall equation describing this process is:



SHS produced essentially pure, single-phase α-sialon, but with a considerably non-uniform morphology and particle size ranging from fine, submicron grains to large, 10 μm irregular particles. Such inhomogeneity was a result of the very rapid and complex gas-phase reactions that occur during SHS. Both Ca²⁺ and Mg²⁺ cations were found to be stabilising the single-phase α' product, a feature difficult to obtain via reaction sintering or CRN, but which was assisted here by the very high temperature (>2000°C) providing greater diffusivity to the gas-phase and liquid-phase reactants. A small amount of glass was also expected to be present in the products.

The very rapid, high-temperature process produced an α' product that was metastable and underwent phase transformations during sintering (Jin and Guo 2003). The SHS-α' powder partially decomposed to β-sialon and glass when hot-pressed at temperatures >1450°C. The extent of decomposition, however, was found to be less than that for (Ca,Mg)-α-sialons produced via the SHS of laboratory reagents (SiO₂, CaO, MgO etc). The addition of 10 wt%

slag or CaCO_3 to the SHS powder as a sintering aid provided glass-forming species to the system, thereby prevented the α' from decomposing into glass and β -sialon.

The SHS process offers some potential advantages over CRN: it is a fast, high-volume, low energy process; contaminants may be volatilised by the high temperatures produced; and a single-phase α' material may be formed where it was not possible using conventional sintering. However, this process is very difficult to control due to the highly exothermic nature of the reaction and the extremely rapid reaction rate. The main parameters for process control are compositional, and due to the dual role of the Al and Si metal powder in providing fuel for combustion and providing the species for α -sialon production, the range of compositions able to be fabricated by this method will be limited by the SHS process requirements. The wide inhomogeneity of the α' powder, the metastability of the α -sialon formed and the need to use a sintering aid for densification introduces additional complexity to the production of homogenous, stable, bulk materials from this powder.

Despite the longer reaction times, the CRN process may afford a much higher degree of process control, allow a broader range of starting materials and compositions to be used for α' production, and produce stable α -sialon powders that do not decompose during sintering. Therefore a detailed investigation into the production of α' from slag and clay mixtures is warranted, investigating not only the α' -forming CRN reaction processes but also the fabrication and evaluation of bulk materials from this CRN- α' powder. This is the aim of this thesis.

Chapter Three

Experimental Procedure

This chapter describes the experimental procedures used during the work undertaken for this thesis. The specifications of the raw materials are given in Section 3.1, composition selection and fabrication methods are detailed in Section 3.2, and the firing schedules for CRN are given in Section 3.3. Section 3.4 describes the various analytical methods used.

3.1 Raw Materials

The chemical compositions of the four main minerals slag, clay-K, clay-P, and sand, are summarised in Table 3.1 from data provided by the manufacturers.

3.1.1 Slag

The slag used in this investigation was supplied from Steel Cement Ltd. (now Independent Cement and Lime). It originated from BHP's Port Kembla steelworks, and is a ground, granulated iron blast-furnace slag, which has been tapped off from the furnace, quenched in water and then crushed to a fine powder. Approximately 5% gypsum ($\text{CaSO}_4 \cdot 2\text{H}_2\text{O}$) was added by the cement company for its intended application in cements. Gypsum dehydroxylises upon heating at $\sim 200^\circ\text{C}$ to form anhydrite (CaSO_4) which decomposes at $\sim 1020^\circ\text{C}$ (Grimshaw 1971).

The composition of the slag is given in Table 3.1. When calculating the molecular weight of the slag, the 2.17 wt% of unquantifiable 'others' was not included, resulting in a molecular weight of 62.55 g/mol. The slag is processed on site by the cement manufacturer and not sold as a regular commodity *per se*, but it is considered to have an approximate cost of \$90/ton (ICL 1999).

3.1.2 Clay-K (Kaolinite)

The kaolinite-based clay used in this project was Clay HR1-F, from Commercial Minerals Ltd. A chemical breakdown is given in Table 3.1. In addition to kaolinite, 17.6 wt% of the total silica is present as SiO_2 quartz. From the data supplied, its molecular weight was calculated to be 69.75 g/mol. The cost of clay-K is \sim \$450/ton (quoted for a one-off purchase of 1 ton (Unimin 2003)).

Table 3.1 Chemical composition and approximate cost of minerals (slag, clays, and sand) used for CRN.

Compound	Slag ICL (wt%)	Clay-K CM - HRI-F Kaolinite (wt%)	Clay-P CM - PPPG/300 Pyrophyllite (wt%)	Sand Pilkington (wt%)
SiO ₂	33.06	53.3	76.7	99.7
Al ₂ O ₃	12.94	30.3	17.9	0.1
CaO	39.46	0.2		
MgO	6.19	0.2		
Na ₂ O	0.88	0.2	0.2	0.04
Fe ₂ O ₃	0.18	1.2	0.4	0.029
TiO ₂	0.44	2.6	0.2	0.04
K ₂ O	0.37	0.5	1.2	
P ₂ O ₅	0.06			
MnO	0.44			
SO ₃	3.22			
BaO	0.14			
S ²⁻	0.45			
H ₂ O	-	11.4		1.2
Others	2.17		(LOI) 3.8%	
<i>Mw (g/mol) [calculated]</i>	62.55*	69.75	64.34*	60.08
<i>Approx. Cost per ton (AUD\$)</i>	\$90 ^a	\$450 ^b	\$450 ^b	\$10 ^c

* Note that the unquantifiable molecular weight of 'others' or LOI have not been included in this calculation.

^a Estimate of cost, not usually sold as a commodity (ICL 1999).

^b cost quoted for one-off shipment of 1 ton (Unimin 2003).

^c bulk order cost to glassmaker (Pilkington 1999); one-off shipment cost = \$100 (Unimin 2003).

3.1.3 Clay-P (Pyrophyllite)

The pyrophyllite used in this project was supplied by Commercial Minerals Ltd (now Unimin Australia, Ltd), product code PPPG/300. The composition is given in Table 3.1, and 5.1% of the SiO₂ is present as quartz. Its calculated molecular weight is 64.34g/mol, excluding the loss on ignition (LOI). The cost of clay-P is similar to that of clay-K, ~\$450/ton.

3.1.4 Sand (Quartz)

Glassmaking sand supplied by Pilkington Ltd. was used as a source of essentially pure SiO₂. Initially the sand had a particle size of ~1mm, and was aggressively ball milled for 72 hours to reduce the particle size, with the largest particles subsequently being ~300µm. BET analysis

showed it to have a surface area of $0.46 \text{ m}^2/\text{g}$. The cost of sand was quoted as \$90 /tonne for a single shipment of 1 ton (Unimin 2003), however this cost can be as low as $\sim \$10/\text{ton}$ under long-term contract (Pilkington 1999).

3.1.5 Carbon-Black

The standard carbon-black used as a reducing agent was ACB chemicals Tintacarb 130. BET analysis showed it to have a surface area of $121 \text{ m}^2/\text{g}$.

3.1.6 Silicon Nitride

$\alpha\text{-Si}_3\text{N}_4$ powder was used to seed the samples. The powder used was HCST grade M-11, with the $\alpha\text{-Si}_3\text{N}_4$ content determined to be 91.3%, and the remaining 8.7% being $\beta\text{-Si}_3\text{N}_4$. The mean particle size is $0.65 \mu\text{m}$.

3.1.7 Nitrogen Gas

High Purity N_2 from BOC gases was used as the nitrogen source in all furnaces. The oxygen content was $<10\text{ppm}$, and moisture $<12\text{ppm}$.

3.2 Composition Selection and Specimen Preparation

This section will present the selection criteria and nomenclature relating to the main compositions created and investigated in this study.

3.2.1 K-Series: Composition Range Testing

The first series of compositions tested were mixtures of slag and clay-K, (kaolinite). A Microsoft Excel spreadsheet was developed to calculate the required amounts of reagents based on three user variables: slag:clay-K molar ratio, desired total batch mass, and Si_3N_4 seed addition in wt%. The calculated molar weights listed in Table 3.1 were used for this calculation.

A series of 12 compositions was selected with varying slag:clay-K molar ratio, from 0.10:1 to 3.28:1, to test the compositional limits of the CRN process. The 12 specific compositions investigated are listed in Table 3.2. This series was designated as the K-series, and each individual composition uses the nomenclature Kxx, where xx is a two digit suffix indicating 10x the slag:clay-K ratio, rounded to 2 significant figures. For example, the 3.28:1 slag:clay-K composition is referred to as K33, and 0.19:1 as K02.

The carbon content was fixed at 25 wt% of the total batch mass, the level found to be most successful from the preliminary study by Walker (1997). The amount of α - Si_3N_4 added to 'seed' the samples was based on findings from the preliminary investigation and the assumption that the Si_3N_4 seeds interact solely with SiO_2 during CRN. Hence the quantity of Si_3N_4 was pegged to 20 wt% of the SiO_2 content of each composition, rather than being a simple proportion of the total batch mass. Since the slag contains less SiO_2 than the clay, the amount of seeds decreases slightly from 7.75 wt% to 5.42 wt% as the slag content of the compositions increases. Details of the K-series compositions are given in Table 3.2. The Si_3N_4 addition was not counted as part of the target batch weight but as an additional component.

Table 3.2 Slag:clay-K molar ratio of K-series compositions and seeding content for K-series compositions

Composition	K01	K02	K03	K05	K06	K07	K09	K10	K14	K19	K26	K33
slag/clay-K (moles)	0.10	0.19	0.34	0.47	0.62	0.73	0.88	1.00	1.42	1.93	2.55	3.28
% Si_3N_4 seeds	7.75	7.55	7.29	7.10	6.91	6.79	6.66	6.56	6.30	6.07	5.88	5.73
wt% C	25	25	25	25	25	25	25	25	25	25	25	25

A total powder mass of 15g of each composition was initially prepared for this series. The relevant amounts of the four reagent powders (slag, clay-K, carbon-black, Si_3N_4) were weighed out to $\pm 0.1\text{mg}$, then added to an agate mortar and pestle and mixed with isopropanol to form a slurry which was hand mixed continuously for 20 minutes. The isopropanol was evaporated in a drying oven overnight, and the dried powder briefly reground in the mortar and pestle for two minutes to counter any possible settling effects and to break up aggregates.

Approximately 1.5g of powder was transferred to a 1cm diameter cylindrical steel die. The powder was uniaxially pressed in two stages, holding briefly at $\sim 10\text{MPa}$, followed by several minutes at $\sim 15\text{MPa}$. This produced a cylindrical pellet roughly 1cm high. One pellet was placed in the centre of a 10cm long, high-purity Al_2O_3 boat for firing according to the firing schedule presented in Section 3.3.1.1.

3.2.2 K-Series: Intermediate Reaction Product Testing

Three compositions (K06, K10, and K19) were chosen for a more detailed investigation of the intermediate phases formed during firing. For these experiments a greater quantity of the

batch powder was produced, totalling 40g, which necessitated the use of ball milling rather than hand mixing. The measured powders were placed into 600ml polyethylene jars into which 150ml isopropanol and 300g of Si_3N_4 milling balls were added. These were then placed onto a rotary mill for 12 hours, after which the powder and milling media were separated and the powder placed in a drying oven overnight. The powder was then reground briefly by hand in a mortar and pestle to counter any settling effects and break up aggregates.

Difficulties previously experienced when compacting the powders were attributed to excessive pressure, thus the pressing procedure was altered such that approximately 1.5g of powder was uniaxially pressed in the 1cm die at a maximum of 10 MPa. Pellets were fired in an Al_2O_3 boat following a variation to the standard firing schedule as detailed in Section 3.3.1.2.

3.2.3 P-Series: Pyrophyllite-Based Compositions

Three compositions of interest from the K series, K02, K06, and K15, were chosen to be emulated using clay-P, the higher Si-containing, pyrophyllite clay. A spreadsheet was created to determine the amount of clay-P required to provide the same overall SiO_2 content found in the equivalent K-series compositions. Carbon-black was unchanged at 25 wt%. The seeding addition was set at a uniform 6.3 wt% Si_3N_4 across all three compositions, this being the average seeding level used in the K-series compositions. Following the nomenclature established for the K-series, the three P-series compositions are designated P02, P08, and P20, reflecting 10x the slag:clay-P molar ratio.

Wet mixing and drying of the powders proceeded as detailed in Section 3.2.2. Firing proceeded as per the standard firing schedule described previously, but with one main alteration: loose powders were fired instead of uniaxially pressed pellets. It was discovered by this stage that minimising the density of the powder compacts enhanced nitridation, hence uniaxial pressing was seen as an unnecessary complication. Approximately half a teaspoon (~1.5g) of powder was simply placed in the centre of the boat, forming a small heap.

It was discovered that a longer time of 18 hours of firing was required for CRN in these samples, thus in all future experiments involving these compositions, the standard CRN condition was firing at 1450°C for 18 hours, not the standard time of 12 hours.

3.2.4 S-Series: Sand-Based Compositions

The same three K-series compositions chosen for emulation using pyrophyllite (K02, K06, K15) were chosen for emulation using sand as SiO_2 source. A modification to the spreadsheet described above was used to calculate the required amounts of slag and sand to maintain the

same overall SiO_2 content as the base compositions. These compositions are designated S03, S10, and S24, reflecting 10x the slag:sand molar ratio. The carbon-black content remained unchanged at 25 wt% of the batch. The seeding level of these compositions was raised to 10 wt% Si_3N_4 for all three compositions due to a perceived need for increased assistance via seeding.

3.2.5 Effect of Firing Parameters

3.2.5.1 Specimen Density and Geometry

To test the effects of powder compaction on the CRN process, four samples of K06 powder were prepared using different pressing pressures. These were: a) a heap of loose powder spooned into the Al_2O_3 boat with no additional pressure; b) a pellet pressed by firm hand pressure on the 1cm diameter cylindrical die plunger; c) a pellet pressed according to the standard conditions of 10 MPa hydraulic pressure in the 1cm diameter die; and d) a 1cm diameter pellet hydraulically pressed at 10 MPa and then cold isostatically pressed (CIP-ed) at 200 MPa.

Later experiments involved filling the 10cm long, 25mm wide and 15mm deep boats with powder. A light tamping-down of the powder was performed with a flat tool to prevent the fine powder from being carried down the furnace during pre-firing evacuation and allow more powder to be placed in the boat.

3.2.5.2 Seeding

A batch of the K06 composition but without any Si_3N_4 seeds added was prepared via wet mixing as described in Section 3.2.2. Si_3N_4 powder was mixed into this seedless powder by hand in a mortar and pestle to test the effects of seeding. The amount of seeds added corresponded to 2 and 23 wt%.

3.2.6 High-Temperature Phase Behaviour

Powders from the K02, K06, K33, P02, and P08 compositions were wet mixed (Section 3.2.2) and reacted for CRN according to the process detailed in Section 3.3. Some heat-treatments required the removal of residual carbon-black from the CRN powders, which was performed via an oxidation heat-treatment in a muffle furnace in air at 650°C for 2 hours. Pellets were also pressed from these CRN powders by uniaxial pressing in a 1cm die under 40 MPa pressure. The high-temperature furnace used for these experiments is described in Section 3.3.2, and the specific firing conditions used are given in Chapter 6.

3.2.7 Microstructure and Property Evaluation

The four compositions of interest were K06, K33, P02, and P08. Powders were mixed and reacted for CRN following the procedures detailed in Sections 3.2.2 and 3.3. Hot-pressing proceeded according to the procedure given in Section 3.3.3 to produce dense samples for hardness, toughness, and erosion resistance testing.

3.3 Furnaces and Firing Schedules

3.3.1 Nitridation Furnaces and CRN

Two nitridation furnaces were utilised in this investigation for the CRN reactions, a Lindberg model #54434 using MoSi_2 heating elements, and a model #54233 with SiC heating elements. Other than the type of heating element used, the features on the two furnaces and the operating procedures were essentially the same. Both utilised a 48mm internal diameter high purity (99.9%) Al_2O_3 tube to which a vacuum evacuation and a gas flow system was attached to allow control over the furnace atmosphere. Both furnaces had a 'hot zone' 10cm in length, with the maximum temperature attained in the centre of the zone, and a drop of no more than 5°C at the ends 5cm away.

Initially, high-purity Al_2O_3 boats were used to contain the samples. However these appeared to react with the samples and rapidly became unusable, thus graphite boats were used for later experiments. The dimensions of the boats were 10cm long, 25mm wide, and 15mm deep. Single specimens (either pellets or loose powders depending on the experiment to be performed) were placed in the centre of the 10cm boats to coincide with the centre of the furnace hot-zone. The loading and unloading of the specimens took place with the furnaces held at 400°C . This temperature was selected to minimise unnecessary thermal cycling of the heating elements and to avoid the potential for oxidation of the carbon-black in air at temperatures $>500^\circ\text{C}$.

The operating procedures for the furnaces stipulated a maximum allowable heating ramp rate of $5^\circ\text{C}/\text{min}$ for temperatures below 800°C , and $3^\circ\text{C}/\text{min}$ above 800°C to avoid thermal shock of the alumina tube. The maximum ramp rates were used at all times.

3.3.1.1 Standard CRN Firing Schedule

The standard firing schedule for all CRN experiments, unless otherwise specified, is shown schematically in Figure 3.1, and is detailed as follows:

- i. The boat was slowly advanced to the hot zone via a pushrod such that the centre of the boat was located in the centre of the hot zone.
- ii. The tube was sealed and evacuated by means of a rotary pump to $<5 \times 10^{-2}$ torr, flushed with N_2 gas and re-evacuated. This flush was repeated twice to ensure no air remained.
- iii. The tube was then backfilled to atmospheric pressure with N_2 gas and set flowing at a rate of 30 litres/hr using a calibrated flowmeter.
- iv. The furnace control program was started, the furnace heating up at the maximum allowable ramp rates of $5^\circ\text{C}/\text{min}$ to 800°C and $3^\circ\text{C}/\text{min}$ to 1450°C .
- v. The furnace was held at 1450°C for 12 hours for completion of the CRN reactions.
- v. The furnace was then cooled at $3^\circ\text{C}/\text{min}$ to 800°C then $5^\circ\text{C}/\text{min}$ to 400°C . Nitrogen gas flow was maintained throughout the cooling period.
- vi. N_2 gas was turned off, the samples slowly removed from the tube and air cooled to room temperature.

Where carbon was removed after CRN, a separate oxidising heat treatment was performed in a muffle furnace at 650°C in air for 2 hours.

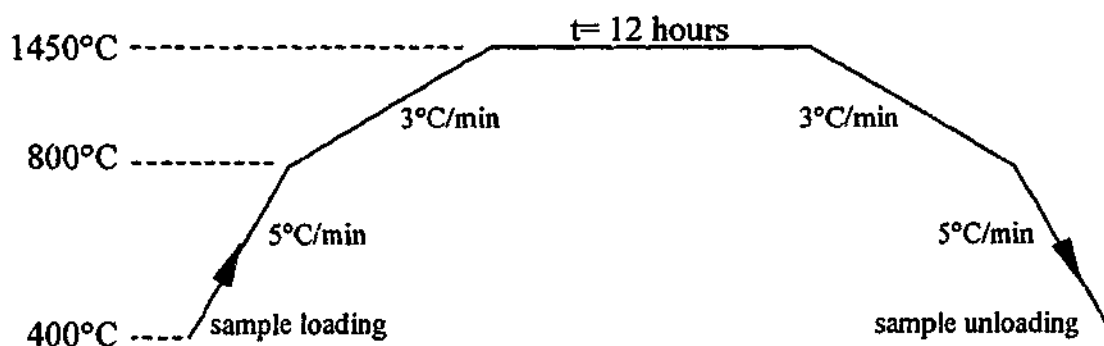


Figure 3.1 Standard firing schedule.

3.3.1.2 Determination of Intermediate CRN Reaction Products

For the series of experiments in Section 4.3 investigating the intermediate reaction processes, the CRN firings were programmed to interrupt the standard schedule at various intermediate

points. For temperatures below 1450°C, the samples were held for 1 minute at the desired temperature before cooling the furnace as usual. At 1450°C, the pellets were held for various times of 1min, 30min, 3 hrs, 12hrs, and in the case of K10, 6hrs. A schematic of these firings is given in Figure 3.2.

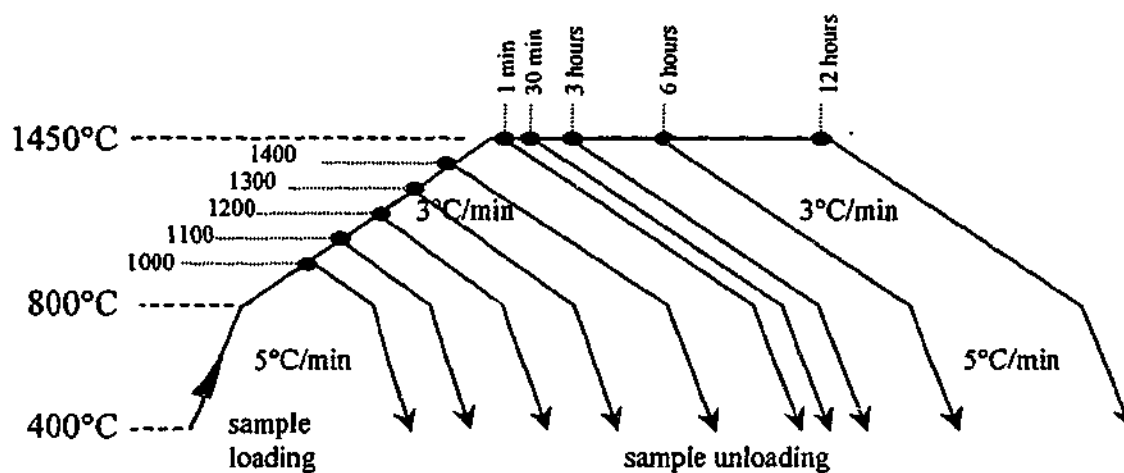


Figure 3.2 Firing schedule for determining the intermediate reaction products.

3.3.2 High-temperature Furnace

A Thermal Technology Labmaster Model 1000-4560-FP20 graphite resistance furnace was used for experiments at temperatures $>1450^{\circ}\text{C}$ detailed in Chapter 6. Samples were pre-loaded in graphite crucibles, the furnace evacuated and flushed with N_2 , and heated at a rate of $30^{\circ}\text{C}/\text{min}$. A pyrometer focused on the graphite crucibles was used to determine the temperature. The furnace was held under vacuum up to 900°C at which the point furnace was backfilled with N_2 gas and a slight positive pressure of N_2 gas set flowing to prevent oxidation of the graphite elements. The furnace was cooled at its natural rate by switching off the power after the desired dwell time was reached.

Firing was performed both without and with packing powder to separate the samples from contact with the graphite crucible. Loose CRN powders and uniaxially pressed pellets were placed in small graphite crucibles 20mm in diameter, 20mm high, and 2mm thick for firing without packing powder. Alternatively, a large graphite crucible 80mm in diameter, 75mm high, with 5mm thick walls and lid was filled to 10mm below the top with a packing powder comprising of 45 wt% BN, 45 wt% Si_3N_4 , 10 wt% SiO_2 and a teaspoon of slag. The pellets

embedded within the crucible such that they were at least 10mm away from the crucible floor and walls.

3.3.3 Hot-pressing

A Thermal Technology Laboratory Hot-press Group 1400 Model HP20-4560-20 with a 1 inch graphite die was used to densify the CRN powders. The powders were first uniaxially pressed at 10 MPa to form 1 inch pellets, and then the diameter was reduced by manually grinding the circumference of the pellets on SiC papers to allow easier entry to the die. The die parts were coated in BN to prevent sticking by mixing BN and ethanol into a paste, painting it on the parts and allowing the ethanol to dry off. BN was also used as a packing powder, with 1 teaspoon of BN placed above and below the pellets in the die, and packed as tightly as possible between the pellet and the die wall to avoid expansion of the pellet.

Heating started at a rate of 30°C/min, using a pyrometer to determine the temperature. The furnace was held under vacuum up to 900°C at which point furnace was backfilled with N₂ gas and a slight positive pressure of N₂ gas set flowing to prevent oxidation of the graphite elements. The pressing pressure was applied once the furnace reached 1300°C and slowly increased to 20 MPa. The sample was held under pressure at 1700°C for 1 hour. The furnace was cooled at its natural rate by switching off the power. On cooling the pressure was maintained to 1200°C.

3.4 Analytical Techniques

Various analytical techniques were used during this investigation. This section will describe the salient features of the apparatus and the methodologies used for analyses.

3.4.1 XRD

In most cases the samples after firing were in a powder form, and although some cohesion was sometimes found in the pelletised samples, powder could be collected for analysis by scraping with a spatula. The collected powder was placed into a small agate mortar and pestle, ethanol was added to form a slurry, and the powder was intensively ground by hand until the slurry was smooth. Drops of the slurry were then placed onto a glass microscope slide using a pipette such that the coating on the slide was opaque, thus ensuring sufficient film thickness to prevent sampling from the glass substrate. The sample was allowed to dry naturally at room temperature.

Two x-ray diffractometers were used in this investigation:

- a Rigaku X-ray diffractometer using a 40kV, 22.5mA beam, $\frac{1}{2}^\circ$ divergence and antiscatter slits, 0.3mm receiver slit, a Cu source and Ni filter, or
- a Philips X-ray diffractometer using a 40kV, 25mA beam, 1° divergence and antiscatter slits, 0.1mm receiver slit, a Cu source and graphite monochromator.

Scan conditions for phase identification were usually $1^\circ/\text{min}$ in steps of 0.04° over a 2θ range of $10\text{-}80^\circ$.

3.4.1.1 Phase Content Analysis

An estimate of the phase content in the samples was obtained from the scans using TRACES[®] Peak Analysis software (Version 6.0, Diffraction Technology Pty. Ltd). Accurate quantitation of the phase content was not possible due to the difficulty in maintaining constant conditions between the different XRD apparatus used, the large variations in specimen composition, and the extremely high level of peak convolution in many of the spectra. Solely for comparative purposes, it was possible to approximate the phase content using peak heights, based on a grading system for the XRD peak intensity. The categories were: strong ($>80\%$), medium strong (60-80), medium (45-60), medium weak (30-45), weak (10-30%) very weak ($<10\%$) intensity. The strongest characteristic peaks were used for this analysis. A quasi-quantitative analysis of the relative amounts of α' and E' phases based on XRD peak intensity was developed for use in Chapter 6, and will be described in detail in Section 6.1.1.

3.4.1.2 Determination of Ca-content in α -Sialon

The α -sialon m- and n- values define the amount of substitution of Al^{3+} and O^{2-} into the α - Si_3N_4 structure according to the formula:



It has been shown that these values can be calculated from the lattice parameters of the α -sialon unit cell according to Equations 3.2a and b (van Rutten, Hintzen, *et al.* 1996).

$$a (\text{\AA}) = 7.749 + 0.0023n + 0.0673m \quad [3.2a]$$

$$c (\text{\AA}) = 5.632 - 0.0054n + 0.0550m \quad [3.2b]$$

For increased precision, the lattice parameters were determined via a slow scan on the XRD using a small amount of ThO_2 powder mixed in with the CRN powder to act as an internal standard. Scans were performed at $0.2^\circ/\text{min}$, with a step size of 0.02° . The lattice parameters were calculated from the peak positions on the XRD traces using the CELLSIZ program (Scott 1986).

3.4.2 DTA

Differential thermal analysis (DTA) was performed using a Rigaku Thermoflex DTA apparatus to identify phase changes in the system during heating. A heating rate of $20^\circ\text{C}/\text{min}$, a maximum temperature of 1100°C , and a chart speed of $2.5\text{mm}/\text{min}$ were determined to be optimal for these materials. A straight baseline was generally not obtained on this apparatus, however the peaks corresponding to structural events were clearly observable. These scans were performed in air.

3.4.3 TGA

Thermogravimetric analysis (TGA) was performed to determine the residual carbon content of samples after CRN. The apparatus used was a SETARAM TG92, and scans were run in an atmosphere of flowing air using a heating rate of $10^\circ\text{C}/\text{minute}$.

3.4.4 Optical Microscopy

An Olympus PMG3, reflected light microscope was used for preliminary microstructural imaging. Images were recorded digitally.

3.4.5 SEM

Scanning electron microscopy (SEM) was used for morphological analysis of the powders and sintered samples.

Two SEMs were used:

- a JEOL JSM840A using a tungsten element and fitted with an Oxford EDXS detector with an ultra-thin aluminium/mylar window. Images were recorded either digitally or on photographic film. EDXS spectra were obtained over a 100s live time, using a voltage of 20kV.

- A JEOL JSM6300F using a cold field emission gun (FEG) and fitted with an Oxford EDXS detector with an ultra-thin aluminium/mylar window. Images were recorded digitally. EDXS spectra were obtained over a 100s live time, using a voltage of 15kV.

3.4.5.1 Powder Sample Preparation

Powder specimens were prepared by ultrasonically dispersing the powder in ethanol and transferring a small amount of the suspension via a pipette onto a brass stud. The ethanol was allowed to evaporate and the brass stud was stuck to an aluminium baseplate using conductive carbon tape or carbon paint. The surface was sputter-coated with a layer of carbon to provide electrical conductivity.

3.4.5.2 Thermal Etching of Densified Pellets

The various Ca-Si-Al-based phases in this system produce little contrast in the SEM. Therefore the surfaces were etched in molten NaOH to remove the grain boundary glass and highlight the grain morphologies.

First, polished surfaces of the densified pellets were prepared for etching by grinding on successively finer SiC papers down to 120 grade, followed by 3 μ m and 1 μ m polishing using diamond paste on a cloth lap. NaOH granules were placed in a Ni crucible and heated over a Bunsen burner until the molten NaOH solution was clear and free from bubbles, corresponding to >400°C. The polished surfaces were immersed in the molten solution and held for 10s after the first appearance of bubbles around the pellet edge; this is an indicator that etching is proceeding effectively. After removal from the etchant, the samples were immediately rinsed under running water for at least 10 minutes. The samples were then mounted on Al discs using carbon paint, and sputter-coated with a conductive layer of carbon.

3.4.6 TEM

Transmission electron microscopy (TEM) was used to allow a more detailed examination of the K06 sample's microstructure. The TEM used was a Philips CM20 running at 200kV and fitted with an Oxford EDXS detector with an ultra-thin aluminium/mylar window. EDXS spectra were collected for qualitative analysis operating in nanoprobe scanning mode with a 5nm nominal beam width and a 100s live time. The specimens were mounted in a low background double-tilt sample holder.

3.4.6.1 Sample Preparation

A ceramic foil was prepared from the K06 and K33 pellets hot-pressed at 1700°C for one hour via the following method: wafers ~1mm thick were cut out of the pellets using a diamond edged wafering saw. Discs 3mm in diameter were ultrasonically cut from these wafers using B₄C as a cutting medium. These discs were mounted onto brass studs using a mounting wax, and then polished using successively finer grades of SiC paper followed by 3µm and 1µm diamond paste to a thickness of ~250µm, before demounting, reversing and polishing down to a thickness of 100µm. One side was dimpled until the thickness at the bottom of the dimple was less than 20µm, and polished using 1µm paste. The sample was soaked overnight in acetone to fully remove the wax. Final thinning was performed on a Gatan dual beam ion mill using two 0.5A beams of ionised argon under an accelerating potential of 4kV. Discs were rotated during milling, and the impingement angle was 12° for the first 4 hrs, and lowered to 8° thereafter. After perforation, the samples were coated with a thin layer of carbon.

3.4.7 Density Measurement

The bulk density of hot-pressed pellets was determined using the Archimedes principle with water as a medium. Samples were boiled for 1 hour prior to immersion to remove errors associated with the open porosity. The density was calculated using Equation 3.3 (Jones and Berard 1993).

$$\text{Bulk density} = \frac{W_D \times \rho_L}{W_S - W_{SS}} \quad (\text{g/cm}^3) \quad [3.3]$$

where ρ_L is the liquid (water) density

W_D is the dry mass measure in air

W_S is the mass after saturation (boiling) measured in air

W_{SS} is the saturated mass measured while submerged in water

3.4.8 Hardness & Fracture Toughness Measurement

Hardness testing was performed on samples hot-pressed at 1700°C for 1 hour. The pellets were ground and polished flat down to a 1µm finish. Tests were conducted with a Vickers diamond-pyramid indenting device using a load of 10kg. This produced diamond-shaped indentations with cracks emanating from the corners. The length of the indent diagonals (2a)

and the end-to-end distance of the cracks ($2c$) in both directions were measured from 5 indentations made on each of two pellets. The hardness (H_v) and fracture toughness (K_{IC}) were calculated using Equations 3.4 and 3.5 (from Evans and Charles 1976).

$$H_v = 0.1855P/2a^2 \quad (\times 10^7 \text{ Pa}) \quad [3.4]$$

$$K_{IC} = 10H_v\sqrt{a} / 0.15\phi k (c/a)^{-3/2} \quad (\text{MPam}^{1/2}) \quad [3.5]$$

where P is the load in N

a is in mm (for H_v calculation)

\sqrt{a} , a , and c are in meters (for K_{IC} calculation)

$$\phi = 3$$

$$k = 3.2 \text{ if } c/a > 2$$

3.4.9 Erosion Resistance

The specimens used for erosion testing were pellets of K06, K33, P02 and P08 hot-pressed at 1700°C for 1 hour. The pellets were polished on successively finer SiC papers down to 1200 grit. It was not necessary to achieve a mirror finish, as any polished surface layer must be removed before steady-state erosion is achieved.

Erosion resistance testing was performed in a gas-blast type erosion test rig developed by Zhang as shown schematically in Figure 3.3. Abrasive grit is carried by compressed air through the nozzle and blasted onto the densified samples at a chosen angle of incidence. A succession of timed doses is impacted onto the sample, with the sample weighed in between each dose to determine the weight loss. The tests are stopped after several successive doses produce essentially constant weight loss, which corresponds to steady-state erosion of the material.

The abrasive used was a commercial SiC grit (Norton Black), with particles ranging in size between 210 and 500 μm (mean $d_{50} = 388\mu\text{m}$) and irregular in shape. The sample-nozzle stand-off distance was 13.8mm, the particle velocity 20m/s, and tests were undertaken at both 30° and 90° impact angles. The erodent dosage rate was measured to be 210g/min. Mass loss from the target materials was measured on an analytical balance with an accuracy of $\pm 0.1\text{mg}$. For erosion testing the samples were polished down to a 1200 grit finish using SiC paper.

The erosion rate (ΔE) was determined from the steady-state erosion regime, according to Equation 3.6. The cumulative volume loss was calculated by multiplying the cumulative mass loss by the target specimen density.

$$\Delta E = \text{volume loss from specimen} / \text{mass of particles used (m}^3/\text{kg)} \quad [3.6]$$

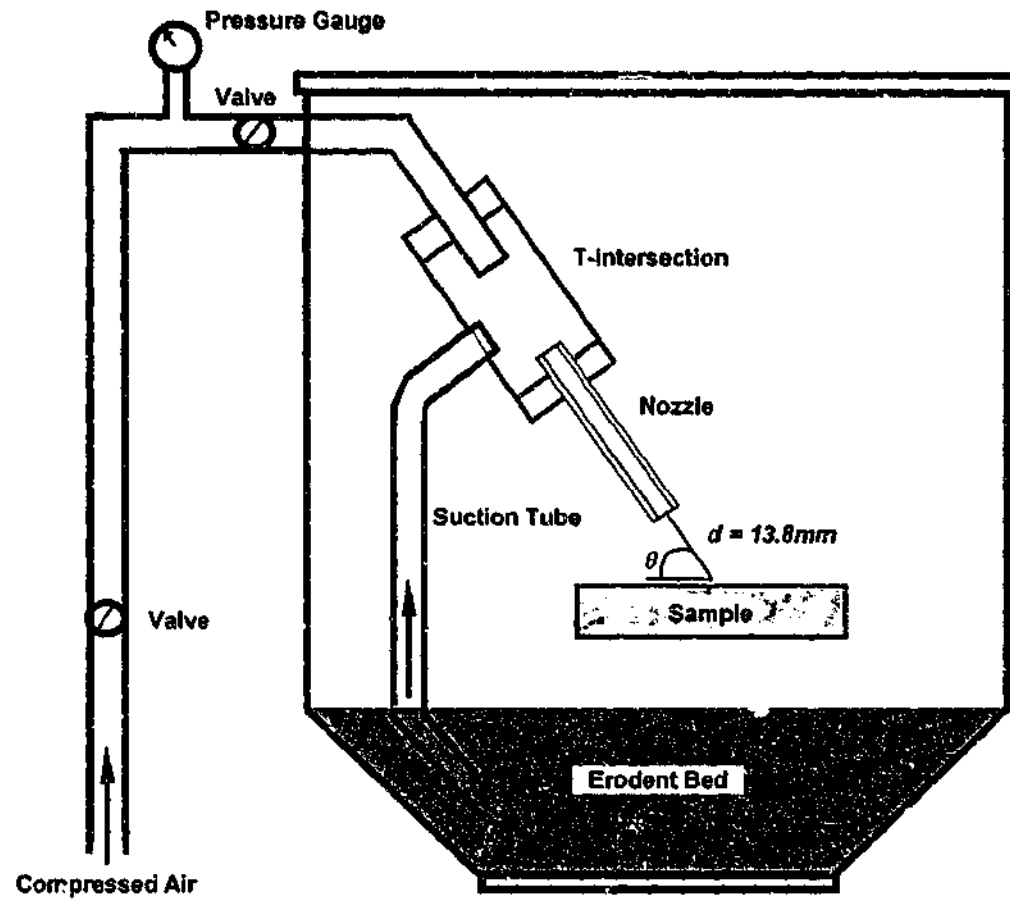


Figure 3.3 Schematic of gas blast erosion rig (after Zhang 2002).

Chapter Four

Fundamental Reaction Processes During Carbothermal Reduction-Nitridation of Slag and Clay Mixtures

The first step in developing the CRN process to produce a bulk α -sialon material from slag and clay is to gain an understanding of the fundamental reaction processes that convert the oxide raw materials into α -sialon. This is the focus of the work presented in this chapter. First, some analyses of the reactants used in this chapter are presented in Section 4.1, followed in Section 4.2 by an investigation of the products of CRN of a range of slag and clay-K mixtures. This will determine the range of compositions over which α -sialon can be produced and allow the identification of successful compositions that will be used in further work investigating and optimising the CRN process. The intermediate CRN reaction products are investigated in Section 4.3 to elucidate the mechanism of CRN in this system.

4.1 Analysis of the Raw Materials

Some chemical and physical properties of the component raw materials as provided by the material suppliers were given in Section 3.1. Additional analyses of the raw materials used in this chapter were performed via x-ray diffraction (XRD) and scanning electron microscopy (SEM) to establish the characteristic signatures of these raw materials before reaction.

4.1.1 Slag

An XRD trace of the slag powder is presented in Figure 4.1. The crystalline peaks correspond to ~5% gypsum ($\text{CaSO}_4 \cdot 2\text{H}_2\text{O}$) that had been added by the manufacturer for the original purpose of slag as an additive in cement. CuK_α radiation was used for all XRD analysis in this investigation, and the amorphous hump at this wavelength lies in the 2θ range of 20 – 30° . The slag XRD trace has a particularly large and distinct amorphous hump, reflecting the amorphous nature of the quenched slag. A micrograph of the powder is shown in Figure 4.2. The sharp angular particles are indicative of glass shattered via quenching and post-quench crushing. A wide particle size distribution is evident, ranging from 2 to $30\mu\text{m}$.

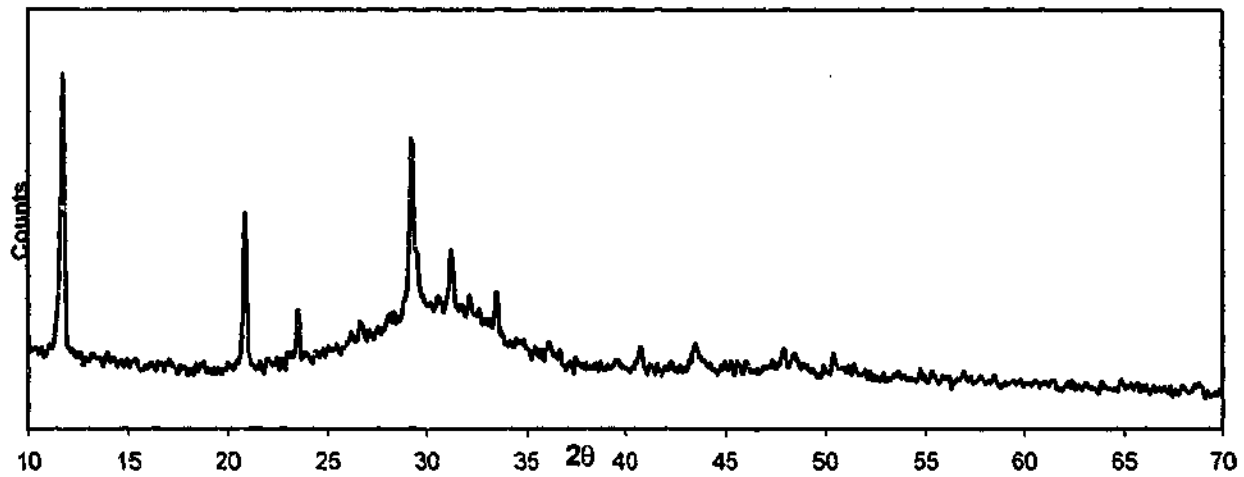


Figure 4.1 XRD trace of slag. All peaks correspond to gypsum ($\text{CaSO}_4 \cdot 2\text{H}_2\text{O}$).

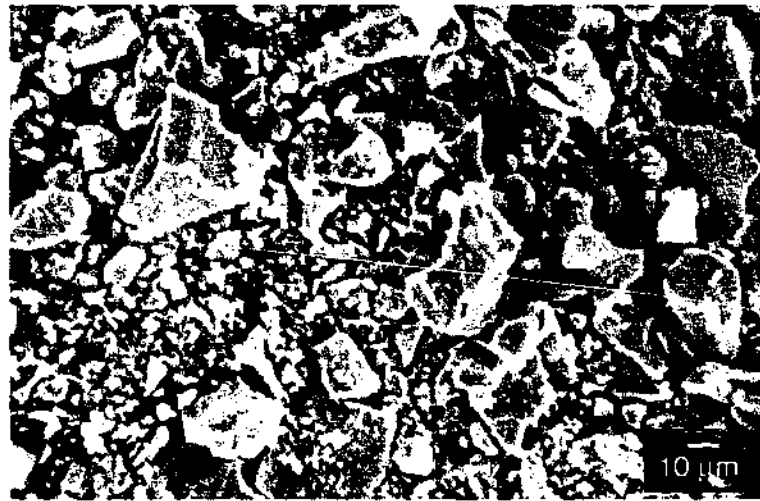


Figure 4.2 SEM micrograph of slag.

4.1.2 Clay-K (Kaolinite)

Figure 4.3 presents an XRD trace of clay-K, with the quartz peaks labelled, and all remaining peaks can be indexed as kaolinite. The quartz signal is very strong and dominates the XRD trace. This is due to the high scattering strength of quartz; being a well-crystallised phase it produces sharp, distinct peaks in clay minerals even when concentrations are $<1\%$ (Brindley and Brown 1984). Clay minerals tend to have thin, poorly crystallised crystals with disordered layer stacking, thus generally produce broad, low intensity XRD peaks.

An SEM micrograph of the clay powder is shown in Figure 4.4. The particles are generally round/hexagonal, flat plates with a particle size around $1\mu\text{m}$. The supplied data sheet states

that 65% of the particles are below $1\mu\text{m}$, with a maximum particle size of $38\mu\text{m}$, and a specific surface area of $25.3\text{ m}^2/\text{kg}$.

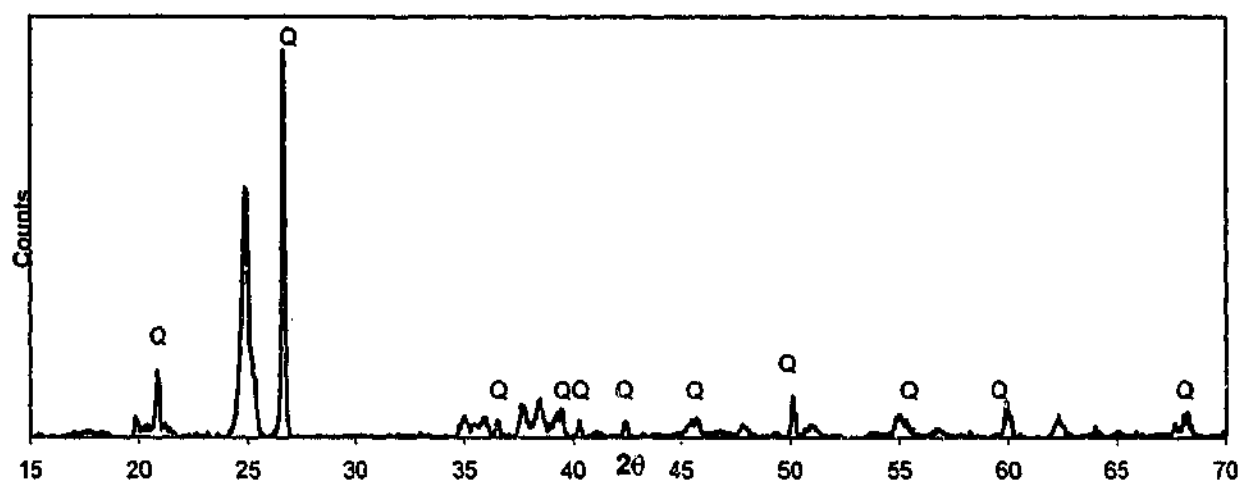


Figure 4.3 XRD trace of clay-K. The peaks corresponding to SiO_2 quartz are indicated; all other peaks correspond to kaolinite.

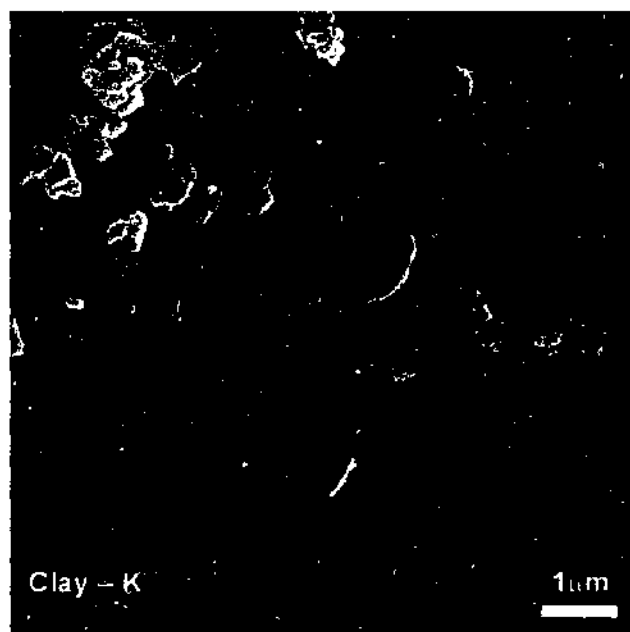


Figure 4.4 SEM micrograph of clay-K.

4.1.3 Silicon Nitride Seeds

An XRD trace of the silicon nitride used to seed the samples is presented in Figure 4.5. Only the peaks corresponding to the ~9 wt% β - Si_3N_4 content are indicated; the remainder correspond to α - Si_3N_4 . The fine particle size is evident in the SEM micrograph given in Figure 4.6, with many of the grains seen to be 0.1-0.2 μm in size. The average grain size was specified as 0.65 μm .

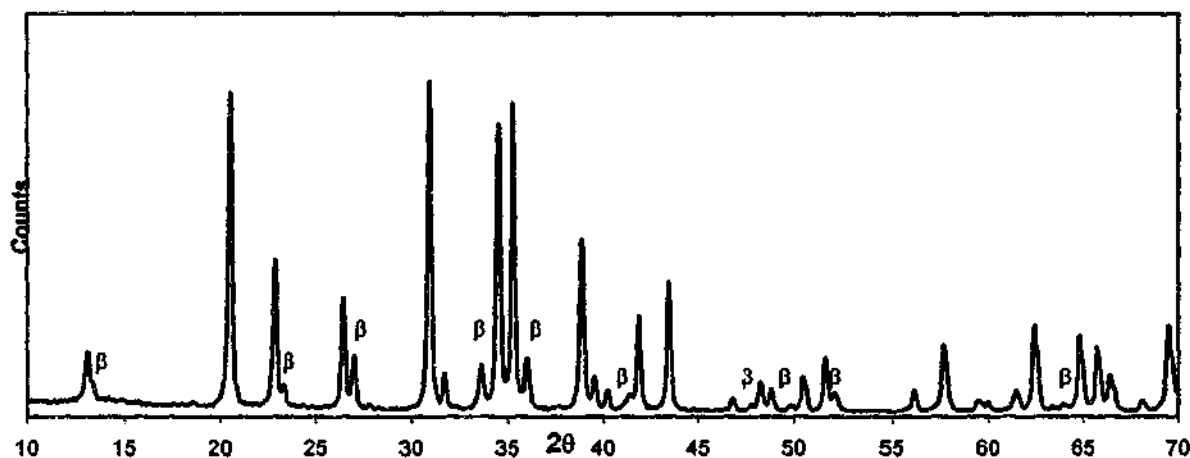


Figure 4.5 XRD trace of Si_3N_4 seeds. The peaks unique to β - Si_3N_4 are labelled 'β'; all other peaks correspond to α - Si_3N_4 .

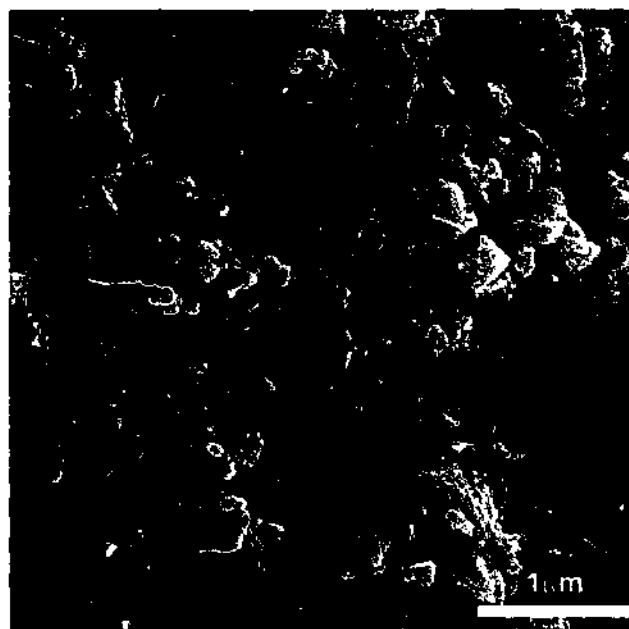


Figure 4.6 SEM micrograph of Si_3N_4 seeds.

4.2 K-series Firings: Slag + Clay-K (Kaolinite)

4.2.1 Experimental Procedure

The equation describing Ca- α -sialon compositions is given in Equation 4.1, and it can be seen that for a typical Ca- α -sialon with $m=1.6$ and $n=1.2$ (JCPDS PDF #33-0261) the ratio of Ca:Si:Al required is $\sim 1:9:1$, which is very Si-rich. The composition of the slag is much lower in Si than this, having an almost 1:1:1 Ca:Si:Al cation ratio, and for this reason the Si-content of the sample must be boosted by the addition of Si-rich kaolinitic clay-K to the slag.



Twelve different compositions were created with slag:clay-K molar ratios ranging from 0.1:1 to 3.3:1, as listed previously in Table 3.2 (Chapter 3). The nomenclature of Kxx uses two digits to describe 10x the slag:clay-K molar ratio rounded to two significant figures, i.e. the 0.19:1 slag:clay-K composition is referred to as K02. The carbon-black content was fixed at 25 wt% of the batch, and content of α - Si_3N_4 seeds decreased slightly from 7.7 wt% in K01 to 5.7 wt% in K33 as described in Section 3.2.6. The pellets were prepared and fired according to the procedures described in Chapter 3; a maximum temperature of 1450°C was used in all CRN firings, and the furnace was held at this temperature for 12 hours with N_2 gas flowing at 30ℓ/hr.

4.2.2 Appearance of Fired Pellets

Visual inspection of the pellets after firing at 1450°C showed that most pellets were bloated, with the side edges splayed out in ridges. No appreciable densification was obtained in any of the pellets after firing; many of the post-fired pellets in fact had less cohesion than in the pre-fired state and crumbled easily during handling.

Ca- α -sialon produced via pure laboratory reagents has a light grey colour, thus any residual carbon-black after CRN will darken the colour of the powder. Most pellets were a light/medium grey colour, with the higher slag compositions K19 (1.9:1 slag:clay-K) and above being indistinguishable in colour to the black raw batch powder. Many samples were found to have a distinct surface layer on the top and side edges that was a lighter grey colour than the core, which indicates that less residual carbon-black may be present on the surfaces of these pellets. Sometimes this layer was only a small patch on the top face of the pellet, but in some samples the layer penetrated to a depth of ~ 0.5 -1mm. Often these surface layers had noticeably higher cohesion than the bulk pellet material, and required scraping with a spatula

to remove material for analysis. This surface layer was also analysed via XRD where sufficient material could be obtained without significant contamination from the core powder. The residual carbon-black content of the powders is investigated in Section 4.2.4.

A sulphurous smell could sometimes be detected when the pellets were removed from the furnace boats. This indicates that the gaseous SO_3 , decomposition product from gypsum ($\text{CaSO}_4 \cdot 2\text{H}_2\text{O}$) had not been fully removed from the sample during firing. Other unidentified volatiles originating from the 2.17% of 'other impurities' in the slag may also remain in the CRN powders after firing.

4.2.3 Phase Analysis of K-series Powders After CRN

This section presents the results of phase analysis of the fired CRN powders, based largely on the results obtained via XRD. Due to the complex chemistry of the raw materials, many possible phases can be formed from the various impurity elements, and consequently several minor peaks found in the XRD traces from the samples after firing were unable to be identified via XRD alone, and remained unidentified throughout much of this investigation. This was due to their small number (only one or two peaks), low intensity, and partial overlaps with other peaks; many of these phases were only identified via SEM and TEM analyses performed in later stages of this investigation. In addition, several of the major phases identified via XRD appeared to be solid-solutions, evidence of which was also obtained during later work. To avoid unnecessary complication and qualification, the following presentation of the XRD data and phase identification discusses all phases identified, including those identified later using non-XRD techniques. Furthermore, these phases will initially be discussed in terms of their standard, stoichiometric composition. Following this in Section 4.2.2.1 will be a brief explanation of the features that allowed these minor phases to be unambiguously identified, and Section 4.2.2.2 will discuss the evidence regarding the solid-solution nature of these phases.

A summary of the phases identified in the twelve CRN powders after firing at 1450°C for 12 hours is presented in Table 4.1 using indicators from 'strong' to 'very weak' to describe the XRD peak intensities, which are related to the relative phase content. Representative XRD traces from six compositions (K01, K02, K05, K09, and K33) are presented in Figure 4.7. α -Sialon is the desired product phase in this investigation, and the term 'secondary phase' will be used during this discussion to refer to phases formed in large quantities in competition with α '.

Table 4.1 Phases identified in various slag:clay-K compositions fired at 1450°C for 12 hours.

Composition: slag:clay-K (molar):	K01 0.10:1	K02 0.19:1		K03 0.34:1	K05 0.47:1		K06 0.62:1	K07 0.73:1	K09 0.88:1		K10 1.0:1	K14 1.42:1		K19 1.93:1	K26 2.55:1	K33 3.3:1
Phase	core	core	surf	core	core	surf	core	core	core	surf	core	core	surf	core	core	core
α -Si ₃ N ₄	s	w	vw													
β -sialon	ms															
Ca- α -sialon	s	s	s	s	s	s	s	s	s	s	s	mw	s	vw	vw	vw
gehlenite (Ca ₂ Al ₂ SiO ₇)				mw	s	s										
E-phase (CaAlSiN ₃)							vw	vw	m	w	s	s	w	s	s	s
AlN	s	w	w	w	vw	vw	vw	vw	vw		vw	vw		vw?	vw?	vw?
FeSi	w	w	vw	vw	vw	vw	vw	vw	w	w	w	w		w	vw	vw
TiN	w	vw	vw	vw	vw		vw	vw	vw	vw	vw	vw?	vw?	vw?	vw?	vw?
SiC-2H	ms						vw?		vw?	vw?	v?	w?	w?	w?	w?	w?
SiO ₂ (quartz)	w?															
amorphous [†]	s	Δ	Δ	Δ	Δ	Δ	Δ	w	w	w	Δ	w	w	w	Δ	Δ

Key to XRD intensity: s=strong, ms=medium-strong, m=medium, mw=medium weak, w=weak, vw = very weak, ? = difficulty estimating from scan.

[†] The amorphous phase is difficult to detect via XRD, thus is only described as having a 'strong' or 'weak' presence.

^Δ An amorphous phase is expected to be present, but not able to be detected above the background noise in the XRD.

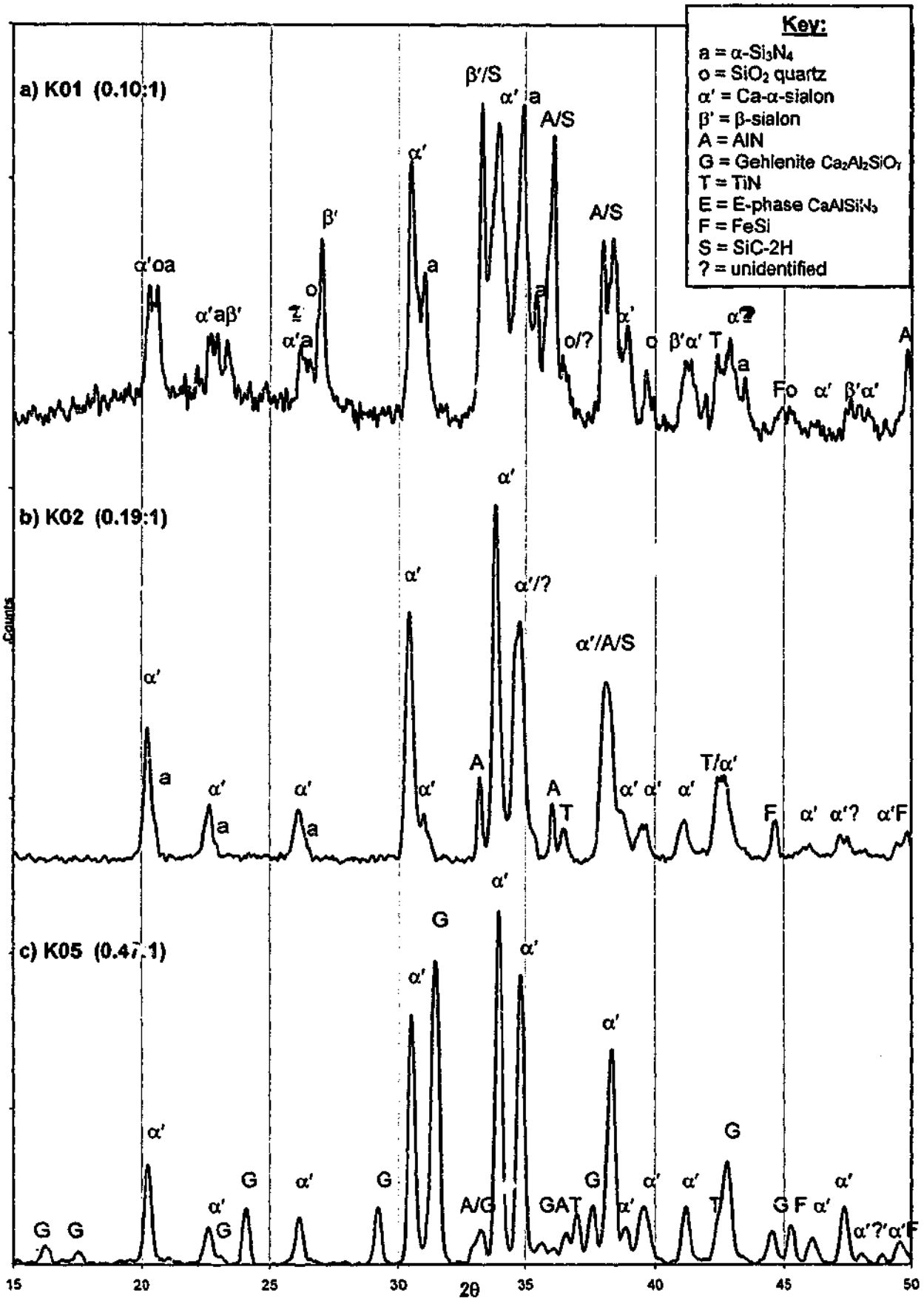


Figure 4.7 XRD traces of various slag:clay-K compositions fired for 12 hours at 1450°C: (a) K01, (b) K02, (c) K05. Continued next page.

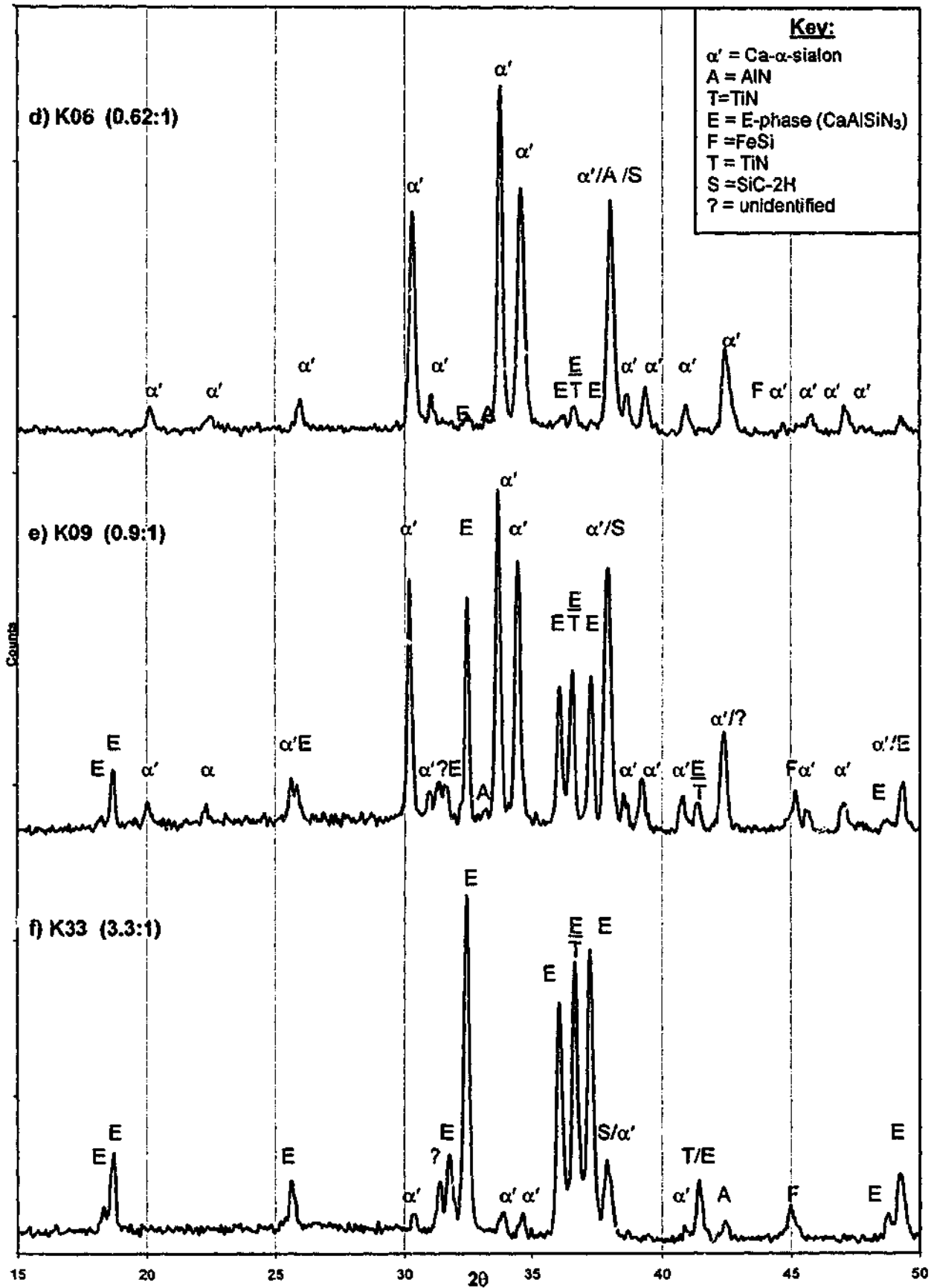


Figure 4.7(cont.) XRD traces of various slag:clay-K compositions fired for 12 hours at 1450°C:
(d) K06, (e) K09, (f) K33.

The lowest slag-containing sample K01 (0.1:1 slag:clay-K) shows an inability to fully form α -sialon. The product phases are mainly α - Si_3N_4 , α -sialon, β -sialon, AlN, SiC, quartz (SiO_2), and amorphous glass (Figure 4.7a). β -Sialon was distinguished from β - Si_3N_4 by the use of an internal Si standard, and is a commonly seen CRN intermediate phase during α' formation (van Rutten, Terpstra, *et al.* 1995). SiC is an intermediate phase commonly seen during the CRN of clays to form β -sialon (Mazzoni and Aglietti 1993), but has only previously been detected in the amorphous state in studies of CRN- α' formation (Ekstrom, Shen, *et al.* 1998). α - Si_3N_4 has not been reported as an intermediate CRN phase in the literature, and it is not possible to determine whether the α - Si_3N_4 seen in this XRD trace corresponds to the initial Si_3N_4 seeds or is a product of CRN. FeSi and TiN are impurity phases that originate from the Fe and Ti impurities present in both the slag and clay. Neither slag nor kaolinite from the starting mixture were detected in this sample after firing, however quartz was still present and this is likely to correspond to part of the 17.6% quartz impurity present in initial clay-K.

The phase assembly in the K02 (0.19:1 slag:clay) composition after CRN is distinctly different from both the lower-slag K01 composition and the next highest slag K03 (0.34:1 slag:clay-K) composition. The K02 reaction product is dominated by α -sialon (Figure 4.7) with a 'weak' amount of α - Si_3N_4 also visible, seen as the slight broadening of the α - Si_3N_4 / α -sialon peaks and the small shoulders on the higher 2θ side of some α' peaks. Minor amounts of impurity phases FeSi, and TiN, and AlN are also present. AlN was the main secondary phase found in the work on the CRN of Ca- α' using laboratory chemicals by Hotta and co-workers (Hotta, Tatami, *et al.* 2002), and AlN or one of a series of AlN-polytypes are often found in equilibrium with α -sialon in Ca- and Al-rich Ca-Al-Si-O-N compositions (Wood and Cheng 2000). The diagram of the α' -plane (Figure 2.4) shows that various triangular phase compatibility regions exist between α -sialon, AlN or an AlN-polytypoid, and liquid (i.e. grain boundary glass on cooling), which suggests that a small amount of grain boundary glass is also likely to be present in all compositions produced here. However glass is transparent to XRD, and was not clearly visible in these low-slag compositions. FeSi and TiN impurity phases were also detected in this sample, and SiC may also be present but is difficult to determine due to peak overlap.

The slight increase in slag from K02 (0.19:1 slag:clay-K) to K03 (0.34:1) produced a significantly different phase assembly, with gehlenite ($\text{Ca}_2\text{Al}_2\text{SiO}_7$) as the main secondary phase to α' . Further increasing the Ca level in the system by raising the slag content to that of K05 (0.47:1) further increases the proportion of gehlenite formed to 'strong', matching that of α' in

this composition. The impurity phases AlN, FeSi, and TiN are also present, but there is no evidence of any residual α -Si₃N₄. Gehlenite has been seen in Ca- α -sialon systems as an intermediate phase produced during reaction-sintering (van Rutten, Hintzen, *et al.* 1996) and as the main devitrification product of the residual glass (Hewett, Cheng, *et al.* 1998).

Raising the slag content slightly from K05 (0.47:1 slag:clay-K) to K06 (0.62:1) produced another abrupt change in phase behaviour, with this composition being dominated by α -sialon. Gehlenite is not present, but a small amount of E-phase (CaAlSiN₃) is now detected in addition to the impurity phases AlN, TiN and FeSi. This sample is the lowest slag-containing composition where E-phase is detected, and increasing the slag content from 0.62:1 increases the amount of E-phase formed, at the expense of α' . At a 1:1 molar slag:clay-K ratio (K10) both α' and E-phase are present in an equally 'strong' amount, and further raising the slag content results in powders dominated by E-phase. E-phase has been reported to form simultaneously with AlN within the 3CaO·Si₂N₂O-2CaO·Si₃N₄-AlN system hot-pressed above 1500°C (Huang, Sun, *et al.* 1985). It was also found to be a decomposition product of M-phase (2CaO·Si₃N₄·AlN) above 1450°C, however no M-phase was detected in these samples. The presence of AlN in the higher slag compositions above K06 is difficult to ascertain due to peak overlap, as indicated by the '?' in Table 4.1, but is likely to be minor. The quantity of glass produced in these higher slag samples is often great enough to be visible in the XRD, and simply listed as 'weak' due to an inability to accurately quantify this amorphous phase.

Distinct compositional differences were detected between the dark grey core of the pellets and the light grey, more cohesive surface layers. These differences were most noticeable in compositions K09 and K14 where more α' and less secondary and impurity phases are found on the surface when compared to the core. XRD traces for the core and surface regions of the K09 pellet are shown in Figure 4.8. This difference is due to the greater extent of reaction possible at the pellet surface which is directly exposed to the N₂ gas flow, resulting in a more complete removal of carbon-black. This is discussed further in Section 4.2.4.

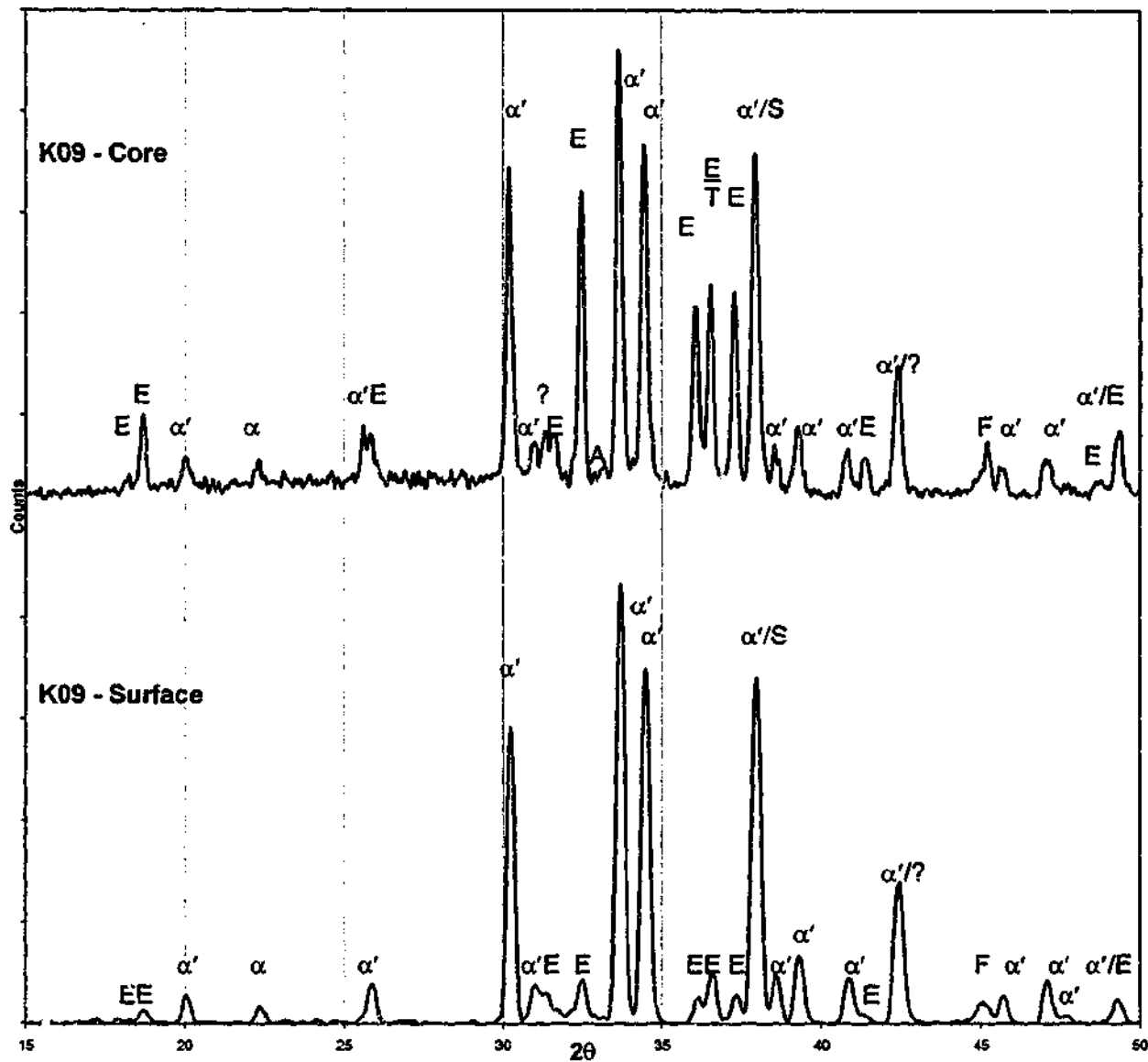


Figure 4.8 XRD traces of the surface and core regions of the K09 pellet.

[Key: α = α - Si_3N_4 , A= AlN , α' =Ca- α -sialon, E=E'-phase, F= FeSi , T= TiN , ?=unidentified].

4.2.3.1 Identification of Minor Phases

Differentiation between α' and α - Si_3N_4 , relies upon two features of the XRD scans: 1) the angular shift of the α' peaks to lower values of 2θ ; and 2) corresponding changes in the relative intensities of the peaks between α' and α - Si_3N_4 , both of which are features resulting from the increase in cell dimensions caused by the Al-N substitution for Si-N in the lattice. These peak shifts can be small and difficult to resolve for low m - and n -value α -sialons (Equation 4.1) which will have very similar lattice parameters to the parent Si_3N_4 . In the case of α -sialon, two α - Si_3N_4 peaks display particularly distinct changes when α -sialon is formed; the 78% intense α - Si_3N_4 (101) peak at $2\theta=20.59^\circ$ and the 100% α - Si_3N_4 (201) peak at 30.99° . In the α' sialons produced here, which are similar to the $m=1.6$, $n=1.2$ Ca- α -sialon reference

listed in the JCPDS Powder Diffraction File (PDF #33-0261), these peaks display a large change in intensity of 78%→35% and 100→75%, respectively, and peak shifts to lower 2θ values of $\sim 20.29^\circ$ and $\sim 30.58^\circ$. Thus these two peaks are good indicators of α -sialon formation as distinct from α - Si_3N_4 . For ambiguous cases, Si powder was added to the sample as an internal standard to remove any calibration error.

The minor impurity phases FeSi and TiN could only be unambiguously identified from the TEM work to be presented in Chapter 7. Only the two strongest peaks from TiN are visible in the XRD, and the 100% (111) TiN peak at 36.6° overlaps directly with that of E-phase. Only the 100% FeSi (210) peak is seen in these XRD scans, which is in accord with previous observations that FeSi_x phases in CRN systems produce only one characteristic XRD peak (Mazzoni, Aglietti, *et al.* 1992a). Slight deviations are seen from the predicted peak positions of these impurities, $\sim \pm 0.15^\circ$, but are up to -0.4° for the FeSi (210) peak. 2H-SiC (α -SiC) was identified via the high-temperature stability work presented in Chapter 6, where very large amounts of SiC are produced and the peak positions can be clearly seen. Only one characteristic 2H-SiC peak is generally visible in the XRD scans produced here, this being the 100% intense peak at 38.1° which overlaps both α' and AlN peaks. SiC can therefore only be seen clearly in high-slag samples where the volumes of α' and AlN are low but the 38.1° peak remains abnormally intense. The lower intensity 2H-SiC peaks also directly overlap with α' and E-phase peaks, and hence are not detected.

4.2.3.2 Identification of Solid-solution Phases

It has been noted that phases such as E-phase (E) and gehlenite (G) produced XRD traces with slightly different 2θ positions (i.e. d-spacing), and relative peak intensities to the pure stoichiometric phases listed in the relevant JCPDS PDF cards. Individual XRD peaks were shifted by up to $\pm 0.25^\circ$, and these variations to individual peaks were consistent between samples and could not be attributed to error in the XRD equipment. An example is given for E-phase in Table 4.2, which lists the JCPDS data and the experimentally observed data averaged from five different XRD scans.

It is important to recognise that these peak shifts were not so large that the phases were unable to be unidentified (except for the impurity phases FeSi and TiN which did not have a sufficiently strong presence in the XRD), but that there was a small, consistent deviation from the standard data presented in the JCPDS. This indicates that the phases identified are solid-solutions, where the similarly sized Ca, Al, Si, and Mg cations are able to be substituted for

each other as long as the change in cation charge is compensated elsewhere in the structure. These substitutions will slightly distort the crystal structures, producing the observed variation to XRD peak positions and intensity. These changes are similar to the way in which α - and β -sialon XRD patterns are related to the parent α - and β - Si_3N_4 patterns, with the difference observed in peak positions and intensity increasing as the level of Al-N and Al-O solid-solution increases.

Table 4.2 Comparison of experimental E-phase XRD peak positions and intensities to JCPDS standard (listed for $\text{CuK}\alpha$ radiation).

JCPDS PDF #39-0749 E-phase (CaAlSiN_3)		Experimental Results E'-phase		
2θ ($^\circ$)	Intensity (%)	2θ ($^\circ$)	Intensity (%)	Peak Shift ($^\circ$)
18.32	10	18.30	12	-0.02
18.51	10	18.76	21	+0.25
25.56	10	25.67	24	+0.11
31.72	50	31.73	23	+0.02
32.26	100	32.50	100	+0.24
35.95	100	36.10	83	+0.15
36.60	100	36.62	84	+0.01
37.09	100	37.31	93	+0.22
41.32	20	41.44	21	+0.11

In addition to the various cation substitutions possible in this system, anion substitutions of N^{3-} for O^{2-} are also possible. As with α -sialons, any excess negative charge must be balanced by changing the cation composition, which may be achieved via various solid-substitutions as discussed above. For example, the gehlenite ($\text{Ca}_2\text{Al}_2\text{SiO}_7$) seen here and in previous studies may be nitrogenous, as described by the formula $\text{Ca}_2\text{Al}_{2-x}\text{Si}_{1+x}\text{O}_{7-x}\text{N}_x$ (van Rutten, Hintzen, *et al.* 1996).

It is likely that most phases produced in this system are solid-solutions, and later chemical analysis via SEM and TEM in Chapter 7 will provide direct evidence for this. For example

FeSi is found to have a significant substitution of Ti^{4+} for Si^{4+} (Figure 7.6), and AlN contains a small amount of Mg^{2+} and Si^{4+} substitution for Al^{3+} , and is thus a variation of the AlN' solid-solution discovered by Wood and Cheng (Wood and Cheng 2000). Due to the level of substitution being very low in AlN', no distinct peak shifts are observed in the XRD traces, which is also the case for TiN where only a low level of Si^{4+} for Ti^{4+} is found.

For the remainder of this thesis, the variable solid-solution nature of these phases will be explicitly referred to by the use of the prime symbol (') added to the phase name (ie. G', AlN', E'-phase or E'). Note that α' (α -sialon) and β' (β -sialon) are already differentiated as solid-solutions of α - Si_3N_4 and β - Si_3N_4 , respectively. As the exact composition of these phases is not known, the nominal stoichiometric formula will be used when describing the chemical composition of these phase, for example when listing the phase composition in tables, unless stated otherwise.

The results of some additional analyses of these CRN powders is presented in the following sections, after which a discussion of the significance of these results in terms of the CRN process will be presented in Section 4.2.7.

4.2.4 Carbon Content of Selected Compositions

The difference in colour between various compositions, and between the surface and core regions of some high-slag samples, was previously attributed to differences in the residual C-content (Section 4.2.2). Carbon-black is amorphous and cannot be easily detected via XRD, thus TGA was used to determine the weight loss due to oxidation of the C to $CO_2(g)$ in air above 500°C. The results of residual C determination for selected compositions are presented in Table 4.3. All weight loss in the range 500-650°C is attributed to C burnout alone. Only the high-slag K33 sample experienced an additional weight loss event of ~1.6 wt% at 300°C. This may be due to the oxidation of unknown slag-based impurity phases that have remained in the sample after firing.

There is no clear correlation between residual C and extent of α' formation via CRN. Ideally, completion of the CRN reactions should involve the complete consumption of C and other reactants from the starting batch to produce a final product consisting solely of α' . Here however, the essentially single-phase α' compositions K02 and K06 have higher residual C-contents than that of other compositions that produced significant quantities of secondary phases, such as the $\alpha'+G'$ in K03, and the $\alpha'+E'$ surface of the K09 pellet. Specimen colour and residual C-content are thus not reliable indicators of the extent of CRN. This is because C

consumption is not directly related to α -sialon formation. All powders after oxidation were the same light-grey colour, similar to that of α' .

Table 4.3 Residual carbon content of selected K-series compositions after CRN for 12 hours at 1450°C as determined via TGA (initial C-content=25 wt%).

Sample	Main Phases Present	Colour Before Oxidation	Residual Carbon (wt%)
K01	$\alpha'(s)$ α -Si ₃ N ₄ (s)	medium grey	0.80 ± 00.01
K02	α' (s)	medium grey	1.60 ± 0.01
K03	α' (s), G' (mw)	light grey	0.17 ± 0.01
K06	α' (s)	light grey	0.80 ± 0.01
K09- core	$\alpha'(s)$, E'(m)	medium grey	0.70 ± 0.01
K09-surface	$\alpha'(s)$, E'(w)	light grey	0
K33	E'(s), α' (vw)	black	3.50 ± 0.01

Key to XRD intensity: s=strong, m=medium, mw=medium weak, w=weak, vw = very weak.

Carbon is consumed in the early stages of CRN by the formation of intermediate phases such as SiO(g) and SiC(s), which are then required to further react with the liquid and N to produce α -sialon. This process may be retarded, for example by a lack of sufficient liquid, thus α' formation will be hindered despite full consumption of the carbon. This was seen in the K01 composition which contained very little residual C but displayed incomplete CRN; large amounts of intermediate phases SiC and β' were present after 12 hours of reaction (Figure 4.7a).

The black powder from K33 did contain considerably more residual carbon-black (3.5 wt%) than the lighter coloured powder produced from lower-slag compositions, amounting to 14% of the initial 25 wt% C in the starting powder. This indicates that the C-consuming CRN reactions did not proceed extensively in this high-slag composition, a fact also reflected by the very low α' content produced. This suggests that higher temperatures or longer reaction time may be required to achieve a greater extent of CRN and produce α' rather than E'-phase in high-slag compositions.

The complete removal of C from the surface of the pellet in high-slag compositions such as K09, together with the observed higher extent of α' formed and the very low quantity of secondary phases such as E', indicates that the CRN reactions proceed more fully on the surface of the pellets. This is due to being in direct contact with the N₂ gas flow, which plays a role in both providing reactant N for nitridation, and removing gaseous CRN by-products that can impede the CRN reactions (Mazzoni, Aglietti, *et al.* 1993). Therefore the surface of the pellets have enhanced reactivity.

4.2.5 SEM Analysis of Selected CRN Powders

SEM micrographs representative of some of the powders produced after CRN at 1450°C are presented in Figure 4.9. The powders were ultrasonically dispersed in ethanol, transferred onto a brass stud and sputter coated with a conductive carbon layer.

The essentially single-phase α' products found in K02 and K06 are shown in Figure 4.9a, and c, respectively. The α' particles are generally equiaxed and have a fine particle size of 0.5-1 μ m, forming in agglomerates up to 10 μ m across, which is a similar size to the Ca- α' grains produced via CRN of laboratory chemicals (Mitomo, Takeuchi, *et al.* 1988; van Rutten, Terpstra, *et al.* 1995), and also similar to the Mg- α' sialons produced from talc and clay mixtures (Zhang, Komeya, *et al.* 2000).

XRD analysis of the K05 powder showed this composition to be a combination of α' and G' in equally strong amounts. The powder consists mostly of equiaxed grains with a diameter of ~1 to 3 μ m, with a few large, irregular particles present as indicated in Figure 4.9b. No distinctive morphological features of the gehlenite formed in Ca- α' systems have been reported in the literature, hence distinguishing between α' and G' is not possible via morphology alone, and extensive EDXS analysis of individual particles was not performed here. This composition produces more grains with a size >1 μ m than the other compositions, which may correspond to gehlenite particles rather than Ca- α' . The large, irregular grains have a morphology that may correspond to gehlenite that has formed via crystallisation of the glass.

The XRD trace of the high-slag sample K19 showed that it contained mostly E'-phase (CaAlSiN₃) with only a minor amount of α' present, hence this abundance allowed unambiguous identification of the E'-phase shown in Figure 4.9e. E'-phase consists of large plates ~10-15 μ m in diameter and several microns thick, randomly oriented in agglomerates up to 100 μ m in size. In the 1:1 slag:clay-K K10 composition, (Figure 4.9d) the CRN product phases are a mixture of α' and E' in roughly equal amounts, and the distinct particle

morphologies of these two phases are clearly distinguishable; a large 40 μm agglomerate of E'-phase plates is indicated, surrounded by smaller agglomerates of <1 μm α' grains. These α' grains are similar in size and morphology to those seen in the lower-slag K02 and K06 samples. An unidentified fibre phase is also present in this sample, and fibres have been occasionally seen in other samples investigated in this investigation. Si_3N_4 -whiskers are often seen in various CRN systems, and are evidence of gas-phase reaction processes (Cho and Charles 1991b).

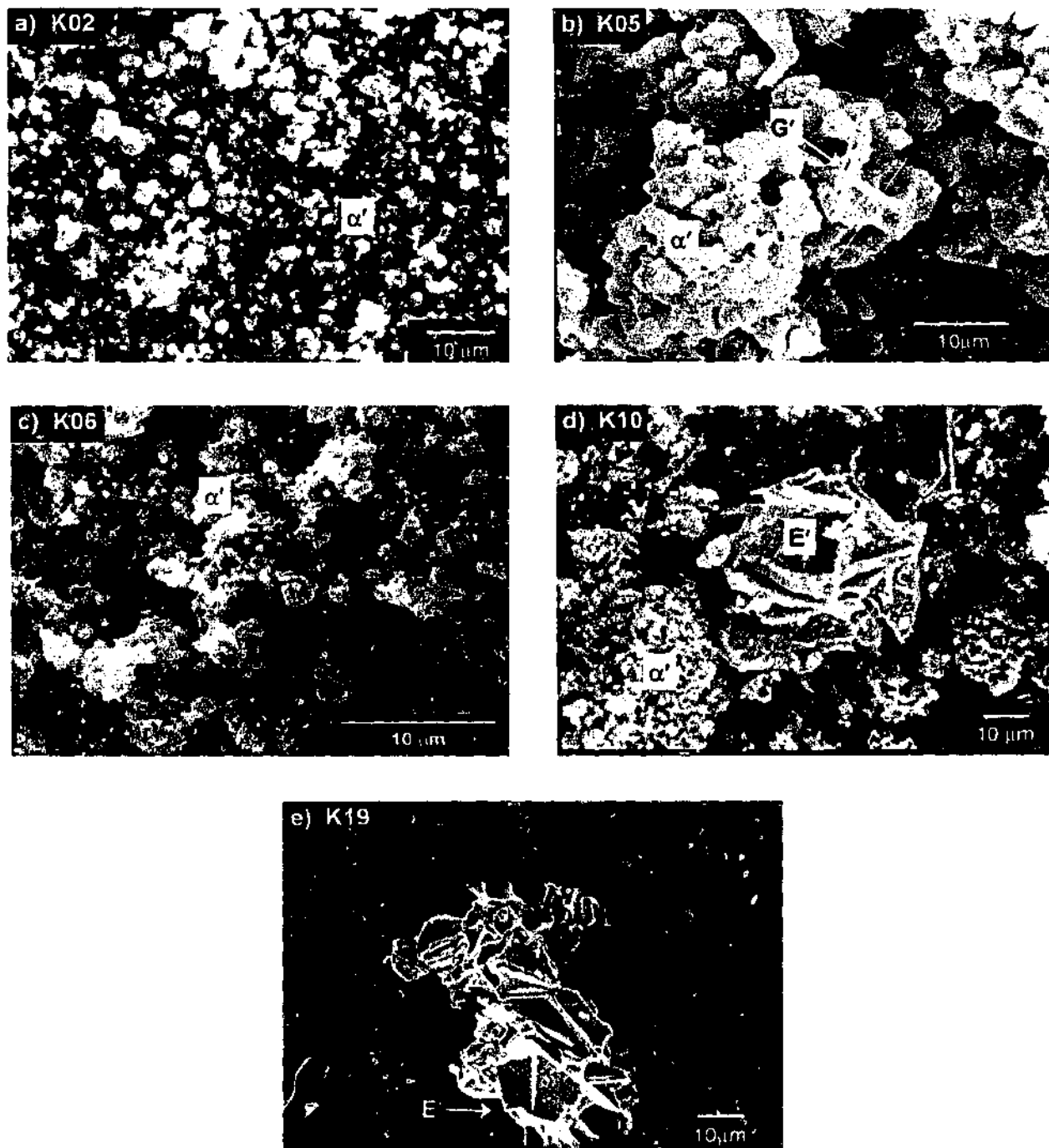


Figure 4.9 SEM micrographs of various CRN powders formed after firing for 12 hours at 1450°C: (a) K02 [α'], (b) K03 [α' +G' gehlenite], (c) K06 [α'], (d) K10 [α' +E'], (e) K19 [E'].

AlN' and other impurity phases such as FeSi' , TiN' and SiC were not identified via SEM in these samples due to their low concentration in the final products.

The K06 composition was the highest slag-containing composition that formed essentially single-phase α' under the CRN conditions used, and was therefore of greater interest than K02 and adopted as the standard α' -forming composition throughout this investigation. SEM analysis of various K06 CRN powders showed the formation of some unique α' morphologies. Hollow balls of α' , such as those shown in Figure 4.10a, were occasionally seen. These hollow balls are 15-25 μm in diameter and composed of several layers of $\sim 1\mu\text{m}$ α' grains, and are much larger than the hollow balls produced by Hotta and co-workers via the CRN of laboratory chemicals, which were 0.5 μm in diameter and composed of 30-50nm α' grains (Hotta, Tatami, *et al.* 2002). Rod-like α' grains have also been observed (Figure 4.10b), which maintain the sub-micron diameter of the α' grains usually found in the K06 powder, but have an elongation of up to $\sim 2\text{-}3\mu\text{m}$. These different α' morphologies were not the dominant morphology produced from K06 powders after firing, and there was no clear indication as to what caused them to be formed. However the possibility of forming α' with unique morphologies such as elongated α' grains via the CRN of slag and clay does exist.

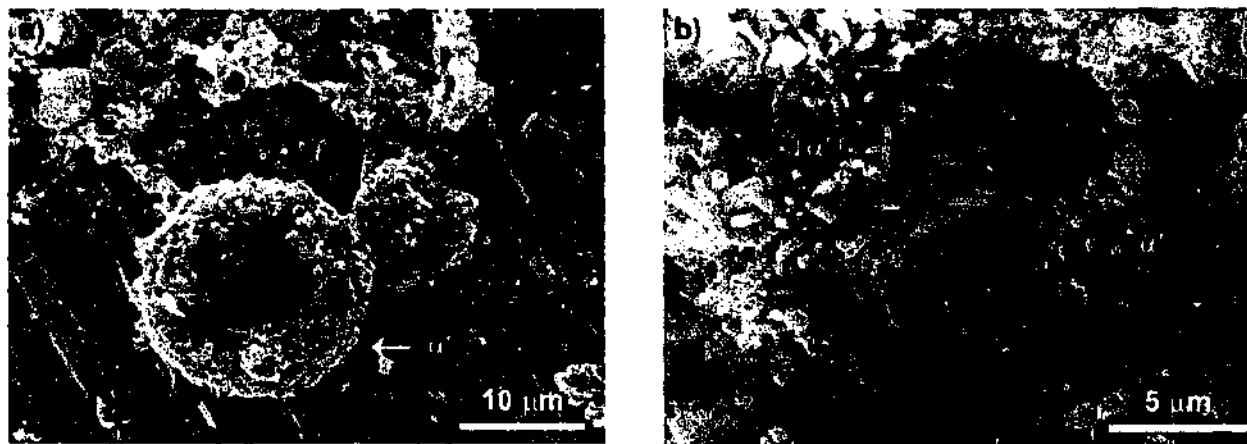


Figure 4.10 SEM micrographs of K06 α' -sialon powders with various morphologies (a) hollow balls, (b) elongated α' rods.

Chemical analysis of the CRN powders was performed using EDXS in the SEM to gain some compositional information. EDXS spectra typical of α' particles in K06 and E'-phase plates from K19 are given in Figure 4.11. Although it is not possible to accurately quantify the compositions based on these results, a comparative analysis can be performed using the relative EDXS peak heights to estimate the composition. The Al:Si:Ca peak height ratios for α -sialon and E' are tabulated in Table 4.4. The detector efficiency for light elements such as O and N is much lower than for the heavier elements, thus these anion species are considered separately.

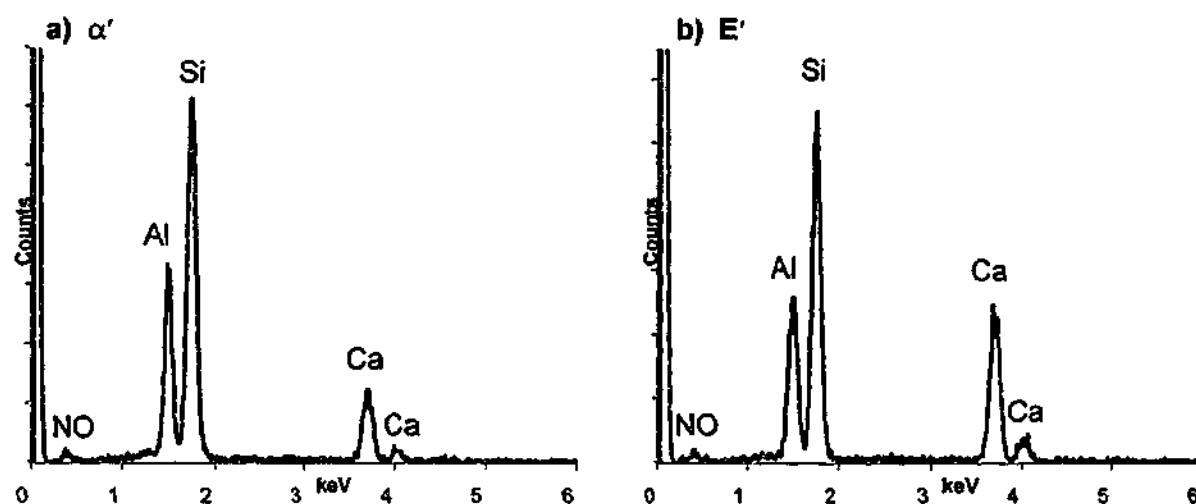


Figure 4.11 EDXS spectra typical of (a) α' grains in K06 powder, (b) E' plates in K19 powder.

Table 4.4 Typical element peak height ratios from EDXS spectra of particles in K06 and K33.

Particle	Al:Si:Ca peak height ratio	O:N peak height ratio
α -sialon (K06)	1: 1.8: 0.3	1: 2.4
E'-phase (K33)	1: 1.9: 0.9	1: 2.0

The Al:Si:Ca peak height ratio for α -sialon is $\sim 1:1.8:0.3$ (Figure 4.11a), which is a Ca- α' phase that is Al-rich. This corresponds to EDXS spectra obtained by Wood from high Ca- and Al-compositions (Wood 2001). It was thought CRN may allow the formation of a multi-cation (Mg,Ca)- α -sialon in this Mg- and Ca-bearing system, however Ca is the only stabilising cation detected in the α' phase. Single-phase Mg- α' -sialon cannot be produced by reaction-sintering

methods, and Wang and co-workers have shown that (Mg,Ca) multi-cation stabilised α -sialons are also difficult to produce via reaction-sintering because Ca enters the α' structure in preference to Mg; and even when the Mg:Ca ratio was 50:50 in the starting powders very little Mg entered the α' , the Mg preferring to form Mg-containing AlN-polytypoid phases such 21R (Wang, Zhang, *et al.* 1999). However, work on the CRN of Mg-bearing talc by Zhang and co-workers showed that single-phase Mg- α -sialon could be produced by the CRN method (Zhang, Komeya, *et al.* 2000), thus it seemed possible that some of the ~6% Mg contained in the slag could enter into the α -sialon formed via CRN here. The EDXS analysis shows that this did not occur and the α' formed is simply a Ca- α -sialon.

EDXS spectra typical of E-phase plates have an Al:Si:Ca ratio of ~1:2:1, which is different to the 1:1:1 CaAlSiN₃, reported by Huang and co-workers (Huang, Sun, *et al.* 1985), but corresponds to the ~1:2:1 reported by Thompson (Thompson 1989). Correspondence with the authors of the original work on E-phase suggested that various discrepancies were not fully resolved at the time of publishing the results, and that the E-phase was seen to be more Si-rich than allowed by the assigned composition of CaAlSiN₃. Clearly, pure E-phase is not well understood, and the potential for various substitutions in this slag-based system does not allow a rigorous analysis to be performed here. The reported composition of CaAlSiN₃ will continue to be used when referring to the nominal composition of E'-phase.

4.2.6 Calcium Content of α -sialon

Following the method described in Section 3.4.1.2, the α' lattice parameters a and c for eight of the α -containing compositions were determined via XRD. Estimates of the corresponding m - and n -values that describe the α -sialon composition ($\text{Ca}_{m/2}\text{Si}_{12-m-n}\text{Al}_{m+n}\text{O}_n\text{N}_{16-n}$) can be determined from this data from the relations (van Rutten, Hintzen, *et al.* 1996):

$$a (\text{\AA}) = 7.749 + 0.0023n + 0.0673m \quad [4.2a]$$

$$c (\text{\AA}) = 5.632 - 0.0054n + 0.0550m \quad [4.2b]$$

The n -values not discussed here, because the m -value is the dominant term in these relations and directly corresponds to the Ca-content of the α' phase. Only samples between K02 and K19 were tested because K01 did not produce any α -sialon, and the higher slag compositions K26 and K33 contained too little α' for accurate analysis. The cell parameters, estimate of m -value and Ca-content for compositions K02 to K19 are listed in Table 4.5.

Table 4.5 Calculated lattice parameters, corresponding estimate of m -values and Ca-content of α -sialon produced from various slag:clay compositions.

	K02	K03	K05	K06	K09	K10	K14	K19
a (Å)	7.897	7.879	7.885	7.91	7.947	7.96	7.958	7.924
	±0.003	±0.003	±0.011	±0.013	±0.004	±0.006	±0.018	±0.028
c (Å)	5.745	5.732	5.737	5.762	5.758	5.754	5.771	5.775
	±0.003	±0.003	±0.011	±0.014	±0.003	±0.006	±0.020	±0.035
m	2.16	1.90	1.99	2.39	2.77	3.00	2.96	2.86
	±0.001	±0.001	±0.005	±0.006	±0.001	±0.003	±0.01	±0.01
Ca/unit cell ($x=m/2$)	1.08	0.95	1.00	1.20	1.39	1.50	1.48	1.43

The m -values determined for the α' produced here are considerably higher than the $m=1.2$ and $m=1.8$ reported for the Ca- α' in other CRN studies (Metselaar, Exalto, *et al.* 1996; Mitomo, Takeuchi, *et al.* 1988), but less than the upper reported limit of $m=2.8$ for Ca- α' produced via reaction-sintering (Huang, Sun, *et al.* 1985). There is a trend towards increasing m -value, i.e. increasing Ca-content, with increasing slag:clay-K ratio of the samples from K02 to K10, although the gehlenite-forming compositions K03 and K05 appear to be anomalous with this trend. The main factor promoting the increase in Ca-content of α' with increasing slag content is the higher Ca- and Al-content provided by the higher amount of slag in the starting batch, allowing higher m -value α' to form. The Ca-content of the α -sialon in K03 and K05 ($m < 2.0$) is lower than in neighbouring compositions K02 and K06 ($m > 2.16$) due to the formation of the Ca- and Al-rich gehlenite phase (nominally $\text{Ca}_2\text{Al}_2\text{SiO}_7$), which consumes the Al and Ca available for α' . However, despite the overall lower Ca-content determined for K03 and K05, the general trend of increasing m -value with increasing slag content is observed, with the higher slag K05 producing a higher m -value Ca- α' than K03.

Increasing the slag content to that of K06 changed the phase behaviour such that E'-phase is stable with α' rather than gehlenite. E'-phase (nominally CaAlSiN_3) contains less Ca and Al per mol than gehlenite, hence there is more Al and Ca available in the system to produce a higher m -value α' . Beyond K10, a slight decrease in the observed m -value is seen above compositions K10, which may be due to increasing uncertainty in the calculation arising from the relatively low α' -content in these samples.

4.2.7 Phase Formation in the Slag–Clay–K system

The results of the previous phase analysis allow the twelve slag and clay-K compositions to be divided into three different regions of phase behaviour. The first region is occupied by the lowest slag-containing samples K01 and K02 and is characterised by the formation of α - Si_3N_4 in addition to α -sialon. The second distinct area of phase compatibility is represented by the 'medium' slag-containing compositions K03 and K05, which produced gehlenite (G') as a secondary phase, and the third, 'high' slag region encompasses all compositions K06 and above which produced E'-phase (E') as the main companion to α '.

It should be noted that kinetic factors may prevent the thermodynamically favoured phases from being able to be formed under the conditions used for CRN here, thus the phases formed in this system may not necessarily be the thermodynamically predicted equilibrium phases. The phase assembly discussed here is specific to the CRN conditions used of 1450°C, 12 hours of reaction, and N_2 flowing at 30ℓ/hr. Altering any of these conditions may result in a different phase assembly being produced.

4.2.7.1 Low-Slag Compositions K01 and K02

Large quantities of phases known to be intermediate CRN products were detected in the lowest slag K01 (0.10:1 slag:clay-K) sample, including β -sialon, SiC, and an amorphous phase. In addition, some SiO_2 quartz was detected in the sample, which is most probably a leftover from the 17.6 wt% quartz component of clay-K; free quartz is known to remain uninvolved in early-stages of CRN when producing β -sialon, being incorporated into β' only during the last stages of reaction (Mazzoni, Aglietti, *et al.* 1993). The amorphous phase corresponds to liquid formed at high temperatures (~1300-1400°C) from which the various CRN-derived phases such as β' and α' , are precipitated. The large quantities of intermediate phases, the presence of residual components from starting powder, the low proportion of α' formed, and the conversion of most of the C to SiC, suggest that the CRN reactions have only just begun in this K01 composition. The XRD trace in Figure 4.7a is essentially a snapshot of the system at an early stage of CRN.

The lack of completion of the CRN reactions suggests that the reaction rate at 1450°C was very slow. Previous studies have shown that inadequate liquid formation during the CRN of clays impedes the diffusive CRN reactions and prevents the full conversion of reactants to sialon (Morrison, Maher, *et al.* 1989). This is the situation in the K01 sample where the composition is essentially pure clay-K (0.1:1 slag:clay-K) with very little slag to promote liquid

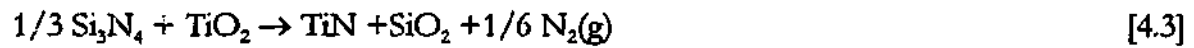
formation. Moreover, the small amount of liquid formed in the clay-rich K01 sample will be dominated by SiO_2 , and will thus have a higher viscosity than CaO-rich liquids produced in higher slag compositions (Dumbaugh and Danielson 1986). This will further retard the CRN process because high rates of diffusion are needed to allow the solution-precipitation of product phases to occur through this liquid. The effects of SiO_2 enrichment on CRN are further explored in Chapter 5.

In the current investigation, doubling the slag content to that of K02 (0.19:1) appears to promote sufficient liquid formation for CRN, and no residual starting materials or known intermediate oxynitride CRN products were found in any composition with this slag content or higher.

$\alpha\text{-Si}_3\text{N}_4$ has not been seen in any previous studies of α' formation via CRN, and it is not clear whether the $\alpha\text{-Si}_3\text{N}_4$ detected in the K01 sample is from the unreacted $\alpha\text{-Si}_3\text{N}_4$ seeds added to the starting powder, or produced via CRN of SiO_2 within the liquid, which may occur according to the reaction $3\text{SiO}_2 + 6\text{C} + 2\text{N}_2 \rightarrow \text{Si}_3\text{N}_4 + 6\text{CO}$. The presence of $\alpha\text{-Si}_3\text{N}_4$ seeds have been seen to promote this reaction by acting as nucleation sites for $\alpha\text{-Si}_3\text{N}_4$ formation (Kang, Komeya, *et al.* 1998). Results to be presented in Chapter 5 from the slag-clay-P system show that $\alpha\text{-Si}_3\text{N}_4$ can in fact be produced as an intermediate CRN reaction product, and is converted to α' with extended reaction times. Therefore it is possible that significantly extending the reaction time of the K01 composition may allow α -sialon to be produced and these intermediate phases consumed. Increasing the reaction temperature may also promote an increased reaction rate and allow the reactions to proceed more fully, however the final compatible phases that form during CRN are temperature dependent (van Rutten, Hintzen, *et al.* 2001), thus increasing the temperature may change the compatibility of phases eventually produced via CRN of the K01 composition.

AlN' is a phase often found in equilibrium with Ca- α' (Wood and Cheng 2000), and can be formed during CRN via the direct nitridation of Al_2O_3 liberated from the transient liquid, which cannot redissolve back into the sialon solution (Higgins and Hendry 1987). No crystalline Al_2O_3 was detected in these samples. The TiN' and FeSi' impurity phases seen in all K-series compositions are formed from the TiO_2 and Fe_2O_3 impurities present in both the slag and clay-K. Their presence in the K01 products shows that they are formed in the very early stages of CRN. Fe-Si has a low eutectic temperature around 1212°C , and the Fe-Si liquid that forms is known to catalyse the nitridation reactions, but is detrimental to the purity and properties of CRN powders due to the residual, hard FeSi_2 particles (Boyer and Mouison

1978). TiN phases have been seen in the CRN products of various Ti-contaminated clays (Fabbri and Dondi 1991). TiN can readily form from TiO_2 in the presence of Si_3N_4 at temperatures above 1000°C , according to the redox reaction given in Equation 4.3 (Trigg and McCartney 1981).



TiO_2 has also been seen to react with AlN in a similar redox reaction to produce TiN and Al_2O_3 (Hong, Lumby, *et al.* 1993). In the TiO_2 -containing slag system, TiN may be produced after N has been incorporated into the system via redox reactions with $\alpha\text{-Si}_3\text{N}_4$ or other oxynitride intermediate phases. The oxygen-rich product of this reaction will be either further nitrated or simply remain in the glass.

The K02 composition (0.19:1 slag:clay-K) produced an essentially single-phase α' product, with only 'weak' amounts of AlN' and $\alpha\text{-Si}_3\text{N}_4$ present in addition to the TiN' and FeSi' impurities. The β -sialon intermediate phase was not detected, but a small amount of intermediate SiC may remain in the sample. This composition therefore appears to have undergone very extensive CRN, facilitated by doubling the slag content from that of K01, providing more CaO and Al_2O_3 to the system which allows for the greater production of lower-viscosity liquid, and thus enhanced Ca- α -sialon formation. The minor amount of $\alpha\text{-Si}_3\text{N}_4$ may be a metastable intermediate phase that can be converted to α -sialon with extended reaction times, however this has not been determined.

It is possible to schematically represent the phases produced after CRN on a phase compatibility diagram based on the Jancke prism as shown in Figure 2.3b. A maximum of four phases are required to form the corners of a phase compatibility tetrahedron located within this 3-dimensional representation of the Me-Al-Si-O-N system. The K02 composition formed $\alpha\text{-Si}_3\text{N}_4$, α -sialon, AlN', and the residual grain boundary glass that is assumed to be present. Hence the appropriate phase compatibility tetrahedron is bounded by the four phases $\alpha\text{-Si}_3\text{N}_4$ - α' -AlN'-glass, and is shown schematically in Figure 4.12. Recall that this diagram does not represent true thermodynamic equilibrium, but what is essentially the 'steady-state' phase assembly of the system after 12 hours of reaction at 1450°C under N_2 flowing at 30ℓ/hr. The K01 composition was clearly not at steady-state, thus it is not possible to accurately define an appropriate phase compatibility region for this composition.

The insert in Figure 4.12 shows the approximate location of the K02 composition on the ternary oxide end of the phase diagram, which is given in equivalent-%. The small amount of MgO in the slag is included together with CaO when indicating the starting compositions in these diagrams. It was seen in Section 4.2.5 that the final products of CRN such as α' and E' do not contain any of the ~6 wt% MgO contributed to the starting batch by the slag, and results in Chapter 7 will show that most of this Mg is located within the grain boundary glass, with a very small amount contained in the AlN' solid-solution. In terms of glass formation, MgO and CaO are both alkaline earths which behave similarly, and are thus often considered together (Dumbaugh and Danielson 1986).

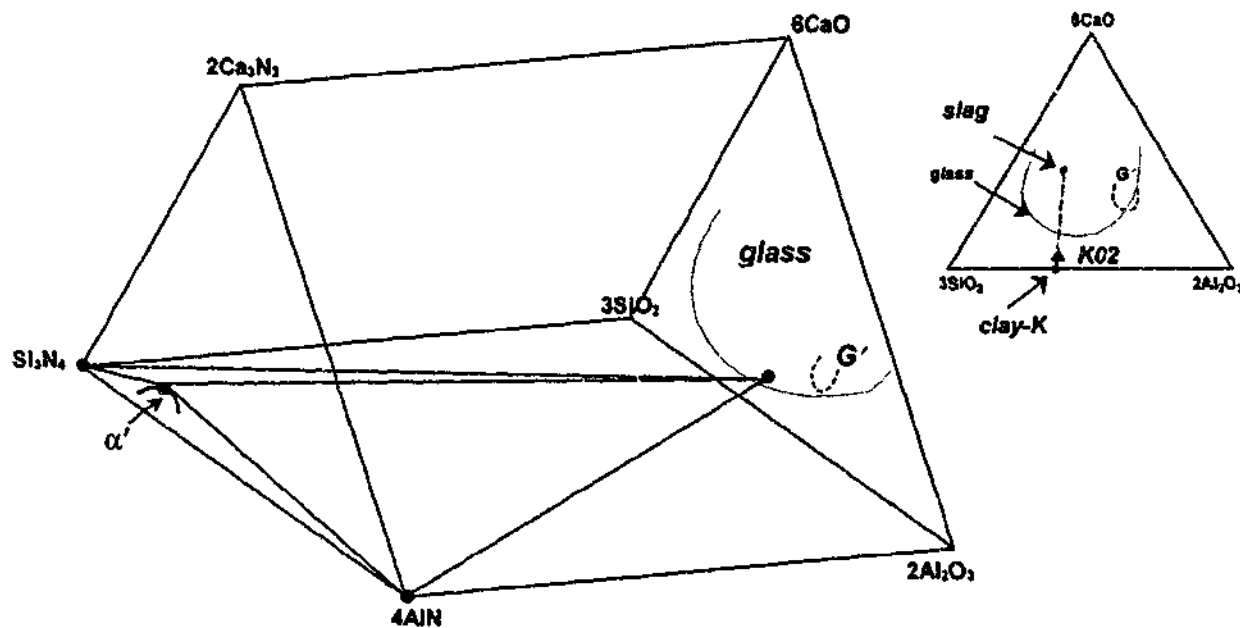


Figure 4.12 Schematic showing phase compatibility region for composition K02 after CRN for 12 hours at 1450°C. The insert shows the overall composition of the oxide starting powders. Both diagrams are given in equivalent-%.

The dotted and dashed lines indicate the approximate boundaries of the glass and gehlenite (G') phase regions, respectively. The exact width of these regions (ie. the range of glass-forming compositions and the extent of G' solid-solution) are not precisely defined, nor is the depth of penetration into the prism (ie. level of N incorporation). Therefore, the precise location of the endpoint in the glass end is not accurately defined and is just shown schematically in Figure 4.12. The G' phase region is located roughly within the potential glass-forming region, which correlates to previous findings that gehlenite is the main devitrification product of the grain boundary glass in reaction-sintered Ca- α -systems (Hewett, Cheng, *et al.*

1998). The curve near α' indicates the approximate extent of the single-phase α' region as located on the α' -plane (Figure 2.3b). To avoid confusion, the α' -plane is not shown.

4.2.7.2 Medium-Slag Compositions K03 and K05

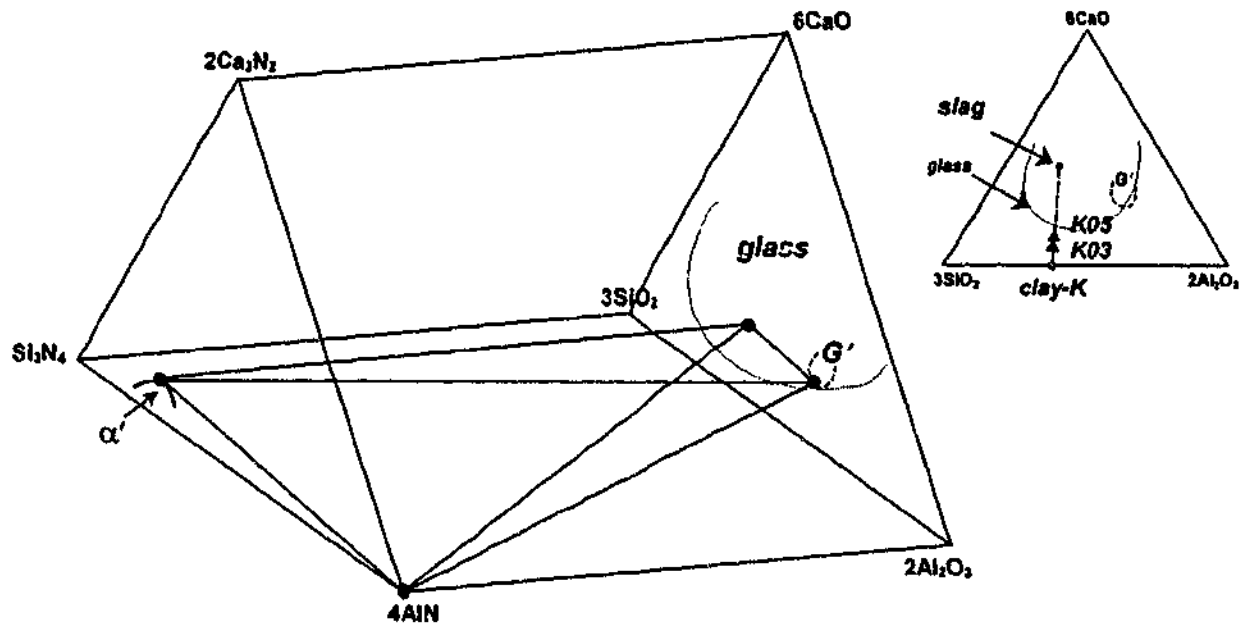
Slightly increasing the slag:clay-K ratio from K02 (0.19:1) to K03 (0.34:1) produced an abrupt change in phase behaviour; significant amounts of G' (gehlenite $\text{Ca}_2\text{Al}_2\text{SiO}_7$) were produced in addition to α -sialon, together with the minor AlN, TiN' and FeSi' phases. This discontinuity in phase behaviour was also reflected in the m-values of the Ca- α' phases in these compositions (Section 4.2.6); the m-values for K03 and K05 were both lower than for the neighbouring compositions K02 and K06. Increasing the slag content from K03 to K05 decreased the proportion of α' in the system and boosted G' formation.

As seen in the K01 sample, kinetic factors may prevent the CRN reactions reaching 100% completion within the 12 hours provided for reaction. The very low residual C-content (0.17 wt%) and lack of clear evidence of intermediate SiC amongst the final phases suggests that the CRN reactions have proceeded quite thoroughly in this composition, and CRN may be essentially complete. It is still possible, however, that the G' phase is a metastable intermediate phase, and may be converted to α' with increasing reaction time. This will require residual C or SiC formed during CRN to be present to further continue the CRN reactions. This possibility was not directly investigated in this study, however the results of high-temperature heat-treatments to be presented in Chapter 6 suggest that it may be possible because some SiC is present within the powders after CRN, probably in an amorphous form within the glass, which is invisible to XRD. The three phases α' , G', AlN', and a grain boundary glass define a tetrahedral phase compatibility region for these medium-slag content compositions shown schematically in Figure 4.13a.

4.2.7.3 High-Slag Compositions K06→K33

Increasing the slag content further from K05 (0.47:1 slag:clay) to K06 (0.62:1) changed the phase assembly such that E'-phase (nominally CaAlSiN_3) was produced as the main secondary phase to α' . The relevant phase compatibility region α' -E'-AlN'-glass is shown schematically in Figure 4.13b. Comparing the phase regions defined in Figure 4.13a and b for the medium- and high-slag compositions shows that they are essentially stacked vertically along the Ca axis, which represents the direction of compositional change resulting from increasing the slag content. Similarly, the α' - α - Si_3N_4 -AlN'-glass phase region shown in Figure 4.12 for the low-

a) Medium slag compositions K03 & K05



b) High slag compositions K06 → K33

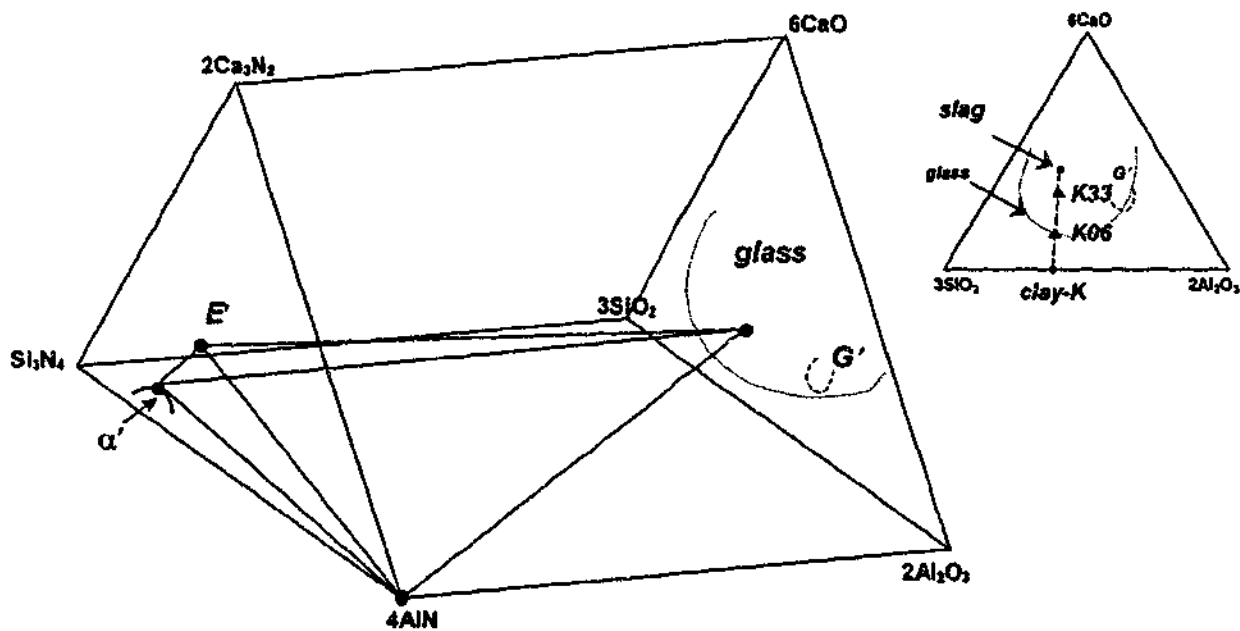


Figure 4.13 Schematic showing phase compatibility regions for compositions (a) K03 and K05, and (b) K06 to K33, after CRN for 12 hours at 1450°C. The inserts show the overall compositions of the oxide starting powders. All diagrams are given in equivalent-%.

slag K02 sample lies below the α' -AlN'-G'-glass tetrahedron. The two phase regions in Figure 4.13 appear to share a common triangular plane connecting α' , AlN', and glass, which

are phases common to both phase compatibility regions. However this may be an artefact of the diagram; the composition of the grain boundary glass has been drawn to be the same for all compositions, which may not be the case.

The K06 (0.62:1 slag:clay-K) composition produced a highly α' product, with only a small amount of E'-phase formed, and further increasing the slag content of the compositions produced greater amounts of E' at the expense of α' . Slag-rich compositions produce E' in preference to α' because E' (nominally 1:1:1 Al:Si:Ca, but may be 1:2:1 via EDXS) is much closer in composition to the \sim 1:1:1 Al:Si:Ca ratio in the slag. α -Sialon formation requires a considerably higher Si/Ca ratio than E'-phase, hence the success of relatively low-slag, high clay-containing samples K02 and K06 in producing essentially single phase α' . This is a disappointing result in terms of recycling the slag because these two successful α' -forming compositions contain more clay than slag.

The high residual C content seen in the high-slag samples after firing (\sim 3.5 wt% in K33) indicates that the CRN reactions may not have gone to completion in high-slag compositions, thus the E'-phase that dominates these CRN products may in fact be a metastable, intermediate CRN phase that is converted to α' with extended firing times. Further evidence of this metastability will be given in Chapter 6.

4.2.8 Summary

The main findings from this initial investigation of the 12 different slag+clay-K compositions are:

- α -Sialon-containing powders were formed by carbothermal reduction-nitridation of mixtures of slag and clay-K at 1450°C for 12 hours, across a wide range of compositions ranging from 0.10:1 to 3.3:1 slag:clay-K molar ratio.
- Two compositions with molar slag:clay-K ratios of 0.19:1 (K02) and 0.62:1 (K06) resulted in almost single-phase α -sialon powder. Compositions in between K02 and K06 produced a gehlenite solid-solution (G', nominally $\text{Ca}_2\text{Al}_2\text{SiO}_7$) in equilibrium with α' , and raising the slag content to K06 produced E'-phase (nominally CaAlSiN_3) as the secondary phase. AlN' was detected in all samples, and a grain boundary glass phase was also assumed to be present. Ti and Fe impurities in the slag produced minor amounts of TiN' and FeSi' impurity phases.

- The surfaces of the samples in direct contact with the flowing N_2 experienced a greater extent of CRN than the interior core material, producing a higher yield of α' . This showed that diffusion of N_2 into the pellet and removal of gas by-products are important reaction parameters.
- The low-slag, Si-rich K01 composition displayed retarded reaction kinetics, showing that the CRN reactions start before all of the reactants are fully melted, and that intermediate CRN phases include β -sialon, SiC, and possibly α - Si_3N_4 .
- The most successful α' -forming compositions were K02 and K06, but these contained more clay-K than slag, by weight. From a commercial point of view, the higher slag-containing K06 composition may be of most interest.
- The α -sialon produced via CRN was stabilised solely by Ca, with no Mg incorporated into the structure. The Ca-content (m-value) of the Ca- α -sialon tended to increase with higher slag content in the starting mixture. The Ca- α' particles were generally $\sim 1\mu m$ in diameter, and equiaxed. Other phases produced in this system are also likely to be solid-solutions.

4.3 Intermediate Phase Formation

The CRN reactions during intermediate stages of firing are investigated in this section to provide greater insight into the CRN process. Previous studies have shown that CRN occurs via several stages, the first of which is the decomposition of the mineral reactants during heating, followed by melting of the reactants and early stage CRN reactions at $\sim 1300^\circ C$ to produce intermediate oxynitride phases, followed by the late-stage CRN reactions and production of equilibrium phases (Zhang, Komeya, *et al.* 2000).

Three compositions were chosen for further investigation in this section; K06 (0.62:1 slag:clay-K), K10 (1:1) and K19 (1.9:1). With the desire to maximise the amount of slag used to produce α' , the focus is on high-slag-containing compositions. K06 produced essentially single-phase α' , as did K02, but is more slag rich and hence of greater interest. K19 was chosen to investigate the factors that promote E'-phase formation rather than α' in very slag-rich compositions, and K10 has a slag content intermediate to these two compositions.

4.3.1 Low Temperature Mineral Phase Changes During Heating in Air

4.3.1.1 Experimental Procedure

This section investigates the first phase reactions during heating up to 1200°C. Previous studies have shown that the only reactions occurring during this low temperature heating stage are mineral decomposition reactions, which are independent of the furnace atmosphere (Mazzoni, Aglietti, *et al.* 1992b; Zhang, Komeya, *et al.* 2000), hence these reactions were investigated using XRD and DTA performed in air. First, the phase transformations occurring in the slag and clay were investigated individually, followed by an examination of mixtures of slag and clay-K combined in the K06 (0.62:1) and K19 (0.19:1) molar ratios. Carbon and the α -Si₃N₄ seeds are also not expected to be involved in these mineral decomposition reactions, hence were not included in the samples. DTA was performed at 20°C/minute under flowing compressed air; and XRD phase analysis was performed on larger samples of powder heat treated in a muffle furnace for 1 hour at various temperatures up to 1200°C, in air. Any difference in the onset temperature for the observed phase transformations due to performing the DTA in air and not N is not likely to be large or significant for the qualitative discussion presented here.

4.3.1.2 Phase Transformations in Slag

A DTA trace and the XRD phase analysis of powders heat-treated at various temperatures in air are shown in Figure 4.14 and Table 4.6. There is significant baseline drift in DTA spectra obtained from this apparatus but this does not affect the location of the recorded peaks. The shape of the baseline is shown in the insert in Figure 4.14. Peaks above the baseline are from exothermic reactions, and endothermic reactions lie below the baseline. Note that the nominal, stoichiometric compositions of the phases are given, however these (Ca, Mg)-aluminosilicate phases may all be solid-solutions with some deviation from stoichiometry, as previously discussed in Section 4.2.3.2.

The phases found in the XRD analysis of the heat-treated powders appear at lower temperatures than the corresponding peaks in the DTA, which is a consequence of the relatively fast heating rate used during DTA. This shifts the recorded temperature for the DTA events to higher temperatures due to thermal lag during heating. The slag was held for 60 minutes in the furnace before air-cooling, which provided considerably greater time for the phase transformations to proceed.

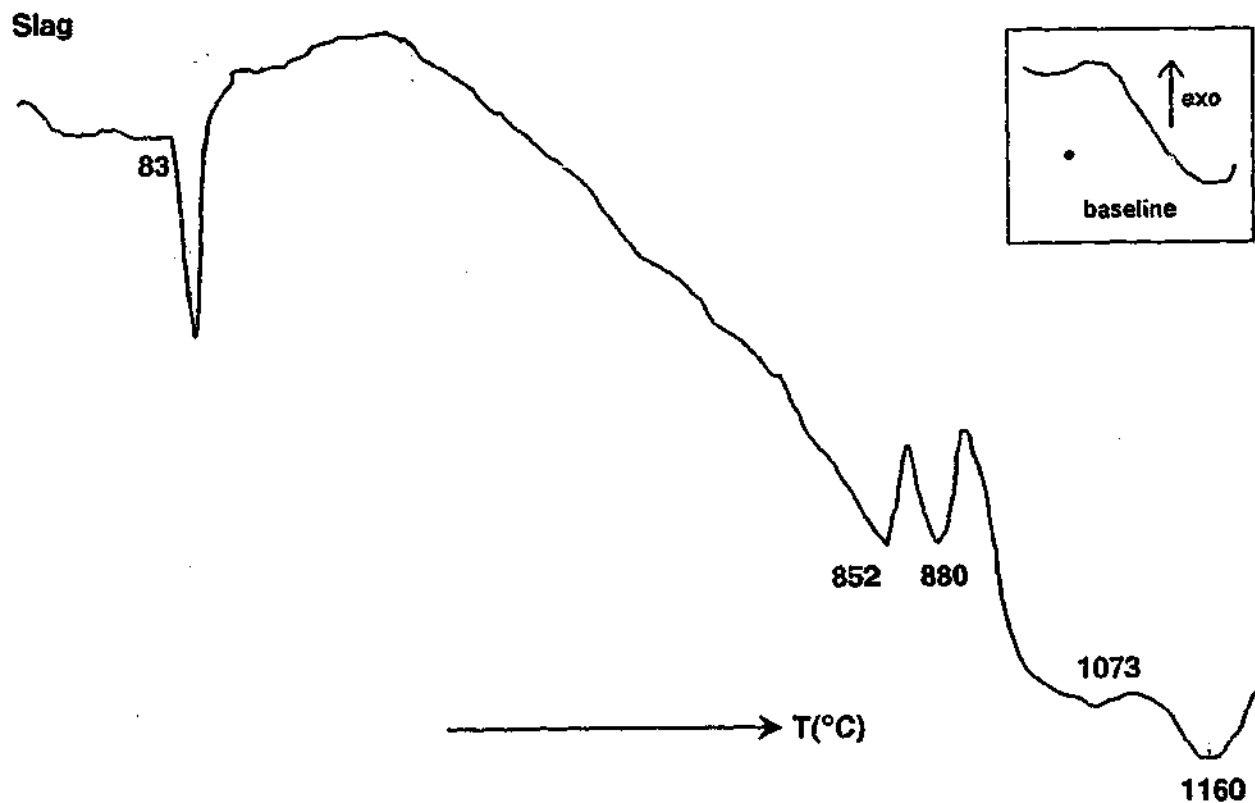


Figure 4.14 DTA curve of slag during heating in air. The insert shows the shape of the baseline.

Table 4.6 XRD analysis of slag after heating in air for 1 hour at various temperatures.

Slag	Holding Temperature (°C)							
	100	600	700	800	900	1000	1100	1200
Phases: [*]								
gypsum (CaSO ₄ ·2H ₂ O)	s							
anhydrite (CaSO ₄)		s	ms	m	w	w		
merwinite (Ca ₃ Mg(SiO ₄) ₂)				s				
gehlenite (Ca ₂ Al ₂ SiO ₇)					s	s	s	s
amorphous (estimate)	s	s	s	w	vw	vw	vw	vw

Key to XRD intensity: s=strong, ms=medium-strong, m=medium, w=weak, vw = very weak.

^{*}The nominal stoichiometric compositions are given but the phases may be solid-solutions.

According to these results, the reactions occurring during heating of the slag are:

- Dehydration of the gypsum addition ($\text{CaSO}_4 \cdot 2\text{H}_2\text{O}$) above 100°C to form anhydrite (CaSO_4) and water.
- Gradual decomposition of the anhydrite (CaSiO_4) between 600°C and 1000°C , probably via dissociation into Ca, O and $\text{SO}_3(\text{g})$. No crystalline CaO was detected in these XRD spectra, which is most likely due to the Ca-O being dissolved into the amorphous phase present at these temperatures.
- Merwinite (nominally $\text{Ca}_3\text{Mg}(\text{SiO}_4)_2$) was precipitated at 800°C , and was totally consumed by the formation of gehlenite (nominally $\text{Ca}_2\text{Al}_2\text{SiO}_7$) at 900°C , possibly via redissolution into the (liquid) amorphous phase.
- CaSO_4 dissociation is almost complete at 1000°C , but above 1100°C , G' was the only crystalline phase detected. A small amount of amorphous phase was present.
- Slag melted at $\sim 1300^\circ\text{C}$.

4.3.1.3 Phase Transformations in Clay-K

The phase transformations occurring in kaolinite clays during heating have been very well studied (Wendlandt 1986) thus detailed XRD experiments were not performed here. A DTA trace of clay-K is presented in Figure 4.15, and contains the expected thermal events; at $\sim 430^\circ\text{C}$ kaolinite ($\text{Al}_2\text{Si}_2\text{O}_5(\text{OH})_4$) decomposes to form amorphous metakaolin ($\text{Al}_2\text{Si}_2\text{O}_7$) and water. From this amorphous state, mullite ($\text{Al}_6\text{Si}_2\text{O}_{13}$) and SiO_2 cristobalite precipitate at $\sim 1060^\circ\text{C}$. The quartz impurity remains uninvolved in these reactions.

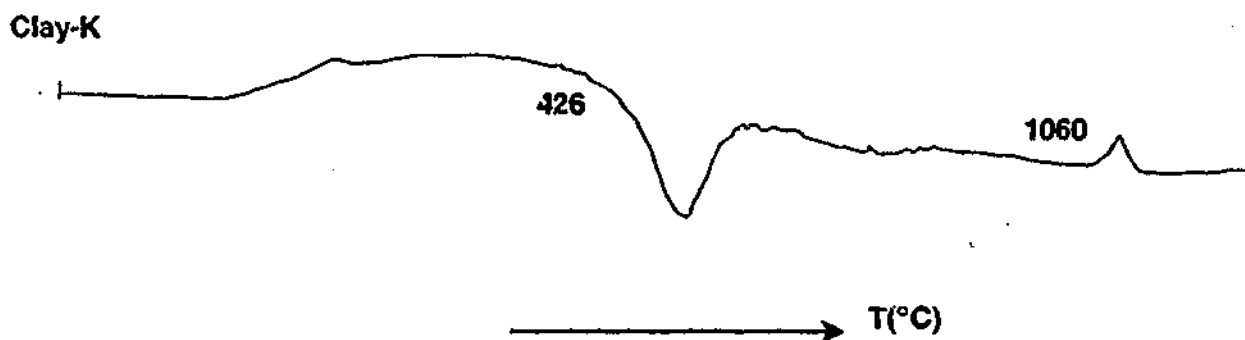


Figure 4.15 DTA curve of clay-K during heating in air.

4.3.1.4 Phase Transformations in Slag+Clay-K Mixtures

Slag+clay-K mixtures equivalent to the molar ratio in K06 (0.62:1) and K19 (0.19:1) were subjected to DTA analysis and furnace heat treatments for XRD analysis, to determine their interactions during heating. The results are shown in Figure 4.16 and Table 4.8 for K06, and Figure 4.17 and Table 4.7 for the K19 composition.

In the 0.62:1 sample clay-K is the dominant reactant, therefore the typical kaolinite decomposition reactions were observed, namely the loss of crystalline kaolin above $>420^{\circ}\text{C}$, and the precipitation of mullite and cristobalite at 970°C . An exothermic event detected via DTA at 744°C remains unidentified.

The XRD results give evidence of several crystallisation events that are not clearly seen in the DTA curve. Gehlenite (nominally $\text{Ca}_2\text{Al}_2\text{SiO}_7$) was produced at 900°C , and appeared to be consumed by the increasing formation of anorthite (nominally $\text{CaAl}_2\text{Si}_2\text{O}_8$) above 1000°C . Anorthite was not seen in the previous heat treatment of the pure slag, which may be because it requires twice as much Si for formation as gehlenite, hence required the Si boost provided by the addition of clay-K. Anorthite has been seen as a devitrification product of grain boundary glass in Ca-Al-Si-O and Ca-Al-Si-O-N systems (Thompson and Hendry 1991). Merwinite, which was seen in the heat treatment of the pure slag at 800°C , was not formed in this sample.

Mullite ($\text{Al}_6\text{Si}_2\text{O}_{13}$) was precipitated at 970°C , which is a lower temperature than found for the decomposition of the pure clay (1060°C). This is most likely due to a lowering of the energy barrier to mullite crystallisation by the formation of a low temperature eutectic liquid in this (CaO, MgO)- Al_2O_3 - SiO_2 system. The SiO_2 quartz component of clay-K was uninvolved in these phase transformations between the slag and clay, and remained in 'strong' quantities up to 1100°C , beyond which the quantity started to decrease, most probably due to dissolution into the amorphous phase.

The 1.9:1 composition was slag-rich, therefore the slag-related phases seen previously in Section 4.3.1.2 such as the amorphous hump, CaSO_4 , gehlenite, and merwinite were observed at the same temperatures as in the pure slag, but in smaller quantities. The clay-based decomposition products mullite and cristobalite were more difficult to detect. Anorthite, which was not detected in either of the pure reactants, was detected here at 1000°C .

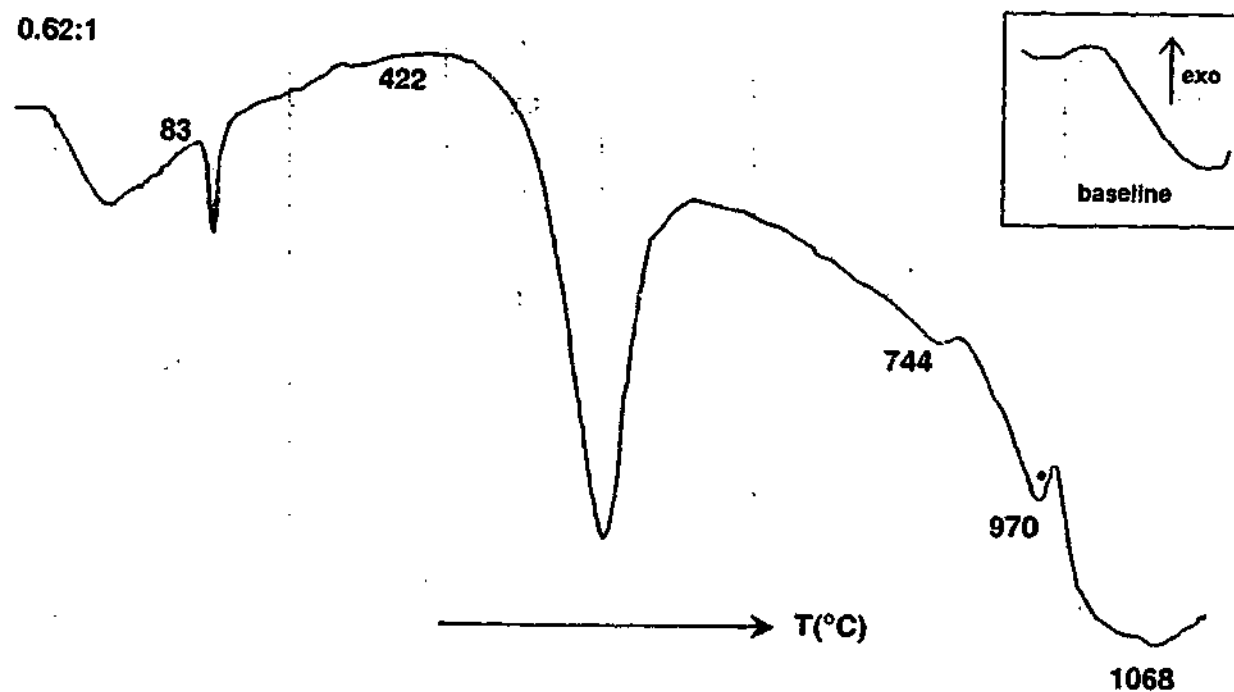


Figure 4.16 DTA curve of 0.62:1 slag:clay-K mixture during heating in air.
The insert shows the shape of the baseline.

Table 4.7 XRD analysis of 0.62:1 slag:clay-K mixture heated in air.

K06	Holding Temperature (°C)							
	400	600	700	800	900	1000	1100	1200
Phases: ^a								
anhydrite (CaSO ₄)	mw	w	w	w	w	w	vw	
kaolinite (Al ₂ Si ₂ O ₅ (OH) ₄)	s							
quartz (SiO ₂)	s	s	s	s	s	s	s	ms
gehlenite (Ca ₂ Al ₂ SiO ₇)					ms	ms	ms	w
anorthite (CaAl ₂ Si ₂ O ₈)						vw	mw	s
crystobalite (SiO ₂)							w	w
mullite (Al ₆ Si ₂ O ₁₃)						vw	w	w
amorphous		w	w	w	w	w	w	w

Key to XRD intensity: s=strong, ms=medium-strong, m=medium, mw=medium weak, w=weak, vw = very weak.

^a The nominal stoichiometric compositions are given but the phases may be solid-solutions.

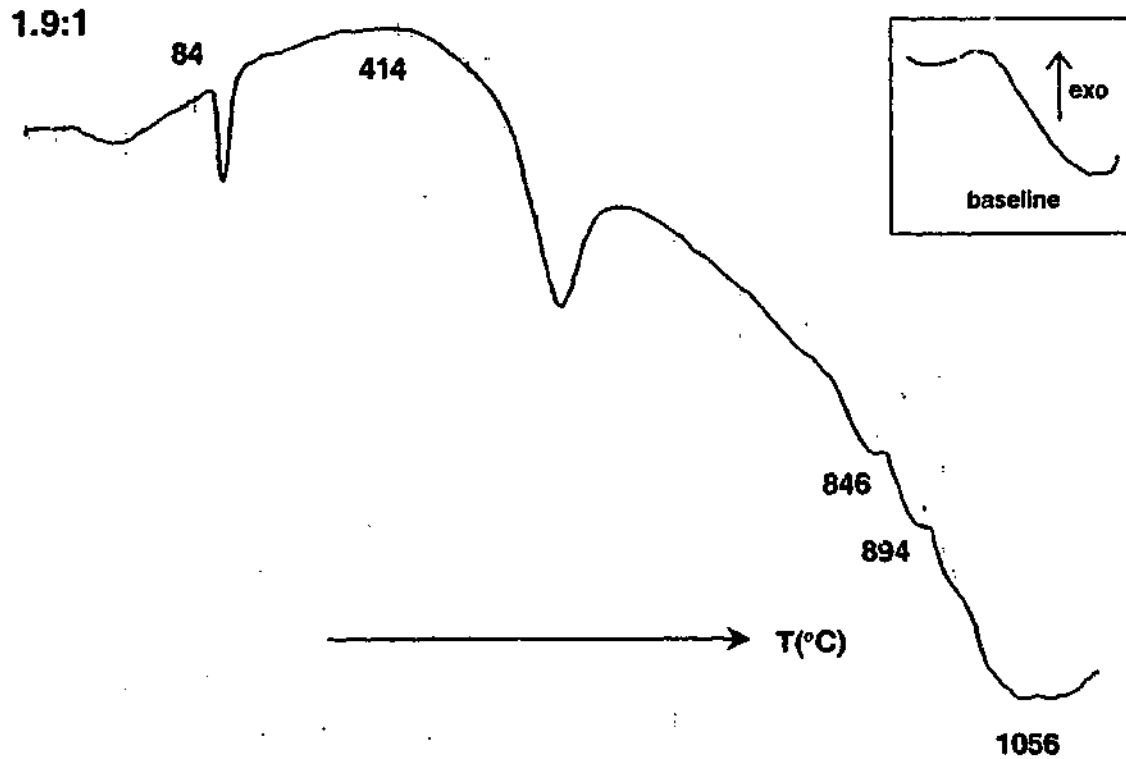


Figure 4.17 DTA curve of 1.9:1 slag:clay-K mixture during heating in air. The insert shows the shape of the baseline.

Table 4.8 XRD analysis of 1.9:1 slag:clay-K mixture heated in air at various temperatures.

KI9	Holding Temperature (°C)						
	400	600	700	800	900	1000	1100
Phases: [*]							
anhydrite (CaSO ₄)	mw	mw	mw	mw	w	w	
kaolinite (Al ₂ Si ₂ O ₅ (OH) ₄)	s						
quartz (SiO ₂)	s	s	s	s	mw	mw	w
merwinite (Ca ₃ Mg(SiO ₄) ₂)				w			
gehlenite (Ca ₂ Al ₂ SiO ₇)					s	s	s
anorthite (CaAl ₂ Si ₂ O ₈)						w	mw
mullite (Al ₆ Si ₂ O ₁₃)							vw
amorphous	s	s	s	s	vw	vw	vw

Key to XRD intensity: s=strong, ms=medium-strong, m=medium, mw=medium weak, w=weak, vw = very weak.

^{*} The nominal stoichiometric compositions are given but the phases may be solid-solutions.

Quartz from the clay-K was stable up to 800°C, but raising the temperature caused it to be consumed by the amorphous phase. This is a lower temperature for quartz dissolution than observed in the 0.62:1 mixture, where it was stable up to 1100°C. This shows that the liquid formed from the higher slag (ie. higher CaO, MgO, Al₂O₃) compositions is more reactive at lower temperatures than the SiO₂-rich liquid produced when clay dominates the composition. The quartz is thus more stable in SiO₂-rich compositions, which explains the detection of residual quartz in the lowest slag K01 composition (Section 4.2.3) at 1450°C after 12 hours of reaction.

4.3.2 CRN Reaction Sequence

The previous section investigated the phase reactions during heating in air to 1200°C, which were not expected to involve C, α -Si₃N₄, or N. At temperatures above 1200°C CRN reactions involving N will start to produce N-containing phases. Therefore the investigation of the higher temperature CRN reactions must involve the complete slag-clay-C-Si₃N₄ batch mixture, fired as per the standard CRN process parameters used previously: N₂ flowing at 30ℓ/hr and a holding temperature of 1450°C. The standard K06, K10, and K19 compositions were prepared and fired according to schedule given in Section 3.3.1.2, halting the firings at various stages between 1000°C and 1450°C to determine the phases present at intermediate stages of CRN. This is aimed at developing a good understanding of the reaction sequence and phase evolution in various high-slag compositions during CRN.

XRD phase analyses of the products formed from the three compositions are presented in Tables 4.9a, b, and c, for K06, K10, and K19, respectively. Note that the amorphous phase cannot be easily quantified, thus its presence is only be indicated as 'strong' or 'weak'. Except for the presence of the additional α -Si₃N₄ seeds, the phases formed in the K06 and K19 compositions fired in N₂ between 1000°C and 1200°C, are seen to be the same as those observed in the heat treatments of slag and clay mixtures in air (Section 4.3.1.4). This validates the previous assumption that the initial reactions during heating are thermally activated interactions between the slag and clay only. A discussion of the reactions observed above 1200°C for the three compositions are presented in the following sections.

4.3.2.1 Intermediate Reactions in Composition K06

Some XRD traces taken of powders halted at various stages during the CRN reaction sequence for composition K06 are presented in Figure 4.18. As seen in the previous section, heating the K06 (0.62:1 slag:clay-K) composition to 1200°C produces the oxide phases

anorthite ($\text{CaAl}_2\text{Si}_2\text{O}_8$), gehlenite ($\text{Ca}_2\text{Al}_2\text{SiO}_7$), mullite ($\text{Al}_2\text{Si}_2\text{O}_7$), and cristobalite (SiO_2) from reactions between the slag and kaolinite in clay-K. Free quartz from the clay-K, the $\alpha\text{-Si}_3\text{N}_4$ seeding addition, and a small amount of the FeSi' impurity phase are the only other phases found at 1200°C (Table 4.9a), in addition to a small amount of an amorphous phase that was barely visible in the XRD.

By 1300°C, melting of the reactants has started and a large amount of liquid is produced via melting of the oxides gehlenite, mullite and cristobalite, which are no longer detectable via XRD (Figure 4.18). Anorthite and a small amount of quartz are still present at this stage. Melting continues up to 1400°C, consuming the anorthite and quartz such that the amorphous phase now dominates the XRD trace, and the crystalline peaks are broad and have low overall counts. At this temperature, no crystalline oxide phases are detected in the XRD, and the first N-containing products β -sialon, M-phase (nominally $\text{Ca}_2\text{AlSi}_3\text{O}_2\text{N}_2$), Ca- α' , and TiN', are formed (Figure 4.18). This shows that at this temperature, N from the furnace atmosphere has been incorporated into the liquid via CRN reactions, and the first precipitation of oxynitride crystalline phases has begun. The onset of CRN for the K06 composition is therefore between 1300 and 1400°C.

M-phase ($2\text{CaO}\cdot\text{AlN}\cdot\text{Si}_3\text{N}_4$) is a metastable oxynitride phase reported in the literature to be stable up to 1400°C in reaction-sintered Ca- α -sialon systems (van Rutten, Hintzen, *et al.* 1996) and up to 1450°C during the hot-pressing of $2\text{CaO}\cdot\text{AlN}\cdot\text{Si}_3\text{N}_4$, beyond which it decomposes to E'-phase (CaAlSiN_3), AlN, and glass (Huang, Sun, *et al.* 1985). As with most crystalline phases in this system, the M-phase is likely to be a solid-solution, and therefore is designated M'. β -Sialon has been noted as a common intermediate phase to α' in previous CRN studies, and the small displacement of the β' XRD peaks relative to $\beta\text{-Si}_3\text{N}_4$ (equivalent to a $z=0$ β') indicates that the β' phase was of a low z -value, ie. low Al-O content. It was also a relatively short-lived intermediate phase, being detected only during heating at 1400°C and 1450°C; after 30 minutes of holding at 1450°C β' could no longer be detected. No other intermediate phases previously reported to form during the CRN of α' such as $\text{Si}_2\text{N}_2\text{O}$, X-phase, AlON, or crystalline SiC, were detected here, however the broad nature of many of the peaks, and the large extent of peak overlap indicate that minor amounts of these or other phases, perhaps poorly crystallised, may be present but are unable to be clearly identified.

Table 4.9a XRD phase analysis of samples taken at various intermediate points between 1000-1450°C during firing of composition K06.

K06	Temp (°C)	1000	1100	1200	1300	1400	1450	1450	1450	1450	1450			1450	
	Hold Time:	1 min	30 min	3 hrs	6 hrs	6 hrs		12 hrs							
Phase: (nominal composition)		core	surf	core	side	core	surf	core	surf						
α -Si ₃ N ₄		mw	mw	mw	mw	mw	mwvw	w							
quartz (SiO ₂)		s	s	ms	mw										
gehlenite (Ca ₂ Al ₂ SiO ₇)		ms	mw	w											
anorthite (CaAl ₂ Si ₂ O ₈)		w	mw	s	s										
crystobalite (SiO ₂)		vw	vw	w											
mullite (Al ₄ Si ₂ O ₁₃)		vw	w	w											
amorphous (s/w only)		w	w	w	s	s	s	w	w	w					
β -sialon						ms	w								
M'-phase (Ca ₂ AlSi ₃ O ₂ N ₃)						mw	ms	ms							
AlN'							w	w	vw	vw				w	
E'-phase (CaAlSiN ₃)									w	mw				w	
Ca- α -sialon						w	mw	ms	s	s				s	
TiN'						w	w	w	vw	w				vw	
FeSi'				vw	vw	vw	vw		vw	vw				vw	
? = unidentified phase		vw	vw	vw	w	w	w	vw	vw	vw				vw	

Key to XRD intensity: s=strong, ms=medium-strong, m=medium, mw=medium weak, w=weak, vw = very weak.
* The nominal stoichiometric compositions are given but the phases may be solid-solutions.

Table 4.9b XRD phase analysis of samples taken at various intermediate points between 1000-1450°C during firing of composition K10.

K10	Temp (°C)	1000	1100	1200	1300	1400	1450	1450	1450	1450	1450	1450	1450
	Hold Time:	1 min	30 min	3 hrs	6 hrs	12 hrs							
Phase: (nominal composition)		core	core	core	core	core	core	core surf					
α -Si ₃ N ₄			mw	mw	mw	w	w	w vw					
quartz (SiO ₂)			ms	w									
gehlenite (Ca ₂ Al ₇ SiO ₇)			s										
anorthite (CaAl ₂ Si ₂ O ₈)			mw	s	s								
crystobalite (SiO ₂)													
mullite (Al ₆ Si ₂ O ₁₃)			w	vw									
amorphous (s/w only)			w	w	w	s	s	w w					
β -sialon						w	vw						
M'-phase (Ca ₂ AlSi ₃ O ₂ N ₃)						vw	w	mw w					
AlN'								vw vw		vw vw	vw vw	vw vw	
E'-phase (CaAlSiN ₃)								s		ms mw	ms		
Ca- α -sialon						w	w	mw s	s	s	s s	s s	
TiN'					vw	vw	vw	vw vw	vw	vw vw	vw vw	vw vw	
FeSi'				vw	vw	w	vw	vw		vw	vw vw	vw vw	
? = unidentified phase			vw	w	vw	w	w	vw vw	vw	vw	vw vw	vw vw	

Key to XRD intensity: s=strong, ms=medium-strong, m=medium, mw=medium weak, w=weak, vw = very weak.

* The nominal stoichiometric compositions are given but the phases may be solid-solutions..

Table 4.9c XRD phase analysis of samples taken at various intermediate points between 1000-1450°C during firing of composition K19.

K19	Temp (°C)	1000	1100	1200	1300	1400	1450	1450	1450	1450	1450	1450	1450		
	Hold Time:	1 min	30 min	3 hrs	12 hrs	12 hrs	6 hrs	6 hrs							
Phase (nominal composition)		core	surf	core	core	surf	surf	core	surf						
α -Si ₃ N ₄		mw	mw	mw	mw	mw	mw	w							
quartz (SiO ₂)		m	m	mw											
gehlenite (Ca ₂ Al ₂ SiO ₇)		s	s	s	s	s	ms	w	vw	vw					
anorthite (CaAl ₂ Si ₂ O ₈)			mw	mw	mw										
crystobalite (SiO ₂)															
mullite (Al ₆ Si ₂ O ₁₃)															
amorphous (s/w only)		w	w	s	s	w	s	w	s	-					
β -sialon							vw								
M'-phase (Ca ₂ AlSi ₃ O ₂ N ₃)							vw	ms	ms	m					
AlN'							mw	w	w	w				w	
E'-phase (CaAlSiN ₃)									w	s				s	
Ca- α -sialon							vw	w	m	s	w			w	
TiN'							vw	vw	vw	vw	w				
FeSi'				vw	vw	vw	vw	vw	vw	vw					
? = unidentified phase		vw	vw	vw	vw	vw	w	vw	vw	vw					

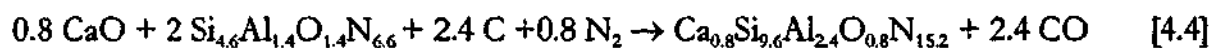
Key to XRD intensity: s=strong, ms=medium-strong, m=medium, mw=medium weak, w=weak, vw = very weak.

* The nominal stoichiometric compositions are given but the phases may be solid-solutions.

Ca- α -sialon was first detected at 1400°C, together with the intermediate phases β' and M' . It is possible that the dissolution of β' and M' phases into the liquid was followed by precipitation of α' , but it is also possible that the first α' was precipitated from reaction between just the α - Si_3N_4 seeds and the Ca-Al-Si-O-N liquid, and did not involve these intermediate phases. The role of the α - Si_3N_4 seeds remains unclear; they may provide nucleation sites for α' , or may be dissolved into the liquid and be a reactant for α' formation. β' , M' , and α - Si_3N_4 are all present after 30 minutes of reaction at 1450°C, though only the M' -phase is still detected after 3 hours, which suggests that the production of α' occurs via the further formation of intermediate M' -phase once the α - Si_3N_4 seeds are exhausted.

AlN' was first detected once the sample had reached 1450°C, although peak overlap with M' makes identification difficult. After 30 minutes, E' -phase was also detected for the first time, but only on the surface of the pellet. The CRN reactions proceeded more rapidly on the surface, with more Ca- α' and E' , less M' , and no α - Si_3N_4 detected on the surface when compared to the core.

In the study by van Rutten and co-workers, the process by which the intermediate β' was converted to α' was seen to be a CRN reaction between β' , C, and the Ca-Al-Si-O-N liquid, as given in Equation 4.4 (van Rutten, Terpstra, *et al.* 1995).



This CRN process relies on solution-precipitation: the β' - phase and additional N are dissolved into the liquid, from which α' is subsequently precipitated. A similar process is likely to operate in slag+clay-K system studied here, whereby the intermediate β' and M' -phases are converted to α' by continued CRN reactions involving solution-precipitation from the liquid phase.

After 3 hours of reaction, phase formation appears complete; no intermediate phases are detected, and the sample is predominantly α' plus a small amount of E' , AlN' , and glass. Increasing the reaction time to 12 hours produced a small decrease in the quantity of E' in the sample, suggesting that the E' -phase is in fact a metastable phase that can be slowly converted to α' with increasing reaction time, i.e. it is an intermediate CRN product that remains amongst the final products after CRN at 1450°C for 12 hours due to incomplete conversion to α' .

4.3.2.2 Intermediate Reactions in Composition K10

The XRD phase analysis for the K10 (1.0:1 slag:clay-K) composition was given in Table 4.9b. K10 behaved very similarly to K06 during heating; melting of the oxides and the onset of CRN occurred at temperatures between 1300 and 1400°C producing TiN', β' , M', and Ca- α' by 1400°C. AlN' was first seen when the sample reached 1450°C; but β' was barely detectable. M'-phase was present for at least the first 30 minutes at 1450°C, and the Ca- α' -content increased with increasing time at 1450°C. The main difference to the K06 sample is that E' was not detected in the sample fired for 30 minutes, but was present after 3 hours at 1450°C.

The K10 composition was the only sample analysed after holding at 1450°C for 6 hours. As with the K06 sample, increasing the reaction from 3 to 6 hours decreased the amount of E' in the products, but further extending the firing time from 6 to 12 hours at 1450°C did not appear to result in a significant change in relative phase content. This suggests that 6 hours may be adequate for CRN at 1450°C. Again, the reactions appeared more complete on the surface of the pellets, with the final products all found after shorter reaction times, and more Ca- α' and less E' present after 12 hours.

4.3.2.3 Intermediate Reactions in Composition K19

The XRD phase analysis for the K19 (1.9:1 slag:clay-K) composition was given in Table 4.9c, and XRD traces taken at various stages during reaction are presented in Figure 4.19. The high-slag K19 composition displayed essentially the same reaction processes as K06 and K10 with one difference; the oxynitride liquid formed at 1400°C crystallised during cooling to produce gehlenite, which was seen in all XRD traces from samples taken after reaching 1400°C.

At 1300°C, a large amount of liquid was produced with the main oxide phases (in this case gehlenite and anorthite) remaining undissolved in this liquid. Recall that Ca-rich gehlenite ($\text{Ca}_2\text{Al}_2\text{SiO}_7$) was favoured over Si-rich anorthite ($\text{CaAl}_2\text{Si}_2\text{O}_8$) when heating the slag rich K19 composition in air (Section 4.3.1.4), and that quartz dissolution occurs at lower temperatures into the Ca, Mg, and Al-rich liquid produced in this sample. According to the results seen for the K06 and K10 compositions, further heating to 1400°C should cause the production of a large amount of liquid (the large amorphous hump in the XRD) and oxynitride CRN products β' , M', and Ca- α' , all of which will precipitate from this N-rich liquid. However in the K19 composition, the XRD reveals only 'very weak' amounts of the amorphous phase and oxynitride CRN products (Figure 4.19), with crystalline gehlenite (nominally $\text{Ca}_2\text{Al}_2\text{SiO}_7$) dominating the phase assembly.

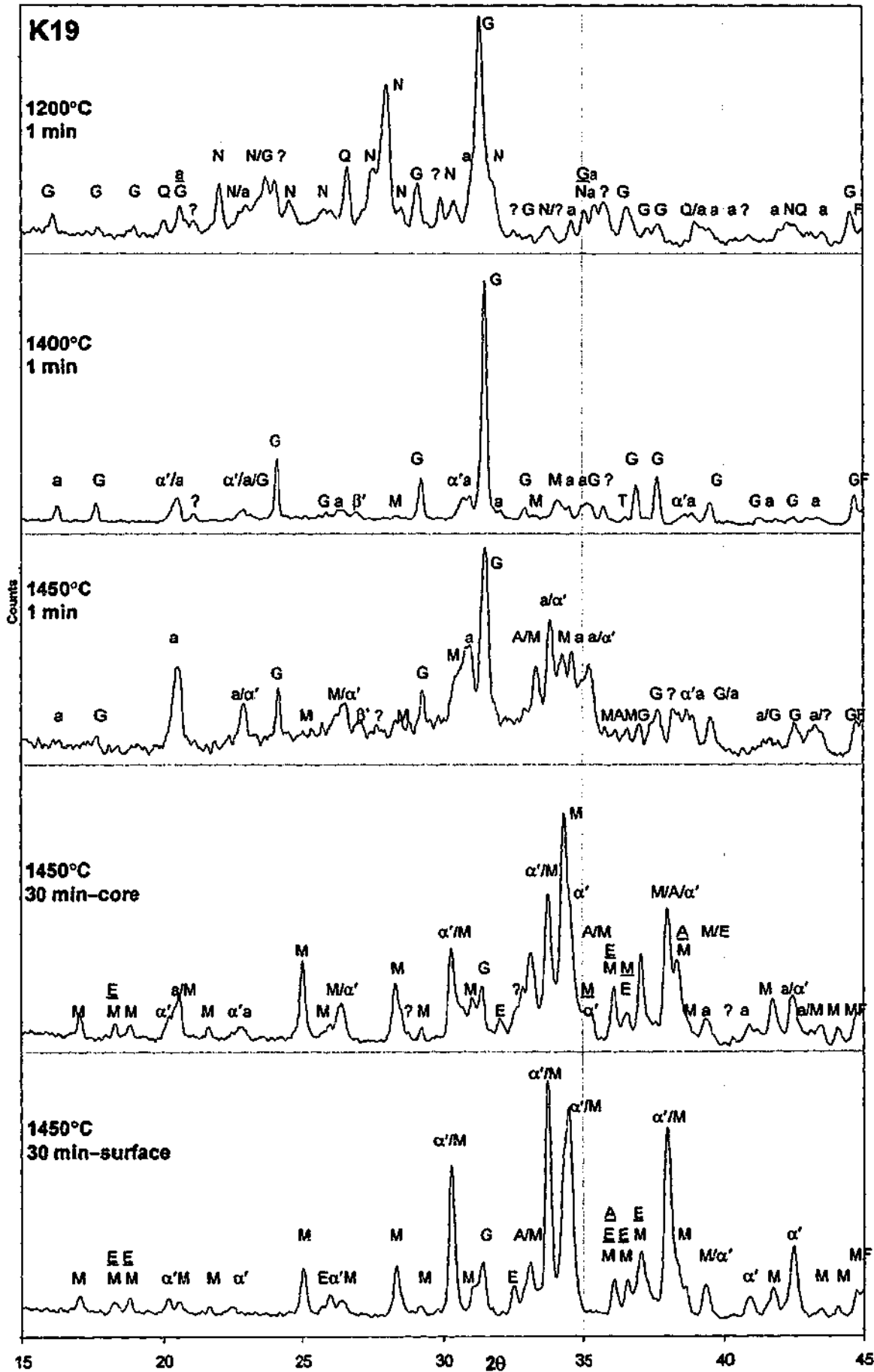


Figure 4.19 XRD traces from samples taken at various intermediate points between 1300-1450°C during firing of composition K19.

[Key: a= α - Si_3N_4 , A= AlN' , α' =Ca- α -sialon, β' = β -sialon, E=E'-phase, F= FeSi' , G=gehlenite, M=M'-phase, N=anorthite, T= TiN' , Q=quartz, ?=unidentified].

Gehlenite has been detected as the main devitrification product of high Ca compositions in the Ca- α -sialon system (Wood and Cheng 2000) and was the dominant phase crystallised from the pure slag and the K19 high-slag composition during heating (Section 4.3.1.4). The glass produced in this higher slag composition is thus closer in composition to gehlenite than that in the lower-slag samples, and was able to crystallise during the slow 3°C/min cooling in the furnace. The presence of oxynitride phases precipitated from the liquid at 1400°C shows that N has been incorporated into this liquid, and thus the gehlenite crystallised from it will be expected to be a N-containing gehlenite, G', (ie. $\text{Ca}_2\text{Al}_{2-x}\text{Si}_{1+x}\text{O}_{7-x}\text{N}_x$).

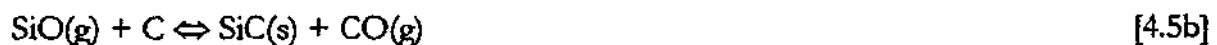
This is a different phase to the pure oxide gehlenite (nominally $\text{Ca}_2\text{Al}_2\text{SiO}_7$) formed via interactions between the slag and clay during heating between 900 and 1300°C, which subsequently melts to produce the liquid.

The large amount of G' formed at 1400°C indicates that as with the K06 and K10 compositions, a large amount of liquid is present at this temperature from which the β' , M' and α' phases are precipitated. The amount of G' seen in the XRD traces taken from further stages of reaction decreases with time spent at 1450°C, demonstrating that the liquid formed in the system is consumed by the continuing CRN reactions. A small peak corresponding to the 100% intense G' peak at $\sim 31.4^\circ$ remains in the XRD trace, even after 12 hours. In fact, a closer inspection of the XRD scans from various K-series compositions produced after 12 hours of CRN (Figure 4.7) shows that an unidentified peak at $\sim 31.4^\circ$ is present in most XRD traces from high-slag compositions K10 and above, which can now be attributed to G' devitrified from the glass upon cooling. This G' is not considered to be a CRN product phase, thus does not alter the phase compatibility behaviour of the high-slag compositions described in Section 4.2.7. However, the G' formed in the medium-slag K03 and K05 compositions is a CRN product phase and cannot be the devitrification product of glass; an extremely large amount of liquid would be required to produce such a high amount of G', and the lack of any other CRN intermediate phases found together with G' suggests that the CRN reactions have progressed quite thoroughly in this sample, with α' and G' being the CRN product phases

Again, the reactions on the surface proceeded faster than in the core of the pellets, and after 3 hours of reaction the final phase assembly of E' and 'weak' amounts of α' and AlN' were produced, with no significant change observed after the full 12 hours was complete.

4.3.2.4 Surface/Core Effect and Influence of Reaction Kinetics

The enhanced rate of reaction observed on the surface of the pellets when compared to the core is unsurprising due to the dual role played by the N₂ gas; it both delivers the reactant N to the pellet, and removes gaseous CRN by-products and thereby encourages further CRN. Work by Higgins and Hendry on the CRN of kaolinite clay for β-sialon production showed that CRN proceeds via reversible equilibrium reactions which produce gaseous reaction products (Higgins and Hendry 1986). For example, the carbothermal reduction of free SiO₂ to SiC proceeds via a gas phase process described by Equations 4.5a and b, and the CRN of mullite to β-sialon occurs via Equation 4.6. Nitridation is favoured by high partial pressures of SiO(g) and low partial pressures of CO(g), and it has been shown in the work by Higgins and Hendry that there exists a maximum CO-content above which the reaction for the reduction of mullite is reversed and β-sialon is not formed. Therefore the CO(g) must be continuously removed to encourage the CRN product formation, rather than the reverse reaction.



The cores of the pellets experience relatively lower N penetration due to the gas having to diffuse through the dense compact, resulting in less efficient removal of CO in the core, and the higher $p[\text{CO}]$ (CO partial pressure) impedes the nitridation process. The CO formed on the surface will be removed much more efficiently by the free-flowing gas, but the heavier SiO(g) will not be swept away as easily, thus increasing the relative $p[\text{SiO}]$ at the surface and promoting the nitridation reactions. This accounts for the more rapid formation of final CRN products such as α' seen on the surface of the all pellets, even after only 30 minutes at 1450°C. The lower quantity of E' formed on the surface of these pellets further demonstrates that E' is a metastable, intermediate CRN product, which can be converted to α' under conditions where CRN is enhanced. It would therefore be expected that firing the powders without pressing would promote the yield of α', and preliminary work in this system suggests that this is true. This will be investigated further in Chapter 6.

4.3.3 Summary

The previous results show that the CRN reaction process is fundamentally the same in all three slag+clay-K mixtures and consists of three stages:

1) Initial reactions [R.T. → 1300 °C]

These reactions during heating involve the thermal decomposition of the mineral reactants and subsequent crystallisation of various oxide phases. This process has two stages:

- loss of physical and structural water and decomposition of the clay and gypsum between 100 and 600°C;
- precipitation of various crystalline phases merwinite, gehlenite, anorthite, mullite, and cristobalite, between 800°C and 1000°C. In lower slag compositions anorthite (nominally $\text{CaAl}_2\text{Si}_2\text{O}_8$) is the main phase produced, and in higher slag compositions gehlenite (nominally $\text{Ca}_2\text{Al}_2\text{SiO}_7$) is the dominant phase.

2) Melting and early stage CRN [1300-1400 °C]

The previously formed oxide phases melt above 1300°C to form a liquid, and N is incorporated into this liquid via CRN reactions. Intermediate oxynitride phases β -sialon and M'-phase are precipitated, as well as the first Ca- α' and the TiN' impurity phase.

3) Final nitride product formation [1450 °C]

The intermediate phases are gradually consumed for final product formation. β' is no longer produced, and the intermediate β' and M' are converted to E', AlN', and Ca- α -sialon. The E' and AlN' phases may in fact be intermediate phases that have not yet been converted to α' and thus appear amongst the final 'steady state' products of CRN after 12 hours at 1450°C. The initial rate of final product formation varies with composition, however 6 hours at 1450°C may be adequate for completion of the CRN reactions at 1450°C in this system. The reactions proceed faster on the surface of the pellets, due to greater contact with the N_2 gas.

4.4 Conclusions for Chapter Four

This chapter presented the results of the first detailed investigation into using CRN to produce α -sialon from mixtures of slag and clay. The main conclusions to be drawn from this chapter are:

- α -Sialon can be produced from mixtures of slag and a kaolinite (clay-K) across a wide range of compositions ranging from 0.19 → 3.3:1 slag:clay-K (molar ratio), after 12 hours of reaction at 1450°C under N_2 flowing at 30ℓ/hr. The most successful compositions that produced predominantly single-phase α' powders were K02 (0.19:1

slag:clay-K) and K06 (0.62:1), both of which were clay rich. The main secondary phases found in these two compositions were α - Si_3N_4 , AlN' and glass for K02, and E' -phase (nominally CaAlSiN_3), AlN' and glass for K06. Impurity phases FeSi' and TiN' were also formed from the impurities present in the slag and clay. The crystalline products were all solid-solutions with some deviation from the defined stoichiometry.

- The slag content of the composition greatly influences the final phases formed; slag contents higher than K02 but below K06 produced gehlenite (G' , nominally $\text{Ca}_2\text{Al}_2\text{SiO}_7$) as the main secondary phase to α' , and E' -phase is produced in increasing amounts as the slag content is raised above K06 (0.62:1). CRN of the K01 (0.10:1) slag:clay-K sample which contained the lowest quantity of slag could not be completed within 12 hours of reaction at 1450°C . This is thought to be due to retarded reaction kinetics in this SiO_2 -rich composition.
- The kinetics of the CRN reactions are controlled by both the composition and access to the flowing N_2 gas stream; the surfaces of the compacted powders exposed to the N_2 gas flow displayed a greater ability to produce α -sialon more rapidly than in the core of the pellets, where the diffusion of gaseous species was hindered.
- The CRN reaction process consists of three stages: 1) decomposition of the oxide reactants and phase transformations during heating to 1300°C , 2) melting of the oxide phases and early stage CRN between 1300 and 1400°C to produce the first oxynitride phases, and 3) final product formation and elimination of intermediate phases with extended holding time at the maximum reaction temperature (1450°C). During Stage 1, the melting, dissolution, and reprecipitation of various Ca-Mg-Al-Si-O phases does not involve N, C, or the α - Si_3N_4 seeds. A low z-value β -sialon and M' -phase (nominally $\text{Ca}_2\text{AlSi}_3\text{O}_2\text{N}_2$) are the two main intermediate phases produced during Stage 2 of CRN, and are rapidly consumed for continued α' formation in Stage 3. The G' , E' and AlN' found in the final products may also be metastable intermediate CRN phases unable to be converted to α' under the conditions used.
- The α' produced from the slag and clay mixtures is stabilised only by Ca, and forms as generally sub-micron, equiaxed grains. The Ca-content (m-value) of the α' tends to increase with increasing slag content of the system. The E' -phase formed in high-slag compositions K06 and above has a coarse, plate-like morphology.

Chapter Five

Effect of Using Concentrated Sources of Silica on the Carbothermal Reduction-Nitridation of Slag

The previous chapter has established that a wide range of slag+clay-K mixtures can be reacted at 1450°C to produce powders containing α -sialon via CRN. Of the twelve compositions tested, however, only two were effective in producing nearly single-phase α' : K02 (0.19:1 slag:clay-K) and K06 (0.62:1). Both of these compositions contain more clay-K than slag by weight, highlighting the role of clay in boosting the SiO_2 -content of the system to allow the formation of Si-rich α' . It is desired in this investigation, however, to recycle as much slag as possible, hence it was thought that it might be possible to minimise the amount of clay added and use more slag in the compositions if clay-K was replaced with a more concentrated source of SiO_2 . Accordingly, two alternative SiO_2 -rich additives were proposed: pyrophyllite clay and sand. Various compositions containing these two SiO_2 -rich additives were fired for CRN, and the effects on the CRN process and final phase formation are presented in this chapter.

5.1 Analysis of the Raw Materials and Experimental Procedure

A description of the two alternative SiO_2 -additives is presented here, followed by details regarding the composition selection and the firing conditions used for experiments in this chapter. A full chemical analysis of all the SiO_2 -additives was given previously in Table 3.1, and this information is summarised in Table 5.1 below.

Table 5.1 Summary of the composition of the SiO_2 -additives used in this investigation.

SiO_2 -additive	SiO_2 (wt%)	Al_2O_3 (wt%)	Volatiles [H_2O & LOI] (wt%)	Others
clay-K (kaolinite)	53.3 (17.6% quartz)	30.3	11.4	5.0
clay-P (pyrophyllite)	76.7 (5.1% quartz)	17.9	3.8	1.6
sand (quartz)	99.7	0.1	0.1	0.1

5.1.1 Clay-P (Pyrophyllite)

Pyrophyllite ($4\text{SiO}_2 \cdot \text{Al}_2\text{O}_3 \cdot \text{H}_2\text{O}$) is the main constituent of clay-P, and despite containing twice as much SiO_2 per mol as kaolinite (the main component of clay-K), the overall SiO_2 -content is not double that of clay-K due to the high level of quartz impurity in clay-K. Clay-P contains 76.7 wt% SiO_2 in the as-received state compared to 53.3 wt% in clay-K, with quartz accounting for 5.1 wt% of this SiO_2 . When using clay-P to provide the same SiO_2 -content (wt%) as was provided by clay-K, the lower Al_2O_3 and moisture content allows a smaller mass of this clay to be used.

An XRD trace of clay-P is given in Figure 5.1. As mentioned when discussing the XRD trace of clay-K (Figure 4.3), quartz is a very strongly diffracting phase even in small amounts, and the quartz peaks in clay-P dominate the XRD trace (Figure 5.1). All of the unlabelled peaks correspond to pyrophyllite. The low, broad nature of the pyrophyllite XRD peaks are a result of the high degree of stacking irregularities which is common in natural pyrophyllite (Brindley and Brown 1984). The SEM micrograph (Figure 5.2a) shows that the particles are generally flat plates with a particle size $\sim 2\mu\text{m}$, which is larger than that of clay-K.

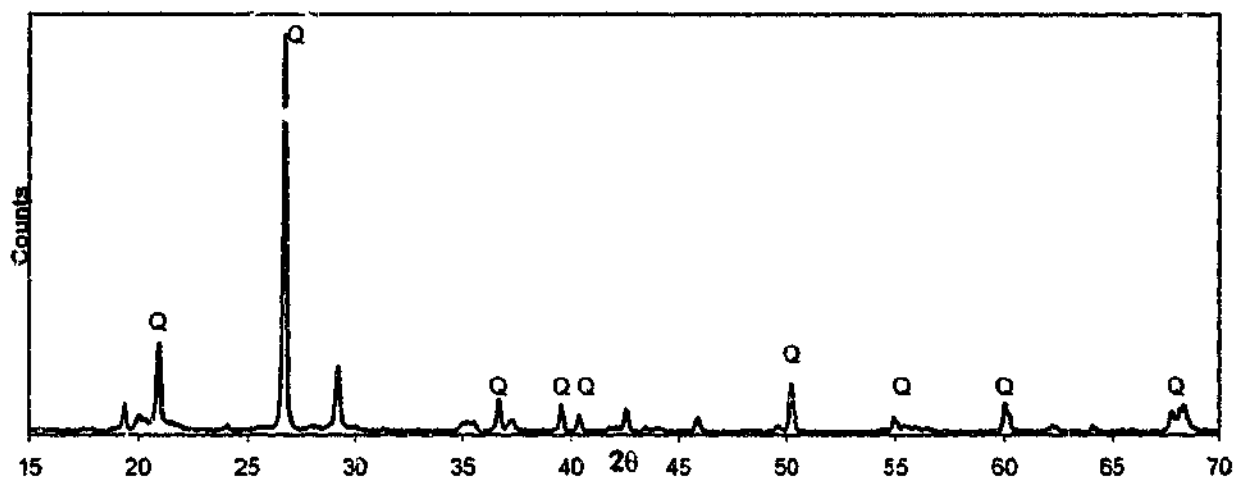


Figure 5.1 XRD trace of clay-P. The peaks corresponding to SiO_2 quartz are indicated ('Q'); all other peaks correspond to pyrophyllite.

5.1.2 Sand (Quartz)

Sand is a mineral source of pure (99.7%) SiO_2 quartz. The sand used here had an as-received particle size of $\sim 1\text{mm}$ which was reduced by aggressive ball milling in alcohol for 72 hours. A wide particle size distribution was produced, ranging from $<1\mu\text{m}$ to a maximum of $\sim 300\mu\text{m}$. An XRD trace of the milled sand is given in Figure 5.3, and an SEM image in Figure 5.2b. The SEM micrograph shows the smaller particles have a fractured appearance from the ball milling.

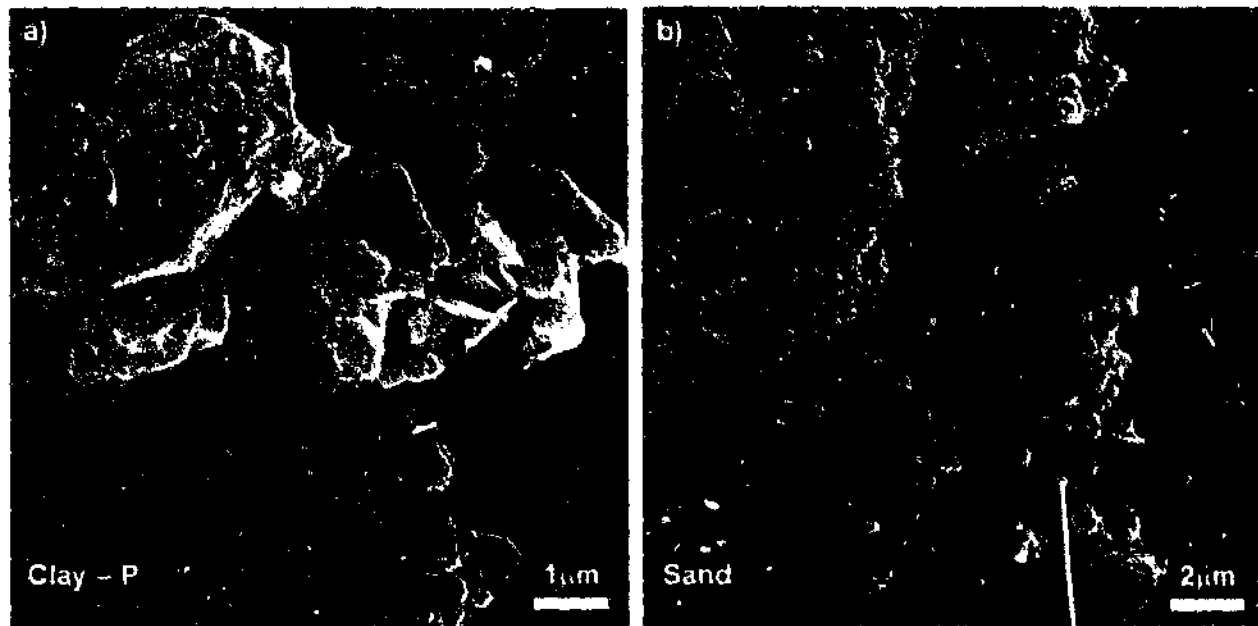


Figure 5.2 SEM micrographs of (a) pyrophyllite clay-P, (b) milled sand.

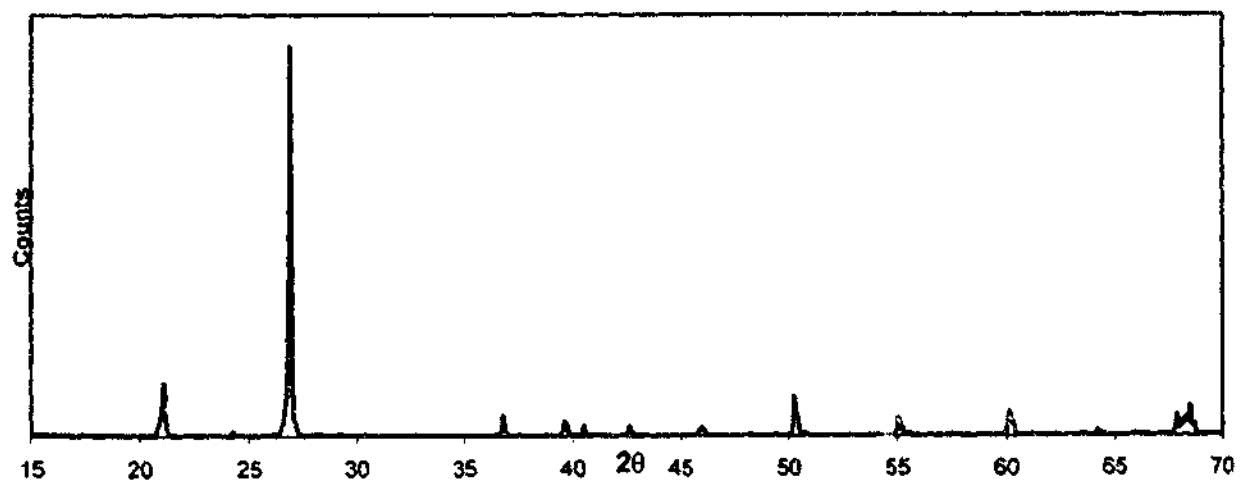


Figure 5.3 XRD trace of sand after milling. All peaks correspond to SiO_2 quartz.

5.1.3 Composition Selection and Firing

Three K-series compositions were chosen for emulation using clay-P and sand: the compositions K02 (0.19:1 slag:clay-K) and K06 (0.62:1) which previously formed nearly single-phase α' , and the equivalent of 1.5:1 slag:clay-K. This was composition not actually investigated in the K-series (the nearest being 1.4:1 K14) but which was chosen here to represent a reasonably high slag-containing composition. The amount of clay-P or sand to be added to the slag was calculated such that the overall SiO_2 -content of the K-series compositions was maintained. The $\alpha\text{-Si}_3\text{N}_4$ seeding level was fixed at 6.3 wt% of the total batch weight for the clay-P samples, which was the average seeding level used in the K-series compositions, and 10 wt% for the sand samples where it was thought that more assistance via seeding may be required.

The same nomenclature used for the K-series will be used for these compositions: Pxx refers to the clay-P samples (P-series), and Sxx refers to the sand samples (S-series) with xx denoting 10x the slag:additive molar ratio. The K-series base compositions and the clay-P and sand equivalents are listed in Table 5.2. The proportion of slag, in terms of the mass percent of the two component slag:additive mixture is also listed.

Table 5.2 Molar ratios of K-series and equivalent P- and S-series compositions, and slag content as a function of just the slag and SiO_2 -additive.

slag:clay-K basis molar ratio [wt% slag / (slag + clay)]	slag:clay-P equivalent molar ratio [wt% slag / (slag + clay)]	slag:sand equivalent molar ratio [wt% slag / (slag + sand)]
0.19:1 (K02) [14.5 wt% slag]	0.25:1 (P02) [19.7 wt% slag]	0.31:1 (S03) [24.2 wt% slag]
0.62:1 (K06) [35.7 wt% slag]	0.82:1 (P08) [44.4 wt% slag]	1.00:1 (S10) [50.9 wt% slag]
1.50:1 (K15) [57.4 wt% slag]	1.99:1 (P20) [65.9 wt% slag]	2.42:1 (S24) [71.6 wt% slag]

Increasing the concentration of SiO_2 by changing the additive did not result in a significant increase in the overall slag content of the compositions based on K02 and K06. The higher slag composition based on K15 received the most benefit, with the slag content of the batch increasing by ~25 wt% when changing from clay-K to sand.

The firing of these samples for CRN followed the same standard firing schedule as used for the K-series compositions (Section 3.1.1.1), with one change made to the sample preparation: loose heaps of powder were fired rather than compacted pellets. By the time these experiments were performed, it was determined that the extent of CRN could be slightly improved and the sample preparation process simplified by not pressing the powders into pellets. This result is discussed in further detail in Chapter 6.

5.2 P-series Firings: Slag + Clay-P (Pyrophyllite)

5.2.1 Firings Performed for 12 Hours at 1450°C

The three clay-P compositions P02, P08 and P20 were each fired for 12 hours at 1450°C. XRD traces are shown in Figure 5.4, and the results of phase analysis are listed in Table 5.3. It is clear that pure α' could not be formed in any of these samples despite P02 and P08 having essentially the same composition as K02 and K06, which did form nearly single-phase α' under the same firing conditions.

α - Si_3N_4 was the main reaction product in the P02 sample, with some α -sialon also detected as seen in the broadening of the α - Si_3N_4 peaks. The amount of α - Si_3N_4 found is much larger than can be attributed to the 6.3% seeding addition in the starting powder. A 'strong' amount of the gehlenite solid-solution phase G' (nominally $\text{Ca}_2\text{Al}_2\text{SiO}_7$) was also detected, which is a phase that was not previously detected in the equivalent K02 composition. Recall that the K02 (0.19:1 slag-clay-K) composition formed α -sialon, α - Si_3N_4 , and AlN' as the main phases, and G' was only formed in compositions when the slag content was raised to 0.34:1 and 0.47:1 slag:clay-K (K03 and K05). The impurity phases FeSi' and TiN' were not detected in this sample.

In the P08 sample, the XRD peak intensities and positions clearly correlate to α -sialon rather than α - Si_3N_4 , and a 'strong' amount of another phase was formed which was identified as D-phase ($2\text{CaO}\cdot\text{Si}_3\text{N}_4$). A similar result was found for the P20 sample, where α' and D-phase are the two main phases formed, both categorised as 'strong'. Slight differences in the D-phase relative peak heights and positions to the JCPDS PDF #38-0945 indicate that this too is a non-stoichiometric solid-solution phase, hereafter referred to as D'. Later EDXS analysis in Section 5.2.2.3 will show that some degree of Al-O substitution does occur within the D-phase structure.

Table 5.3 XRD phase analysis of slag:clay-P samples fired for 12, 18, and 24 hours at 1450°C.

	Phase ^a	Hours at 1450°C			
		12	18	24 ^b	
				core	surf
P02	α -sialon	mw ^c	s	s	
	α -Si ₃ N ₄	s	w	w	
	gehlenite (Ca ₂ Al ₂ SiO ₇)	s			
	D-phase (Ca ₂ Si ₃ O ₂ N ₄)				
	AlN ^d				
	FeSi ^d				
	unidentified			vw	
	amorphous	Δ	Δ	Δ	
P08	α -sialon	s	s	s	
	α -Si ₃ N ₄				
	gehlenite (Ca ₂ Al ₂ SiO ₇)				
	D-phase (Ca ₂ Si ₃ O ₂ N ₄)	s	m	m	
	AlN ^d				
	FeSi ^d	vw	vw	vw	
	unidentified	m	w	mw	
	amorphous	Δ	Δ	Δ	
P20	α -sialon	s	s	s	m
	α -Si ₃ N ₄	mw	m	w	vw
	gehlenite (Ca ₂ Al ₂ SiO ₇)				
	D-phase (Ca ₂ Si ₃ O ₂ N ₄)	s	s	s	m
	AlN ^d	mw	m	w	vw
	FeSi ^d	vw	vw	vw	vw
	unidentified	m	m	mw	w
	amorphous	Δ	Δ	Δ	Δ

Key to XRD intensity: s=strong, ms=medium strong, m=medium, mw=medium weak, w=weak, vw=very weak, ?=difficult to determine due to peak overlap

* The nominal stoichiometric compositions are given but the phases may be solid-solutions.

^b Only in the P20 sample was a distinct surface layer produced and analysed separately from the core material.

^c An amorphous phase is expected to be present, but not able to be detected above the background in the XRD.

Pure D-phase (2CaO·Si₃N₄) has only been reported in the literature once, in the same study that first identified E-phase (Huang, Sun, *et al.* 1985). The subsolidus phase diagram of the Si₃N₄-AlN-CaO system (Figure 2.6) shows that D-phase has an extensive region of compatibility with α -sialon, co-existing over a wide range of compositions. The crystal structure remains unknown.

AlN' was only detected in the P20 sample fired for 12 hours, and not in P02 or P08. This is due to the lower Al₂O₃-content of clay-P of 18 wt%, compared to 30 wt% in clay-K, so the clay-rich P02 and P08 samples contain much less Al than the equivalent K-series compositions. This may also account for the formation of the Al-poor D'-phase, which is nominally Al-free (2CaO·Si₃N₄), in the high-slag P-series compositions, rather than the higher Al-containing E'-phase (nominally CaAlSiN₃), as formed in high-slag K-series compositions.

An FeSi' impurity was detected in weak amounts in P08 and P20, but TiN' and SiC were unable to be identified due to overlap with the D'-phase peaks. A considerable number of relatively intense peaks remain unidentified in both the P08 and P20 samples. It is possible that the unidentified peak at ~26.8° may correspond to β-sialon, but overlap of other phases with all other β' peaks means that this identification cannot be made with any confidence. Identification of the unidentified peaks was attempted by comparison to the phases commonly formed in the (Ca/Mg)-Al-Si-O-N system and various subsystems, however no close match was found. Identification of these phases by XRD alone is very difficult due to: a) the high degree of peak overlap; b) the variable nature of peak positions and intensities arising from the probable solid-solution nature of these phases; c) the large number of possible elements that may be combined to produce phases in this system; and d) the possibility of these peaks corresponding to more than one phase. Similar problems were encountered for the K-series compositions as described in Chapter 4, where further analyses using electron microscopy were required to unambiguously identify the impurity phases. Such detailed analyses were not performed on the P-series powders produced here.

These experiments at 1450°C for 12 hours show that the higher proportion of slag in each of the clay-P compositions produced a phase assembly similar to what would be expected from the K-series equivalent compositions with similarly elevated slag contents. The P02 composition behaved more like K03 than the K02 base composition by producing G'. The P08 sample behaved more like K10 than the K06 basis by producing a 'strong' amount of a secondary phase to α', in this case D', which is also likely to be a metastable intermediate phase. The presence of stronger amounts of intermediate CRN phases α-Si₃N₄, G', and D' in the final P-series products indicates that a lesser extent of CRN was achieved in these samples compared to the K-series compositions. This may be due to insufficient time or temperature provided for the CRN reactions to occur. Thus, in order to investigate whether α-sialon can be formed and the relative levels of both α-Si₃N₄ and D'-phases can be reduced to similar levels as in the K-series compositions, the firing time was extended to 18 and 24 hours.

5.2.2 Firings Performed for 18 and 24 Hours at 1450°C

XRD traces of the firings for 18 hours are presented in Figure 5.5, and for the P20 composition fired for 24 hours in Figure 5.6. The results of phase analysis were given previously in Table 5.3.

Extending the firing time to 18 hours at 1450°C significantly increased the α -sialon content of the P02 sample, with only a weak trace of α - Si_3N_4 remaining, and no G' detected. This phase assembly is essentially the same as that seen in the K02 equivalent composition fired for 12 hours, except that AlN' is not produced due to the very low Al-content in this composition. The large quantity of α - Si_3N_4 produced in P02 after 12 hours of CRN and its subsequent conversion to α -sialon by 18 hours is the clearest evidence yet that the α - Si_3N_4 detected here and in the lowest-slag K-series compositions is in fact an intermediate CRN product phase and a precursor to α' .

In the higher-slag P08 composition D'-phase is still present after 18 hours of CRN. However the amount is reduced and α -sialon now becomes the dominant phase. Although greatly reduced, the amount of D' relative to α' is still higher than the amount of E' found relative to α' in the K06 equivalent composition fired for 12 hours. The α' -content in the P20 sample after firing for 18 hours appeared to decrease slightly from 'strong' to 'medium strong', with D' remaining the dominant phase. P20 contains the highest amount of slag, so it is also the most Al-rich of the three P-series compositions, and AlN' could be clearly identified in this sample.

Further extending the firing time to 24 hours did not reduce the amount of residual α - Si_3N_4 nor produce any other noticeable change in the P02 sample. The P08 sample also remained essentially unchanged after firing for 24 hours, however the highest slag P20 composition did experience some increase in the amount of α' produced, with a corresponding decrease in D'-content. In fact, a surface/core effect was produced in the P20 composition, with the surface of the powder being noticeably lighter in colour than the bulk underlying powder. XRD analysis (Figure 5.6) reveals that a very large amount of α' was produced on the surface with correspondingly low quantities of D', AlN' , FeSi' , and unidentified peaks present. The bulk of the powder displayed a slight increase in the α'/D' ratio compared to the 18 hour firing, but far less than that found on the surface. Such a surface/core effect was seen in the K14 composition in Chapter 4, which is the composition closest to the 1.5:1 clay-K basis for P20. This surface/core effect is a result of the CRN reactions proceeding more fully on the surface

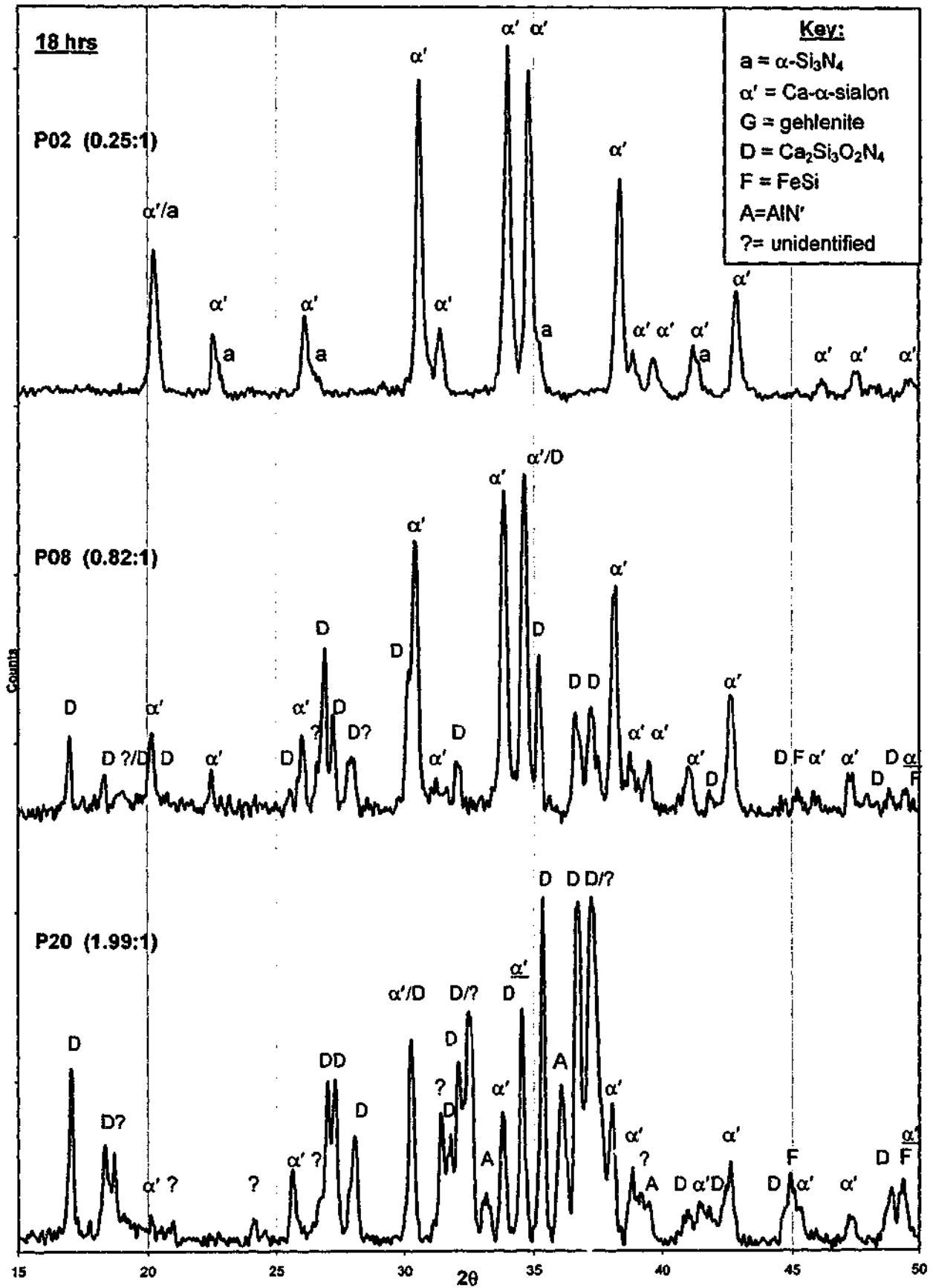


Figure 5.5 XRD traces of slag:clay-P samples fired at 1450°C for 18 hours.

of the sample which is in direct contact with the flowing N_2 reactant gas. These results demonstrate that like E' in the K-series compositions, D' -phase is a metastable CRN product that may be converted to α -sialon under more favourable CRN conditions. It also shows that even for an uncompacted powder where diffusion is less hindered than in a pressed pellet, the diffusion of gases into and out of the bulk of the powder is a limiting factor for completing the CRN reactions throughout the sample mass.

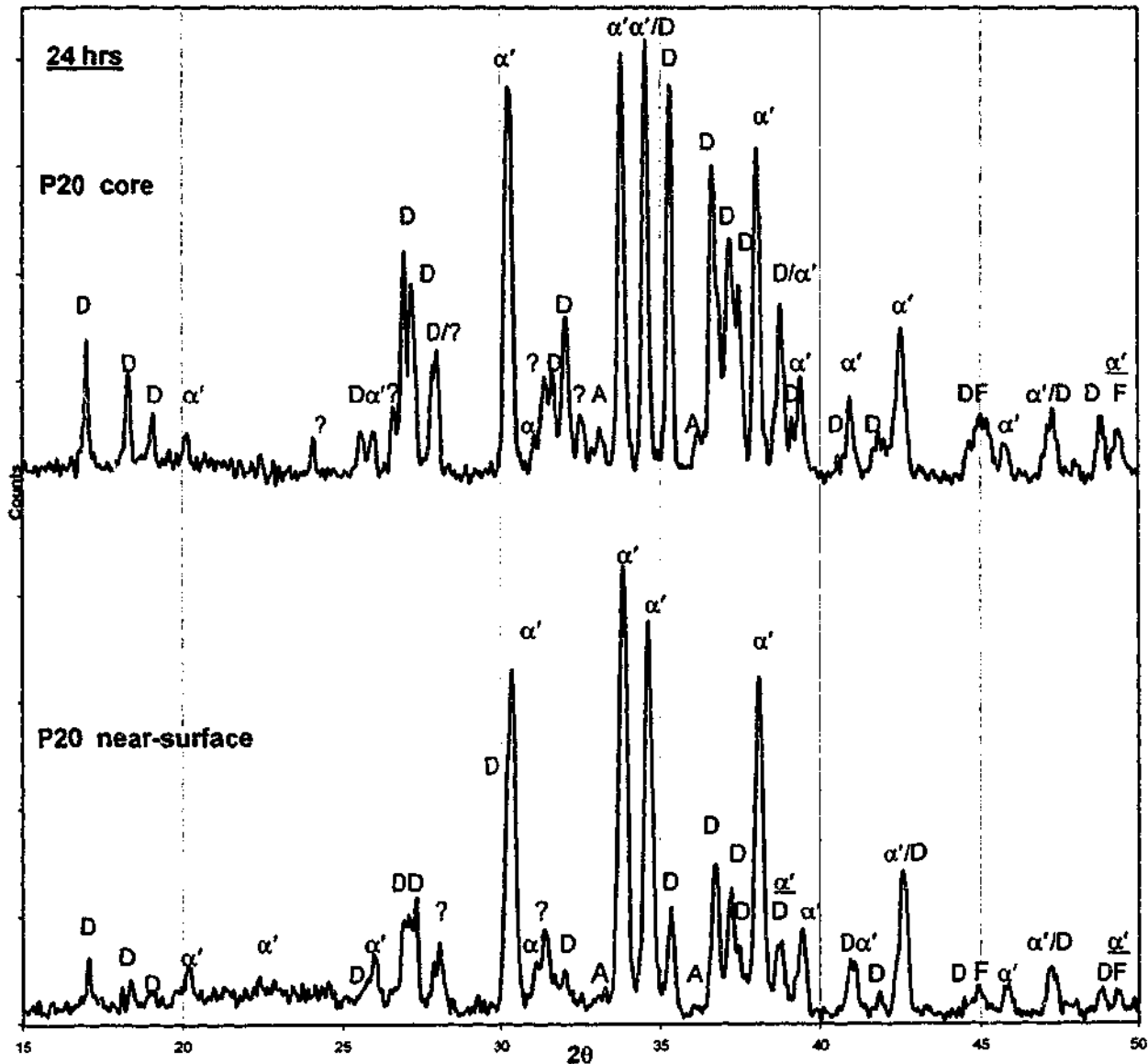


Figure 5.6 XRD traces of surface and core of P20 fired for 24 hours at 1450°C.

[Key: α' = α -sialon, A=AlN, D= D' -phase, F= $FeSi'$, ?=unidentified phase.]

Except for the surface of P20, there was no significant change to the phase assembly of any of the three samples when the firing time was increased from 18 to 24 hours. This indicates that the maximum extent of CRN achievable in this system at 1450°C under the present

processing conditions was attained by 18 hours, and extending firing beyond this time is unnecessary.

The powders produced after CRN for 18 hours will be investigated using SEM to gain further insight into α' formation in this system. To differentiate these powders from those fired under the standard conditions of 12 hours at 1450°C (ie. all clay-K CRN powders), they will be referred to as P02-18, P08-18, and P20-18.

5.2.2.1 Ca-Content of α -Sialon in P-series CRN Powders

The lattice parameters, estimates of m-value, and Ca-content of the α' phase in the P02-18 and P08-18 powders are given in Table 5.4, using the same procedure as performed for the K-series compositions as described in Section 3.4.1.2. The XRD signal for the α' phase was not sufficiently clear in the P20-18 powder for accurate analysis.

Table 5.4 Calculated lattice parameters, corresponding estimate of m-values and Ca-content of α -sialon produced from P02 and P08 compositions fired for 18 hours at 1450°C.

	P02-18	P08-18
a (Å)	7.873 ± 0.002	7.891 ± 0.004
c (Å)	5.729 ± 0.002	5.752 ± 0.009
m	1.82 ± 0.004	2.13 ± 0.006
Ca/unit cell ($x=m/2$)	0.91	1.07

As with the K-series equivalent compositions, increasing the slag content increased the Ca-content in the α -sialon, from 0.91 to 1.07 Ca^{2+} /unit cell in P02-18 and P08-18, respectively. The compositions K02 and K06 were calculated to have 1.08 and 1.20 Ca^{2+} /unit cell, which is higher than that produced in both P-series samples, despite their having lower slag contents (by mass) than the P-series equivalents. With reference to the α -sialon equation ($\text{Ca}_{m/2}\text{Si}_{12(m+n)}\text{Al}_{m+n}\text{O}_n\text{N}_{16-n}$), the lower Ca-content (m-value) in the α' phase of the P-series samples than in the K-series equivalents means that the α' phase will be richer in Si and lower in Al in these P-series samples. The lower Ca-content in the α' phase may be due to the lower overall Al-content of the system: less Al is able to be incorporated into the α' lattice thus less Ca is required to maintain electronegativity.

5.2.2.2 SEM Analysis of P02 Powder Fired for 18 Hours

The P02-18 powder was ultrasonically dispersed onto a brass stud and coated with carbon for investigation in the SEM. A low magnification overview of the predominantly single-phase α' powder from this composition is shown in Figure 5.7a. The streaking in the image is an artefact caused by an inadequate carbon coating on the sample. The majority of the particles are sub-micron in size and found in agglomerates up to 10 μm in diameter. These are agglomerates of the abundant α' particles, which in the higher magnification image (Figure 5.7b) are shown to be generally equiaxed and with a size of 0.5-1.0 μm , similar to those seen in the clay-K compositions. Long 10-20 μm fibres such as that labelled 'f' are also prevalent, and investigation at higher magnification reveals the presence of 2-4 μm spherical particles with an irregular surface, as indicated by 'x' in Figure 5.7b. EDXS spectra of the three types of particles seen in the P02-18 powder are given in Figure 5.8. The brass substrate has contributed to the signal in all three spectra and is the cause of the overlapping Cu_L and Zn_L peaks at 0.94 and 1.01keV, respectively. The α' spectrum (Figure 5.8a) was taken from a large agglomerate to minimise the influence of the brass stud and is representative of numerous spectra taken from small particles. Figures 5.8b and c were taken from the fibre (f) and large particle (x) as indicated in Figure 5.7.

The approximate peak height ratios of the elements detected in the various EDXS spectra are given in Table 5.5. The Al:Si:Ca ratio of 1:4.1:0.4 for the P02- α' is considerably higher in Si (and thus lower Ca and Al) than that found in the K06 powder (1:1.8:0.3 Al:Si:Ca), which is consistent with the results of m-value determination described in the previous section.

The large, irregular particles are Si- and N-rich and may be $\alpha\text{-Si}_3\text{N}_4$ particles formed during CRN, with the Al and Ca contribution to the spectrum provided by a small amount of Ca-Al-Si-O-N grain boundary glass coating the particle. A number of fibres are also observed, which have a Ca-Al-Si-O-N composition similar to α' . Fibre formation is indicative of gas-phase interactions, and Si_3N_4 fibres have often been seen during the CRN production of Si_3N_4 powder from SiO_2 and β' from clays (Cho and Charles 1991a; b). There is a possibility that these fibres are α' , which could form via reactions between gaseous species such as SiO(g) and the Ca-Al-Si-O-N rich liquid, which will therefore have a different composition to the α' formed via solution-precipitation from the melt. The identity of this fibre phase cannot be confirmed without further experimental evidence.

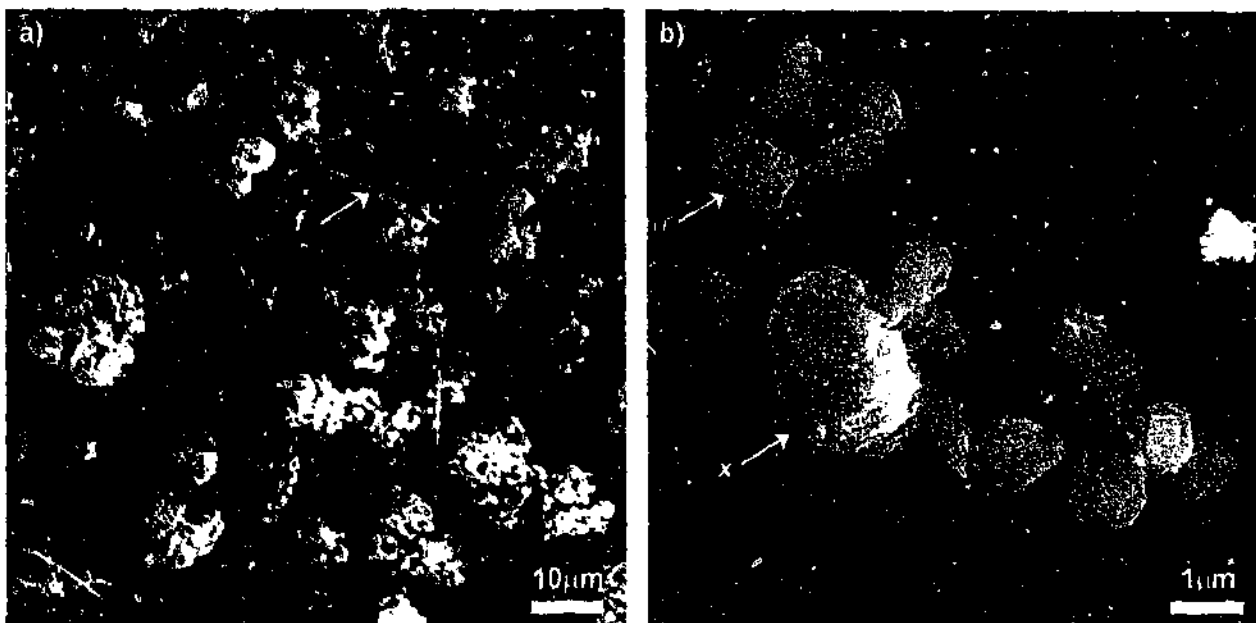


Figure 5.7 SEM micrographs of P02-18 powder fired for 18 hours at 1450°C: (a) low magnification image, (b) high magnification image.

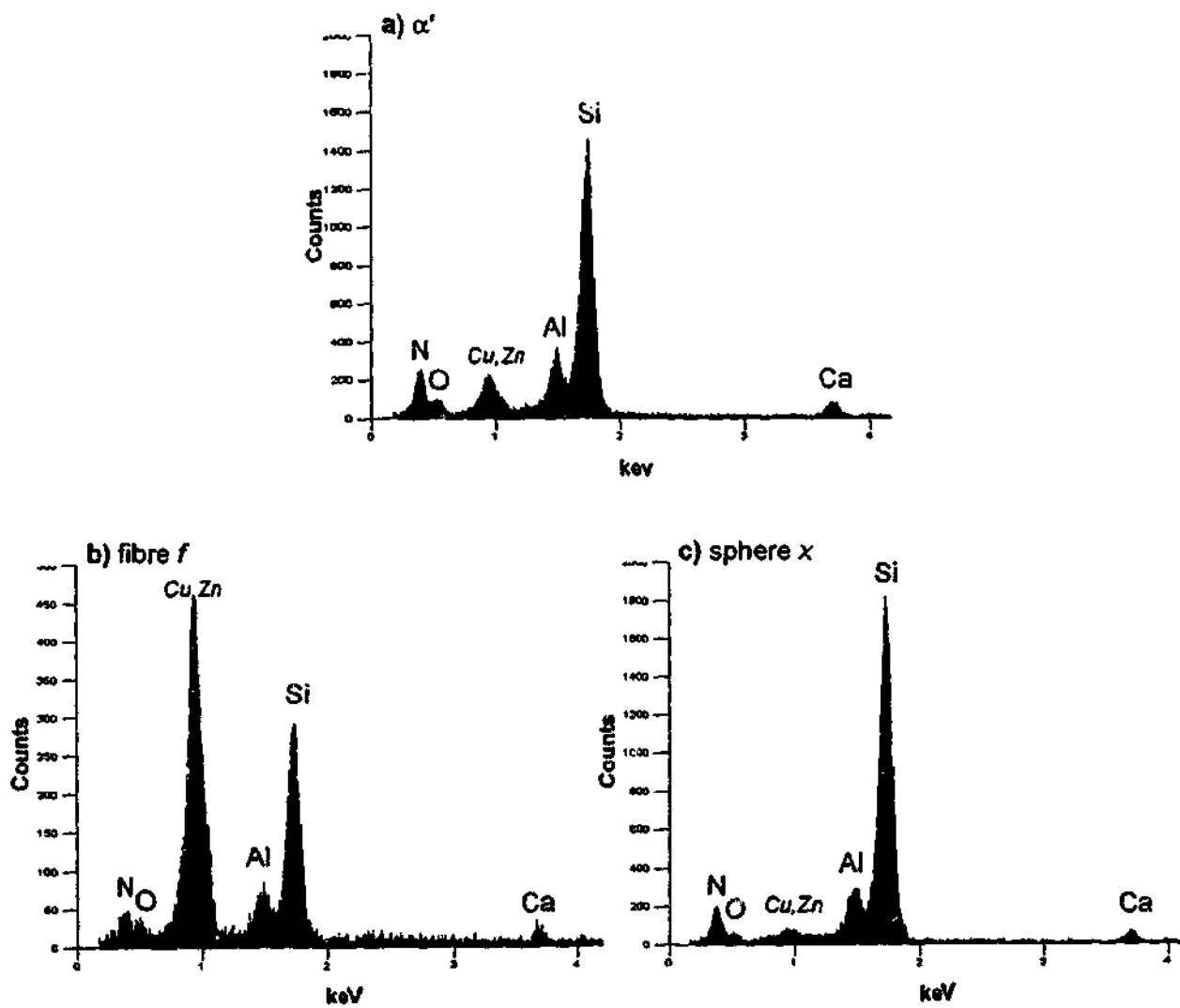


Figure 5.8 EDXS spectra of various particles in P02 powder fired for 18hrs at 1450°C: (a) small α' sialon particles, (b) fibre 'f' and (c) particle 'x' indicated in Figure 5.7. Note the Cu_L and Zn_L signals are artefacts from the brass substrate.

Table 5.5 EDXS peak height ratios of 3 types of particle found in composition P02 fired for 18hrs at 1450°C.

Particle	Al:Si:Ca peak height ratio	O:N peak height ratio
α' (average)	1: 4.1: 0.4	1: 2.4
fibre <i>f</i>	1: 3.6: 0.4	1: 1.6
particle <i>x</i>	1: 6.5: 0.2	1: 3.0

5.2.2.3 SEM Analysis of P08 Powder Fired For 18 Hours

XRD analysis of the P08-18 sample showed that it consisted largely of α -sialon, with a significant amount of D' -phase and a small amount of an unidentified phase present. SEM analysis reveals that three distinct particle morphologies were present with distinct chemical signatures: fine equiaxed grains, larger rod-like particles, and large, irregular particles (Figure 5.9). These have been attributed to α' , D' , and the unidentified phase, respectively. Typical EDXS spectra from the three types of particles are given in Figure 5.10, and the relative peak heights are tabulated in Table 5.6. Fibres are also present in this sample, but are much rarer than in the P02-18 powder.

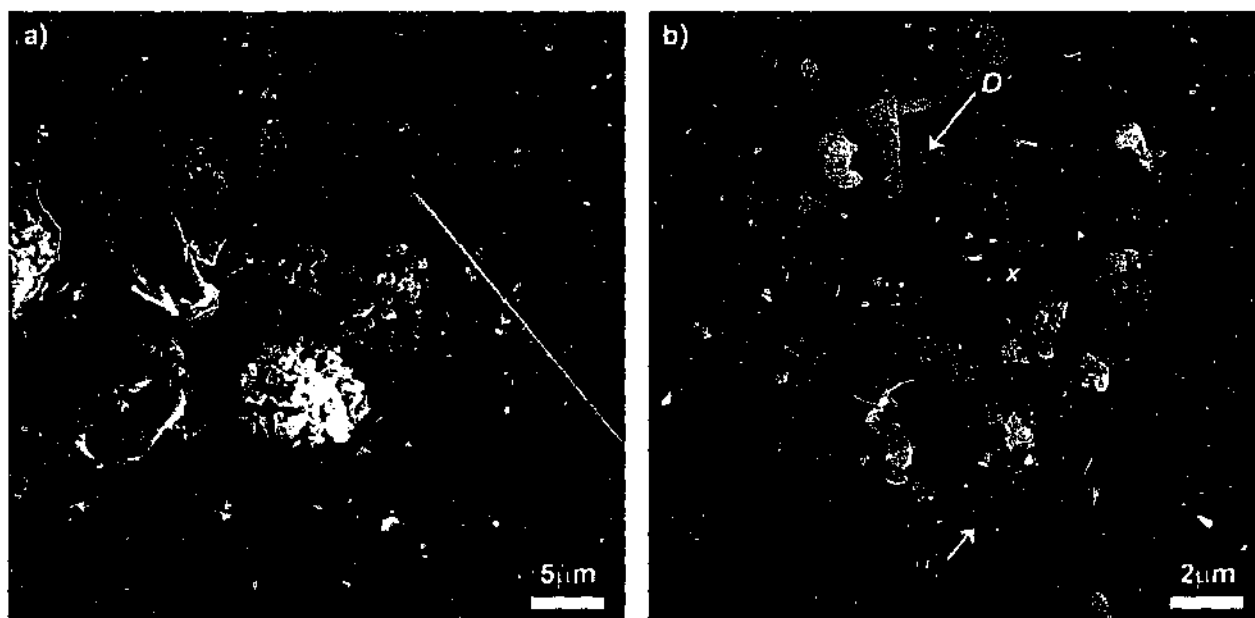


Figure 5.9 SEM micrographs of P08-18 powder fired for 18 hours at 1450°C.

The α -sialon particles were identified by having the similar submicron equiaxed morphology as seen previously in compositions K06 and P02-18. The Al:Si:Ca ratio of 1:3.4:0.3 in the P08- α' is lower in Si and higher in Al and Ca compared to the P02- α' (1:4.1:0.4 Al:Si:Ca), which would be expected from the higher m-value as determined in Section 5.2.2.1.

The D'-phase particles have a distinctly different morphology to α' , forming as larger, elongated rods several microns in length (Figure 5.9b). This is different to the morphology shown in Figure 1 in the paper by Huang and co-workers for pure D-phase ($2\text{CaO}\cdot\text{Si}_3\text{N}_4$) produced via hot-pressing, which is not very clear but appears to show a morphology of square plates of unknown size (Huang, Sun, *et al.* 1985). The chemistry of D' (Al:Si:Ca ratio of $\sim 1:3:0.3$ by EDXS) is different to that of the pure D-phase (0:3:2 Al:Si:Ca). The large reduction in Ca-content may be a result of Al substituting for Ca, with each Al^{3+} replacing 1.5 Ca^{2+} cations. The presence of oxygen indicates that some O^{2-} for N^{3-} substitution has also occurred in this phase, thus the exact nature of the substitutions are unknown and would require further detailed work to clarify its composition. The abundance of the rod-like D' grains in the microstructure corresponds well with the 'medium' intensity of D' seen in the XRD trace (Figure 5.5).

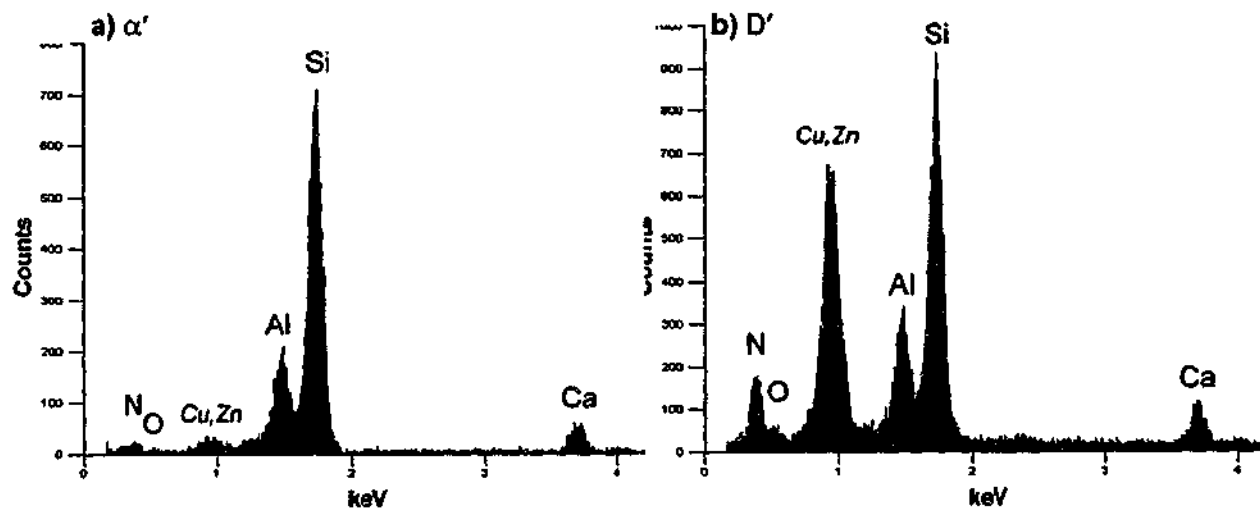


Figure 5.10 EDXS spectra of P08-18 particles: (a) small equiaxed particles found in agglomerates, (b) small rod-like grains. The Cu_α and Zn_α peaks are artefacts from the brass substrate.

Table 5.6 Measured EDXS peak height ratios of particles found in composition P08-18 fired for 18hrs at 1450°C.

Particle	Al:Si:Ca peak height ratio	O:N peak height ratio
α' (average)	1: 3.4: 0.3	1: 1.8
D' (average)	1: 2.8: 0.3	1: 2.8
particle x	1: 6.2: 2.1	1: 2.1

At first glance the unidentified particles appear to have a more D'-like chemistry than the rods; they are rich in Si and Ca. However they are considerably richer in Si than required for $2\text{CaO}\cdot\text{Si}_3\text{N}_4$, they also do not have a plate-like appearance, and there are simply insufficient numbers of these particles to account for the amount of D' expected in the sample. Further SEM analysis of bulk materials hot pressed from this powder (to be presented in Chapter 7) show that the phase assembly of $\alpha'+\text{D}'$ was maintained after hot-pressing, and the microstructure contains an abundance of rod-shaped grains with a chemistry similar to that seen in here in the powder; i.e. closer to α' than $2\text{CaO}\cdot\text{Si}_3\text{N}_4$. No Si-, Ca-rich phase similar to the unidentified phase in this powder was detected in the hot-pressed material, hence this phase cannot be D'.

5.2.3 Discussion of CRN of the P-series Compositions

It was seen in Chapter 4 that kinetic effects determined the extent of CRN and that sufficient time must be provided for the diffusive solution-precipitation reactions to be completed. For the K-series compositions fired at 1450°C, a 12 hour dwell was seen as the practical limit beyond which no significant CRN was obtained. The two compositions K02 and K06 were found to be favourable for essentially single-phase α' formation under these conditions. Other compositions produced secondary phases such as G' or E', depending on the slag content. These two phases are metastable, and although they are thermodynamically compatible with α' during firing at 1450°C, their formation may be less favourable under different CRN conditions, such as at higher temperatures.

The P-series compositions were designed to maintain the same mass ratio (and thus molar ratio) of $\text{CaO}:\text{SiO}_2$ as found in the K-series base compositions (not including the minor 0.4 wt% $\text{CaO}+\text{MgO}$ impurity in the clay-K). Replacing clay-K with clay-P essentially enriches the compositions in SiO_2 at the expense of Al_2O_3 , and this change in chemistry has had two important effects on the CRN of these compositions. First, the chemistry of the phases

produced during CRN reflects the low Al-content of the system. Al-rich phases seen in the K-series samples were not easily formed here; AlN' was not detected in the clay-rich samples P02 and P08, and D'-phase (nominally Al-free $2CaO \cdot Si_3N_4$, but containing a small Al-O substitution) was formed instead of E'-phase ($CaAlSiN_3$) in the higher slag P08 and P20 compositions. The α -sialon formed in the P-series compositions was also lower in Al, and therefore Ca, despite more Ca being available for stabilisation in these higher slag compositions. Therefore more Ca will be available for grain boundary glass formation or the production of Ca-containing secondary phases, both of which are likely to degrade the mechanical properties of a material produced from this powder.

The other effect of SiO_2 enrichment is a significant retardation of the kinetics of CRN in the clay-P-containing samples. It was seen that 18 hours at $1450^\circ C$ was required to allow completion of the CRN reactions, compared to 12 hours in the K-series compositions. This was most clearly demonstrated by the P02 composition, which produced a nearly identical phase assembly as the equivalent K02 composition, but required an additional 6 hours of reaction time to do so. In the other P-series compositions, higher levels of the intermediate secondary phase D' were found after 12 hours compared to the amount of secondary E'-phase found in the equivalent K-series compositions. This is due to slower reaction kinetics resulting from retarded diffusion through the SiO_2 -rich liquid produced in this system.

The liquid formed from melting of the components is essentially a molten glass with a composition dominated by CaO , Al_2O_3 , SiO_2 , and MgO , ie. it is an alkaline-earth aluminosilicate glass. The effect of SiO_2 -content on the viscosity of various glasses is shown in Figure 5.11. Pure SiO_2 (fused silica) has the highest viscosity of all glasses at all temperatures. Decreasing the purity to 96% SiO_2 lowers the viscosity of the glass, and the other glasses with even lower SiO_2 contents have even lower viscosity; a typical commercial aluminosilicate or borosilicate glass contains ~60-70% SiO_2 (Dumbaugh and Danielson 1986). This shows that there is a clear relationship between increasing the SiO_2 -content and increasing the viscosity of the glass.

The glass viscosity is an important parameter affecting CRN because α' formation is a solution-precipitation process that relies upon the diffusion of species through this liquid (Edrees and Hendry 1995). The CRN reactions involve reaction between the C or SiC reductant, N_2 from the furnace environment, and Si-based phases in the liquid. The intermediate oxynitride phases β' and M' are precipitated from this liquid, and subsequently further reacted via CRN to redissolve and precipitate the product phases α' , E', and D'. This

requires a significant diffusive migration of species such as Ca and Al through the oxynitride liquid. Consequently, the viscosity of this liquid will greatly affect the rate and extent of final CRN products able to be formed in this system. Enriching the SiO_2 -content of the liquid by using SiO_2 -rich clay-P significantly increased the viscosity of the liquid, retarding the rate of the diffusion, thereby preventing extensive α' formation within 12 hours at 1450°C , and necessitating the use of a longer reaction time of 18 hours.

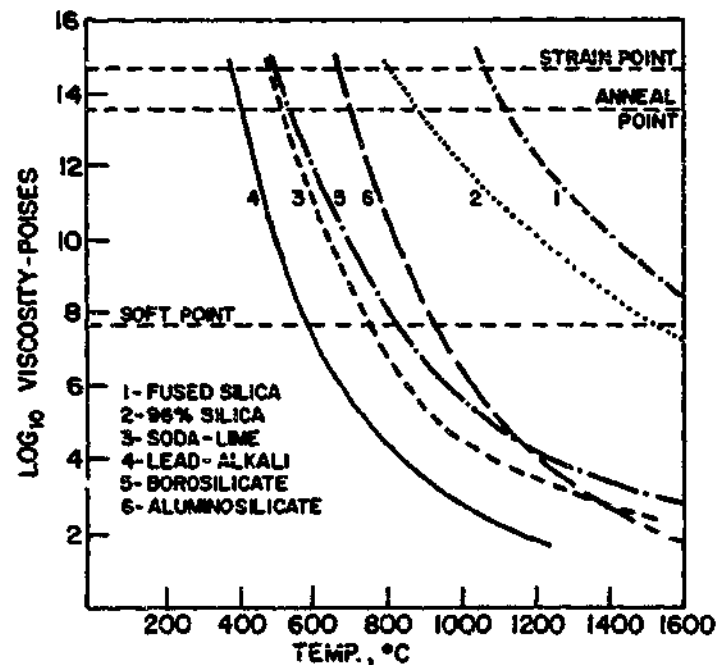


Figure 5.11 Diagram showing the relationship between glass viscosity and temperature for a variety of glass compositions (after Dumbaugh and Danielson 1986).

This effect of SiO_2 enrichment on retarding the rate of CRN was previously found to have contributed to the low extent of CRN achieved in the K01 sample (Section 4.2.7.1). This displayed very retarded reaction kinetics, with residual quartz from the clay-K still present after 12 hours of reaction at 1450°C . The very low slag content of the that sample (0.19:1 slag:clay-K) resulted in a composition that formed only a small amount of SiO_2 -rich liquid, thus hindering CRN. A similar effect was also observed in the study on the CRN of fly ash (Kudyba-Jansen, Hintzen, *et al.* 2001). In that study, one of the fly ashes ('Demkolec') produced a significantly lower α' -content (8 wt% compared to >51 wt%) than the others, though no explanation was given for this phenomenon. The Demkolec fly ash contained 68% SiO_2 , which is 14% richer in SiO_2 than in the other four fly ashes used. Therefore the retarded

diffusion through the higher viscosity SiO_2 -rich liquid as seen here, can explain the difficulty observed in achieving a high extent of α' formation in the Demkolec composition.

Elevating the reaction temperature to increase the fluidity of the liquid has been seen to promote the more rapid solution-precipitation of product phases during CRN (Edrees and Hendry 1995). This may be an effective method to improve the extent of α' in these SiO_2 -rich compositions, however a different thermodynamic equilibrium will operate at higher temperatures which may change the balance of phases compatible with α' .

It can therefore be predicted that CRN in the S-series system using pure SiO_2 sand to replace clay-K will be even more difficult to achieve than in the P-series system. This is investigated in the following section.

5.3 S-series: Slag + Sand

Loose heaps of the three slag:sand compositions listed in Table 5.2 were fired at 1450°C for 12 hours. As with the P-series compositions, 12 hours was insufficient for CRN thus the S03 and S10 compositions were fired for 24 hours. The phase results are listed in Table 5.7, and the XRD trace for S03 is given in Figure 5.12.

Table 5.7 XRD phase analysis of slag:sand samples fired for 12 and 24 hours at 1450°C .

	Phases	Hours at 1450°C	
		12	24
S03	$\alpha\text{-Si}_3\text{N}_4$	s	s
	D-phase ($\text{Ca}_2\text{Al}_2\text{SiO}_7$)*	w	w
	unidentified	mw	mw
S10	$\alpha\text{-Si}_3\text{N}_4$		
	D-phase ($\text{Ca}_2\text{Al}_2\text{SiO}_7$)*	s	s
	unidentified	m	m
S24	$\alpha\text{-Si}_3\text{N}_4$		
	D-phase ($\text{Ca}_2\text{Al}_2\text{SiO}_7$)*	s	
	unidentified	mw	

Key to XRD intensity: s=strong, m=medium, mw=medium weak, w=weak,

* The nominal stoichiometric composition is given but the phase may be a solid-solution.

The lowest slag sample S03 formed mostly $\alpha\text{-Si}_3\text{N}_4$ and D'-phase; which were seen as intermediate CRN phases in the P-series compositions (Section 5.2.1). This indicates that a

small extent of CRN was achieved, but not enough to form α -sialon. Many peaks remain unable to be identified (Figure 5.12). No detectable change to the phase assembly was produced by increasing the reaction time to 24 hours.

D'-phase was the dominant phase found in the higher slag-containing compositions S10 and S24, where neither α - Si_3N_4 nor α -sialon could be positively identified. As with the S03 composition, many XRD peaks remain unidentified in these samples, and no change was seen in the phase assembly of the S10 composition when extending the firing time to 24 hours. The S24 composition was not tested at this longer reaction time.

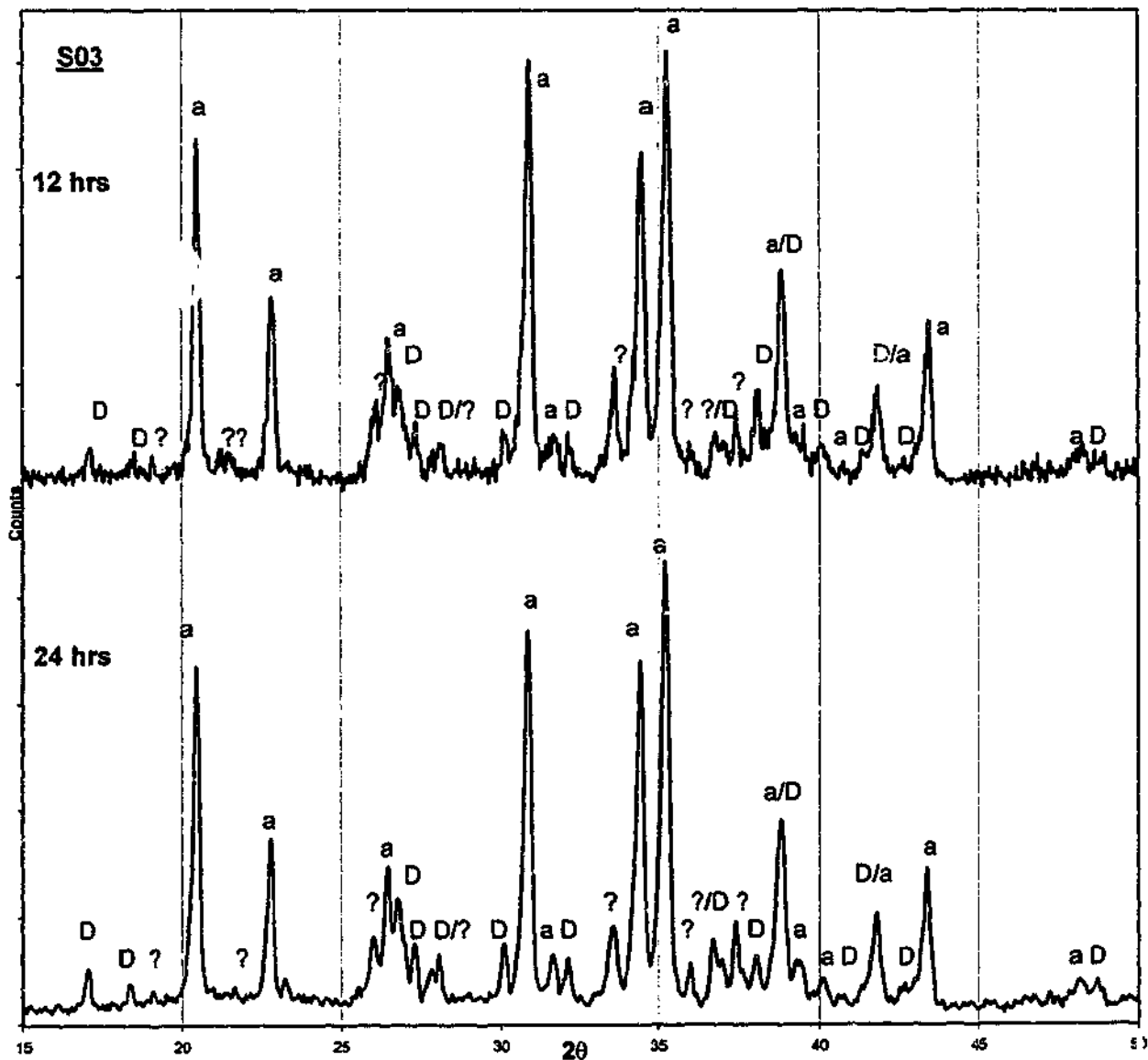


Figure 5.12 XRD traces of S03 sample fired for 12 and 24 hours at 1450°C. a= α - Si_3N_4 , D=D' phase (nominally $2\text{CaO}\cdot\text{Si}_3\text{N}_4$), ?=unidentified.

These results indicate that pure SiO_2 is inappropriate for the CRN production of α' at 1450°C because no α -sialon was formed in any of the samples tested, even those fired for 24 hours. This is consistent with the previous findings for the clay-P compositions where the increase in SiO_2 -content was found to hinder CRN due to the high viscosity of the liquid phase formed during CRN. The S02 sample is ~ 83 wt% SiO_2 , compared to 68 wt% in P02, and 50 wt% in K02, which will result in a very SiO_2 -rich glass with very high viscosity (Figure 5.11), and thus low diffusivity, thereby retarding the rate of dissolution and precipitation of CRN product phases.

In addition to the enrichment of the system in SiO_2 , there are two additional factors that may have contributed to hindering the rate and extent of CRN in this system: a) the large particle size of the quartz (up to $300\mu\text{m}$); and b) the low C/ SiO_2 ratio in these compositions. A fine particle size will allow for a greater number of contacts between the C and SiO_2 particles, a feature known to be necessary for improving the rate of CRN for Si_3N_4 production from SiO_2 (Weimer 1997). Si_3N_4 formation occurs, however, via gas-phase reactions, with no reliance on liquid phase diffusion. In the slag+sand system, reducing the particle size of the quartz alone may not be sufficient to overcome the problem of retarded diffusion through the molten reactants. It was seen in the study of the fly ash system that the fine, amorphous, 'Demkolec' fly ash was considerably more reactive than the other coarser, semi-crystalline fly ashes. However, the increased reactivity was only operative during early stages of CRN before the reactants had melted; the onset temperature of the early-stage CRN reactions was lowered and the gas-phase reactions started earlier than in the other fly ash compositions, but α' production was the lowest of any of the fly ashes tested (8 wt% vs. >51 wt%) (Kudyba-Jansen, Hintzen, *et al.* 2001). As per the discussion in Section 5.2.3, this lack of α' formation can be attributed to the considerably higher SiO_2 -content of the Demkolec fly ash compared to the other, coarser, fly ashes. Therefore the viscosity of the liquid during later stages of CRN is a limiting factor, and is far more significant than the initial particle size.

A high C/ SiO_2 ratio is also an important parameter found to enhance the CRN of SiO_2 when producing Si_3N_4 powder, with ratios ~ 4 (double the stoichiometric amount) found to be optimum (Weimer 1997). In the slag-based systems studied here, the C-content of the batches was maintained at 25 wt% across all compositions. Calculation of the C/ SiO_2 molar ratio for the K02, P02, and S03 equivalent compositions shows that C/ SiO_2 decreased from 3.3 in K02 to 2.4 in P02, and 2.0 in S03. The effect of this reduction in the C/ SiO_2 ratio is unlikely to be significant; the P02 and S03 compositions have very similar C/ SiO_2 ratios, yet S03 was totally unable to form α' , whereas P02 could produce nearly single-phase α' . The higher C/ SiO_2 ratio

produced in higher-slag compositions is also no guarantee of increased α' yield. For example, the 4.5 C/SiO₂ ratio in K33 did not produce a significant amount of α' . Other factors such as composition and reaction temperature are more influential on the extent of CRN experienced by these compositions.

The slightly increased seeding level of 10% α -Si₃N₄ used in these compositions, which is well above the 3% used for such an effect in other CRN systems (Zhang, Komeya, *et al.* 2000), was unable to overcome the unfavourable CRN conditions. The effect of seeding is studied further in Chapter 6.

Extending the CRN reaction time beyond 24 hours will not be expected to significantly improve the yield of α' . In addition to being commercially impractical, it would also be non-productive since no change at all was observed in the phases formed between the 12 hour and 24 hour firings. Increasing the CRN reaction temperature may be the only effective way to increase α' formation by increasing the fluidity of the liquid phase. Care must be taken, however, to avoid the increasingly favourable SiC formation at elevated temperatures.

5.4 Conclusions for Chapter 5

This chapter investigated the replacement of clay-K by more concentrated sources of SiO₂, pyrophyllite (clay-P) and sand, with the aim of minimising the mass of SiO₂ additive required and maximising the amount of slag used for α -sialon production. The major findings were:

- SiO₂-additives of higher SiO₂ concentration reduced the extent of CRN able to be performed at 1450°C, discouraging α -sialon formation. This is due to the system becoming richer in SiO₂ at the expense of Al₂O₃, which produces a liquid with a high viscosity at the CRN temperature. This slows the rate of diffusion for the solution-precipitation of CRN product phases.
- 12 hours was inadequate for the CRN of slag:clay-P compositions at 1450°C and a reaction time of 18 hours was required for the reactions to reach their maximum extent. Only the lowest slag composition P02 (0.25:1 slag:clay-P) produced a nearly single-phase α' product after CRN at 1450°C for 18 hours. The higher slag compositions P08 and P20 produced mixtures of α' and a solid-solution based on D-phase (2CaO·Si₃N₄). Pure SiO₂ in the form of sand was totally unable to form α -sialon.

- The α -sialon particles produced from the CRN of P02 and P08 powders for 18 hours at 1450°C are generally equiaxed and $<1\mu\text{m}$ in size. The Ca-content of the α -sialon was determined to be lower than that of the α' produced from the slag:clay-K powders. The D'-phase grains are slightly elongated rods, several microns in length, with a different chemistry to the nominal composition of $2\text{CaO}\cdot\text{Si}_3\text{N}_4$ due to the incorporation of Al and O in solid-solution.
- The most successful composition for producing α' at 1450°C was P02, which contains 5% more slag by weight than the K02 base composition, but 15% less than the most successful K-series composition K06.

Chapter Six

Optimisation of the CRN Process

The previous chapters have examined the fundamental phase formation processes that occur within the slag and clay mixtures during CRN, primarily by examining the effects of changing compositional factors such as slag content and clay composition. Several other parameters may also be manipulated to control the CRN process, including specimen factors such as the level of seeding and specimen density, and also firing parameters such as nitrogen flowrate and firing temperature. The work presented in this chapter is an investigation of the effects of these parameters on the phases formed from CRN, with the aim being to produce the highest yield of α' possible. Section 6.1 is a discussion of the experimental procedure and derivation of an equation to quantify the α'/E' ratio. Section 6.2 examines the effects of powder compaction and sample geometry on CRN, and Section 6.3 investigates the effects of changing the N_2 flowrate through the furnace. The type and level of seeding is examined in Section 6.4, and Section 6.5 discusses the effects of increasing the temperature on the stability of the CRN products.

6.1 Experimental Outline

6.1.1 Composition Selection

With the desire to maximise the quantity of slag used in α -sialon formation, the high-slag compositions K06 (0.6:1 slag:clay-K) and K33 (3.3:1 slag:clay-K) are the focus of this chapter. K06 was the highest slag-containing composition that formed nearly single-phase α' , with a small amount of E' phase, AlN' , and $FeSi'$ and TiN' impurities were also produced. K33 was predominantly E' -phase (nominally $CaAlSiN_3$) and contained only a minor amount of α' in addition to the impurity phases $FeSi'$ and TiN' . The E -phase is thought to be a metastable CRN product able to be converted to α' , thus this composition can be used to determine whether the low α' content of very slag-rich compositions can be increased.

6.1.2 Quantitation of α -Sialon / E' -phase ratio

Improving the α' content of the sample by reducing the amount of secondary E' -phase in the K-series compositions is the main aim of the work in this chapter, hence a method to quantify the change in the relative proportion of the α' and E' phases is needed. Quantitative XRD

analysis or electron microscopy based-methods would require considerable effort due to the complexity of this multi-component system, thus a simple 'quasi-quantitative' measure of the α'/E' ratio was used, based on their relative peak intensities in the XRD.

A quantitative approach to determining the β/α ratio in silicon nitride and sialon systems via XRD has been developed by Kall, and the equation is given in Equation 6.1, where $I\beta$ and $I\alpha$ are the integrated intensities of the planes specified (Kall 1988).

$$\% \beta = \frac{I\beta_{(101)} + I\beta_{(210)}}{I\beta_{(130)} + I\beta_{(002)} + I\alpha_{(102)} + I\alpha_{(210)}} \quad [6.1]$$

α content is given by $1 - \% \beta'$, and in sialon systems the same crystal planes of the α' and β' phases can be used to determine the α'/β' ratio. The $\alpha'(102)$ and $\alpha'(210)$ planes are best suited for quantification because they were seen to be the most immune to compositional variation arising from the incorporation of the metal cation into the structure. Deconvolution of overlapping peaks was also required for accurate quantification. It was seen that in the Si_3N_4 system the half-widths of the strong α - and β -peaks did not differ significantly, therefore the integrated intensity is proportional to peak height and this simplification can be used for quantification.

To estimate the change in the relative proportions of the α' and E' -phases in the CRN powders, Equation 6.1 was used as the basis for Equation 6.2, which gives a quasi-quantitative estimate of the α'/E' ratio in the XRD scans.

$$\% \alpha' = \frac{I\alpha'_{(102)} + I\alpha'_{(210)}}{IE'_{(130)} + IE'_{(002)} + I\alpha'_{(102)} + I\alpha'_{(210)}} \quad [6.2]$$

The same, α' peaks as used in Equation 6.1 are used in Equation 6.2, which in these scans correspond to the two most intense α' peaks at $2\theta = \sim 33.8^\circ$ (100% intensity) and $\sim 34.7^\circ$ (80% intensity) respectively. The two E' -phase peaks chosen for analysis are $E'(130)$ ($2\theta = 32.3^\circ$) and $E'(002)$ (36.1°), which are high intensity, characteristic E' -phase peaks. Visual inspection of these peaks in numerous XRD scans showed them to have no significant overlaps and consistent relative intensities. The background radiation was subtracted before calculating peak height.

This equation can only be used to compare XRD results between scans to evaluate trends in the α'/E' ratio. It should be noted that several assumptions and simplifications have been

made in establishing this equation, thus it does not allow for accurate quantitative determination of the α' content of these samples. Firstly, it is assumed that the samples are simple binary mixtures of the phases of interest, α' and E'; the other minor phases AlN', TiN', FeSi', SiC, and glass are considered to be constant between scans. Second, it is assumed that the solid-solution compositional change has no significant effect on the relative peak heights of the E' phase peaks chosen for analysis. Previous EDXS evidence suggests the E'-phase is a solid-solution, and some variation in the relative peak heights was observed between samples, but the effect of composition is unknown. The two E' peaks chosen for analysis were the most consistent, as determined by visual inspection. The third assumption is that the peak height is directly proportional to the integrated intensity.

An uncertainty level of $\pm 1\%$ α' has been determined for this equation, which is the resolution limit when comparing results from different XRD scans. It must be remembered that the value derived from this equation is not the absolute quantity of α' in the phase mixture, but a semi-quantitative approximation of the α'/E' content, and can only be used for comparative purposes. Absolute values of α' or E' in a sample may easily differ from these calculations by 10% or more, reflecting the many assumptions listed above, as well as equipment factors such as the minimum detection limit of $\sim 4\%$, and natural variation in the quantity of products formed between firings. For relative comparison, the E' content is simply defined as $100\% - \alpha'$.

6.2 Specimen Density & Geometry

The presence of a difference in the appearance and phase composition of the surface and core of uniaxially pressed K-series pellets suggests that the specimen density and geometry are important factors affecting the CRN process (Section 4.3.2.4). The CRN process is governed by both gas-phase reactions and solution-precipitation processes, and diffusion of gases into and out of the samples is vital for the gas-phase CRN reactions to proceed effectively. In addition to the packing density of the powder, the geometry and size of the sample may also be important factors affecting the flux of N_2 experienced by the sample. The effect of these two factors on the yield of α' have been investigated and the results are presented in this section.

6.2.1 Powder Packing Density

Four samples of K06 powder (slag:clay-K 0.62:1) of different packing density were fired to determine the effects of powder compaction on α' -sialon formation. The samples were: a) a heap of loose powder spooned into the Al_2O_3 boat with no additional pressure; b) a pellet

pressed by firm hand pressure on the 1cm diameter cylindrical die plunger; c) a pellet pressed according to the 'standard' conditions of 10 MPa hydraulic pressure in the 1cm diameter die, as used in Chapter 4; and d) a pellet of 1cm diameter hydraulically pressed at 10 MPa and then cold isostatically pressed (CIP-ed) at 200 MPa. These samples were fired as per the standard condition (12 hours at 1450°C in N₂ flowing at 30ℓ/hr).

A surface/core effect was noticeable in all the fired samples, including the loose powder, which had a lighter-coloured layer of grey powder on the surface. Underneath the surface, the bulk material tended to be a dark grey colour. The surfaces of the pellets were all more cohesive than the darker core material, which had basically no resistance to scratching. In the case of the CIP-ed pellet, the surface was considerably more cohesive than usual, requiring significant force to break through to expose the core, but the core material was not noticeably firmer than in the other samples. This is a clear demonstration that the green-bodies cannot be simultaneously converted to α' via CRN and densified in a one-step process.

The XRD traces are shown in Figure 6.1, with tabulated estimates of α' content given in Table 6.1. Samples for analysis were taken from the core regions of the pellets. The data presented in Table 6.1 clearly shows a trend towards decreasing α' content with increasing powder compaction. The sample with the lowest density, the heap of loose powder, produced the highest relative quantity of α' , of 94% (6% E'). Hand pressing in a die to form a pellet doubled the E' formed to ~13%, and hydraulically applied pressure of 10 MPa doubled again the amount of E' formed to 25%. Further application of pressure via CIP did not have any further effect on the α' /E' ratio. No significant effect could be seen on the amount of AlN' or other secondary phases formed.

It should be noted that the amount of E' detected in the core of the standard 10 MPa pressed pellet (25%) is significantly higher than the 12% E' calculated for the standard K06 sample as shown in Figure 4.7d. The main reason for this is that a degree of variation exists between different firings of the same composition, which may be due to several parameters over which there is a relatively poor degree of control. The two most likely variables are the uniaxial pressing pressure, which may be up to 25% uncertain, and the N₂ flowrate during CRN which is affected by the buildup of reaction products in the filter as particles are swept down the tube. Although the results have been checked for consistency, some small variations in the relative proportions of the phases present have been detected between different firings, and only the most consistent ones have been presented here. A detectable surface/core effect

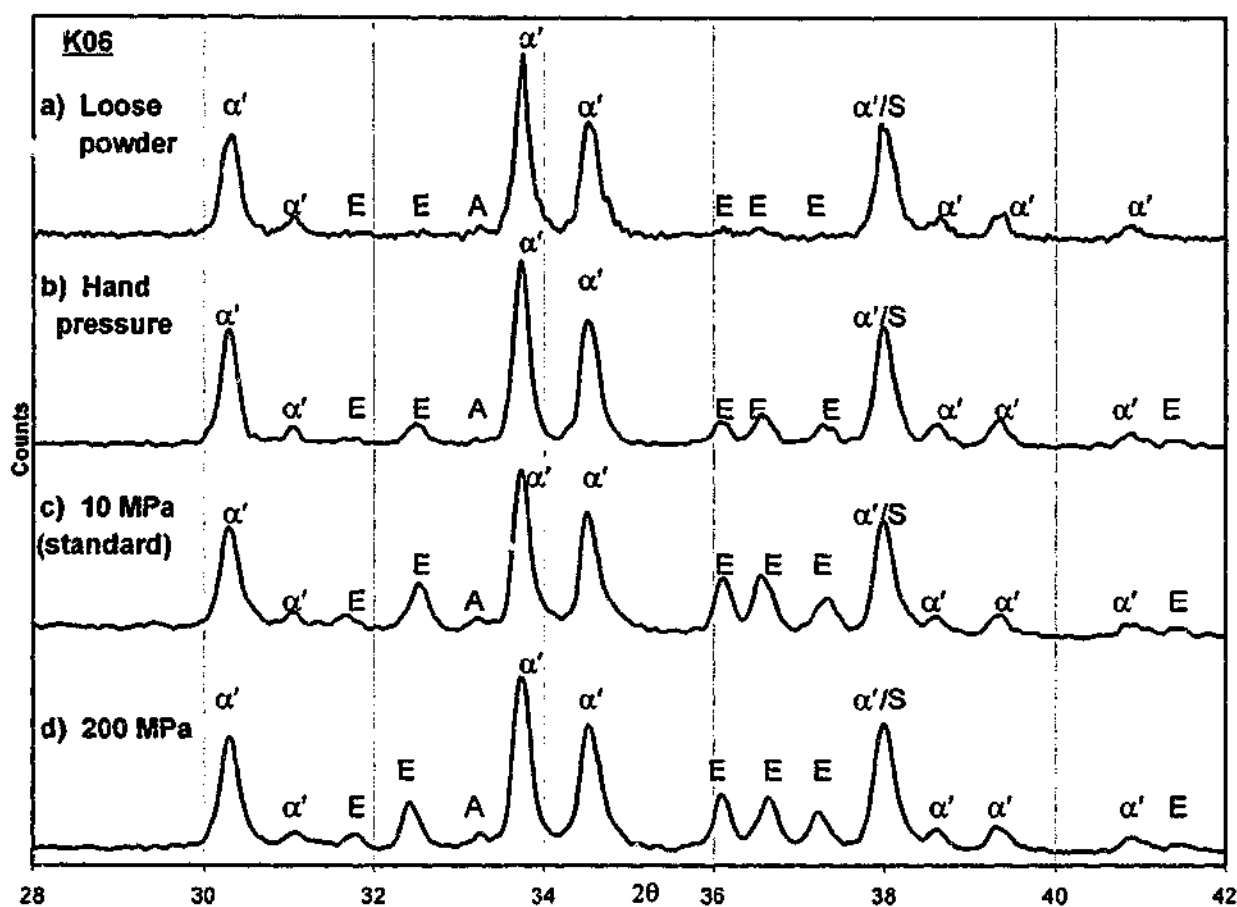


Figure 6.1 XRD of fired K06 powder compacts of varying compaction density.

[Key: α' = α -sialon, A = AlN', E=E'-phase, S=2H-SiC. TiN' at 36.6° not labelled].

Table 6.1 α' / E' ratios in fired powder compacts of different compaction density.

Sample	% α'	% E' (=1-% α')	Other phases
Loose powder	94	6	AlN' - vw TiN' - vw FeSi' - vw SiC - vw?
Hand pressed pellet	87	13	AlN' - vw TiN' - vw FeSi' - vw SiC - vw?
10 MPa hydraulically pressed pellet (standard)	75	25	AlN' - w TiN' - vw FeSi' - vw SiC - vw?
200 MPa CIP-ed pellet	74	26	AlN' - w TiN' - vw FeSi' - vw SiC - vw?

Error = $\pm 1\%$.

Key to XRD intensity: w=weak, vw=very weak, ?=unable to be accurately quantified due to peak overlap.

was produced in the K06 pellets fired for these experiments, whereas no such effect was seen in the first K06 pellet fired, possibly as a result of such variations between firings.

The reduction in α' content with increasing powder packing density can be clearly attributed to the increasing difficulty of gas penetration into and out of the compacted samples. Gas penetration into the pellets is clearly important for providing the reactant N required for nitridation, and increasing the degree of pellet compaction will block the porous pathways that help the N_2 gas gain access to the interior of the sample. Access to the gas is also important for the removal of gaseous by-products such as $CO(g)$ out of the sample. The CRN reactions such as $SiO_2 + 3C \rightleftharpoons SiC(s) + 2CO(g)$ are reversible, equilibrium reactions, as detailed in Section 2.2.2 and discussed in Section 4.3.2.4. To maintain the CRN reactions moving in the forward direction and keep producing the desired CRN products, (ie. to prevent equilibrium from being attained), $CO(g)$ must be continually removed, and the sweeping action of the N_2 gas flow will be hindered by increasing the powder packing density.

Previous work on the CRN formation of β' from clays showed that the powder compaction pressure has two competing effects on the extent of CRN. Excessive pressure was found to prevent CRN due to $CO(g)$ build-up in isolated regions (Higgins and Hendry 1986), however increasing the level of compaction could also produce greater contact between the C and other components, thereby enhancing CRN (Mazzoni, Aglietti, *et al.* 1993). In the present experiments, it appears that the contact between C and the other components was adequate and was not improved by higher compaction pressures, rather the increased specimen density directly impeded the gas flow and hindered α' formation. The loose powder without any compaction provided the easiest access to gas diffusion, and thus produced the highest extent of α' . The maximum hindrance to CRN- α' formation was produced by a pressing pressure somewhere between hand pressure and 10 MPa, above which further increasing the pellet density did not alter the extent of CRN.

In densely packed samples, only the surface layers can achieve easy gas penetration, which results in the surfaces undergoing more extensive CRN than the underlying bulk material. The α' content of the surfaces of all three pelletised specimens was found to be ~93%, which is higher than for all the core powders. The surface layer on the loose heap of powder had 97% α' , which is also higher than in the core (94%). α -Sialon production is clearly favourable in areas with easy access to the N_2 gas. The formation of a small difference in the α' content on the surface of the heap of loose powder that was totally uncompacted suggests that the extent

of CRN is extremely sensitive to gas penetration, which has strong implications for the consistent production of uniform powders by this method.

6.2.1.1 Mass Production of α -Sialon (Sample Size and Geometry)

So far, all of the CRN firings have involved only a small amount of powder (~1.5g) placed in the centre of a 10cm long furnace boat, which allows for easy access to the N₂ gas flowing along the horizontal tube. The size of the sample and the location in the furnace boat may influence the flux of N₂ experienced by the sample, for example the front wall of the furnace boat may partially shield any powder immediately adjacent to it from the gas flow. The CRN process was scaled-up to fire the maximum mass of powder possible in the laboratory furnaces, to examine the effect of increasing the sample size and determine whether N₂ penetration is consistent throughout the sample.

The tube furnaces have a defined hot zone 100mm long, with the maximum temperature obtained in the centre and the drop in temperature experimentally determined to be no more than 5°C at the ends. The standard furnace boats used in this investigation were 100mm long to match the length of the hot zone, and 15mm deep, and 25mm wide. To react the maximum possible quantity of powder in one firing, these boats were filled to the brim with the reactant mixture. A light tamping-down with a flat tool was used to slightly consolidate the fine powder and prevent it from being carried down the furnace during pre-firing evacuation, and also to allow more powder to be packed into the boat. In this way approximately 17g of powder was reacted in one firing, compared to the ~1.5g fired previously.

After firing the K06 powder under the standard conditions (1450°C, 12 hours, 30ℓ/hr N₂), the surface of the powder bed had a thick lighter-coloured surface layer, to a depth of ~3mm. Samples were taken from the bulk of the powder immediately adjacent to the front and rear walls of the boat, as well as from midway down the boat. The surface layer was sampled only at the midway point. The calculated α' content for these regions of the powder mass is given in Table 6.2.

Table 6.2 α' content after firing a full boat of powder at 1450°C for 12 hours.

Sample Location	% α'	%E' (=1-% α')	Other phases
front (bulk)	88	12	AlN'-vw TiN'-vw FeSi'-w SiC - vw?
center (bulk)	88	12	AlN'-vw TiN'-vw FeSi'-w SiC - vw?
rear (bulk)	87	13	AlN'-vw TiN'-vw FeSi'-w SiC - vw?
center (surface)	90	10	TiN'-vw FeSi'-vw SiC - vw?

Error = $\pm 1\%$

Key to XRD intensity: s=strong, ms=medium strong, m=medium, mw=medium weak, w=weak, vw=very weak, ?=unable to be accurately quantified due to peak overlap.

The core material from all points sampled along the length of the boat contained essentially the same level of α' (~88%), indicating that CRN was able to proceed equally effectively at all points in the powder bed. No problem was detected due to shielding of the material at the front of the boat from the N_2 flow. The α' content of 88% is basically the same as that found in the hand-pressed sample discussed in the previous section, which is less than the 94% formed in the smaller heap of loose powder. This lower α' content in the boat full of powder may be the combined result of the much larger size and mass of the sample, and the pressure applied when tamping down the powder. The applied pressure, although less than that used when hand-pressing the pellet in Section 6.2.1, may be sufficient to hinder nitridation when compared to the loose powder. Recall from the previous discussion that even in the uncompacted small heap of loose powder the extent of α' formation was very sensitive to N_2 diffusion, and the bulk of the loose powder contained slightly less α' than the surface (Section 6.2.1). As with the pelletised specimens, the top surface layer of the powder was able to undergo a greater extent of nitridation as evidenced by the slightly higher α' content (90%). This surface material contained less of the impurity phases than the bulk, with no AlN' detected and less FeSi'.

The XRD traces from the bulk of the powder showed no significant variation to the content of the TiN', FeSi', and SiC impurity phases in the three locations along the boat.

These results demonstrate that the powder packing density has a significant effect on the extent of α' formation. CRN is enhanced by direct contact with the N_2 gas stream, and any

degree of powder compaction will hinder the extent of CRN. Even loose heaps of powder without any compaction displayed inhomogeneous α' formation between the surface of the powder and the underlying material. This implies that for the commercial production of α' via this process, an alternative furnace geometry may be useful to allow even gas flow throughout the sample, such as a fluidised bed or a rotating tube furnace.

6.3 Nitrogen Flow Rate

The previous section has shown that gas penetration is an important variable governing the effectiveness of the carbothermal reduction-nitridation reactions. Gas penetration will also depend on the flowrate of N_2 gas through the furnace during firing. In the current investigation 30ℓ/hr was set as the standard flowrate based on the results of the preliminary investigation by Walker (1997), and is comparable to other CRN studies where high flowrates between 30-42ℓ/hr were successfully used to produce predominantly α' products (Hotta, Tatami, *et al.* 2002; Zhang, Komeya, *et al.* 2000). To examine the effects of N_2 flowrate in this system, tests were performed on small heaps of loose powder placed in the centre of the furnace boats from the K06 (0.62:1 slag:clay-K) and K33 (3.3:1) compositions. The minimum N_2 flowrate achievable in the furnace of 3ℓ/hr, and the maximum achievable flowrate of 52ℓ/hr, were used for CRN at 1450°C for 12 hours. The results of phase analysis, including % α' content, are tabulated in Table 6.3 and XRD traces for the K33 sample are given in Figure 6.2. Powder was sampled from the bulk of the powder heaps.

Increasing the N_2 flowrate from 30ℓ/hr to 52ℓ/hr to achieve greater N_2 penetration did not increase the amount of α' formed in either of the specimens; the K06 sample showed no detectable increase in α' and the K33 composition exhibited a slight decrease in α' of ~4%. In addition, the formation of a small amount of an unidentified phase was detected in the products fired under the higher N_2 flowrate. The opposite effect was found by decreasing the flowrate to 3ℓ/hr; the α' content of the K06 sample increased by 8%, and a dramatic increase in α' from 5% to 55% was detected in the K33 sample, however this figure may be influenced by the large amount of M' -phase also formed which partially overlaps the α' XRD peaks. A small amount of AlN' was also detected in K33 sample fired at 3ℓ/hr, which was not present when higher N_2 flowrates were used.

Table 6.3 Phase analysis and α' content for samples fired under varying N_2 flow rates at $1450^\circ C$ for 12 hours.

	Phase ^o	N_2 flowrate (l/hr)		
		3	30	52
K06	α -sialon ^A	98%	90%	90%
	E' (CaAlSiN ₃) ^A	2%	10%	10%
	AlN'	vw	vw	vw
	FeSi'	w	w	w
	TiN'	vw	vw	vw
	SiC	vw?	vw?	vw?
	unidentified			vw
K33	α -sialon ^A	55%	5%	1%
	E' (CaAlSiN ₃) ^A	45%	95%	99%
	M' (2CaO·Si ₃ N ₄ ·AlN)	ms		
	G' (Ca ₂ Al ₂ SiO ₇)	vw?	vw?	vw?
	AlN'	vw		
	FeSi'	vw	vw	vw
	TiN'	vw	vw	vw
	SiC	w?	w?	w?
unidentified			vw	

Key to XRD intensity: s=strong, ms= medium strong, m=medium, mw=medium weak, w=weak, vw=very weak, ?=unable to be accurately quantified due to peak overlap.

^A Error = $\pm 1\%$.

^o The nominal stoichiometric compositions are given but the phases may be solid-solutions.

This result is a little surprising, as a survey of the literature suggests that CRN is generally enhanced by higher gas flowrates due to achieving better penetration of the reactant N_2 into the pellet and more efficient removal of unwanted gaseous reaction by-products (Mazzoni, Aglietti, *et al.* 1993). It has been noticed, however, that increasing the N_2 flowrate can also increase the extent of $SiO(g)$ loss due to the increased sweeping action of the faster flowing gas (Mazzoni and Aglietti 1998), causing enrichment of the products in Al, and the formation of Si_3N_4 whiskers in cooler parts of the tube (Cho and Charles 1991b). $SiO(g)$ is formed as an intermediate step during the carbothermal reduction of SiO_2 to form SiC (Equations 6.3a and b). Unlike the $CO(g)$ reaction product, which must be continually removed to allow the CRN reactions to progress, it is not desired to remove $SiO(g)$ from the system because of its further involvement in CRN. Moreover, $SiO(g)$ loss will deplete the system of Si needed for α' formation. It was shown in Chapter 4 that Si-poor compositions (ie. siag-rich compositions) favour the production of E' (nominally 1:1:2 Ca:Al:Si) rather than α' (~1:3:6 Ca:Al:Si (Table 4.4)) due to the lower Si content required for E'. Therefore excessive $SiO(g)$ loss will promote the formation of Si-poor phases rather than α' .

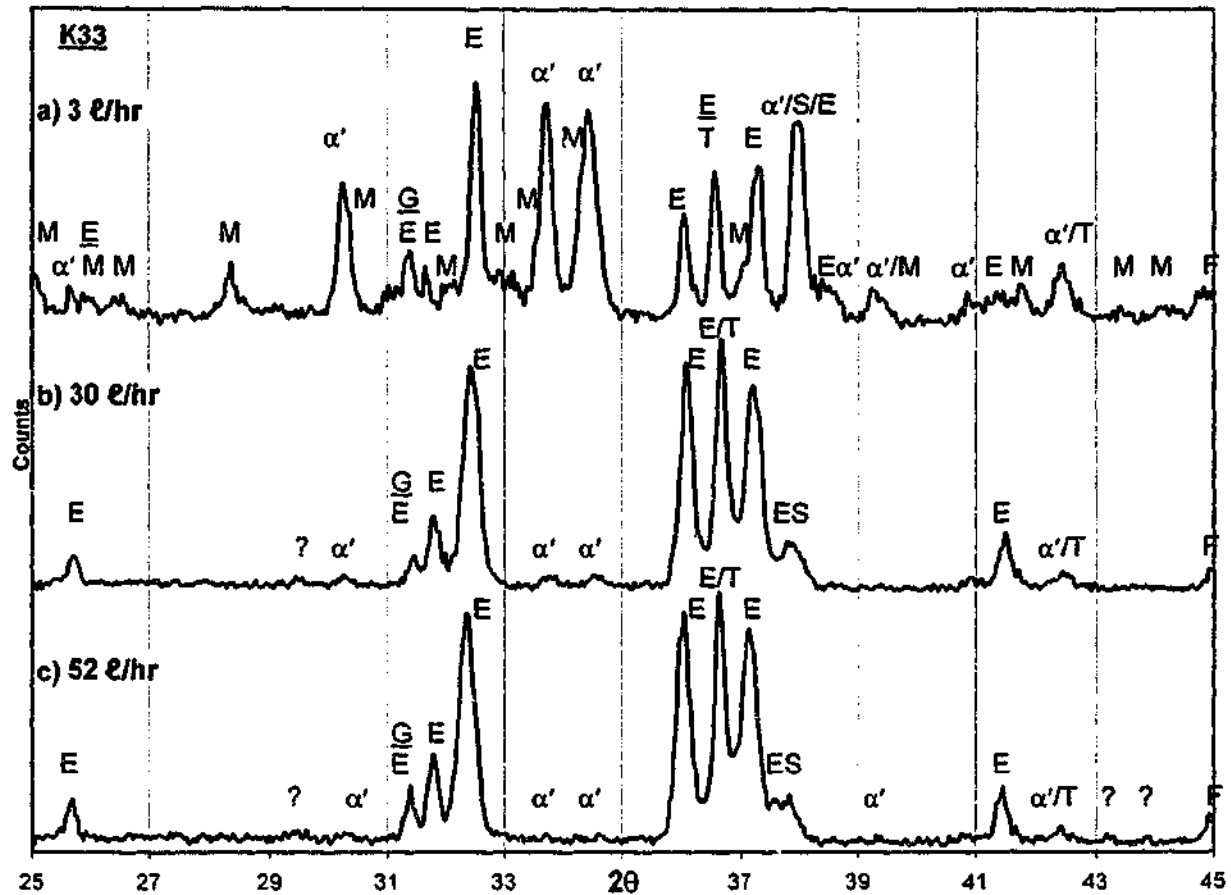


Figure 6.2 XRD traces of K33 powder fired at 1450°C for 12 hours under different N_2 flowrates: (a) 3 l/hr, (b) 30 l/hr (standard), (c) 52 l/hr.

[Key: α' = α -sialon, M=M'-phase, E=E'-phase, G=G'(gehlenite devitrification product), T=TiN', S=SiC, F=FeSi', ?=unidentified].

The higher molecular weight of SiO (44 g/mol) compared to CO (28 g/mol) makes the SiO(g) more difficult to sweep away in the N_2 gas than the CO(g). Therefore only at higher flowrates will SiO(g) loss become significant and the resultant low SiO(g) partial pressure ($p[\text{SiO}]$) have a noticeably negative effect on CRN. The flowrate above which SiO(g) loss will be detrimental to α' formation will depend on factors relating to furnace and specimen geometry (ie. tube diameter, specimen size and density), and also on composition; Si-rich compositions may accommodate higher SiO(g) losses and thus endure higher N_2 flowrates without significantly affecting α' formation.

This effect may explain the different behaviour between the K06 and K33 compositions. The low flowrate of 3ℓ/hr produced the highest amount of α' in both compositions, and corresponds to the least amount of SiO(g) loss expected from the sweeping action of the gas. Considerably more α' was formed under a 3ℓ/hr flowrate than when the composition was fired under the higher, more aggressively sweeping 30ℓ/hr flowrate. The higher flowrate increased the extent of SiO(g) loss, and the Si-rich K06 composition was able to more easily accommodate this loss and still produce a predominantly α' -bearing powder, albeit with a small reduction in α' content of 8%. The K33 composition, which contained much less SiO₂, could not accommodate the extensive SiO(g) loss, forming only 5% α' . Further increasing the flowrate to 52ℓ/hr essentially prevented α' from forming in this composition.

Admittedly, the CRN reactions were not fully complete in the K33 sample fired at 3ℓ/hr, as evidenced by the presence of M'-phase in the products after 12 hours. M'-phase was previously found in equilibrium with α' and E' only during intermediate stages of CRN, where it was consumed to form the final $\alpha'+E'$ 'steady state' CRN product phases (Section 4.3.2). The presence of M'-phase in the K33 sample fired at the low N₂ flowrate suggests that although α' formation is now clearly more thermodynamically favourable, the low N₂ flowrate has slowed the rate of the CRN reactions such that they could not be completed in this sample within the 12 hour dwell at 1450°C. This is a direct result of the reduced CO(g) sweeping efficiency; the higher $p[CO]$ retards the reaction rate. Therefore, the use of lower N₂ flowrates at 1450°C for α -sialon production may entail reaction times longer than 12 hours to ensure completion of the reactions and final phase formation.

It was seen in Chapter 5 that the clay-P and sand based samples did not produce significant amounts of α' after CRN for 12 hours at 1450°C with N₂ flowing at 30ℓ/hr. This was attributed to a retardation of the diffusion kinetics resulting from the higher viscosity, SiO₂-rich liquids formed in these compositions. The formation of nitride phase such as α -Si₃N₄ and D'-phase (nominally 2CaO·Si₃N₄) indicates that N has been incorporated into the system via CRN, but further CRN reactions involving the solution and precipitation of crystalline phases through the liquid could not proceed adequately. Altering the N₂ flowrate is therefore unlikely to have a significant effect on the clay-P or sand samples, but to test this assertion the P02 (0.25:1 slag:clay-P) and S03 (0.30:1 slag:sand) compositions were fired using the lower flowrate of 3ℓ/hr for 12 hours at 1450°C. As expected, no significant change to the phase assemblies of these samples could be detected via XRD, with neither sample producing significant amounts of α' . Diffusive reaction kinetics are clearly a limiting factor in controlling the extent of α' formation via CRN.

The above experiments have shown that by manipulating the N_2 flowrate, it may be possible to significantly alter the equilibrium CRN conditions to allow an essentially single-phase α' product to be formed from very high-slag compositions which were previously unsuccessful at producing α' . The optimum N_2 flowrate for α' formation will depend on the composition of the specimen, and will also be related to other factors such as sample density, furnace geometry, and the fundamental CRN parameters of reaction temperature and time. It may even be possible to produce highly α' -bearing powder from just slag alone, without any clay additions, by optimising the N_2 flowrate and other parameters. The economic advantage in using lower N_2 flowrates to achieve highly α' -bearing powders from high-slag compositions, however, may be offset by the longer reaction time required to complete the CRN reactions.

6.4 Seeding

The previous work on Mg- α' formation via the CRN of talc and clay minerals demonstrated that the addition of 3% α - Si_3N_4 seeds almost tripled the quantity of α' formed, from 35% to >90%, as shown in Figure 2.8 (Zhang, Komeya, *et al.* 2000). Seeding has also commonly been used to boost the α - Si_3N_4 content of Si_3N_4 powders produced via CRN of SiO_2 (Kang, Komeya, *et al.* 1996), by lowering the energy barrier to nucleation through the provision of pre-formed nuclei in the system. The choice of the seeding content for the K-series compositions was discussed previously in Section 3.2.1, and was on average 6.5 wt% of the total batch weight. This section presents the results of experiments designed to determine the effectiveness of the α - Si_3N_4 seeds added to the batch, as well as to investigate the possibility of self-seeding the samples with CRN- α' powder rather than α - Si_3N_4 .

6.4.1 Effect of α - Si_3N_4 Seeds

The standard K06 (0.62:1 slag:clay-K) composition contains 6.9 wt% α - Si_3N_4 seeds, which is higher than the 3 wt% successfully used for Mg- α' formation (Zhang, Komeya, *et al.* 2000). Three K06 compositions were created to investigate the effect of α - Si_3N_4 on α' formation: 0%, 2 wt% and 23 wt% α - Si_3N_4 seeds. The 23 wt% α - Si_3N_4 sample does not really represent a 'seeding' addition but was produced to investigate the effect of excessively high α - Si_3N_4 content. For these experiments, the samples were uniaxially pressed under 10MPa to form pellets for firing under the standard conditions (1450°C for 12 hours, 30ℓ/hr N_2).

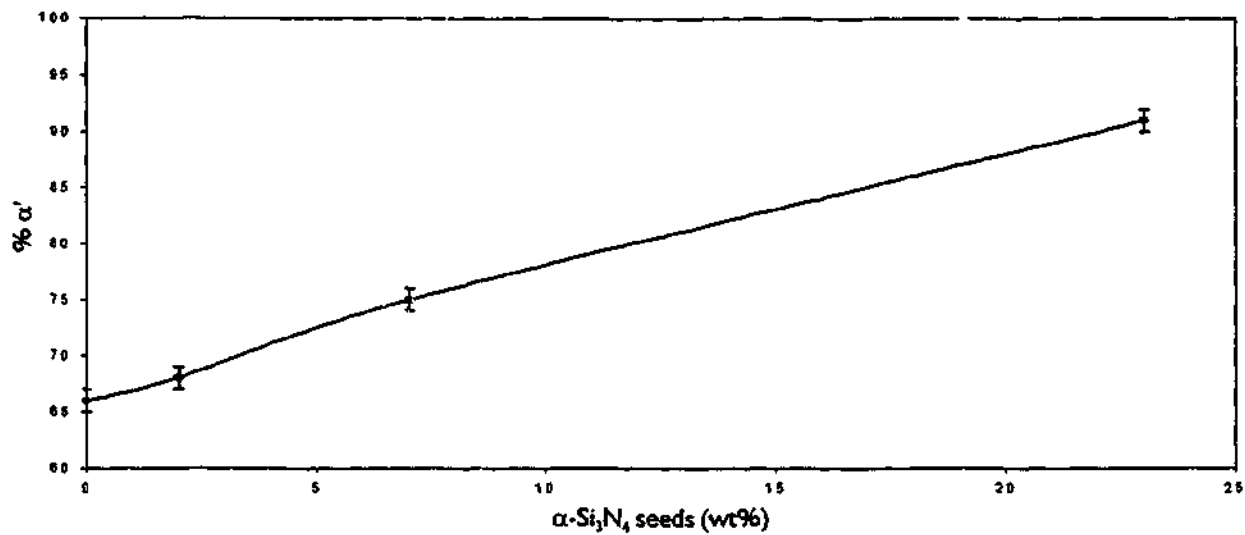


Figure 6.3 α' formation as a function of α -Si₃N₄ seeding content for K06 pellets fired at 1450°C for 12 hours under N₂ flowing at 30l/hr.

No trace of α -Si₃N₄ was detected in any of the samples after firing, indicating that all of the α -Si₃N₄ had been converted to α -sialon, even in the 23 wt% α -Si₃N₄ sample. Figure 6.3 shows that the relationship between α' content and seeding is essentially linear, which does not represent a seeding effect; the small addition of just 2 wt% seeds should have produced a dramatic increase in α' content if a seeding effect was operational, which was not the case. The increase in seed content results in an essentially monotonic increase in α' ; the unseeded K06 sample formed 66% α' , and the addition of 2 wt% seeds increased the α' content by 2% to 68%. The 7 wt% seed addition increased α' by 9%, and the 23 wt% addition increased the α' content by 25%.

It is clear that the α -Si₃N₄ additions increased the yield of α' in these K06 pellets, but this occurred via direct α -sialon formation rather than by promoting α' nucleation. α -Sialon can form directly from α -Si₃N₄ by a solution-precipitation reaction with the Ca-Al-Si-O-N liquid produced at >1300°C in the same way as α -Si₃N₄ powder is converted to α -sialon during reaction-sintering (van Rutten, Hintzen, *et al.* 1996). This direct α' formation may account for the α' observed at very early stages of CRN (Section 4.3.2.1), where α' was first detected at the same point during CRN as the intermediate β' and M'-phases were first detected, together with a large amount of liquid. It is not possible to determine whether the dissolution of pre-existing α -Si₃N₄ into the liquid and subsequent precipitation of α' occurs before or concurrently with the CRN formation of α -sialon, however these processes appear to be independent and α' formation via CRN is not influenced by the α -Si₃N₄ seeds in these

samples. A different result was found, however, for loose powder samples that were not compacted into pellets. This is discussed in the following section.

6.4.2 Self-Seeding with CRN- α' Powder

In the case of α - Si_3N_4 formation via CRN of SiO_2 powders, the reactants are 'self-seeded' with the desired final product, usually α - Si_3N_4 seeds to promote α - Si_3N_4 production over the undesired β - Si_3N_4 phase (Kang, Komeya, *et al.* 1996). In a similar manner, rather than using α - Si_3N_4 powder to promote α' nucleation, CRN- α' powder was used here as a 'self-seeding' addition to the K06 slag+clay-K mixture. CRN- α' powder from previously fired K06 samples was hand ground in an agate mortar and pestle to reduce the particle size, and 5 wt% was added to the unseeded K06 batch mixture. In these experiments, loose heaps of both the unseeded K06 powder and the CRN- α' seeded samples were reacted according to the standard conditions. Table 6.4 lists the α' content of these powders, along with the standard K06 composition with 7 wt% α - Si_3N_4 seeds (fired as a loose powder), for comparison.

Table 6.4 Effect of type of seed on α' content of loose K06 powder fired at 1450°C for 12 hours in N_2 flowing at 39l/hr.

K06 Sample	% α'	% E' (=1-% α')	Other phases
0 seeds	70	30	AlN' - mw TiN' - vw FeSi' - w SiC - vw?
5% CRN- α' seeds	81	19	AlN' - w TiN' - vw FeSi' - vw SiC - vw?
7 wt% α - Si_3N_4 seeds	94	6	AlN' - vw TiN' - vw FeSi' - w SiC - vw?

Error = $\pm 1\%$

Key to XRD intensity: s=strong, ms= medium strong, m=medium, mw=medium weak, w=weak, vw=very weak, ?=unable to be accurately quantified due to peak overlap.

In the previous experiment using compacted pellets, the 7 wt% α - Si_3N_4 seeding addition did not produce a seeding effect, with the increase of 9% α' corresponding to direct α' formation from the α - Si_3N_4 addition. In the case of firing loose powders, a seeding effect has been detected from samples using both the α - Si_3N_4 and CRN- α' seeds. The 7 wt% α - Si_3N_4 seeding addition boosted the overall α' content by 24%, resulting in a >90% α' product, which is indicative of a seeding effect.

The K06 CRN- α' powder was much less effective as a seeding agent than α -Si₃N₄, with the 5 wt% α' addition producing only a 11% increase in α' formation, including the 5 wt% contribution of α' seeds in the starting mix. One reason for this lack of effectiveness may be the larger particle size of the CRN- α' powder compared to the α -Si₃N₄ powder, ($\sim 1\mu\text{m}$ versus $0.65\mu\text{m}$), and the effective particle size may be larger than this if the hand grinding was unable to fully break up the agglomerates to separate the individual grains.

The difference between the seeding behaviour of α -Si₃N₄ in the loose powder and the previously examined compacted powder may be explained by the effect of compaction in promoting intimate contact between the reactant particles. In the case of the compacted pellet, intimate contact will promote dissolution of the α -Si₃N₄ into the liquid formed at the CRN temperature, which may be the source of α' precipitation at the very early stages of CRN as discussed previously. In this case, the α -Si₃N₄ particles are consumed before they can act as nucleation sites for the subsequent CRN reactions that are beginning to operate. In the loose powder, the less intimate contact between reactants will reduce the rate and extent of dissolution of the α -Si₃N₄ into the melt, which gives the surviving α -Si₃N₄ particles more opportunity to act as nucleation sites for the preferential nucleation of CRN products.

These results suggest that seeding the mixture with α -Si₃N₄ is much more effective than self-seeding the mixture with CRN- α' particles, but only under certain conditions such as low specimen density – seeding did not promote α' formation in compacted samples. Previous results from Section 6.2 suggest that optimising (lowering) the N₂ gas flowrate may be a much more effective way to boost the α' content of a composition, while minimising the cost and complexity of the batch mixture. Therefore, this expensive addition to the batch mix may be unnecessary.

6.5 Effect of Elevated Temperature on CRN Reactions and Phase Stability

The reaction temperature is a fundamental parameter affecting the phases produced after CRN. Previous studies have found that increasing the temperature of the CRN process or heat-treating CRN-derived powders at elevated temperatures could increase the yield of α' in the products (Mitomo, Takeuchi, *et al.* 1988; van Rutten, Terpstra, *et al.* 1995). It was seen in Section 4.3 that the final phase assembly formed via CRN is not necessarily the true equilibrium phase assembly, but the 'steady state' assembly that had formed after 12 hours of reaction at 1450°C. The α'/E' ratio in high-slag K-series compositions increased over the 12 hours of reaction, and may further increase with extended reaction time. However only an

incremental increase in α' was observed after 6 hours of reaction, thus it was assumed that at 12 hours the system was essentially at a steady state. The E' found with α' after CRN is therefore a metastable CRN intermediate phase that has not been converted to α' , but can do so with further CRN, and involving solution-precipitation with the liquid phase.

Raising the temperature for CRN is one method that has been found to increase the yield of α' (van Rutten, Terpstra, *et al.* 1995). However, there may be an upper limit to the benefits of increasing the reaction temperature, as it was found in that study that SiC becomes increasingly favourable over α' formation above 1650°C. Unfortunately it was not possible to directly test the effects of higher CRN reaction temperatures in this investigation, as 1450°C was the maximum temperature achievable in the reaction furnaces used for CRN. It was possible, however, to indirectly obtain some insight into the role of temperature on the CRN reactions by heat-treating previously formed CRN powders at higher temperatures. The furnace used for these heat-treatments cannot replicate the conditions experienced during CRN, but the nitrogen atmosphere and elevated temperatures may promote the continuation of CRN reactions that were kinetically hindered at 1450°C. In addition to the CRN reactions 'continuing' at higher temperatures, non-CRN related phase transformations may also occur in the powders if the phases formed at 1450°C are unstable at higher temperatures. Densification of the CRN- α' powder is likely to require high-temperature firing in the range 1600-1800°C, thus any phase transformations occurring during sintering will have significant implications for the production of bulk materials from this powder. Heat-treating this powder thereby enables an examination of the stability of these powders.

6.5.1 Stability of the CRN Powders at 1600°C.

The predominantly α' K02, K06, and P02-18 CRN powders were investigated here, in addition to the predominantly E'-phase K33 and the α' +D'-phase P08-18 CRN powders. The samples contained varying amounts of residual C after CRN, therefore to remove any influence of this C on the samples during firing, the C was removed via oxidation in air at 650°C for 2 hours in a muffle furnace prior to heat-treatment.

Approximately 1g of oxidised loose powder was placed in individual graphite crucibles and heat-treated at 1600°C for 1 hour under a slight positive pressure of N₂, using in the furnace described in Section 3.3.2. The results of XRD phase analysis of the powders after heat-treatment ('HT') are given in Table 6.5, along with the original phases present in the oxidised powder before heat-treatment ('CRN'), for comparison.

Table 6.5 Phase analysis of oxidised (C-free) CRN powders heat-treated at 1600°C for 1 hour.

Phase*	K02		K06		K33		P02-18		P08-18	
	CRN	HT	CRN	HT	CRN	HT	CRN	HT	CRN	HT
Ca- α'	s	s	s	s	w	w	s	s	s	s
α -Si ₃ N ₄	w						w	mw		
AlN'	w		vw	vw						
E' (CaAlSiN ₃)		w	w	vw	s	s				
D' (2CaO·Si ₃ N ₄)									m	mw
SiC-2H	vw?	w?	vw?	w?	w?	w?	?	?	?	?
TiN'	vw	vw	vw	vw	w	vw				
FeSi'	vw	vw	vw	vw	w	w			vw	vw
G' gehlenite (Ca ₂ Al ₂ SiO ₇)		vw			vw	w				
unidentified									m	m
amorphous	Δ	Δ	Δ	Δ	vw	vw	Δ	Δ	Δ	Δ

Key to XRD intensity: s=strong, ms= medium strong, m=medium, mw=medium weak, w=weak, vw=very weak, ?=unable to be accurately quantified due to peak overlap.

* The nominal composition is given but these phases may be solid-solutions.

Δ An amorphous phase is expected to be present, but not able to be detected above background in the XRD.

The K02 CRN powder (0.19:1 slag:clay-K) displayed a considerable difference in phase assembly after heat-treatment, as shown in Figure 6.4. The kinetic factors preventing complete CRN in the K01 composition was discussed in Section 4.2.7, and in Section 5.2.3 regarding the P-series compositions. Evidence of this kinetic difficulty was the presence of transient CRN phases such as α -Si₃N₄ amongst the final products, of which only a minor amount was present in K02. It has been established that the CRN reactions were hindered by a low volume of high viscosity, SiO₂-rich liquid, impeding the diffusion required to produce α' via a solution-precipitation process. It was suggested that increasing the time and/or temperature for CRN would achieve a greater degree of α -sialon formation, and this appears to be true in this sample fired at 1600°C for 1 hour, where α -Si₃N₄ was no longer detected and appears to be converted to α -sialon and/or E'.

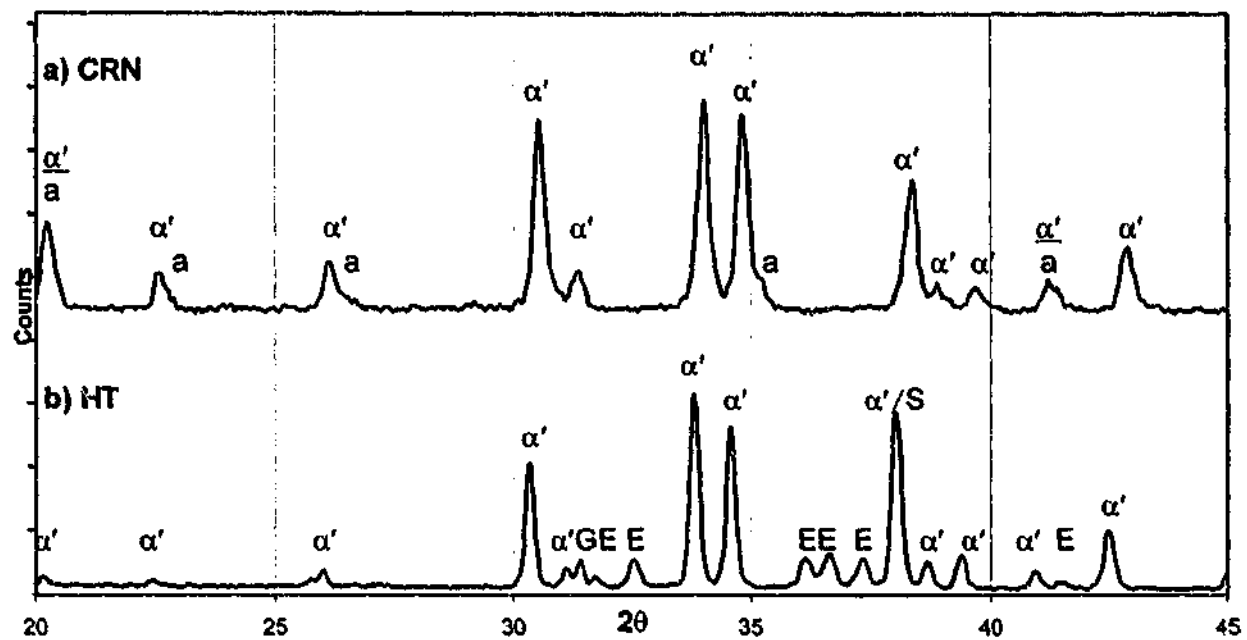


Figure 6.4 XRD of oxidised (C-free) K02 CRN powder: (a) before heat-treatment, (b) heat-treated at 1600°C for 1 hour.

In the case of the P02-18 composition, some reduction in the α - Si_3N_4 content was observed, however a significant amount still remains after heat-treatment. This indicates that the viscosity of the SiO_2 -rich liquid in this composition is very high, and requires temperatures even greater than 1600°C to allow for a sufficiently high degree of diffusivity to promote α' formation.

It was observed by van Rutten and co-workers that Ca- α' formation increased in CRN- α' powders after heat-treatment via the dissolution of β' into the residual liquid and precipitation of α' , a process that did not involve the further incorporation of N via CRN reactions (van Rutten, Terpstra, *et al.* 1995). Similarly in the present system, the removal of residual C prior to heat-treatment suggests that the extra Ca- α -sialon formed in K02 and P02-18 was purely the result of a temperature-enhanced solution-precipitation process involving dissolution of the intermediate α - Si_3N_4 into liquid formed from the molten grain boundary glass. This is due to the liquid having increasingly lower viscosity with elevated temperature, allowing for enhanced rates of solution and precipitation.

However, it is also possible that the CRN reactions did continue somewhat during the heat-treatment. An increase in SiC-content was observed in the K02 powder after firing at 1600°C, despite the removal of residual C from the powder before heat-treatment. The oxidation firing at 650°C for 2 hours should be adequate to remove all of the free-C present in the sample

(Nielsen and Weimer 1997), hence the source of C for SiC formation must come from elsewhere. One possibility is that the SiC may have precipitated from amorphous Si-C contained within the grain boundary glass, a feature discovered in the work by Ekstrom and co-workers on the CRN of halloysite clay (Ekstrom, Shen, *et al.* 1998). Another potential source of SiC formation is from C released from the graphite furnace components such as the heating elements, refractory, and crucibles, during firing. The samples were not shielded from the furnace atmosphere, thus any C that is released into the chamber from the furnace components may enter the sample. A lime-green deposit characteristic of SiC was found on the bottom of the graphite crucibles where there was direct contact with the CRN powder, demonstrating that direct contact with C can result in SiC formation. For this reason, packing powders are commonly used to isolate the samples from the furnace atmosphere (Hampshire 1994). The effects of packing powders on phase transformations in these CRN powders will be discussed in Section 6.5.2.5.

The SiC formed during intermediate stages of CRN acts as a reductant for further CRN reactions between the crystalline phases, N from the atmosphere, and the liquid (Mazzoni and Aglietti 1998). E' is a known CRN intermediate phase, hence it is possible that the small amount of E'-phase (nominally CaAlSiN_3) produced in the K02 sample after heat-treatment was formed as a result of continued CRN between the $\alpha\text{-Si}_3\text{N}_4$, N, SiC, and the liquid. It is interesting to note that both E' and G' (nominally $\text{Ca}_2\text{Al}_2\text{SiO}_7$) were formed in the heat-treated K02 via CRN. Previous results in Section 4.2.7 showed that the closest composition to K02, K03 (0.34:1 slag:clay-K), produced G' gehlenite as the main secondary phase to α' , with E'-forming compositions requiring considerably higher slag contents of 0.62:1 (K06) and above. The formation of G' under the new equilibrium conditions at 1600°C is therefore not surprising, however the formation of E' in the low slag K02 composition clearly demonstrates that the 'steady-state' phase assembly described in Section 4.2.7 does not represent true equilibrium of the system, and only describes the 'local equilibrium' developed during CRN at 1450°C for 12 hours. Quite different equilibrium conditions exist at 1600°C, producing a different balance of phase compatibility. It is possible that the small G' peak at ~31.4°C may be due to devitrification of the grain boundary glass upon cooling, rather than a product of CRN reaction. However it is not possible to determine this without further analysis.

No significant changes to the phase assembly were observed in the other compositions heat-treated at 1600°C for 1 hour. The K06 and P08-18 powders only experienced a slight decrease in the amounts of the respective E'- and D'-secondary phases. This shows that the α' phase is stable at elevated temperatures, and that minor amounts of secondary phases may be

converted to α' during sintering processes. However, it is not entirely clear whether this small extent of conversion is purely due the higher temperature allowing for solution-precipitation, or whether it is due to CRN reactions promoted by minor quantities of SiC, either residual or formed during heat-treatment.

The lack of any change to the E' content of the K33 sample was surprising, as preliminary results showed that some conversion to α' could occur at temperatures $\sim 1500^\circ\text{C}$. With the desire to maximise the amount of slag used in α' production, the possibility of converting E' to α' at elevated temperatures via heat-treatment, or even via additional CRN processes is very attractive, and this is investigated further in the following section.

6.5.2 Factors Affecting the Conversion of E' to α' in K33

The K33 phase assembly after 12 hours of CRN at 1450°C consists of mostly E', with minor amounts of α' , SiC, TiN', FeSi', G' and glass. The previous heat-treatment performed at 1600°C on oxidised K33 powder with the residual C removed did not produce any increase in the α' content, despite preliminary results suggesting this could be achieved. Four factors were investigated here to determine their effect on promoting the conversion of E' to α' : temperature, C-content, powder compaction density and furnace environment (packing powder).

The factors of temperature and C are examined first, using samples of both oxidised (C-free) and as-fired (C-containing) powders heat-treated at 1600, 1700, and 1800°C for 2 hours. XRD scans from the powders after firing are presented in Figure 6.5, and the results of phase analysis in Table 6.6.

6.5.2.1 Effect of Temperature on the CRN Reactions in K33

As with the previous 1 hour firing at 1600°C , extending the heat-treatment of the oxidised (C-free) K33 powder to 2 hours at 1600°C did not produce any significant change in the phase assembly from the initial CRN K33 powder. A large change was observed, however, when the heat-treatment temperature was increased to 1700°C , where both the α' content and the SiC content of the sample increased from 'weak' to 'medium', with the E'-phase remaining 'strong' as the dominant phase. The relative proportion of α'/E' increased during this heat-treatment, rising from $\sim 1:4$ to $\sim 1:2$ $\alpha':\text{E}'$, as calculated using Equation 6.2. Raising the temperature to 1800°C dramatically increased the amount of SiC present in the sample such that SiC became

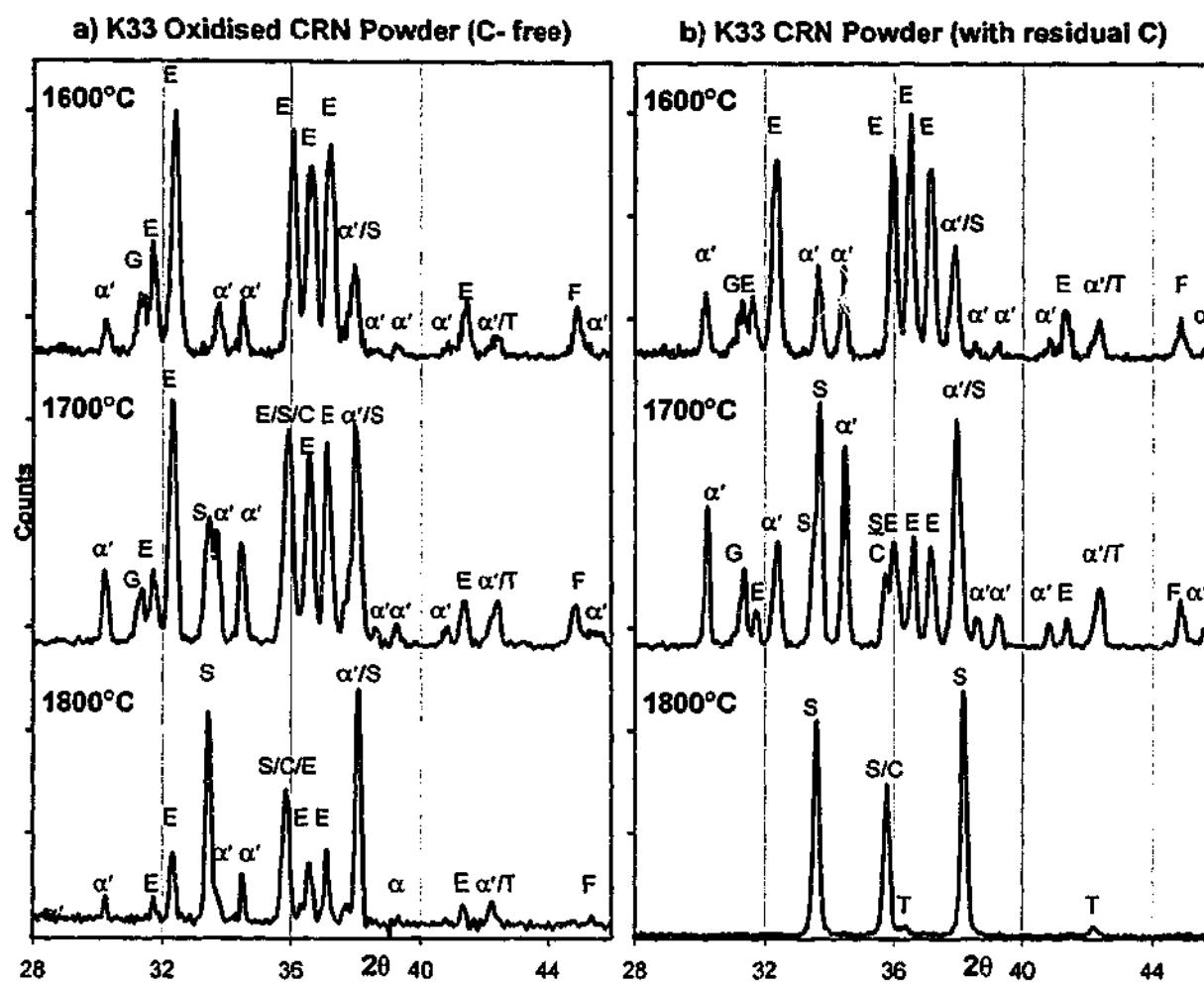


Figure 6.5 XRD scans of K33 powders heat-treated at various temperatures for 2 hours.

[Key: α' = α -sialon, E=E'-phase, S=SiC-2H, C=SiC-3C, G=G' gehlenite, T=TiN', F=FeSi'].

Table 6.6 Phase analysis of oxidised and as-fired K33 CRN powder heat-treated at various temperatures for 2 hours.

Phase	K33 Heat-treatment					
	Oxidised (no C)			As-fired (with C)		
	1600°C	1700°C	1800°C	1600°C	1700°C	1800°C
Ca- α'	w	m	w	mw	s	
E'	s	s	mw	s	ms	
SiC	w?	m?	s?	w?	ms?	s?
TiN'	vw	vw	vw	vw	w	vw
FeSi'	w	vw	vw??	vw	w	
G'	w	w		w	w	
glass	vw	vw	vw			

Key to XRD intensity: s=strong, ms= medium strong, m=medium, mw=medium weak, w=weak, vw=very weak, ?=unable to be accurately quantified due to peak overlap.

the dominant phase, as shown in Figure 6.5a. The strength of the XRD signals of both α' and E' are much lower compared to the SiC, indicating that the SiC has formed at the expense of both of these phases, however the $\alpha':E'$ ratio appeared to further increase to $\sim 1:1$.

It is the strong intensity of the SiC XRD signal produced here that enabled 2H-SiC to be identified in this system. Only the 100% intense 2H-SiC(101) peak is usually observed in the XRD scans from powders reacted at 1450°C, which at $2\theta=38.1^\circ$ overlaps both α' and AlN' , making identification and quantification difficult. All of the other 2H-SiC peaks are also overlapped by other peaks, which provided no means for unambiguous identification in the earlier XRD scans, as discussed in Section 4.2.3.1.

SiC has several different polymorphs with hexagonal, cubic, or rhombohedral unit cells and numerous stacking sequences. The hexagonal SiC polymorphs are commonly referred to as α -SiC, with the 6-layer 6H-SiC being the most common α -SiC polymorph (Lee and Rainforth 1994). The 2H-SiC polymorph detected here is relatively rare. In addition to 2H-SiC, a significant amount of 3C-SiC was also produced after heat-treatment at 1800°C. The 3C polytypoid has a cubic structure with a 3-layer stacking sequence, and is commonly referred to as β -SiC. The phase equilibria governing polytypoid formation are not relevant to the present work and will not be discussed here. The JCPDS PDF defines the 100% intense peak for 3C-SiC at $2\theta=35.63^\circ$ (PDF #29-1126), however the experimentally observed position in these samples is often ~ 35.8 to 35.9° , which can overlap with a main E' peak (83% intense) at 35.9 - 36.1° . This small shift may be due to disturbances in the stacking sequence of the SiC crystals, which is a common feature of SiC (Lee and Rainforth 1994). The other 3C-SiC peaks are much lower in intensity, ~ 20 - 35% , and directly overlap α' , E' , or 2H-SiC peaks, hence this phase has only been unambiguously identified in this and other samples containing very high SiC and very low α' and E' contents (Figure 6.5).

The preferential formation of SiC at elevated temperatures is predicted thermodynamically, as determined in the study by Wada and co-workers of phase equilibria in Si-C-N-O the system (Wada, Warg, *et al.* 1988). Calculations of the equilibrium between solid β - Si_3N_4 and β -SiC as a function of temperature, N_2 partial pressure ($p[N_2]$) and C activity (a_C) show that for the conditions closest to those used here ($a_C=1$ and $p[N_2] = 1$ atm), SiC is in equilibrium with Si_3N_4 at 1374°C, with SiC favoured at higher temperatures and Si_3N_4 at lower temperatures. Increasing the temperature will promote SiC formation at the expense of Si_3N_4 -based materials, and this effect was observed here; a small amount of SiC is produced at the CRN temperature of 1450°C, and increasingly higher amounts of SiC are formed at the expense of

the nitride α' - and E'-phases when firing the powder at temperatures $>1600^{\circ}\text{C}$. The graphite furnace components are the most likely source of C.

The above results showed that the extent of conversion of E' to α' was enhanced by increasing the temperature, however this may be due to the greater formation of SiC at elevated temperatures, which promotes the conversion of E' to α' via CRN. The deliberate promotion of the CRN reactions is examined in the following section, using non-oxidised CRN powders, which contain some residual carbon-black.

6.5.2.2 Effect of Carbon on the CRN Reactions in K33

The results of heat-treating the as-fired K33 loose powder that still contains the residual 3.5 wt% C are listed in Table 6.6 and XRD scans were given in Figure 6.5b. When compared to the oxidised powders, more α' was formed after heat-treatment at 1600°C and 1700°C in the C-containing samples, showing that C has a positive effect on enhancing the conversion of E' to α' . At 1700°C the α' content was greater than that of E', a situation that required the higher temperature of 1800°C to be achieved in the C-free sample. This clearly demonstrates that the formation of α' via CRN can be enhanced at higher temperatures, allowing a greater conversion of intermediate CRN phases such as E' to α' . Hence it may be possible to produce highly α' -containing powder from slag-rich compositions such as K33 if CRN is performed at temperatures $>1450^{\circ}\text{C}$. However, α -sialon formation is in competition with SiC formation, thus there will be an upper limit to the temperature able to be used for CRN. At 1600°C the amount of SiC formed was quite similar in both the C-free and C-containing samples. At 1700°C , however, SiC formation was clearly favoured in the C-containing sample, and increasing the temperature further to 1800°C produced a sample totally dominated by SiC, with no α' or E' detected.

The work by Wada and co-workers in the pure Si-C-N-O system previously discussed in Section 6.5.2.1 predicts increasingly favourable conditions for SiC formation at temperatures above 1374°C (Wada, Wang, *et al.* 1988). It was also shown that SiC formation is enhanced by increasing a_{C} , i.e. increasing the C-content of the system. Hence it would be expected that SiC formation would increase with temperature in all samples above 1374°C , and would also be greater in all C-containing, as-fired CRN-K33 samples than in the C-free oxidised powders, however this was not the case. Carbon was seen to have no significant effect on the extent of SiC formation at temperatures below 1700°C , with SiC formation in the C-containing sample exactly matching that of the oxidised sample at 1600°C . Only at 1700°C did the extra C seem to have an effect, whereby SiC formation was enhanced in the C-containing sample (Figure

6.5b). A similar result was found in other studies of α' production via CRN, where heat-treating the CRN powder at temperatures 1500-1550°C enhanced the conversion of secondary phases to α' , but SiC formation was found to be favoured above 1650°C (Mitomo, Takeuchi, *et al.* 1988) (van Rutten, Terpstra, *et al.* 1995).

The above result suggests that the experimental conditions experienced during heat-treatment are very different from the thermodynamic equilibrium conditions used for the calculation by Wada and co-workers, which do not reflect the complex chemistry of the present system. The lack of increased SiC formation in C-containing samples at 1600°C suggests that there is a threshold temperature below which SiC formation is relatively limited, possibly due to retarded diffusion kinetics. At 1800°C the extent of SiC formation was far greater in the C-containing powder than in the oxidised powder, fully reducing the Si-Al-Ca-O-N phases α' and E' to produce SiC. The Ca, Al, and other metallic species are thought to be partially lost from the sample through volatilisation at the high temperature, with the remainder forming the grain boundary glass. TiN' was the only other phase stable in this sample at 1800°C.

It would appear from these results that temperatures $>1600^\circ\text{C}$ are unfavourable for densification of the CRN powders due to SiC production being thermodynamically favourable. The stability of the nitride phases as opposed to the carbides can be improved however, by reducing the a_c in the system and increasing the $p[\text{N}_2]$ (Wada, Wang, *et al.* 1988). The C effect is stronger and easier to achieve; in the work by Wada and co-workers it was seen that changing the crucible material from graphite to BN raised the stability of Si_3N_4 from 1374°C to 1700°C, under 1 atm N_2 pressure. If the graphite crucible was used, a $p[\text{N}_2]$ as high as 70 atm would be required to compensate and maintain nitride stability at 1700°C. In practice, nitride ceramics are often successfully densified at these temperatures in graphite furnaces using graphite crucibles without any SiC formation. This may be due to two factors not examined by the previous firing of loose powders; compaction of the powder into pellets for sintering, and the use of a packing powder to isolate the pellet from the crucible. These factors are investigated further in the following section.

6.5.2.3 Effect of Compaction Pressure and Packing Powder on the CRN Reactions in K33

It was seen in Section 6.2 that compacting the powder before CRN hinders the ability of the gas-phase reactants to penetrate the pellet and allow the CRN reactions to occur. Therefore, a similar retarding effect on the SiC formation and the CRN E' \rightarrow α' transformation may be experienced if the CRN powders are compacted before heat-treatment to emulate sintering. Furthermore, packing powders ('powder beds') are often used when sintering nitride ceramics

to prevent thermal decomposition of the pellets and side reactions with the crucibles. The packing powders used in sialon studies are commonly a 50:50 mix of Si_3N_4 and BN powders (Hampshire, Lonergan, *et al.* 1999). The Si_3N_4 provides a similar environment to that of the Si_3N_4 -based precursor pellets, and the inert BN helps prevent densification of the packing powder onto the sample. Large graphite crucibles filled with packing powder are used so as to keep the pellets as far as possible from the crucible walls and prevent any harmful decomposition reactions occurring at temperatures in the range 1600-1800°C.

The effects of packing powder and sample compaction on the continued CRN conversion of E' to α' in the E' -phase K33 powder were tested at 1800°C to determine whether SiC formation could be adequately suppressed. The packing powder used was a variation on the 50:50 BN: Si_3N_4 mix commonly used for the sintering of sialons; to account for the higher oxygen content of the CRN powder and minimise diffusion, 10wt% of SiO_2 and one teaspoon of slag was added to a 45:45 wt% mix of BN: Si_3N_4 . Oxidised (C-free) CRN-K33 powder was used to prevent overly aggressive SiC formation at 1800°C, and this powder was uniaxially pressed into 1cm diameter pellets under 40 MPa hydraulic pressure. The pellets were placed in the centre of a large graphite crucible (diameter 80mm) filled with the packing powder described above. Another compacted pellet was fired at 1800°C in a graphite crucible without packing powder as a control, to examine the effect of compaction density alone. The results of firing on the phase assembly are shown in Table 6.7, along with the previous results for the loose powder heat-treated at 1800°C and the original as-fired CRN powder, for reference.

Very different phase behaviour was observed for the two 40 MPa pellets fired at 1800°C for 2 hours with and without packing powder. The pellet fired in a graphite crucible without packing powder produced a cohesive surface layer of 2H-SiC. This may be expected from the previously observed interactions between graphite from the crucible (and possibly the furnace atmosphere) and the Si-rich CRN powder. In the case of the compacted pellet, the reactions on the closely-packed surface produced a dense SiC surface layer, which essentially formed a protective skin that provided no pathway for further diffusion of species (C , $\text{N}_2(\text{g})$ or $\text{CO}(\text{g})$) into or out of the core of the pellet. Hence the core remained reasonably unchanged from the as-fired CRN powder; E' -phase dominates the phase assembly and 2H-SiC is present only in a 'weak' amount, with no extra SiC formation seen. Nitrogen for CRN would also be prevented from migrating to the core of the pellet, and any $\text{CO}(\text{g})$ evolved would also have difficulty escaping. Thus although the 2H-SiC already within the powder could act as a reductant for CRN, the dense SiC skin prevented the expected $\text{E}' \rightarrow \alpha'$ CRN reaction and SiC formation, from occurring within the pellet. The XRD analysis shows that only a small extent of phase

change was able to proceed in the core of the pellet, with the disappearance of the small trace of α' present and the development of an unidentified impurity phase. This change is unique to this pellet, and probably arises from a limited amount of SiC-assisted carbothermal reduction occurring in isolation within the core of the pellet, which may be assisted by the increased contact between powder particles in the pressed pellet, allowing diffusive rearrangement to occur. E'-phase may be more stable than α' in the local equilibrium conditions within the pellet core.

Table 6.7 Phases present after firing oxidised (C-free) K33 powder and pellets at 1800°C for 2 hours, with and without packing powder.

Phase	CRN as-fired K33 powder	Powder HT 1800°C 2hrs	40 MPa pellet, no packing powder, 1800°C, 2hrs		40 MPa pellet, in packing powder, 1800°C, 2hrs	
			surf	core	surf	core
Ca- α'	w	w			s	s
E'	s	mw		s		
SiC-2H	w?	s	s	w?		vw?
SiC-3C						
SiO ₂					s	
TiN'	vw	vw	vw	vw		vw
FeSi'	w	vw	vw	w		vw
G'	w		vw	w		
unidentified			vw	mw		
glass					vw	vw

Key to XRD intensity: s=strong, ms=medium strong, m=medium, mw=medium weak, w=weak, vw=very weak, ?=unable to be accurately quantified due to peak overlap.

The K33 sample fired in the packing powder produced a pellet with an uneven, white deposit adhering to the surface. XRD analysis of the surface, followed by lightly grinding and re-examination showed this deposit was SiO₂ that adhered from the packing powder (Figure 6.6b). The underlying surface of the pellet was found to consist of Ca- α' -sialon, with none of the other impurity phases or E'-phase detected. The core of the pellet was also fully converted

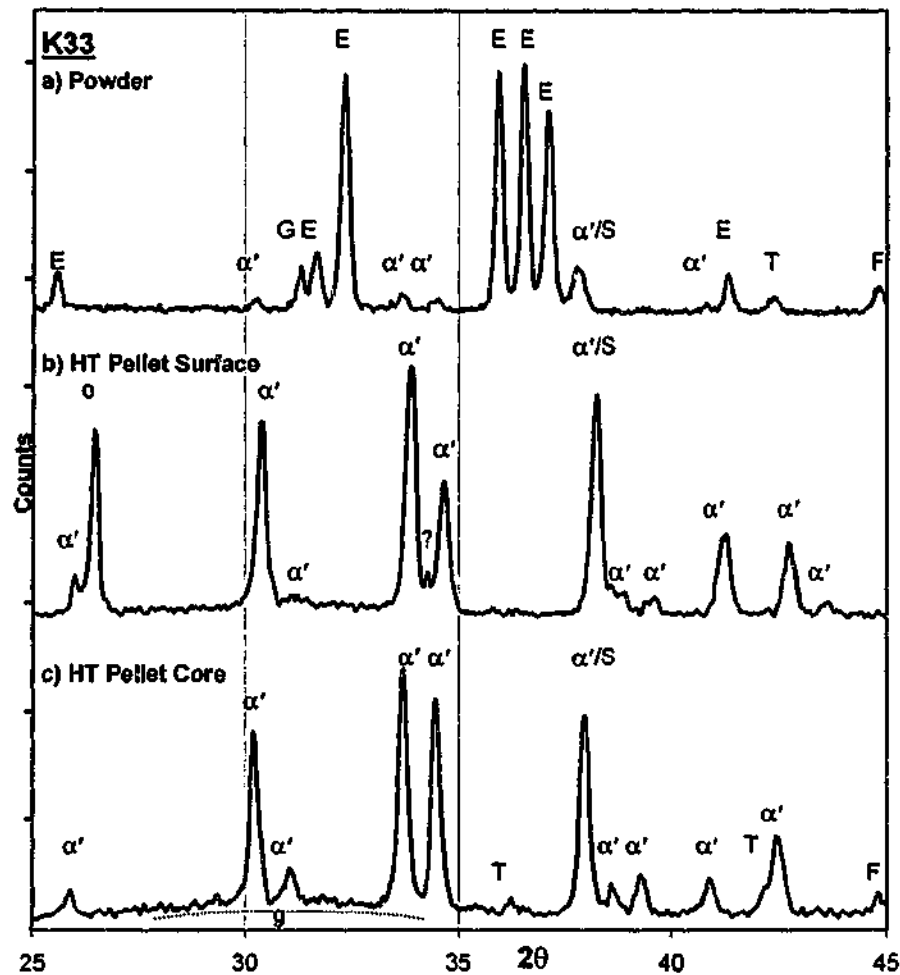


Figure 6.6 XRD of CRN-K33 pellet after heat-treating in packing powder at 1800°C for 2 hours: (a) CRN-K33 powder, (b) surface, and (c) core of fired pellet.

[Key: α' = α -sialon, E = E', T = TiN', F = FeSi', S = 2H-SiC, o = SiO₂, g = glass, ? = unidentified phase].

to α' , with a large amount of glass and no trace of E' present, but the TiN' and FeSi' impurities remained (Figure 6.6c). It would seem that by preventing contact between the graphite crucible and the sample, the E' \rightarrow α' CRN reaction process could occur without competition from the SiC formation reactions. The reductant for CRN was the 2H-SiC already present in the CRN-K33 powder, which is undetected after heat-treatment, indicating that it was consumed during CRN. Nitrogen could be supplied either directly from the Si₃N₄-BN-based packing powder, or from the N₂ furnace atmosphere which penetrates the packing powder. Unlike the pellet fired without packing powder, no dense skin was formed on this pellet, thus the reactants could diffuse through to the core without hindrance. In fact, the compaction of the pellet may have aided the E' \rightarrow α' reaction by increasing the contact

between particles, a feature seen by other workers to be beneficial to CRN (Mazzoni, Aglietti, *et al.* 1993).

This result suggests the possibility that high-slag-containing compositions such as K33 could be used to form solid, essentially pure α -sialon bodies (but relatively high in glass content) from powders containing only a small amount of the desired α' phase after CRN. The requirements for gas penetration into and out of the sample may however produce a relatively porous material with degraded mechanical properties. In the K33 sample the required porosity may result from the intrinsic coarse, plate morphology of the E' being unable to be closely packed, producing large voids between plates through which the gas may travel. The density of the pellet produced after firing in packing powder is investigated in the following section.

6.5.3 Pressureless Sintering of CRN Powders at 1800°C

The previous firing of a pellet of CRN-K33 in packing powder at 1800°C for 2 hours was essentially a pressureless sintering process. Three other compositions, K06, P02-18, and P08-18, were fired according to the same process to gain some idea of the density and phase behaviour of the CRN powders after pressureless sintering. After firing, the SiO₂ from the packing powder that adhered to all four samples was ground off for XRD analysis and density determination using the Archimedes method as outlined in Section 3.4.7. The results are presented in Table 6.8.

XRD analysis of the core material revealed that in all cases the pellets were essentially pure α -sialon, with only 'very weak' amounts of the secondary and impurity phases detected. As with the previously examined K33 pellet where there was total conversion of E' to α' , the D'-phase present in the as-fired CRN-P08-18 powder was also fully converted to α' . No real change was seen in the reasonably pure α' compositions K06 and P02-18, though the minor amounts of AlN' and α -Si₃N₄ in these compositions, respectively, were also removed during sintering. The 'purification' of these powders after firing at 1800°C suggests that small amounts of secondary phases such as E', D' or AlN' may be tolerated after CRN and will be removed during sintering processes.

Table 6.8 Density of pellets pressureless sintered from CRN powders at 1800°C for 2 hours.

Composition	Density (g/cm ³)	Phases present before sintering	Phases present after sintering
K06	2.909 ± 0.007	α' (s) E' (vw), AlN' (vw) FeSi' (vw) TiN' (vw)	α' (s) FeSi' (vw) TiN' (vw)
K33	2.430 ± 0.003	E' (s) α' (vw) FeSi' (vw) TiN' (vw) SiC (w)	α' (s) FeSi' (vw) TiN' (vw) glass (vw)
P02-18	3.04 ± 0.02	α' (s) α -Si ₃ N ₄ (vw)	α' (s) FeSi' (vw)
P08-18	3.05 ± 0.04	α' (s) D' (m) FeSi' (vw) ? (mw)	α' (s) FeSi' (vw)

Key to XRD intensity: s=strong, ms= medium strong, m=medium, mw=medium weak, w=weak, vw=very weak, ?=unable to be accurately quantified due to peak overlap.

Conventional reaction-sintered Ca- α -sialon materials have a theoretical full density of 3.22g/cm³ (JCPDS PDF#33-0261), and all four pressureless sintered compositions are considerably lower than this, including the two essentially single-phase α' compositions K06 and P02-18. This may be due to limited redissolution and mobility of the pre-formed Ca- α -sialon. It will be seen in Chapter 7 that the K33 material contains large voids due to poor packing of the coarse plates (Figure 7.8). Although these voids provide a pathway for the gaseous reactants to complete the E'→ α' CRN reactions, the final density of this material was the poorest of the four compositions tested, ~75% of the theoretical density. Clearly the α' formed could not fill the voids. The α' +D'-containing P08-18 composition produced the highest measured density (~96% of the theoretical density). This is despite some porosity assumed to be present to allow the CRN D'→ α' conversion to occur. The elongated D' rods are several microns in length, (Figure 5.9) which are larger than the equiaxed ~1 μ m α' particles. This bimodal particle size may allow for reasonably efficient packing, but at the same time provide some porous pathways for the reactants to access the pellet for the D'→ α' transformation.

Excluding the very low-density K33 sample, the other three compositions achieved densities >90% of the theoretical density for Ca- α -sialon. This is relatively low compared to the >98% often achievable for conventional reaction-sintered products (Zhang 2002). Densification of these powders via hot-pressing to achieve full density will be investigated in Chapter 7.

6.5.4 Summary of Findings From High-Temperature Heat-treatments

The above results show that under the appropriate conditions (oxidised, compacted powder embedded in a powder bed), the CRN- α' powders K06 and P02-18 are stable up to 1800°C and can be densified to >90% of theoretical density by pressureless sintering at 1800°C. The E'- and D'-containing powders K33 and P08-18 are unstable, but under the same conditions these phases can transform via continuation of the CRN reaction process to α' . In terms of performing the initial CRN production process at higher temperatures, care must be taken to avoid temperatures and conditions such that SiC formation is favourable.

6.6 Conclusions for Chapter 6

This chapter has investigated the role of various processing variables and conditions on the extent of the CRN reactions that produce Ca- α -sialon. The following conclusions can be made:

- The N₂ gas flowrate was the CRN process parameter with the greatest impact on the degree of CRN achievable in a given specimen at 1450°C. A 30ℓ/hr flowrate is generally too high, and removes an excessive amount of intermediate gaseous species required for α' formation in addition to the unwanted gaseous CRN by-products. Lowering the flowrate to 3ℓ/hr achieved a dramatic improvement in the extent of α' formation, especially in the high-slag-containing K33 sample. However it appears that the low flowrate may require longer reaction times (>12 hours) for completion. The optimum N₂ flowrate will therefore need to be determined for each specific composition, sample size, and furnace geometry.
- N₂ gas penetration into the samples can be improved by minimising the density of the green body. Loose powders without any compaction produced the greatest extent of α' formation, and increasing the compaction density reduced the amount of α' formed.
- Si₃N₄ seeds do not promote α' formation in compacted powders, but do have a positive effect on α' formation in uncompact powder samples. It is likely that minimisation of the sample density and optimisation of the gas flowrate can promote α' formation more effectively than seeding, thereby removing the need to add expensive Si₃N₄ to the system. The use of CRN- α' powder to 'self-seed' these powders was not as effective in the uncompact samples as Si₃N₄.

- The CRN reactions may proceed more effectively at higher temperatures, however the CRN reactions may be in competition with SiC formation if sources of C are present. The predominantly α' -containing powders K06 and P02-18 are stable at high temperatures, and the α -Si₃N₄, E', and D'-phases can be converted to α' if SiC formation can be prevented by compacting the powder and embedding the pellets in a nitride powder bed. The transformation to α' during high-temperature firing allows for the possibility of producing Ca- α -sialon materials by sintering high slag, low α' -producing compositions. However the densities achieved via pressureless sintering may be inadequate.

Chapter Seven

Microstructure and Property Evaluation of Ca- α -Sialon Bulk Materials

The previous chapters have focused on gaining a detailed understanding of the carbothermal reduction-nitridation reaction process for producing α -sialon from mixtures of slag and clay. Specific attention was paid to determining the best compositions for α' production, investigating the details of the CRN reaction mechanism, determining the influence of process parameters on the final products, and examining the high-temperature stability of the powders. It has been shown that the CRN reaction process can be controlled via the manipulation of several compositional and process parameters to produce reasonably pure Ca- α -sialon-bearing powders from inexpensive slag and clay mixtures.

The α -sialon product from the CRN process is a powder, not a densified solid body, hence there may be new opportunities for novel applications to be developed for α -sialon powder; for example as abrasive grits, or mixed into other materials as hard inclusions to form new composites. Many conventional applications, however, require bulk materials to be densified from powder precursors, and any economic advantage for producing α -sialons inexpensively from slag can only be realised if the densified material provides a similar level of performance to that expected from conventional α -sialon bulk materials. It is not expected that a Ca- α -sialon material produced from impure, slag waste will exactly match all of the performance characteristics of Ca- α -sialons formed from pure chemicals, especially at high-temperatures. However many low-temperature industrial applications may potentially take advantage of an inexpensive α -sialon material if the performance is not overly compromised and intrinsic properties, such as hardness and wear resistance, remain high. Therefore it is necessary to conclude this investigation with an evaluation of some basic physical and mechanical properties of this material, to gauge its potential for commercial applications.

The four compositions chosen for analysis were those investigated in detail previously: K06, K33, P02-18, and P08-18. Hot-pressing was used to produce fully-dense bulk materials and this process is outlined in Section 7.1. Detailed analyses of the microstructures of the densified materials are given in Section 7.2, and Section 7.3 discusses the results of hardness and

fracture toughness determination; these are parameters important to the dry erosion tests to be described in Section 7.4.

7.1 Hot-Pressing

Previous results in Chapter 6 showed that pressureless sintering was unable to produce fully dense materials from the CRN powders, but the CRN reactions progressed such that all the secondary phases transformed to α' to produce essentially pure α -sialon materials. Hot-pressing is a densification technique used to overcome sintering difficulties, and was used here to produce fully dense samples for microstructural examination and mechanical testing.

7.1.1 Experimental Procedure

The hot-pressing procedure was described in detail in Section 3.3.3 but will be outlined briefly here. The four powders chosen for densification were the predominantly α -sialon K06 and P02-18; the predominantly E'-phase K33; and P08-18 which was a mixture of α' +D'-phase. Residual carbon was removed from the powders after CRN by oxidation at 650°C for 2 hours, and pellets were uniaxially pressed at 10MPa in a 1 inch diameter die. BN powder was used as a packing powder to prevent contact of the pellet with the graphite die parts, and hot-pressing was performed at 1700°C for 1 hour under 20MPa applied pressure. After pressing, the BN that was lightly adhered to the pellet surfaces was removed by sandblasting, and the as-fired surfaces were analysed via XRD. The surfaces were then ground away to enable density determination and XRD analyses of the bulk material.

7.1.1.1 Green-Body Fragility

To improve the transportability of green-bodies, an intermediate step of cold isostatic pressing (CIP-ing) of the uniaxially pressed pellets is often used before hot-pressing. The procedures used here involve first vacuum sealing the uniaxially pressed pellets in two or three layers of polyethylene bags, which acts as an airtight, flexible mold for CIP-ing at 250MPa. CIP-ing has the dual purpose of increasing the green-body density for better handling and slightly reducing the pellet diameter to enable easier insertion of the 1 inch pellet into the 1 inch hot-press die. During these experiments, however, few of the pellets survived the CIP-ing process; extensive cracking or disintegration was observed after CIP-ing, and sometimes after just vacuum sealing, indicating poor compaction density of the CRN powder after uniaxial pressing. Lowering the pressing pressure to avoid excessive elastic springback did not overcome this problem.

Such fragility has generally not been encountered in pellets uniaxially pressed from laboratory reagent powders such as Si_3N_4 , AlN , and SiO_2 when producing reaction-sintered α -sialon materials. The CRN- α' green-bodies are more fragile than those produced from laboratory chemicals due to the CRN- α' powder being considerably harder and coarser than laboratory reagents; the CRN- α' powder has a particle size of $\sim 1\mu\text{m}$ compared to $0.65\mu\text{m}$ or less for commercial Si_3N_4 powder. This indicates that the production of bulk materials from the CRN- α' powder may require an additional processing stage to improve the packing properties of the powder, such as reducing the particle size via milling, for example. The addition of a binder or lubricant may also be useful for improving the green forming properties of the powder, and may allow the use of processes such as tape-casting, slip-casting, or injection moulding to produce α' components with geometries unable to be produced via reaction sintering. However, any additional processing may contribute to increased cost of the final α' components.

For the hot-pressing performed here, the diameter of the uniaxially-pressed pellets was reduced to fit in the die by manual grinding of the circumference of the pellets on abrasive SiC paper.

7.1.2 Density of Hot-Pressed Pellets

A distinct surface layer was noticed on some of the pellets after hot-pressing, and this layer was analysed by XRD before being removed via grinding for density determination. Density determination was performed using the Archimedes method in water, and the average results from two pellets of each composition are presented in Table 7.1, along with the main phases identified in the core of the pellets via XRD. In terms of notation, the pellets pressed from the P02-18 and P08-18 powders will be referred to as simply P02 and P08, respectively.

The theoretical density of Ca- α -sialon ($m=1.6$, $n=1.2$) is generally taken to be 3.22g/cm^3 (JCPDS PDF #33-0261). The three compositions other than K33 produced densities near the theoretical density, with the K06 sample exceeding it. This is due to the higher m -value of the α' -phase in K06 ($m=2.4$), which reflects a higher amount of interstitial Ca^{2+} in the structure that will increase the density. Heavy elements such as Fe and Ti also increase the density, and by producing dense secondary phases such as TiN , which has a density of 5.39g/cm^3 (PDF #38-1420). Therefore, the density of materials densified from heavy metal-containing CRN powders will be intrinsically higher than materials produced from pure Ca-Al-Si-O-N powders.

Table 7.1 Density and phases of bulk pellets hot-pressed at 1700°C.

Pellet	Density of pellet (g/cm ³)	Phases present in pellet core
K06	3.294 ± 0.0005	α' (s) FeSi (vw) E' (vw) TiN (vw)
K33	2.951 ± 0.0003	E' (s) FeSi (vw) α' (vw) TiN (vw)
P02	3.192 ± 0.0008	α' (s) FeSi (vw)
P08	3.196 ± 0.0006	α' (s) FeSi (vw) D' (s) unidentified (vw)

Key to XRD intensity: s=strong, vw=very weak.

All compositions produced a significantly higher density after hot-pressing than was achieved during pressureless sintering, about 10% greater on average. The ranking of pellet densities did not exactly follow the pressureless sintering results (Table 6.8), with K06 producing the highest density after hot-pressing. The two clay-P based pellets P02 and P08 have essentially the same density despite having considerably different phase compositions. Replacing some of the α' seen in P02 with D' as seen in P08 did not significantly alter the final density, which suggests that the density of the pure D'-phase, which has not been reported, is roughly similar to that of α -sialon. K33 remained significantly lower in density than the other three pellets, which reflects the inherent difficulty of densifying a microstructure consisting of coarse, plate-like E' particles without a sufficient amount of a second phase, such as glass, to fill the voids.

7.1.3 Phase Transformations During Hot-Pressing

During the pressureless sintering described in Chapter 6, continuation of CRN >1450°C resulted in all four pellets being fully transformed to α -sialon. This occurred regardless of the starting composition: E' from the K06 and K33 powders; α -Si₃N₄ from the P02-18 powder; and D' from the P08-18 powder were all converted to α' . However the density of these pressureless sintered pellets was low, hence it was thought that it might be possible to obtain single-phase α' materials with full density via hot-pressing these powders. The XRD analysis of the hot-pressed pellets presented here (Table 7.1) shows that this was not in fact possible, and that the expected conversion of secondary phases to α' could only occur on the surfaces of the hot-pressed pellets.

Various sections and orientations of the hot-pressed pellets are discussed in this chapter, hence it is useful to define the terminology used to describe the pellet orientation. A schematic of a hot-pressed pellet is given in Figure 7.1. The pressing direction is indicated, and the round planes parallel to the top surface and normal to the pressing direction will be referred to as the 'flat pellet plane' (Figure 7.1a). Generally, all XRD analyses of the pellet surfaces (before and after grinding) are performed on the flat pellet plane unless otherwise specified. In some cases the pellet is sectioned and the sectioned surface is analysed (Figure 7.1b). This is will be referred to as the 'pellet section', which is parallel to the pressing direction, and thus normal to the flat pellet plane.

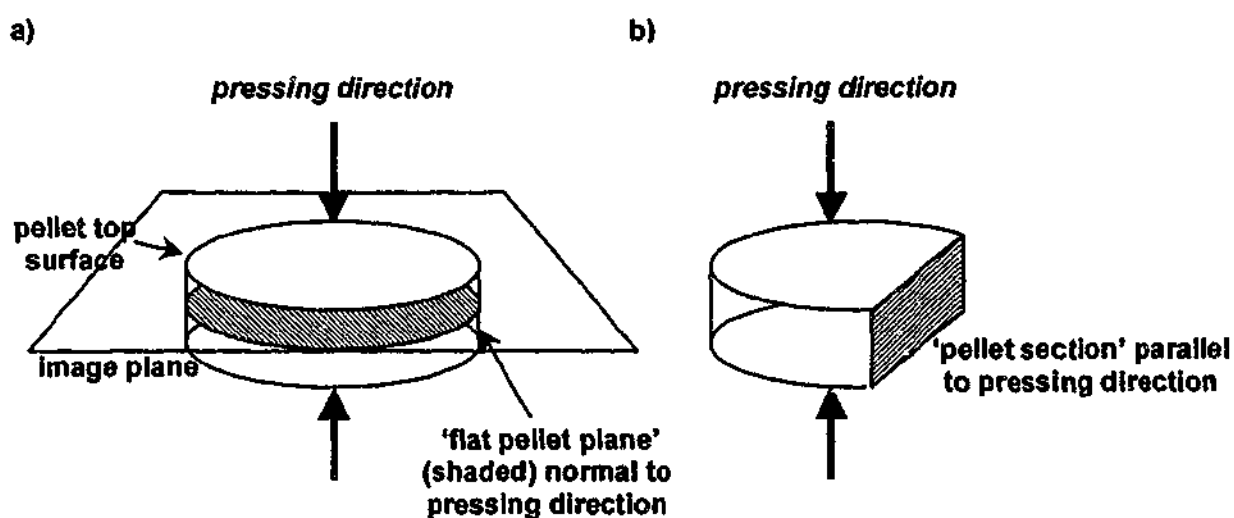


Figure 7.1 Schematic showing orientation of pellets produced by hot pressing: (a) the 'flat pellet plane' normal to the pressing direction, used for all analyses and images presented in this chapter unless stated otherwise, (b) the 'pellet section', parallel to the pressing direction.

It was seen in Section 6.5 that the continuation of CRN reactions involving N_2 from the furnace atmosphere, SiC formed within the sample, and the liquid phase, caused the transformation of minor secondary phases D', E' and α - Si_3N_4 , to α' . This 'purification' of the α' material was also observed after hot-pressing, where the minor trace of E'-phase was removed from both the surface and the bulk regions of the K06 pellet, and α - Si_3N_4 was removed from the surface and bulk of the P02 pellet.

The two pellets K33 and P08 that contained large amounts of the E'- and D'-phases could not fully transform to α' . A highly α' -containing layer was produced on the surfaces of these pellets, but the bulk remained basically unchanged from the CRN powders. Figure 7.2 presents XRD traces of the K33 CRN powder, the transformed pellet surface, and the bulk of

the pellet after removal of the surface layer. The transformed layer is almost fully α -sialon, with only a 'very weak' trace of E' remaining. The core region contains essentially the same phases as the initial CRN powder of E', plus minor amounts of α' and 2H-SiC. A similar result was seen in the α' +D' pellet pressed from P08-18 powder, where the surface was entirely transformed to α' , and the core remains a combination of mostly α' +D' (Figure 7.3). Note that these XRD scans were taken of the flat pellet plane (Figure 7.1a). The depth of these surface layers is investigated via SEM and discussed later in Section 7.2.3.1.

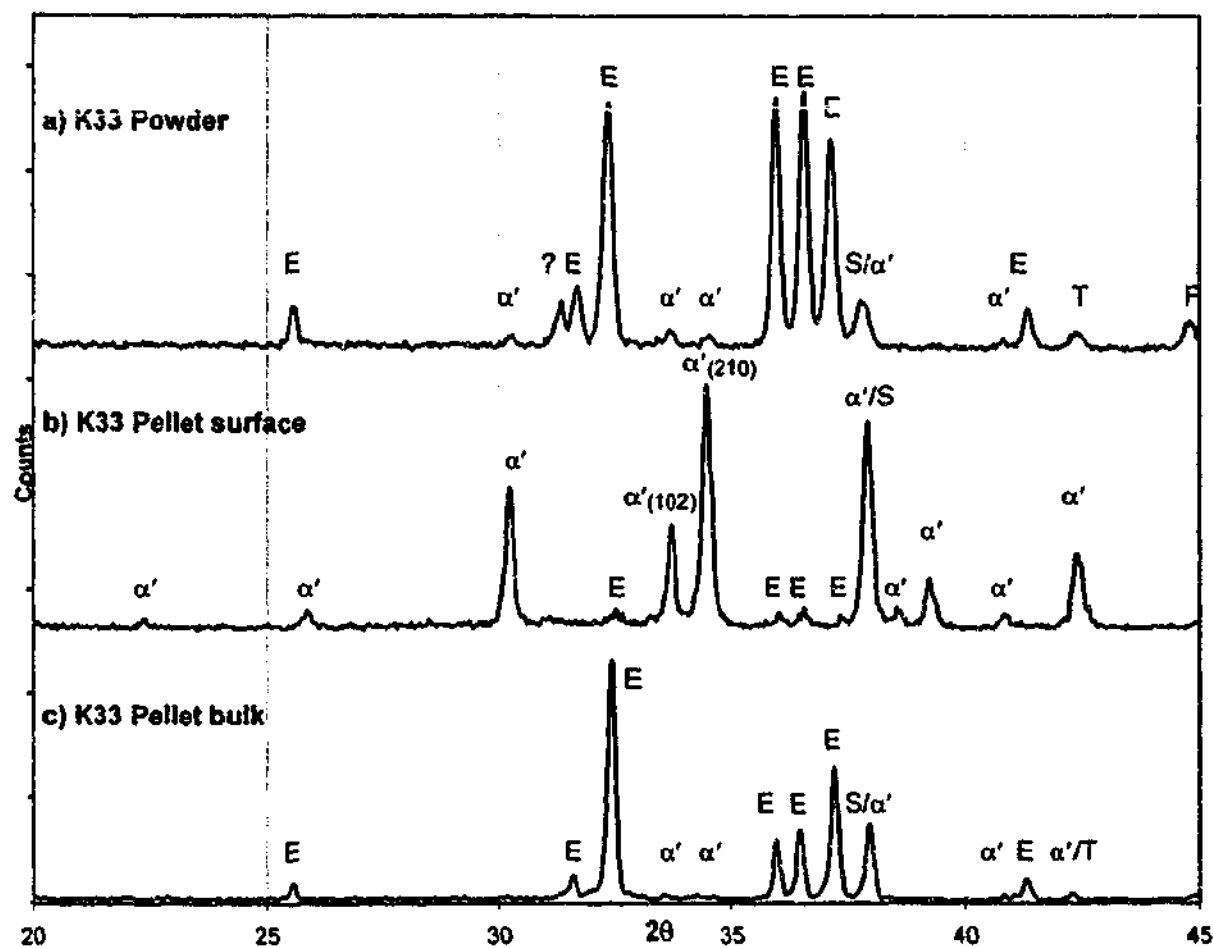


Figure 7.2 XRD showing phase transformations on the K33 pellet surface after hot-pressing at 1700°C: (a) K33 CRN powder before hot-pressing, (b) the as-fired pellet surface, (c) pellet core after surface removal.

These results suggest that small amounts of residual CRN intermediate phases such as E', D', and α -Si₃N₄ may be tolerated in the final CRN powder and will be fully removed during densification. However, the large-scale CRN transformation of massive quantities of residual E'- and D'-phases during hot-pressing is not possible. This is because nitrogen cannot diffuse

through the pellet while it is being densified during hot-pressing, thereby preventing CRN from occurring.

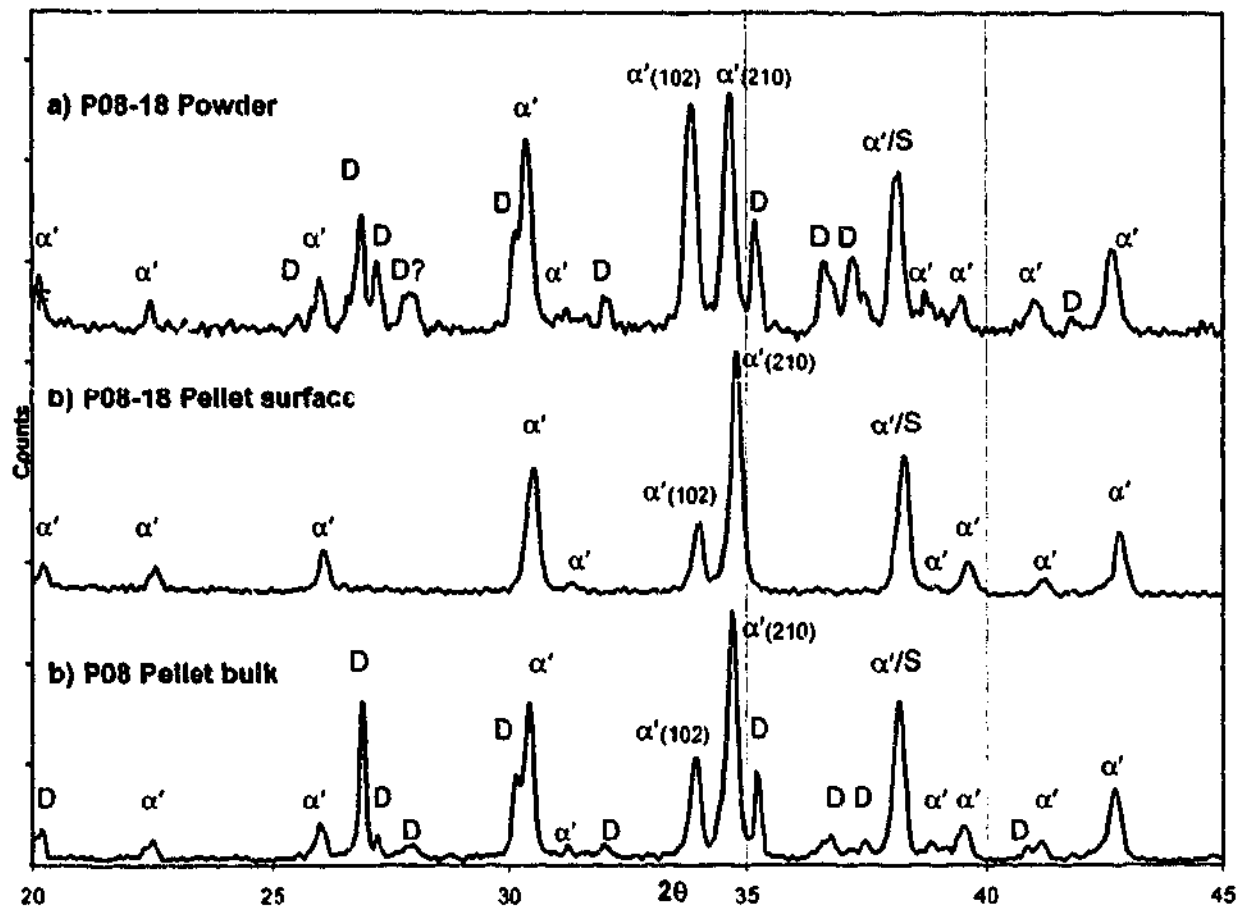


Figure 7.3 XRD showing $D' \rightarrow \alpha'$ phase transformation on P08 pellet surface after hot-pressing at 1700°C: (a) P08-18 CRN powder before hot-pressing, (b) as-fired pellet surface, (c) pellet core after surface removal.

It was shown in Section 6.1 that gas diffusion through the pellets is an important factor in promoting the CRN reactions, both in delivering reactant N_2 and removing gaseous by-products. In the case of pressureless sintering (Section 6.5.3), the pellets were uniaxially pressed before sintering, but were reasonably porous due to the difficulty in compacting the coarse CRN powders. Uniaxially pressed powders typically produce a compact with ~40% porosity (Rahaman 2003), which is enough to allow easy diffusion of gases through the pellets, and thereby allow the CRN reactions to occur. In the case of hot-pressing, the pressure was applied once the sample reached 1300°C which is the approximate temperature at which glass melting (liquid formation) is expected to start. Consequently, the sample is being densified by the time the favourable CRN transformation temperature (ie. >1450°C) is reached. This

prevents the diffusion of gases into and out of the pellet as required for transformation due to the removal of the porous pathways. Consequently, only the surface of the pellet is able to experience sufficient gas diffusion to produce α' ; the N_2 gas cannot penetrate through to the bulk. It is therefore extremely difficult to achieve CRN transformations throughout the bulk of the pellets during hot-pressing. Any phase transformations that do occur within the bulk must be diffusive transformations, such as particle growth or solution-precipitation, that do not rely on gas-phase reactions from the furnace atmosphere.

It is clearly not possible to use hot-pressing to fully transform thick pellets of the E'-phase K33 powder or the highly D'-bearing P08-18 powder to α -sialon while simultaneously achieving full density. Fully transformed components may only be produced if the sections are sufficiently thin, i.e. equivalent to twice the thickness of the transformed surface layer. Later work in Section 7.2.3.1 will show this layer to be only ~ 0.1 mm thick in K33. It is possible that this surface transformation could be utilised to produce core/shell composite materials that have a core of E' or $\alpha'+D'$, surrounded by a shell of transformed α -sialon. The K33 material may be of greater interest because it is less dense than α' , which may result in a lightweight E'-based material protected by a dense and hard α -sialon skin.

7.1.3.1 Preferential Orientation of α -Sialon

Another feature seen in the XRD of the α' phases produced on the surfaces of the K33 and P08 pellets (Figures 7.2b and 7.3b), is that they display considerably different relative peak heights for the α' (102) and α' (210) characteristic peaks than seen in the CRN powders (Figure 4.7, Figure 5.5). Note that these traces were taken from the flat pellet plane. In the powders, the α' (102) peak is usually the strongest α' peak, however in these pellets α' (102) is much weaker than α' (210). Such changes to the relative intensity of these two particular peaks have been attributed to a preferred orientation produced during hot-pressing of reaction-sintered α' materials (Nordberg, Shen, *et al.* 1997; Wang, Cheng, *et al.* 1996). In these studies, it was found that the primary growth of the α' grains precipitated from the M-Al-Si-O-N liquid was anisotropic, producing α' crystals elongated along the c-axis. This growth favoured the direction normal to the pressing direction (i.e. along the flat pellet plane) because diffusion is easier in this direction than normal to the pressure gradient. An additional texture-forming mechanism was detected during the hot-pressing of β - Si_3N_4 materials containing elongated microstructures, where anisotropic growth acted together with rotation of the elongated grains to produce an alignment of the grains parallel to the direction normal to the pressing direction (Lee and Bowman 1992).

In the CRN- α' materials hot-pressed in the present work, the α' grains are pre-existing in the material and are generally equiaxed, hence grain rotation is unlikely to be significant to the texture produced in these samples. The preferred orientation must therefore occur via anisotropic grain growth. A CRN-induced solution-precipitation mechanism is responsible for the conversion of the metastable phase β' to α' , hence the α' precipitated from the liquid may undergo oriented growth in the direction normal to the pressing pressure. Where the CRN reactions are limited, such as in the bulk of the pellet, some dissolution of the pre-existing α' grains into the liquid formed from the molten grain boundary glass will occur, which will then be re-precipitated and grow in the preferred orientation. Evidence of the solution-reprecipitation of α' grains is given in the TEM analysis presented in Section 7.2.2.

A greater extent of orientation was found in the transformed surface layer of the pellets than in the bulk of the pellets. Figure 7.3 shows that the α' (102) peak is slightly higher, relative to the α' (210) peak, than seen in the XRD trace of the pellet surface (Figure 7.3b). This is due to the effect of CRN promoting a higher extent of solution-precipitation on the surface of the pellets than in the bulk.

7.2 Microstructural Analysis

The mechanical properties of bulk materials are heavily dependent on the microstructure formed during sintering. It is therefore useful to examine the microstructures that have developed in the four hot-pressed CRN pellets to gain an understanding of the features that will underpin their in-service performance. In addition, greater insight may be provided into the densification process and surface phase transformations which occur during sintering, which are of interest to the further development of bulk CRN- α' materials.

7.2.1 Experimental Procedure

The methods for preparing specimens for microstructural analysis were detailed in Chapter 3, and will be recapped here. Pellets from the CRN powder were hot-pressed at 1700°C for 1 hour, after which any BN which adhered to the surface was removed via sandblasting. Some samples were lightly polished using 1200 grit paper and 1 μ m diamond paste on a cloth lap for examination of the as-fired pellet surface using a reflected light optical microscope. The surfaces were then ground to remove any transformed surface layer, verified by XRD, and then polished to a 1 μ m diamond finish before etching in molten NaOH at ~400°C for 10s. In some cases both the surface and core regions of the pellets were etched and inspected. Etching was used to remove the grain boundary glass and allow microstructural details to be

observed in secondary electron mode in the SEM. Unlike α -sialon systems stabilised by heavy Y^{3+} or RE-cations, which produce good contrast between phases in backscattered electron mode, very little contrast exists between Ca-Si-Al-containing phases in either secondary or backscattered electron modes. For detailed observation and analysis in the TEM, a foil was made from a hot-pressed K06 pellet without etching.

The micrographs presented here were all taken in the pellet plane (Figure 7.1a), normal to the pressing direction, unless stated otherwise.

7.2.2 K06 Pellet

No significant change to the phase assembly of the K06 pellet was detected after hot-pressing; the pellet remained essentially pure α' with a small amount of AlN' and minor amounts of E' -phase, $FeSi'$, and TiN' impurities present. One difference observed between the powder and the hot-pressed pellet was the development of a preferential orientation of the α -sialon grains, as discussed in Section 7.1.3.1.

No microstructural features were visible in the polished specimen under the low magnification provided by the optical microscope. A K06 pellet was sectioned perpendicular to the pellet plane (Figure 7.1b) and representative micrographs of the etched surface taken via SEM are presented in Figure 7.4. The majority of grains present are α' , but the microstructure is considerably non-uniform. The grains shown in Figure 7.4a display a generally fine, $<1\mu m$ grain size, and are basically equiaxed with only a slight elongation (aspect ratio ~ 1.6) detected. In Figure 7.4b, a few elongated grains with a much higher aspect ratio of >3 can be seen. Although some slightly elongated α' particles were found in the K06 powder (Section 4.2.5), the considerable number of elongated grains seen here suggests that the texture is a result of anisotropic grain growth during hot-pressing. Some large, irregular grains with a morphology indicative of solidification from a transient liquid are also seen in Figure 7.4b, and are features associated with either porosity or the grain boundary glass (which was removed via etching). Chemical analysis via EDXS showed that the fine, equiaxed and elongated grains consisted of Ca, Al, and Si, which would be expected of Ca- α' , and that the large grains were the Fe- and Si-rich $FeSi'$ phase.

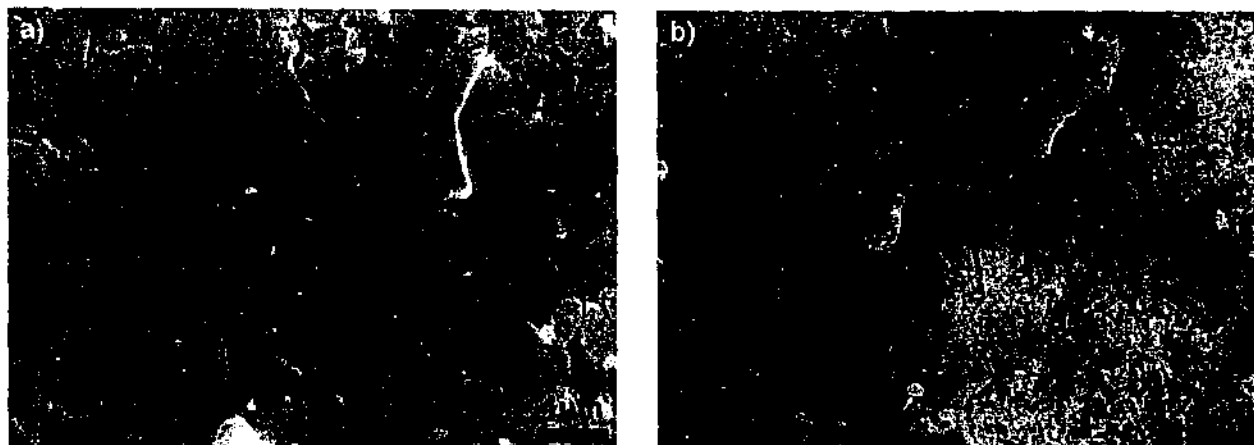


Figure 7.4 SEM micrograph of K06 pellet hot-pressed at 1700°C. Note the grain boundary glass was removed via etching in molten NaOH.

Closer inspection in the TEM (Figure 7.5) reveals finer-scale features not seen in the SEM images shown above. Detailed phase identification was possible via both electron diffraction patterns (CBEDP) and energy dispersive x-ray spectroscopy (EDXS), the results of which are presented in Figure 7.6. It is this work that enabled the unambiguous identification of many of the minor phases discussed throughout this thesis.

Both elongated and equiaxed α' morphologies can be seen in the TEM bright field images presented in Figure 7.5a. Small overlapping 250nm α' grains can be seen in Figure 7.5b with hexagonal facets characteristic of α' . These are likely to be α' grains precipitated from the liquid during hot-pressing. Small 40-100nm inclusions within the α' grains, identified as TiN', are seen throughout the sample, and are indicated by the arrows in Figure 7.5.

The EDXS spectrum for α' in Figure 7.6a clearly shows the Ca- α' -sialon elements Si, Al, O N, and Ca. The Al:Si:Ca peak height ratio is 1:1.7:0.4, essentially unchanged from that seen in the K06 powder (1:1.8:0.3). EDXS analysis of the powder produced by CRN at 1450°C showed that the α' was only stabilised by Ca, and not Mg, and the result from the hot-pressed pellet shows that even at higher temperatures where α' has a higher formability, no Mg has entered the α' structure. The carbon signal is an artefact from the conductive sample coating.

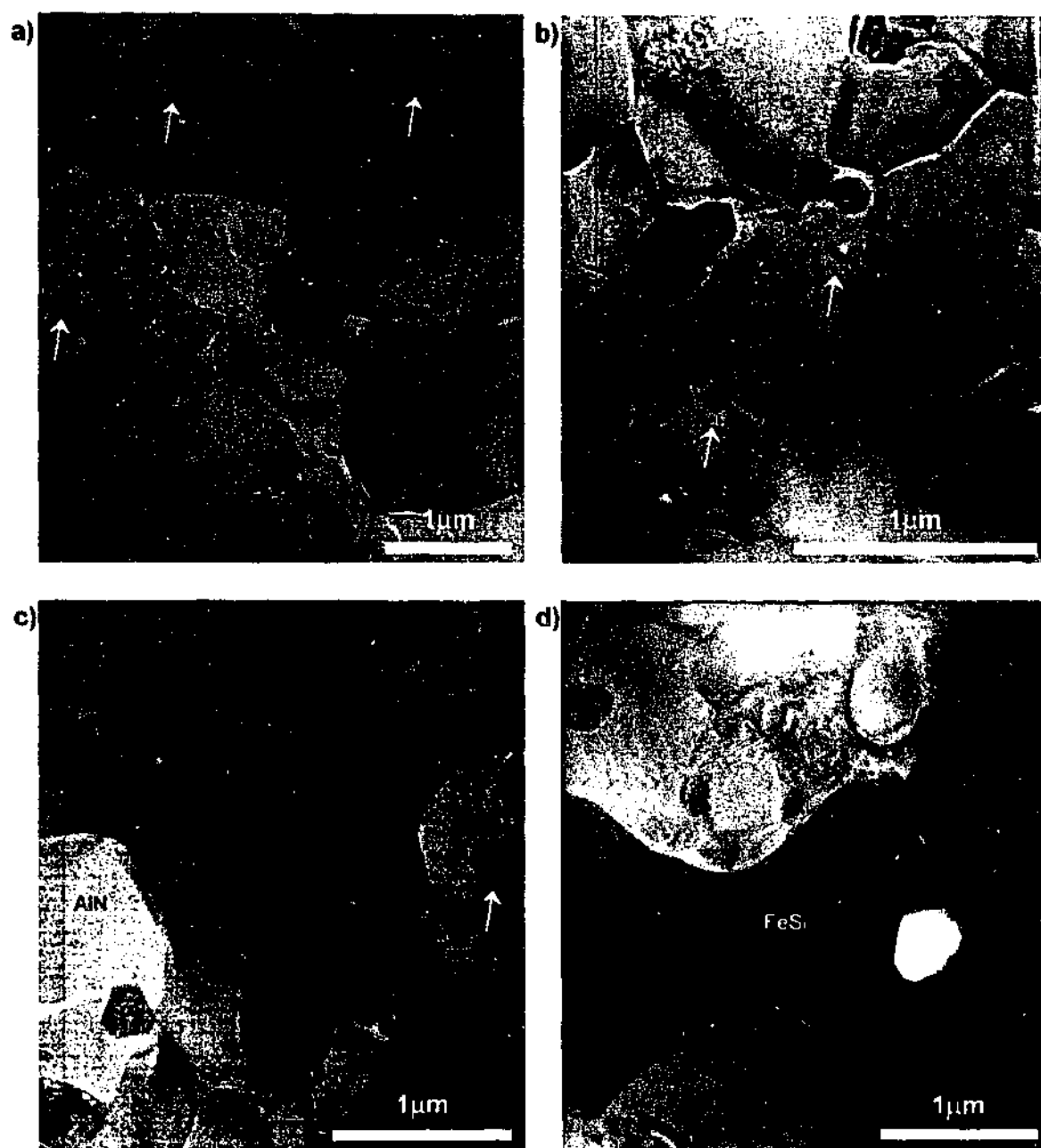


Figure 7.5 TEM bright field overviews of K06 pellet hot-pressed at 1700°C. The phases were identified via EDXS and diffraction pattern analysis presented in Figure 7.6. The arrows indicate TiN' inclusions.

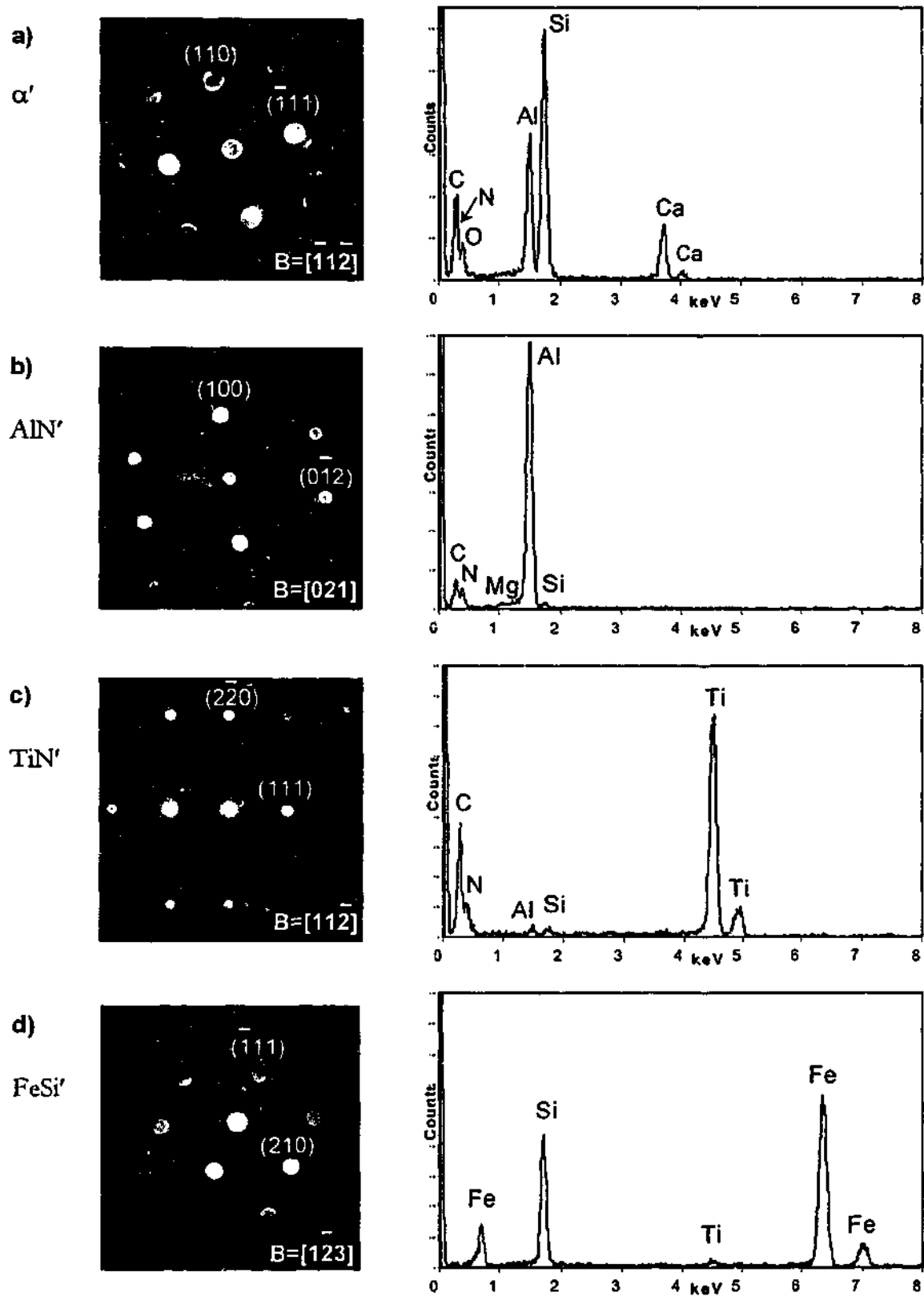


Figure 7.6 Typical convergent beam electron diffraction patterns (CBEDP) and EDXS spectra of grains in the K06 pellet shown Figure 7.6: (a) α' -sialon, (b) AlN' , (c) TiN' inclusions, (d) $FeSi'$ grain.

AlN' was identified as the generally elliptical grains roughly 1 μm in length (Figure 7.5c). This morphology is suggestive of precipitation from the liquid phase (Wood 2001). The large faceted inclusion in the left-hand AlN' grain in Figure 7.5c was found to be α -sialon, and the inclusion indicated by the arrow was found to share the same TiN' chemistry as the smaller ones in Figure 7.5a and b. In the work on the Ca-Al-Si-O-N system, Wood discovered that very small amounts of Si and O could be substituted into the AlN structure, but not enough to allow differentiation between the two phases by XRD or electron diffraction. The AlN produced in this investigation was also indexed as AlN via XRD and CBEDP, but the EDXS results indicate that the solid solution formed is slightly different to the AlN' discovered by Wood; in addition to the aforementioned Si⁴⁺ substitution for Al³⁺, some Mg²⁺ from the slag has also entered this structure (Figure 7.6b). No definitive O signal can be seen in the EDXS spectrum, which may mean that the substitution of Mg²⁺ for Al³⁺ balances the additional charge brought about by the substitution of Si⁴⁺ for Al³⁺. Although this phase should be more properly referred to as Mg-AlN', the label of AlN' to indicate the solid-solution is sufficient for the purposes of the present investigation.

The small inclusions within the α' grains (Figure 7.5) were identified as cubic TiN (Figure 7.6c). The Ti originates from TiO₂ impurities found in both the slag and clay-K. The EDXS spectrum was taken from the large TiN inclusion found in the AlN' grain shown in Figure 7.5c, and reveals that a small amount of Si⁴⁺ substitution for Ti⁴⁺ has occurred, hence the designation of TiN'. The Al signal in the spectrum is from the surrounding AlN' grain.

The dark, strongly diffracting phase in the TEM (Figure 7.5d) corresponds to the large Fe-Si blobs seen in the SEM, and was identified as cubic FeSi with a significant substitution of Ti⁴⁺ for Si⁴⁺ (Figure 7.6d). This large extent of solid-solution accounts for the large peak shifts seen in the XRD, often up to $\pm 0.3^\circ$ for some FeSi' peaks. The Fe is also supplied to the system via impurities in the slag and clay-K. The large size of these grains relative to the other phases in the system, suggests that their presence will have a detrimental effect on mechanical properties.

Analysis of the residual glass is given in Figure 7.7. Given that the Ca content of this system is far in excess of that required for α -sialon formation, it was not surprising to find the SiO₂-based glass to be also very rich in Ca. The remainder of the Mg is also accounted for in the glass, as are many of the other trace impurities. The Mo signal is an artefact from the holder used in the ion-beam thinning process. The sulphur is a residue from the gypsum

($\text{CaSO}_4 \cdot 2\text{H}_2\text{O}$) added to the slag, which decomposes above $\sim 1020^\circ\text{C}$ (Grimshaw 1971). As mentioned in Section 4.2.2, the sulphurous smell detected in the powders after firing indicated that not all of the sulphur was removed from the sample during CRN. Other volatile trace elements from the slag such as chlorine, sodium, and potassium are also not completely removed, having been detected in other glassy pockets analysed via TEM. This also shows that the glass does indeed act as a sink for many of the slag impurities. The lack of any Ti in the glass indicates all of the Ti in the system was either consumed in TiN' formation or entered the FeSi' phase.

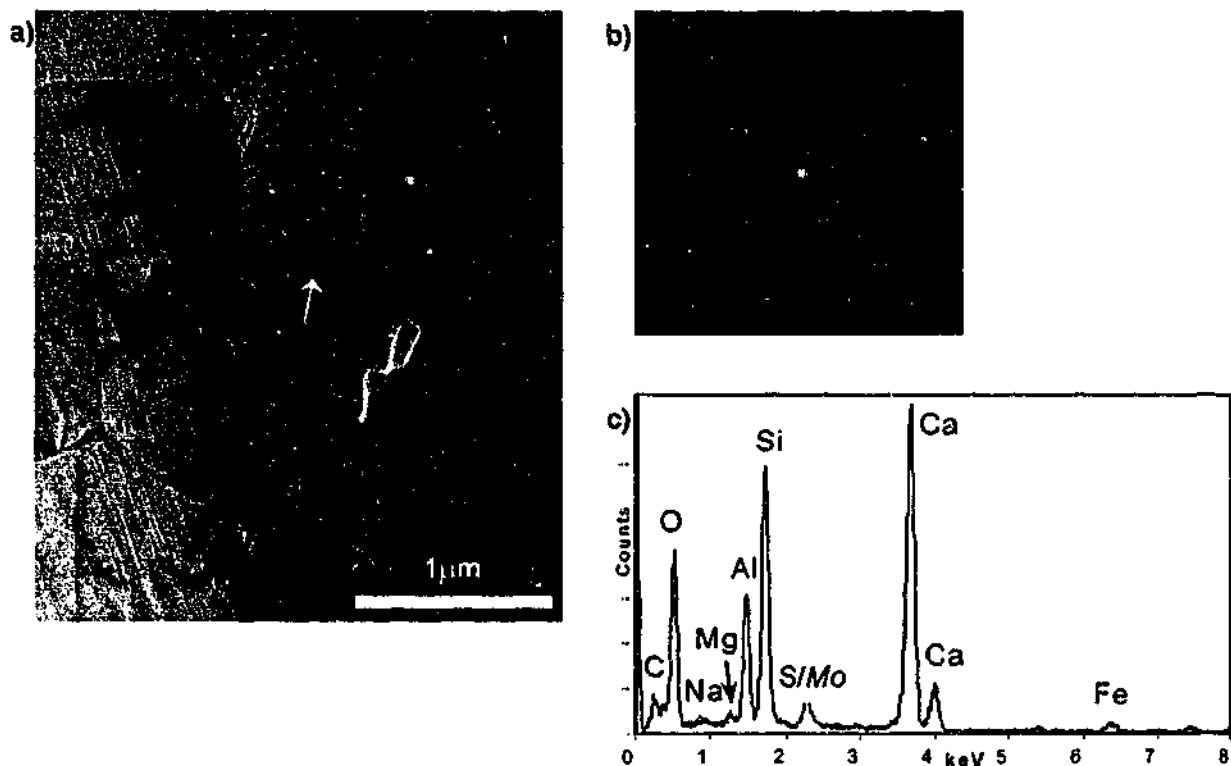


Figure 7.7 TEM micrograph of K06 pellet hot-pressed at 1700°C : (a) bright field image showing glass pocket, (b) amorphous diffraction pattern, (c) EDXS spectrum from point indicated in (a).

7.2.3 K33 Pellet

It was seen in Section 7.1.3 that the metastable E' -phase transformed almost fully to α' during hot-pressing, but only on the surface of the pellets. Understanding and controlling this transformation may eventually allow single-phase α -sialon materials to be produced from high

slag-containing compositions, therefore the both the bulk E' material and the transformed surface layer are examined in detail in this section.

Figure 7.8a is an optical micrograph of the as-fired, transformed surface (in the flat pellet plane) of one such K33 pellet without etching and minimal polishing. Unfortunately, the small amount of polishing performed on the surface was enough to remove some of the transformed layer. XRD analysis showed that the E' from the underlying bulk was now detected, along with the minor α' and 2H-SiC phases. Optical micrographs of the core of the pellet after considerable surface grinding to fully remove this transformed layer are presented in Figure 7.8b and c.

The pellet surface has a highly heterogeneous microstructure. Both large and small pores are distributed throughout the surface, some as large as 10-20 μ m, and others barely resolvable at the magnification used. The light-contrast needles are the dominant phase found in this image, which are up to 10 μ m long and randomly oriented within the plane of the pellet surface. Some are very long and fine. The shorter, fatter needles are most probably E' plates, which appear as laths in cross section and can be identified by having a similar size to the E' plates seen previously in SEM images of the K33 powder (Figure 4.9). In some areas these laths are not densely packed, and are seen to be penetrating into pockets of a medium-grey phase, most likely the intergranular glass. The finer, elongated grains are likely to be elongated α -sialon grains, which grow anisotropically and preferentially along the flat pellet plane of this image. In areas that are considerably denser, the grain size is unresolvable at the magnifications used, which may correspond to regions of the sub-micron α' grains usually seen in various compositions in this system. The bright white spots scattered throughout the image are most likely large, reflective, metal-based inclusions such as SiC or FeSi'.

XRD analysis of the core of the pellet after surface grinding showed that the bulk is essentially pure E'-phase, with some SiC present but no α' detected (Figure 7.2c). The density of this sample was 2.951 g/cm³, which is quite low compared to the predominantly α' K06 pellet. The dark areas in the optical micrographs (Figure 7.8b and c) show that the bulk is extremely porous, much more so than the surface (Figure 7.8a). Some of the pores are as large as 40 μ m in diameter, and using the line-intercept method the porosity was estimated to be ~25%. The E' plates in the bulk of the pellet shown in Figure 7.8c also appear to be slightly coarser than that seen on the surface and in the CRN powder (Figure 4.9). This indicates that some grain growth of the E' plates has occurred during hot-pressing.

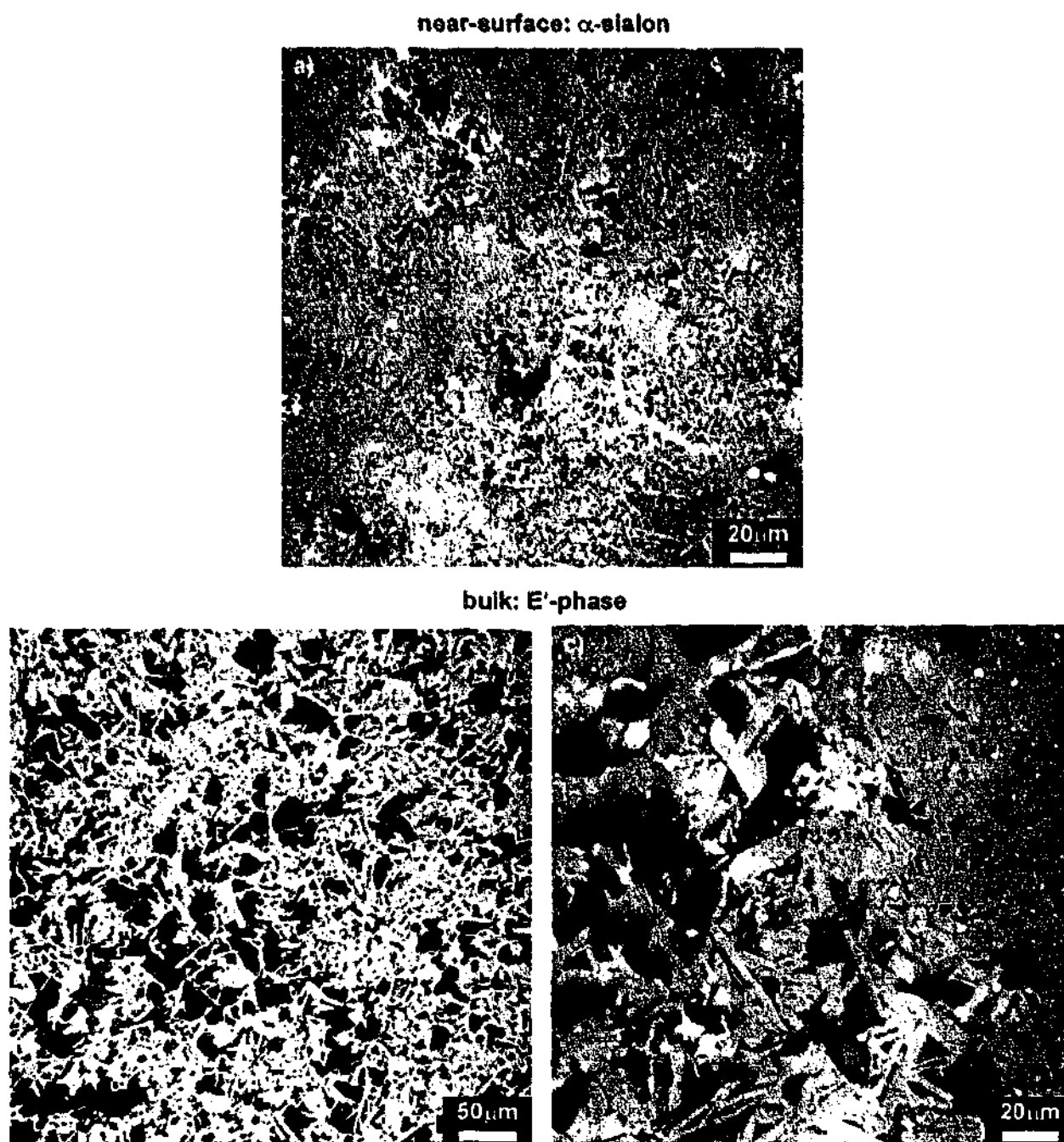


Figure 7.8 Optical micrographs of the K33 pellet hot-pressed at 1700°C: (a) as-fired surface, (b) & (c) pellet core.

The high porosity seen in the bulk of the pellet is a result of the poor packing efficiency of the coarse E'-phase plates, which causes the formation of large voids. Grain boundary glass can be seen in Figure 7.8c to be filling many of the smaller voids, but the amount of glass present is insufficient to fill the large voids. The amount of glass available in the sample will be further depleted via consumption of the liquid for grain growth. The E'-phase plates on the surface of the pellet did not undergo coarsening, but were consumed for α -sialon formation via the CRN reactions, hence the surface contained the lower porosity and finer grain sizes shown in Figure 7.8a.

SEM micrographs of the etched surface and bulk regions of the flat pellet plane of a K33 pellet are shown in Figure 7.9. Pockets of lower density are visible, with some areas higher in porosity or glass (removed via etching) and containing coarse grains; compared to other finer-grained, denser areas. The pellet surface contains mostly fine, highly elongated α' grains with characteristic hexagonal prism morphology indicative of elongation along the c-axis. A small number of E'-phase plates that were also seen to remain on the surface, as indicated in Figure 7.9b. EDXS was used to confirm the identification of the phases, and the results of this analysis will be discussed below. The glass pockets on the surface also appear to be finer and more evenly distributed than in the bulk. The coarse E'-phase grains in the bulk display their characteristic plate morphology (Figure 7.9c and d), with areas of smooth relief being the flat plates aligned planar with the surface and the elongated rectangular rods are plates sectioned edge-on to the surface. Note that the image in Figure 7.9d is taken at a lower magnification than that of the pellet surface in Figure 7.9b. The E'-phase is very soft, and unlike the other three α' -containing compositions which required significant effort to polish, this sample was easily ground on SiC papers, with a high rate of material removal. The arrow marked 'c' in Figure 7.9d indicates some transgranular cracking of the E' plates resulting just from the polishing process. The area indicated by the arrow 'g' is an underlying area of glass not removed via etching, and the small particles visible in Figure 7.9 have been identified via EDXS as either TiN' or FeSi' particles.

Figure 7.10a presents an EDXS spectrum typical of the majority of elongated grains on the pellet surface shown in Figure 7.9b. The Al:Si:Ca peak height ratio is 1:1.6:0.4, which is essentially the same as that found in the α -sialon in K06, indicating that this K33- α -sialon is similarly high in Ca. This is consistent with the trend seen in Chapter 4, where the Ca-content of α' was found to increase with slag content, from $\sim 1.2 \text{ Ca}^{2+}/\text{unit cell}$ for K06 to a maximum Ca-content of $\sim 1.5 \text{ Ca}^{2+}/\text{unit cell}$ for compositions K10 through K19. Therefore the α' phase in K33, which could not be analysed, should be high in Ca, as found in these EDXS results.

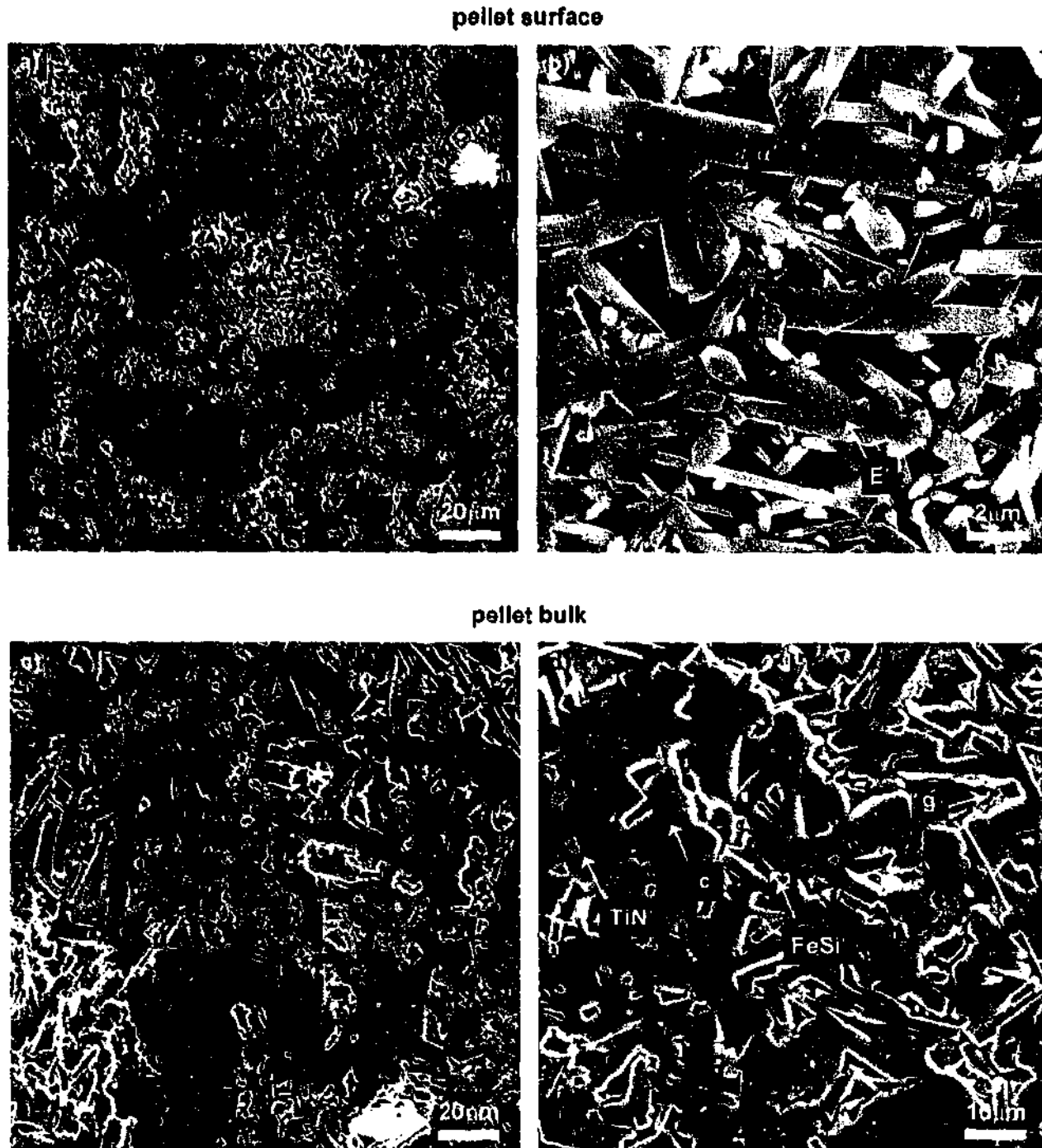


Figure 7.9 SEM micrographs of the etched K33 pellet hot-pressed at 1700°C: (a) & (b) transformed α' surface layer with E' plates indicated, (c) & (d) untransformed predominantly E'-phase core. The arrow 'c' indicates cracking produced during polishing, and 'g' indicates a pocket of residual glass.

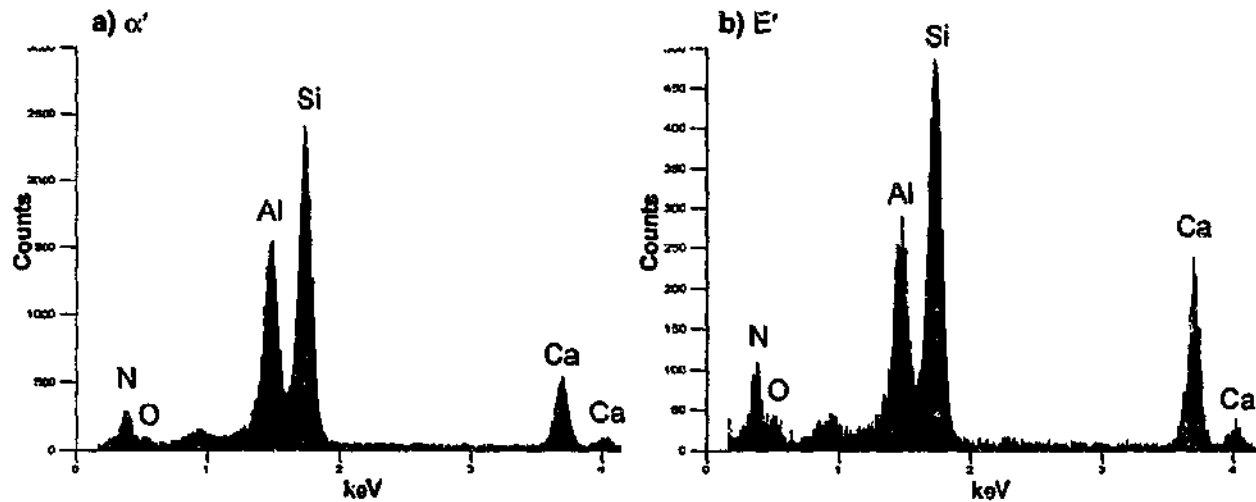


Figure 7.10 EDXS spectra from the K33 pellet hot pressed at 1700°C: (a) elongated α' rods on transformed surface, (b) coarse E' plates from the pellet core.

7.2.3.1 *Depth of the $E' \rightarrow \alpha'$ Transformed Layer in K33*

Unlike the pressureless sintered pellets in Section 6.5.3, the conversion of E' to α' was limited to just the surface of the pellets during hot-pressing. Thick components hot-pressed from K33 powder would thus form an α' shell over an E' bulk, and only thin bodies might fully transform to α' . The depth of this transformation is investigated in this section.

A K33 pellet sectioned along the flat pellet plane and etched in molten NaOH is shown at a low magnification in Figure 7.11a. The curved edge of the 1 inch cylindrical pellet is visible on the right hand side of the image and is bright in contrast due to an electron charging effect. The side-edge has undergone the $E' \rightarrow \alpha'$ conversion, and a dense, finer-grained transformed layer is clearly visible, extending $\sim 100\mu\text{m}$ into the centre of the pellet. Figure 7.11b is an enlargement of the edge area indicated by the square in Figure 7.11a, and EDXS showed that all points in this area corresponded chemically to the α' spectrum shown previously in Figure 7.10a. The α' grains on the surface are fine and often elongated, with a diameter $\sim 1\mu\text{m}$ and $\sim 4\mu\text{m}$ in length.

Although a distinct boundary exists at a depth of $100\mu\text{m}$ between the densified, transformed α' -layer and the underlying core material, the α' formed from CRN extends further into the pellet, with regions $400\mu\text{m}$ from the edge containing significant amounts of fine, equiaxed α' grains nestled in pockets between the coarse E' plates (Figure 7.11c). Only at a distance greater than $\sim 700\mu\text{m}$ from the edge of this 1 inch pellet did E' -phase totally dominate the microstructure, as expected from the XRD results (Figure 7.2).

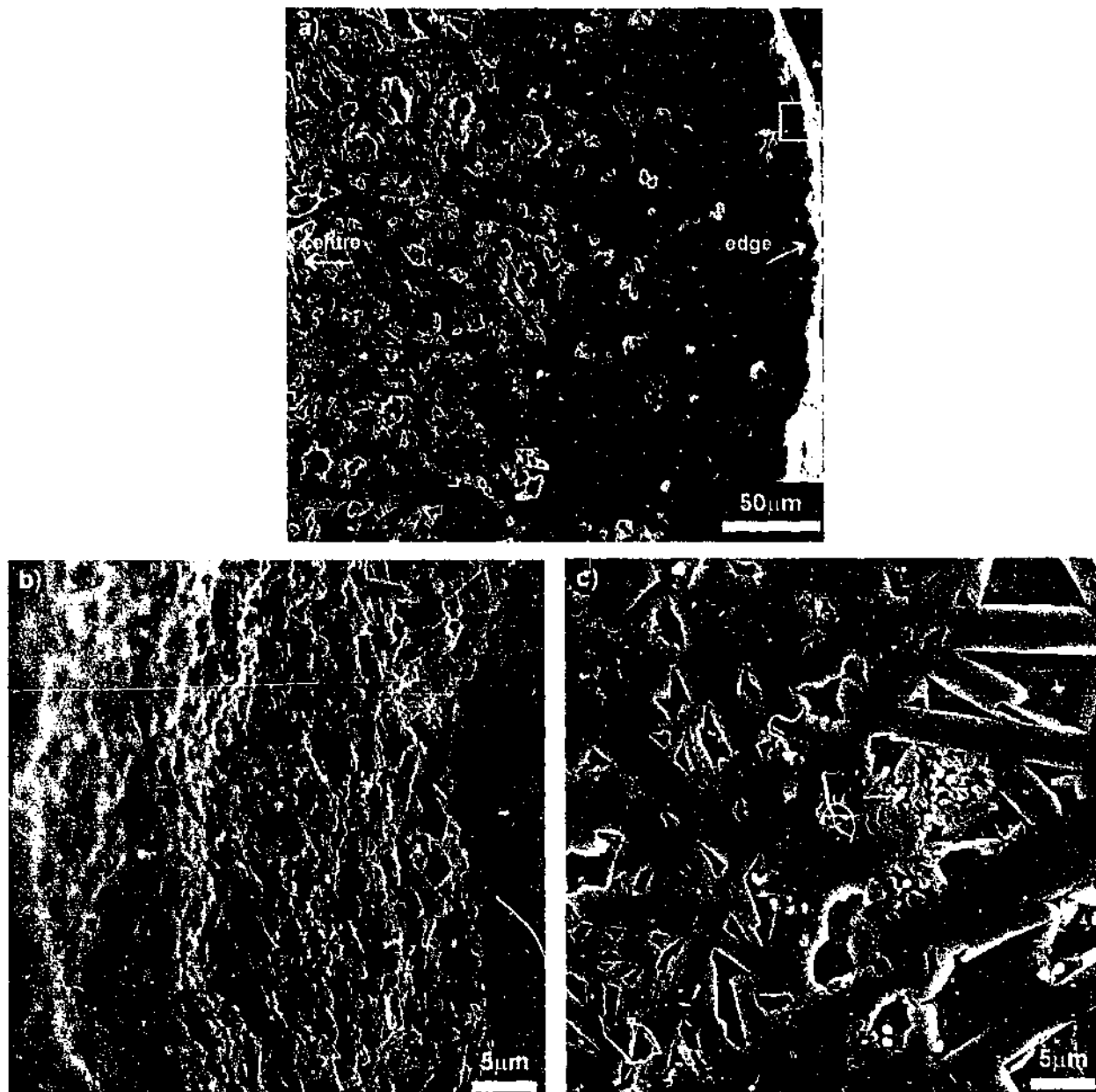


Figure 7.11 SEM micrograph of the etched K33 pellet hot-pressed at 1700°C: (a) low-magnification overview of pellet showing dense surface layer, (b) edge of sample showing fine transformed α' grain structure, (c) intermediate region $\sim 400\mu\text{m}$ from the edge showing pockets of α' (indicated) located in voids between the E' plates.

This shows that some of the N_2 present in the furnace atmosphere was able to diffuse into the bulk of the pellet before densification of the surface layer closed off the porous pathways. Some conversion of E' to α' was therefore possible via CRN at depths below the $100\mu\text{m}$ densified layer.

In the case of an producing an E'/α' core/shell composite material, the discrete boundary between the densified α' layer and the underlying core material may lead to discontinuous

property behaviour if this layer is breached, which may be particularly problematic due to the very soft nature of the E'-phase material.

TEM analysis of the E'-phase in the K33 pellet was attempted, however the specimen preparation technique could not be optimised for the soft, porous E'-phase material in the time given. Excessive material was removed during ion milling, resulting in specimens that were too thick for analysis.

7.2.4 P02 Pellet

The P02-18 powder before hot-pressing consisted predominantly of α' , with small amounts of α - Si_3N_4 and possibly 2H-SiC present. Together with K06, P02 is considered to be a nearly single-phase α' -forming composition. The hot-pressed P02 pellet showed little change in phase composition, with the residual α - Si_3N_4 removed and some texture of the α' produced. An SEM micrograph of an etched P02 pellet is presented in Figure 7.12.

The microstructure is reasonably uniform across the pellet, with no obvious concentrations of glassy pockets or areas of high porosity. Less elongation, and a wider α' grain size distribution of 0.2 to 2 μm is seen in P02 than in K06. The bright white dots on the surface of the specimen are Ni contamination from the apparatus used to sputter coat the sample with carbon.

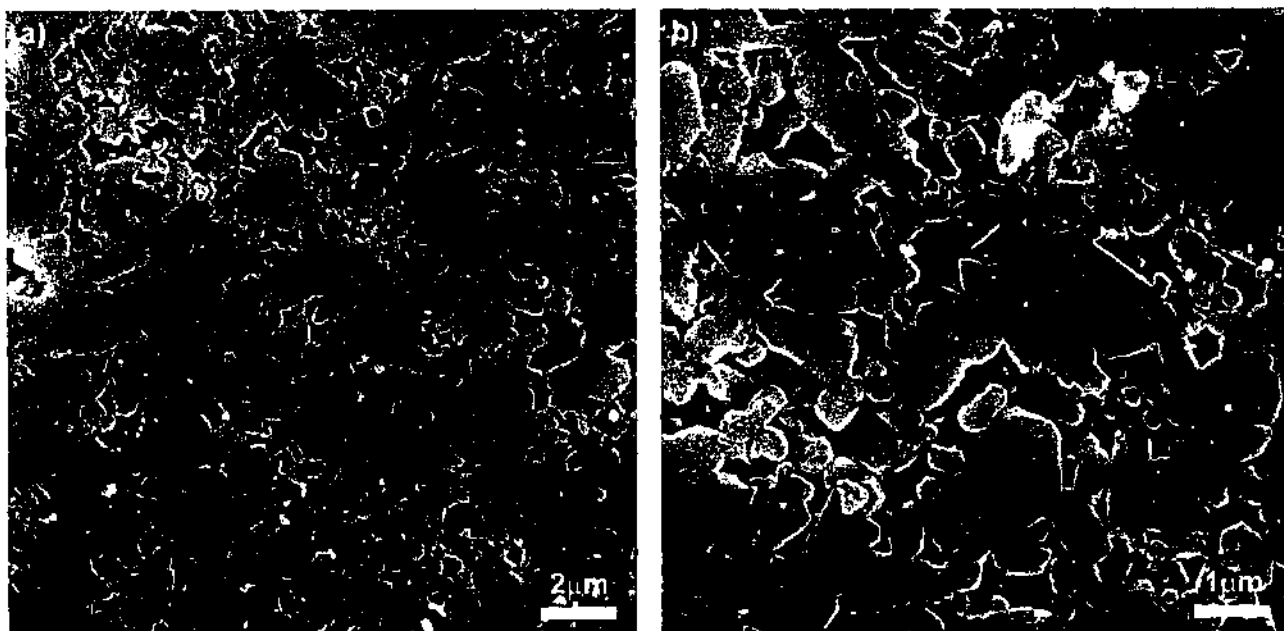


Figure 7.12 SEM micrographs of the etched P02 pellet hot-pressed at 1700°C. All grains are α' , the bright dots are Ni contamination from sputter coating.

An EDXS spectrum typical of the α' grains is given in Figure 7.13, and shows that as in the slag+clay-K system, the α' is stabilised by Ca only and no Mg is incorporated into the lattice after high temperature processing. The Al:Si:Ca peak height ratio is 1:3.8:0.3, which is not dissimilar from the ratio found in the P02 α' powder, which was 1:4.1:0.4. As previously discussed in Section 5.2.2.2, the α' formed in the low-slag P02 composition is much more Si-rich than that in K06.

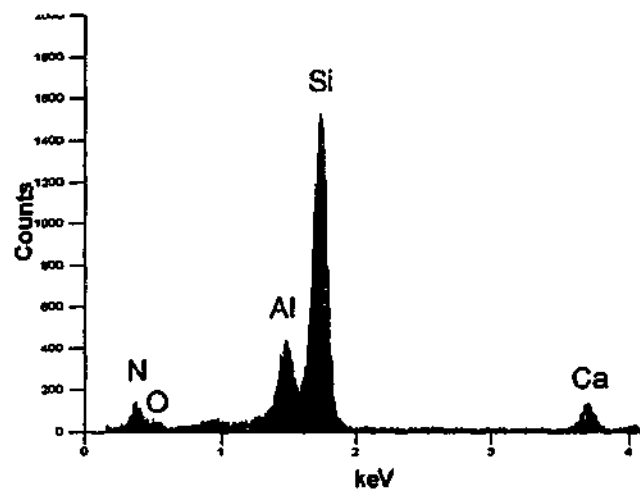


Figure 7.13 EDXS spectrum typical of α' in the P02 pellet hot-pressed at 1700°C.

7.2.5 P08 Pellet

The P08-18 powder contained α' , a large amount of D'-phase (nominally $2\text{CaO} \cdot \text{Si}_3\text{N}_4$), and an unidentified phase in addition to the impurity phases TiN' and FeSi'. The surface of the pellet after hot-pressing was fully converted to α' (Figure 7.3), and the core of the pellet retained a predominantly α' +D' phase assembly. SEM micrographs of the core of the etched P08 pellet are presented in Figure 7.14. The microstructure is non-uniform, with pockets of visibly higher glass content revealed via etching. One such glassy pocket is shown in Figure 7.14a, surrounded by a higher density, lower glass area. Figure 7.15b shows a higher magnification image of the edge of the pocket where the difference in the density is clearly visible. Figure 7.15c is taken from within the pocket to reveal the grain structure.

It was observed previously (Section 5.2.2.3) that the P08-18 powder contained three distinct particle morphologies with distinct EDXS chemical signatures. The α' grains were equiaxed,

submicron, with an Al:Si:Ca ratio of 1:3.4:0.3 and an O:N ratio of 1:1.8. This is higher in Si and lower in N than the larger, elongated D'-phase rods, which had an Al:Si:Ca ratio 1:2.8:0.3 and an O:N ratio of 1:2.8. The third unidentified particle was irregular in morphology and Si- and N-rich.

Differentiation of phases in the hot-pressed pellet was difficult due to a lack of clear distinction between the various particle morphologies and chemistries. A continuous range of grain morphologies is present, including large, 2-3 μm equiaxed grains, elongated grains with aspect ratios >3 , and distinctly fine, rod-like grains with diameters 0.2-0.5 μm and up to 2 μm in length. In terms of the EDXS spectra, the peak height ratios displayed a continuous range of Si- and Ca-contents relative to Al, and N-content relative to O. The Al:Si:Ca ratio of the examined particles ranged from 1:3.0:0.3 to 1:3.9:0.8, and the O:N ratio varied from 1:3.2 to 1:4.6. The grains of similar morphology were ranked in terms of Al:(Si, Ca) ratio, and it was seen that there was a cluster of grains with the highest Si- and Ca-contents combined with low N-content, and these tended to be larger and equiaxed, and were thus designated as α -sialon. The lower Si- and Ca-contents and higher N-contents tended to be associated with elongated grains, and these were designated as L-phase. Without a clear delineation between α' -like features and D'-like features, the cut-off points used for this categorisation were somewhat arbitrary and based on the clustering of Al:Si:Ca ratios. However, many grains such as the grain labelled *x* in Figure 7.14b had an indeterminate morphology and chemical signature that could not be categorised as α' or D'.

The EDXS peak height ratios averaged for the particles categorised as α' and D' are listed in Table 7.2, and representative EDXS spectra of these phases are given in Figure 7.15. No Si-N rich phase seen in the powder (Section 5.2.2.3) was observed in the hot-pressed pellet. The average EDXS peak height ratio for the particles intermediate to the α' and D' particles is also given in Table 7.2. The large variation in particle chemistry observed in this sample may be due to the very wide range of solid-solution found in the D'-phase; it was seen in Section 5.2.2.3 that the composition of D' as determined by EDXS was quite different to that of the pure D-phase (nominally $2\text{CaO}\cdot\text{Si}_3\text{N}_4$). Clearly considerably more work is required to clarify the structure and composition of the D' solid-solution formed in this system, however this is outside the scope of the present study and was not performed.

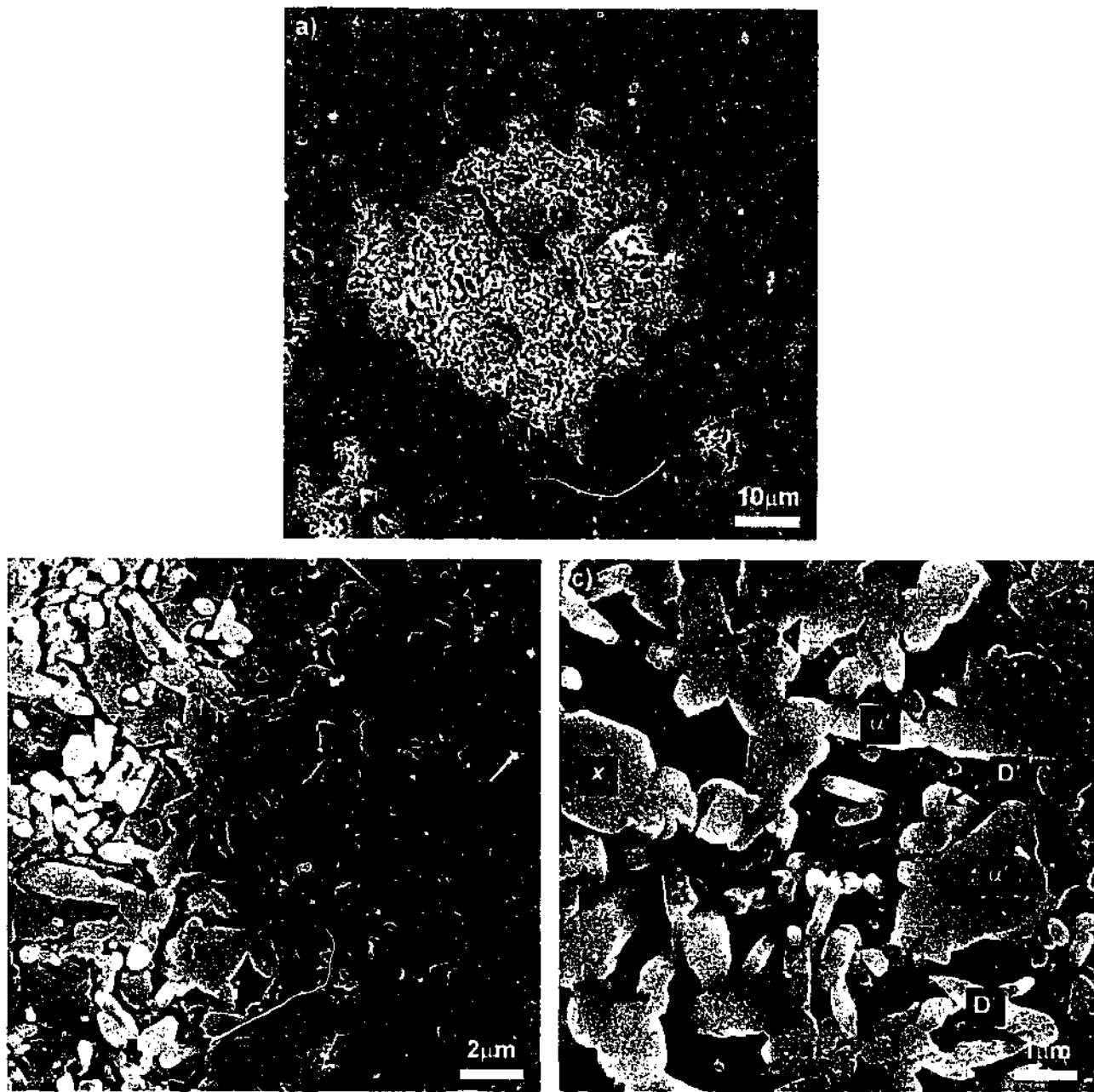


Figure 7.14 SEM micrographs of the etched P08 pellet hot-pressed at 1700°C. Examples of grains assigned to α' , D'-phase, and the unidentified phase (x), are labelled.

Table 7.2 Average EDXS peak height ratios of particles categorised as α' , D', and indeterminate in the P08 pellet hot-pressed at 1700°C. The equivalent EDXS ratios from the P08-18 CRN powder (Table 5.5) are also provided for comparison.

P08 Pellet Particle	Al:Si:Ca peak height ratio	O:N peak height ratio	P08-18 powder (Al:Si:Ca / O:N)
α' (Si >3.6)	1: 3.8: 0.7	1: 3.4	1:3.4:0.3 / 1:1.8
D' (Si <3.2)	1: 3.1: 0.4	1: 4.4	1:2.8:0.3 / 1:2.8
x (Si 3.3-3.5)	1: 3.3: 0.5	1: 3.3	1:6.5:0.2 / 1:3.0

The α' phase in the P08 pellet appears to have a considerably higher Ca content than that seen in the powder, with the Ca peak height after hot-pressing doubling from 9% to 18% relative to Si. This Si:Ca ratio is similar to that seen in the K06- α' material ($\sim 24\%$), and is due to redistribution of the Al and Ca in the system at the hot-pressing temperature of 1700°C. At least one unidentified phase in the powder was seen to have a very high Ca-content (Table 7.2), and also contains some Al. This phase was not detected after hot-pressing, thus the Ca and Al will have been released into the system and become available to form a higher m-value α' phase due to the higher fluidity of the liquid, and the greater extent of the α' -forming region at higher temperatures.

7.2.6 Summary of Microstructural Analysis of Hot-Pressed Pellets

The main findings from the analysis of the hot-pressed pellet microstructures of the four compositions are:

- The two basically single-phase α' powders K06 and P02 produced the most homogenous microstructures, with generally equiaxed grains and the least amount of glass. The K33 and P08 powders, which contained phases other than α' , were more inhomogeneous, and produced larger pockets of glass and porosity.
- The hot-pressed K06 pellet contained generally fine-grained, $\sim 1\mu\text{m}$, α' and AlN' grains, with some elongated α' present. TiN' formed small ($<100\text{nm}$) inclusions found within α' and AlN' grains. FeSi' impurities formed large $2\text{-}5\mu\text{m}$ agglomerates associated with a large degree of inhomogeneity in the pellet.
- The bulk of the K33 pellet contained large E' plates with considerable porosity. The surface was remarkably different, with a fine, elongated α' phase produced via continuation of CRN on the surface of the pellet. A dense α' layer was formed to a depth of $100\mu\text{m}$ in the pellet, with a lesser degree of α' formation observed at greater depths to $\sim 700\mu\text{m}$.
- The P02 pellet had a uniform distribution of Si-rich (Ca-poor) α' grains, roughly equiaxed and $0.2\text{-}2\mu\text{m}$ in diameter, with a low level of glass.
- The bulk of the P08 pellet contained a variety of grain morphologies ranging from equiaxed to fine elongated rods, with a continuous range of chemistries. The grains

categorised as α' tended to be equiaxed and $\sim 1\mu\text{m}$ in diameter, with the grains categorised as D' tending to be elongated.

7.3 Hardness and Fracture Toughness

The characteristic property of α -sialon is its high hardness, therefore any evaluation of the mechanical properties of bulk material produced from the CRN- α' powder must include a determination of its hardness. The fracture toughness of the material is another important property, influencing the crack-forming behaviour of the material during processes such as grinding and polishing, and affecting the erosion response (Xie, Moon, *et al.* 2003). This section presents the results of the determination of the hardness and fracture toughness of the hot-pressed pellets. All tests were performed on the pellet bulk material after surface removal, using the Vickers indentation method under a 10kg load as detailed in Section 3.4.8. The results are summarised in Table 7.3.

Table 7.3 Physical and mechanical property data for K06 K33 P02 & P08 pellets hot pressed at 1700°C.

Sample	Main Phases	Density (g/cm ³)	Hv (GPa)	KIc (MPam ^{1/2})
K06	α'	3.294 \pm 0.0005	14.0 \pm 0.3	4.1 \pm 0.3
K33	E'	2.951 \pm 0.0003	2.7 \pm 0.2	*
P02	α'	3.192 \pm 0.0008	14.8 \pm 0.5	4.1 \pm 0.4
P08	α' , D'	3.196 \pm 0.0006	13.1 \pm 0.9	4.1 \pm 0.6

* Not able to be determined due to extremely high porosity

The hardness was highest for the two predominantly single-phase α' materials K06 and P02, with the clay-P based P02 pellet having the highest hardness of 14.8 GPa. The predominantly α' +D' P08 pellet had a lower hardness than either of the single-phase α' materials of 13.1 GPa, and the predominantly E'-phase K33 pellet had a considerably lower hardness of ~ 3 GPa. The indentations were performed on the least porous areas of the K33 pellet, however it was difficult to accurately determine the hardness due to the considerable amount of damage caused by the indenter head.

The slag-based α' materials produced in this work are expected to be quite glassy due to the high Ca-, Si-, and Al-content of the slag. The 0.25:1 slag:clay-P P02 composition contains considerably less slag than the 0.62:1 slag:clay-K K06 composition, so it is likely to produce less liquid than K06, resulting in a lower amount of residual glass. Although it is difficult to verify any difference in the amount of glass between these two samples by visual inspection alone, a comparison of the SEM images for the P02 and K06 pellets in Figures 7.4 and 7.12 suggests that the P02 sample is slightly less glassy than K06. In the study of reaction-sintered Ca- α' materials by Zhang, it was found that an increase in the glass content was directly related to a reduction in hardness. The lowest hardness of 14.5 GPa was found in the highest glass-containing composition, increasing to 16.4 GPa for a single-phase α' material (Zhang, Cheng, *et al.* 2001). The hardness of 14.0 and 14.8 GPa determined for the predominantly single-phase α' materials in this work are thus comparable to glassy, reaction-sintered Ca- α' materials.

The values for K_{Ic} fracture toughness determined for the three samples K06, P02, and P08 were all basically the same at 4.1 MPam^{1/2}. Fracture toughness was seen in the work by both Zhang and Wood to be heavily dependent on both the aspect ratio of the α' grains and the amount of glass present (Zhang, Cheng, *et al.* 2001; Wood and Cheng 2000). Both K06 and P02 consist of sub-micron, generally equiaxed grains. Although some elongation is observed in K06, any contribution that these elongated grains make to the toughness of K06 may be offset by the large amount of glass present. These compositions have basically the same microstructure and would therefore be expected to have essentially the same fracture toughness, and this was observed here. The value of 4.1 MPam^{1/2} is similar to the 4.5 MPam^{1/2} obtained by Zhang for Ca- α' materials with equiaxed microstructures (Zhang, Cheng, *et al.* 2001) In Zhang's study, toughness was only seen to increase when highly elongated α' grains with aspect ratios >5 were produced, which is considerably higher than the small extent of elongation seen in the present work.

The P08 sample contained D' grains which appeared to have some degree of elongation (Figure 7.14c), but no toughening effect was observed. This may be due to the considerably high amount of glass observed in the P08 pellet, or the D'-phase being intrinsically less resistant to fracture than α' .

The fracture toughness for the K33 sample could not be determined due to the high porosity of the sample; the severe cracking produced by the indenter extended beyond the solid regions and ran into the pores, making accurate measurement of the crack lengths impossible.

The SEM image presented in Figure 7.9d shows transgranular cracking that was produced during the standard grinding and polishing processes, highlighting the poor toughness of this phase, despite its elongated morphology.

7.4 Erosion Resistance

There are many material properties that may be examined to determine the suitability of the slag-based α -sialons for industrial applications, including, oxidation resistance, tensile and compressive strength, high-temperature strength, and corrosion resistance. It is unlikely that the CRN- α' material produced here will be suitable for high-temperature applications due to the high level of glass produced, which can dramatically reduce the high-temperature performance (Hampshire 1994). Consequently, this material will be more suited to low temperature applications. The work by Zhang showed that Ca- α -sialons possess greater resistance to erosion by solid particles compared to other engineering ceramics, including the widely used SiC and Al₂O₃ wear materials (Zhang 2002). Wear resistant linings are therefore one potential application to which a low-cost α' material would be ideally suited. This section presents the results of an investigation into the erosion resistance of α' materials produced via CRN.

7.4.1 Experimental Procedure

Hot-pressed pellets K06, K33, P02-18 and P08-18 were ground to remove the transformed layers and polished down to a 1200 grit finish using SiC paper. Erosion testing was performed using the dry erosion rig as detailed in Section 3.4.9. SiC grit with a mean diameter (d_{50}) of 388 μ m and hardness 30.4GPa was used as the erodent. SiC was chosen based on the findings by Zhang that the commonly used garnet erodent was much less effective at erosion of Ca- α' , due to it having a lower hardness than the α' target material (Zhang 2002). The tests were performed at incidence angles of 30° and 90°, to represent shallow sliding impacts and normal impacts, respectively. The standard dosage used for the 30° impact angle tests was 265g (90s exposure), and 210g (60s exposure) for the more aggressive 90° tests. The samples were weighed after each dose to determine the mass loss. After testing, the materials were coated in carbon and the wear surfaces studied using the SEM.

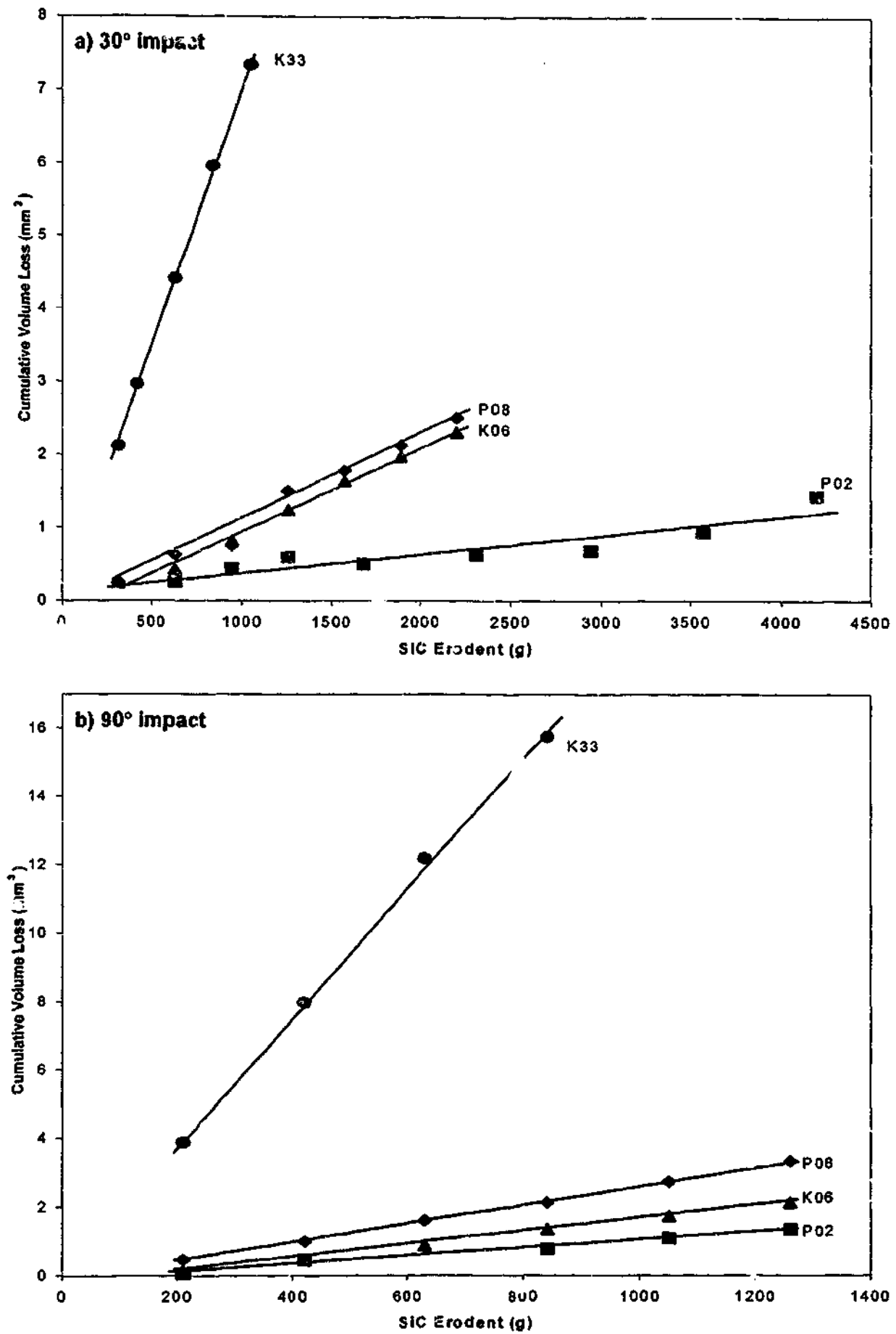


Figure 7.15 Cumulative mass loss of the samples vs. mass of SiC erodent for the four materials K06, K33, P02, P08, under impact angles of (a) 30°, and (b) 90°.

7.4.2 Cumulative Mass Loss

The steady-state erosion response, ΔE , is defined as the slope of the linear region of the graph of cumulative volume loss plotted as a function of the mass of erodent impinging on the material. The graphs of cumulative mass loss for both the 30° and 90° impacts are given in Figure 7.15. A generally linear volume loss regime was experienced by the four samples, and the least squares method was used to fit a line to the data. The values of ΔE calculated for the four materials are given in Table 7.4. The erosion rate for brittle materials is predicted to be the highest for 90° impacts, due to the larger normal component of the impact velocity ($v \sin \theta$) impacting the target (Sheldon 1966). This was found to be true of all four material tested here, displaying higher ΔE under 90° impacts than under 30° impacts.

Table 7.4 Steady-state erosion rates (ΔE) for K06, K33, P02, P08 pellets, ranked in decreasing order of erosion resistance (increasing ΔE).

Sample	ΔE 30° impact ($m^3/kg \times 10^{-10}$)	ΔE 90° impact ($m^3/kg \times 10^{-10}$)
P02 (α')	3.7 ± 0.4	13.4 ± 1.3
K06 (α')	11.3 ± 1.0	18.1 ± 1.4
P08 ($D'+\alpha'$)	11.4 ± 0.9	28.4 ± 1.5
K33 (E')	71.0 ± 1.5	188.7 ± 1.8

The ranking of materials under both impact angles is the same. The worst performing material was the soft E' -phase pellet (K33), which displayed a considerably higher ΔE than the other three materials. The $\alpha'+D'$ P08 composition had the next-highest erosion rate, slightly higher than that of the predominantly α' K06 sample. The P02 α' displayed the lowest erosion rate of the four materials, and in the case of 30° impacts was significantly lower than K06, although some deviations from linearity were observed.

Two theoretical models based on indentation fracture mechanics have been developed to describe the erosion of brittle materials. Both are of the same form, and predict a power-law dependence on the erosion rate (ΔE) on erodent and target properties. The equation for normal impacts is given in Equation 7.1.

$$\Delta E \propto v^n D^{2/3} \rho^p K_c^{-(4/3)} H^q \quad [7.1]$$

Here ΔE is the erosion rate, measured in mass or volume loss per unit mass of erodent, v , D , and ρ are the velocity, mean size and density of the erodent particles respectively, and K_c and H are the fracture toughness and hardness of the target material. The exponents are different for the two models: in the 'dynamic model' the exponents n , p , and q are 3.2, 1.3, -0.25 (Evans, Gulden, *et al.* 1978), and in the 'quasi-static model' are 2.4, 1.2, and 0.11 (Wiederhorn and Lawn 1979). The two models both predict an inverse relationship between erosion rate and both the fracture toughness and hardness of the target material, however the fracture toughness term is dominant. The three compositions K06, P02, and P08 tested here all have the same fracture toughness of 4.1 MPam^{3/2} yet displayed reasonably different erosion responses, which suggests that this model does not correlate well to the Ca- α' materials. This is due to the influence of the more complex microstructures found in these materials than are present in the glasses and single crystals upon which the models are derived. Additionally, there are compositional factors that will also influence the erosion rate. Fracture toughness alone is therefore inadequate for predicting the erosion behaviour of these materials, due to the influence of their complex microstructures.

The erosion rates did, however, follow the inverse of the hardness of the target materials, with the hardest sample P02 displaying the lowest erosion rate. This correlation is less likely to be a true prediction from the theoretical model but a reflection of the large effect of composition on the measured hardness of the pellets. K33 had the lowest hardness and lowest erosion resistance, and is composed of mostly E' (nominally CaAlSiN₃), which was shown to be very soft (Section 7.2.3). In addition to the high-hardness α' phase, the P08 pellet contains D', which has an unknown hardness. The overall hardness of the D'-containing pellet was lower by at least 1 GPa than that of the single-phase α' materials K06 and P02, which may be due to the D' most probably having a lower hardness than α' , and which also may be the result of a high amount of glass in the sample.

7.4.2.1 Comparison of CRN- α' to Reaction-Sintered Ca- α'

Figure 2.5 showed that the reaction-sintered Ca- α' materials tested by Zhang possessed very good erosion resistance, better than many commonly used wear resistant materials such as Al₂O₃ and SiC. The best erosion resistance was found for reaction-sintered Ca- α' materials produced by first pressureless sintering, then hot-pressing at 1700°C for 1 hour to achieve full density. Under 90° impacts using SiC erodent the various Ca- α' compositions were

determined to have values of ΔE between $26\text{--}32 \text{ m}^3/\text{kg} \times 10^{-10}$ (Zhang 2002). The two best performing CRN materials in the present study (K06 and P02) displayed even better erosion resistance, with ΔE between $13\text{--}18 \text{ m}^3/\text{kg} \times 10^{-10}$. These tests were performed on the same erosion rig as used by Zhang and replicating the same experimental conditions. Therefore a direct comparison is possible, and these results clearly show that the slag-based α -sialon materials have a very good erosion resistance, greater than that of the pure Ca- α' materials produced via reaction-sintering. These materials would thus perform significantly better than the SiC and Al_2O_3 materials shown in Figure 2.5, thus demonstrating that this inexpensive Ca- α' material may be well suited to the wear materials market if it can be cheaply densified without affecting its performance.

7.4.3 Eroded Surfaces

It was seen in the study by Zhang that the erosion resistance of the Ca- α' materials were heavily influenced by microstructural features (Zhang 2002). SEM analysis was performed on the wear surfaces to investigate the erosion mechanisms operating in the four materials tested. The erosion craters formed on the pellets were elliptical in the case of 30° impact, and circular in the case of 90° impact. Representative micrographs were taken from the centre of the erosion craters to enable comparison between samples. The four materials are presented in increasing order of erosion resistance, ie. from worst to best.

7.4.3.1 K33

The extremely poor hardness and toughness of the E'-containing K33 pellet has been discussed previously in Section 7.3, where it was that even standard metallographic polishing processes were sufficiently aggressive to cause significant cracking in the sample (Figure 7.9d). The eroded surfaces shown in Figure 7.16 display a very high extent of damage under both 30° and 90° impacts, and have the faceted appearance typical of brittle fracture, with a high degree of material removal occurring via transgranular fracture. Some typical transgranular cracks are clearly visible as indicated by the arrows marked 'c'. Plastic smearing of the sample is evident in the ploughmarks (indicated by 'p') in the sample eroded at 30° , but these ploughmarks appear to be shorter and less common than those seen in the other three materials. Furthermore, considerably more ploughmarks and a larger amount of wear debris are seen in the sample eroded at 30° than that eroded at 90° . Ploughmarks are indicative of plastic deformation, and are longer at low impact angles when the impacting erodent particles have a high horizontal component of velocity (Zhang 2002).

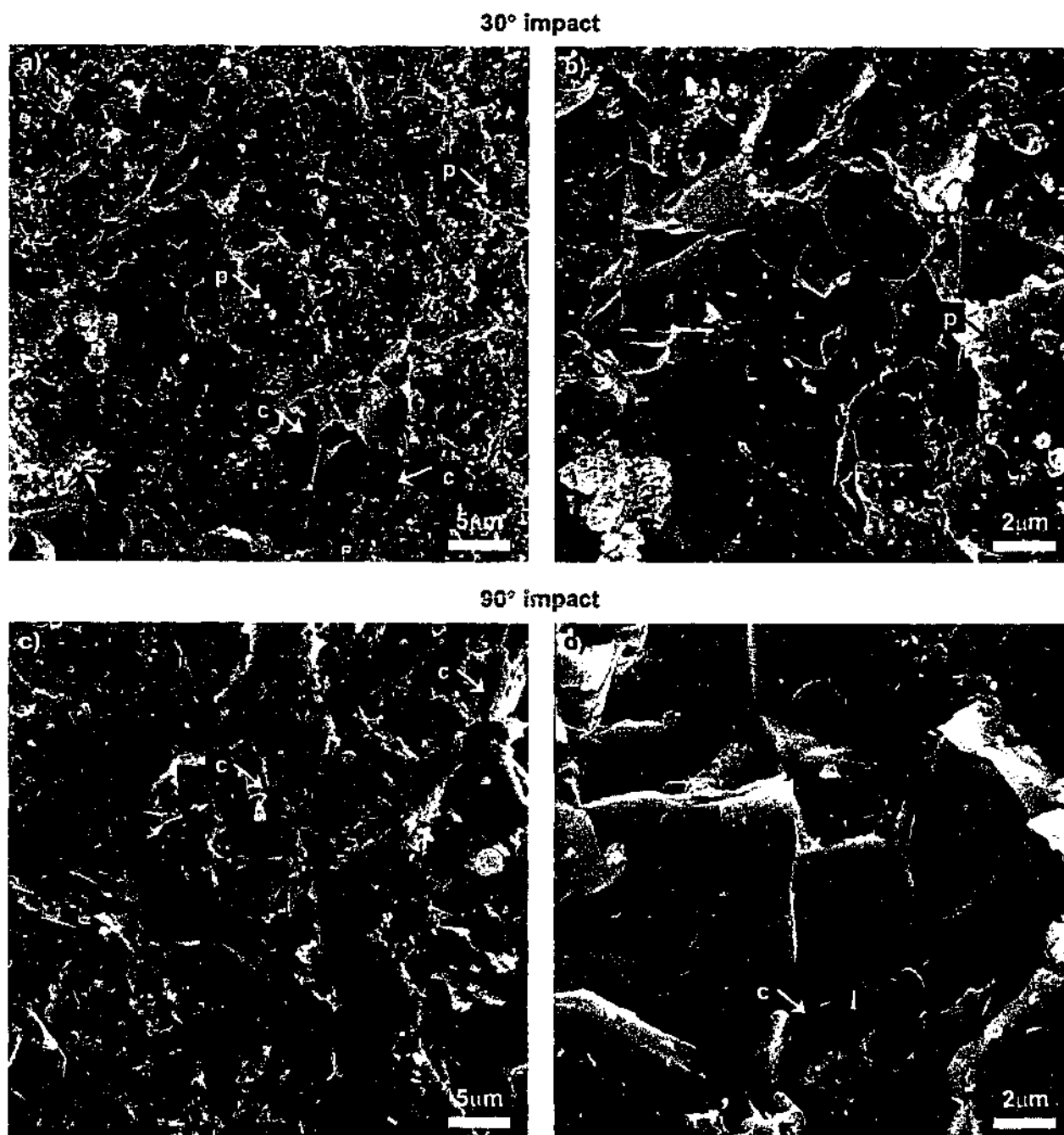


Figure 7.16 Eroded surfaces of the K33 pellet: (a) & (b) 30° impact (the impact direction is from top to bottom in the images), (c) & (d) 90° impingement. Examples of microcracks ('c') and ploughmarks ('p') are indicated.

These erosion features indicate transgranular fracture was the dominant erosion mechanism in this sample. This is largely a result of the microstructure consisting of coarse, interlocking, but soft E' -phase grains, and a very high level of porosity. Pores act as points of stress concentration, enabling easier crack initiation in the surrounding material (Zhang 2002).

7.4.3.2 P08

The erosion rate of the α' +D'-containing P08 sample was nearly the same as that of the predominantly α' K06 sample for 30° impacts, however it was significantly lower under the more aggressive 90° impacts. Previous analysis of the microstructure showed that it contains a coarse morphology consisting of equiaxed α' grains \sim 2-3 μ m in diameter, with elongated D' rods up to 2 μ m in length. A large amount of glass is also present, unevenly distributed in pockets throughout the sample (Figure 7.14). The SEM images of the eroded surfaces of the P08 material are presented in Figure 7.17, and show a large amount of wear damage evident at both low and high magnifications. The cracks indicated in the low magnification view of the P08 pellet eroded at 30° (Figure 7.17a) are long radial cracks. Ploughing and plastic smearing of the material is evident in eroded surfaces under both 30° and 90° impacts. The eroded surface after normal impacts (Figure 7.17c) shows a considerably greater extent of plastic deformation; large flakes of plastically smeared material are visible, with grooves produced from the cutting action of the hard SiC erodent particles.

The higher magnification image in Figure 7.17b clearly shows that the cracks produced after impact at 30° are intergranular, with no evidence of transgranular cracking or fracture present. In the case of normal impacts, the cracking was also generally intergranular, however several regions were revealed where large, plate-like agglomerates were visible after erosion. These may belong to the unidentified phase in the P08 pellet. As with the plate-like E'-phase, a great deal of transgranular fracture has occurred in these coarse, plate-like grains.

Molten drips of material were another feature seen in the P08 sample eroded at 90° (Figure 7.18). The walls of the erosion crater from where this image was taken were reasonably smooth, which suggests that this area was a one of the glass-rich pockets, and the drips are the result of localised melting of the grain boundary glass. The glass in this system may be expected to start melting \sim 1300°C, and it was seen in the work by Zhang that temperatures sufficient to melt the garnet erodent (\sim 1250°C) were generated by from the local heating caused by transfer of energy from the erodent particle to the target. Therefore it may be possible for the glass in this system to be partially melted via this localised heating effect, producing the drip-like formations seen in Figure 7.18. The plastically deformed surface will become smooth rather than ploughed due to the ability of the glass to flow and accommodate the plastic deformation.

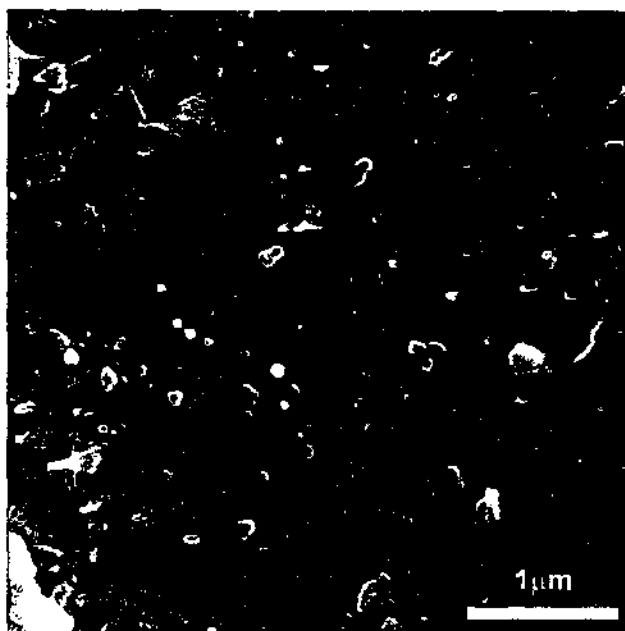


Figure 7.18 Partial melting of grain boundary glass in the P08 pellet eroded at 90°.

7.4.3.3 K06

The K06 sample had a generally finer microstructure than P08, and displayed slightly greater erosion resistance, particularly under 90° impacts. The eroded surfaces of the K06 sample (Figure 7.19) appear to be less damaged and uneven than in the P08 sample. Plastic smearing is visible after both 30° and 90° impacts, and as with the P08 sample larger flakes of deformed material were produced under the more aggressive 90° impacts than under 30° impacts, but these flakes lacked the grooves seen in P08 at low magnifications. At high magnifications, the sample eroded at 30° (Figure 7.19b) shows mostly intergranular cracking, and the 90° eroded surface also contains largely intergranular cracking, but with some evidence of small-scale plastic cutting seen in the step-like groove marks in some areas (Figure 7.19d). Few elongated grains were observed in the eroded surfaces of these pellets, thus these appear to have no significant effect on erosion resistance.

materials eroded at 30°, often >10 μ m, and are indicative of a large extent of plastic smearing of the deformed material. The smooth surface and lack of wear debris suggests that the impacting particles are causing significant plastic deformation and smearing of the material, but this material is not being removed from the surface, a feature reflected in the extremely low rate of mass loss observed under 30° impacts.

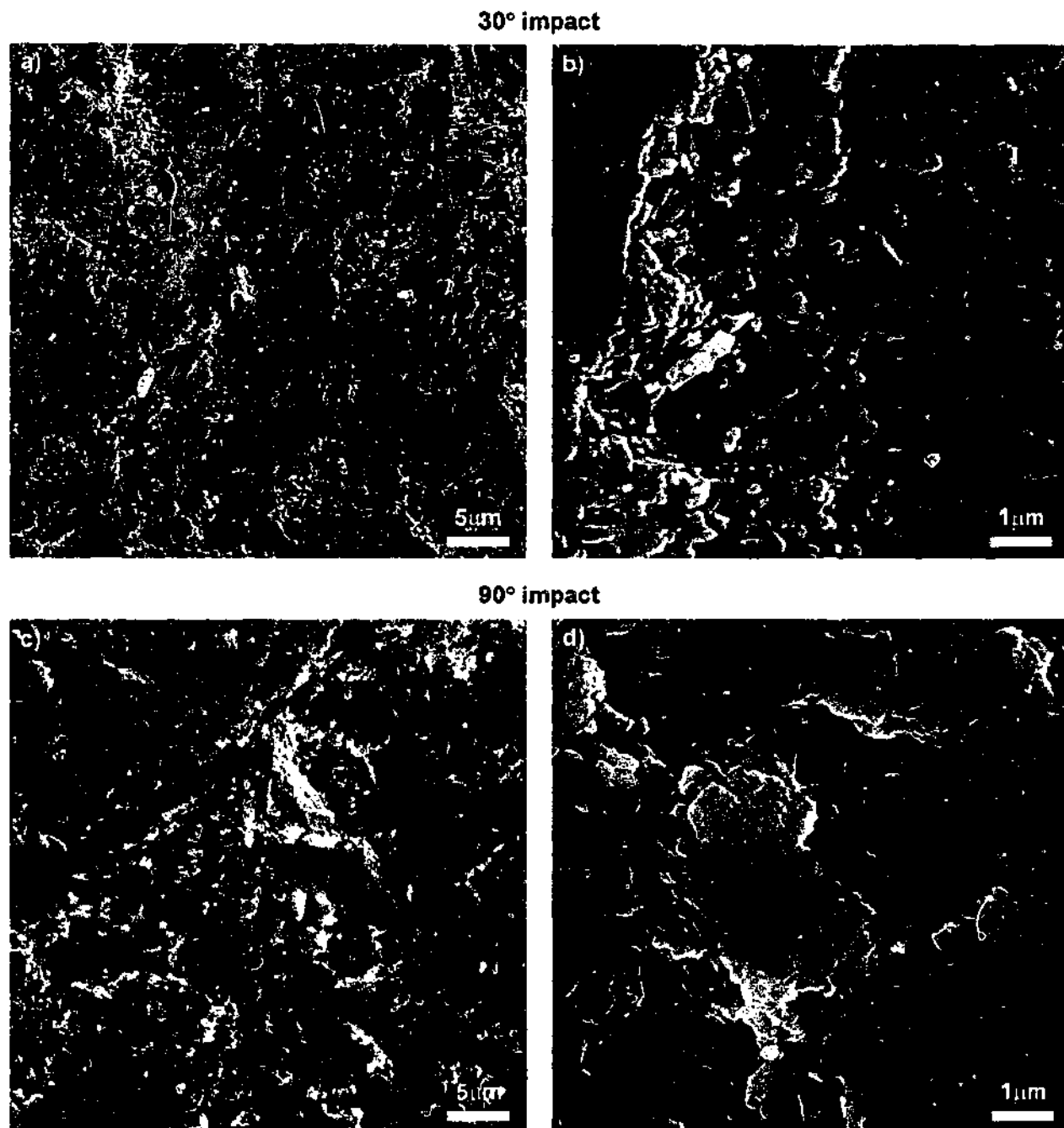


Figure 7.20 Eroded surfaces of the P02 pellet: (a) & (b) 30° impact (the impact direction is from top to bottom in the images), (c) & (d) 90° impact.

In the higher magnification view shown in Figure 7.20b, individual equiaxed α' grains are clearly visible, indicating that cracking is intergranular in nature and follows the grain

boundaries, thereby allowing for grain ejection. The damaged surface of P02 eroded at 90° shows a considerably higher amount of wear damage than that at 30°, indicating that the target material was more effectively removed under this condition. The higher magnification image shows a significant amount of plastic smearing has occurred, but the outline of the grains are still visible, which shows that the cracks are intergranular (Figure 7.20d).

7.4.4 Discussion of the Erosion Behaviour of CRN Materials

All four materials displayed some erosion characteristics as expected from previous work on the erosion of brittle materials. Ploughmarks are the result of plastic deformation by the impacting particles. The ploughmarks formed under 30° impacts were generally long and parallel to the particle impact direction, due to the high horizontal, sliding component of the particle velocity, whereas under 90° impacts the ploughmarks were shorter and more randomly oriented. At 90° erosion, all of the kinetic energy of the impacting particles is transferred to the sample, resulting in higher rates of erosion, a greater extent of material removal, and generally less wear debris remaining on the surface (Zhang 2002).

As seen in the work by Zhang, the erosion mechanism in the Ca- α' materials with fine-grained equiaxed microstructures (K06 and P02) was predominantly intergranular cracking around the grains, followed by grain ejection (Zhang 2002). The intergranular cracks are formed via linking-up of the small-scale lateral cracks produced by repeated particle impacts, which then allows for grains to be ejected. Grain ejection was also the predominant material removal mechanism in the coarser, generally equiaxed P08 material, where the presence of a small volume of fine D'-phase rods did not appear to provide additional toughening mechanisms to the material. Areas with coarse, plate-like grains in the P08 sample, and in the whole of the K33 sample, displayed transgranular fracture to be the main material removal mechanism, as seen in Ca- α' materials with coarse, elongated α' and AlN-polytypoid morphologies in (Zhang, Cheng, *et al.* 2001).

The K33 material, comprising of very coarse E'-phase plates, with some small pockets of α' and extremely high porosity, showed extremely poor erosion resistance. The porosity is a defect that facilitates crack initiation under low stress, which when combined with the apparently low intrinsic hardness of the E'-phase, produces very poor mechanical behaviour. Although it may be expected that the addition of large plate-like grains to a fine, equiaxed microstructure may provide some additional toughening, for example by crack deflection, it is

unlikely that the soft E'-phase would be beneficial to the toughness of α -sialon materials produced here, and thus should be minimised from clay-K based samples.

With a higher glass content and coarser grains, the P08 sample displayed a poorer erosion resistance than the lower-glass, finer grained K06 and P02 samples. The P08 sample has generally equiaxed α' grains 2-3 μm in diameter, compared to K06 with a grain size 0.5-1 μm and P02 with 0.2-2 μm sized grains. The low resistance to erosion was seen in the high degree of plastic deformation and in the partial melting of the glass caused by the heat generated through particle impact. In the work by Zhang it was shown that an excessive amount of glass in Ca- α' compositions was detrimental to erosion resistance due to its intrinsically poorer resistance to fracture than crystalline materials. Also, coarse equiaxed microstructures performed worse than fine equiaxed microstructures due to lower crack-growth resistance to the type of short cracks initiated in erosion (Zhang, Cheng, *et al.* 2001). Therefore it follows that the P08 sample performed worse than the K06 and P02 samples.

The P02 and K06 compositions behaved similarly under 90° impacts, and had the lowest erosion rate of all four materials tested. Both materials had similar hardness, with P02 being slightly harder than K06 (14.8 GPa vs. 14.0 GPa). The microstructure of these two materials is also quite similar, consisting largely of fine equiaxed α' grains, with the P02 appearing to contain less glass and impurity phases such as FeSi' and TiN'. The biggest difference in erosion behaviour was observed for the sliding impacts at 30°, where the material removal rate for the P02 sample was very low.

It is not possible to state with certainty which microstructural features in the P02 sample are responsible for the low erosion rate, or the difference in erosion rate seen between P02 and the similarly α' -containing K06. The K06 sample is more slag-rich, which will cause the formation of greater amounts of impurity phases such as FeSi' and TiN', which may be detrimental to erosion resistance. The K06 sample also contains a small amount of E' which extremely poor erosion resistance. Another candidate is the amount of grain boundary glass in the two samples. Excessive amounts of glass are detrimental to erosion resistance due to its inherent softness, however Zhang has shown that in Ca- α' materials, the presence of some glass can significantly improve erosion resistance, lowering the erosion rate by ~30% in some samples (Zhang, Cheng, *et al.* 2001). The glass cushions the grains from stresses and enhances the bonding between grains; removal of the glass by devitrification heat treatment was found to reduce the erosion resistance of all compositions when compared to the original as-sintered materials. The P02 sample is expected to produce a quite a small amount of glass compared to

the other slag-based samples due to the very low slag content and SiO₂-rich composition of the clay, and this may be below the limit where it becomes detrimental to the erosion resistance.

7.4.5 Summary of Findings from Erosion Resistance Testing of CRN Materials

- The two predominantly single-phase α' materials densified from K06 and P02-18 powder had higher erosion resistance than K33 and P08-18 pellets containing other phases such as E' and D'. These CRN- α' materials may be potentially useful for wear resistant applications.
- The P02 material consisting predominantly of fine-grained α' and a lower amount of grain boundary glass displayed the best erosion resistance, especially under conditions of sliding impacts, than the K06 sample, which also contained fine-grained α' . This difference in behaviour is most likely due differences in the amount and nature of the glass in the two materials, and possibly a result of less impurity phases in P02.
- The P08 material contained an excessive amount of glass and a coarser grain structure, which reduced its erosion resistance. The presence of elongated D'-phase rods did not appear to improve the erosion resistance of this material.
- The K33 sample, consisting of coarse E' plates and extremely high porosity, has extremely poor erosion resistance, and would not be suitable for any wear applications.

7.5 Conclusions for Chapter Seven

Densified materials from several compositions K06, K33, P02-18 and P08-18 were prepared via hot-pressing and their microstructures, hardness, fracture toughness, and solid particle erosion resistance were evaluated. Overall it was found that the materials produced from nearly single-phase α' powders (P02 and K06) displayed the best mechanical properties. Some specific findings from the work presented in this chapter are:

- The K06 and P02-18 powders produced dense α' materials with a generally fine, equiaxed microstructure, low porosity, and low glass. The P08-18 powder produced a coarse microstructure of α' and D'-phase, with a continuous range of chemistries and grain morphologies from equiaxed to slightly elongated. The K33 sample produced a very coarse, plate-like microstructure with ~25% porosity.

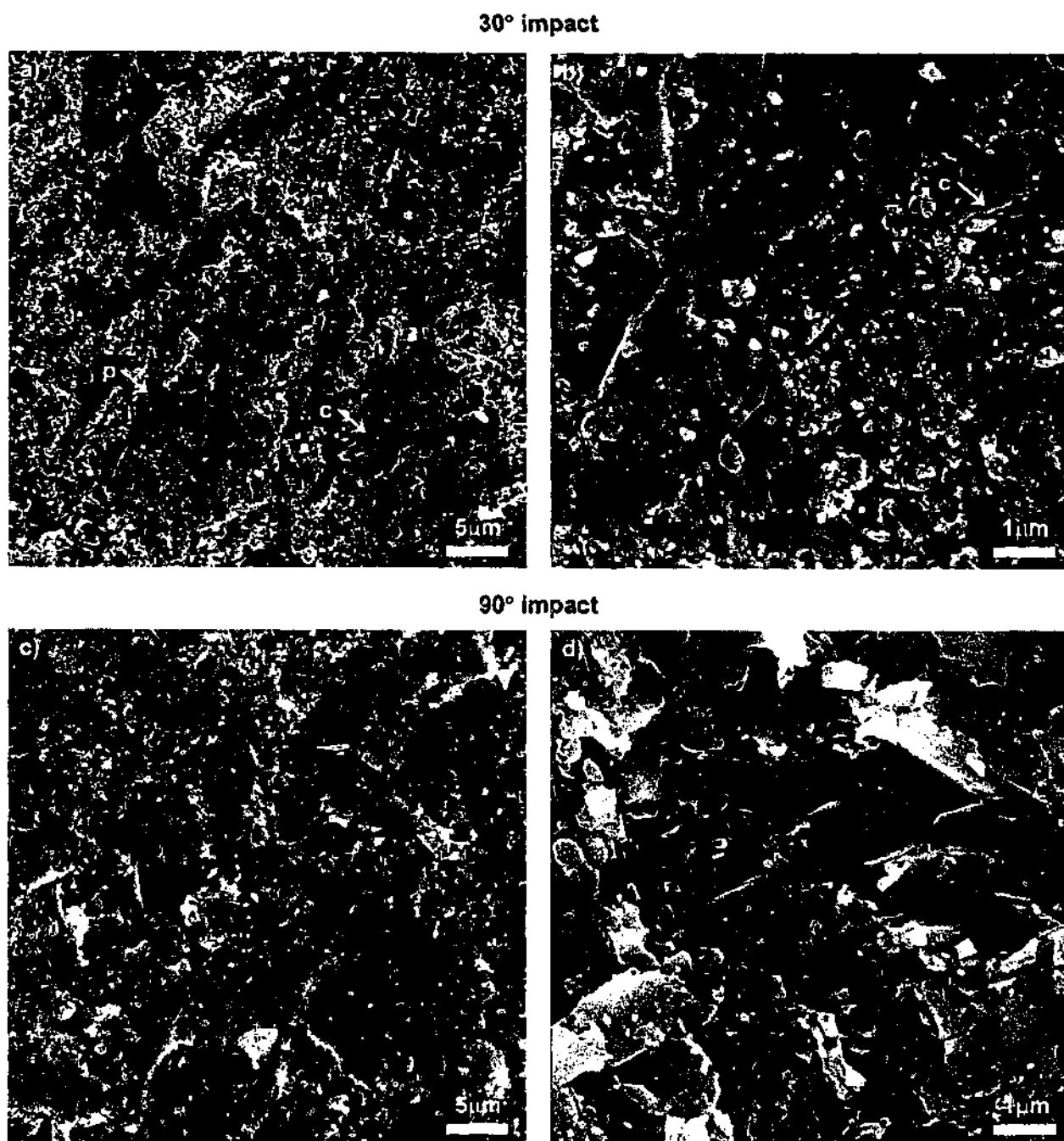


Figure 7.17 Eroded surfaces of the P08 pellet: (a) & (b) 30° impact (the impact direction is from top to bottom in the images), (c) low magnification image of 90° impact, and (d) image of a different area showing transgranular fracture in an agglomerate of plate-like grains eroded under 90° impact. Note that images (c) and (d) are not of the same area.

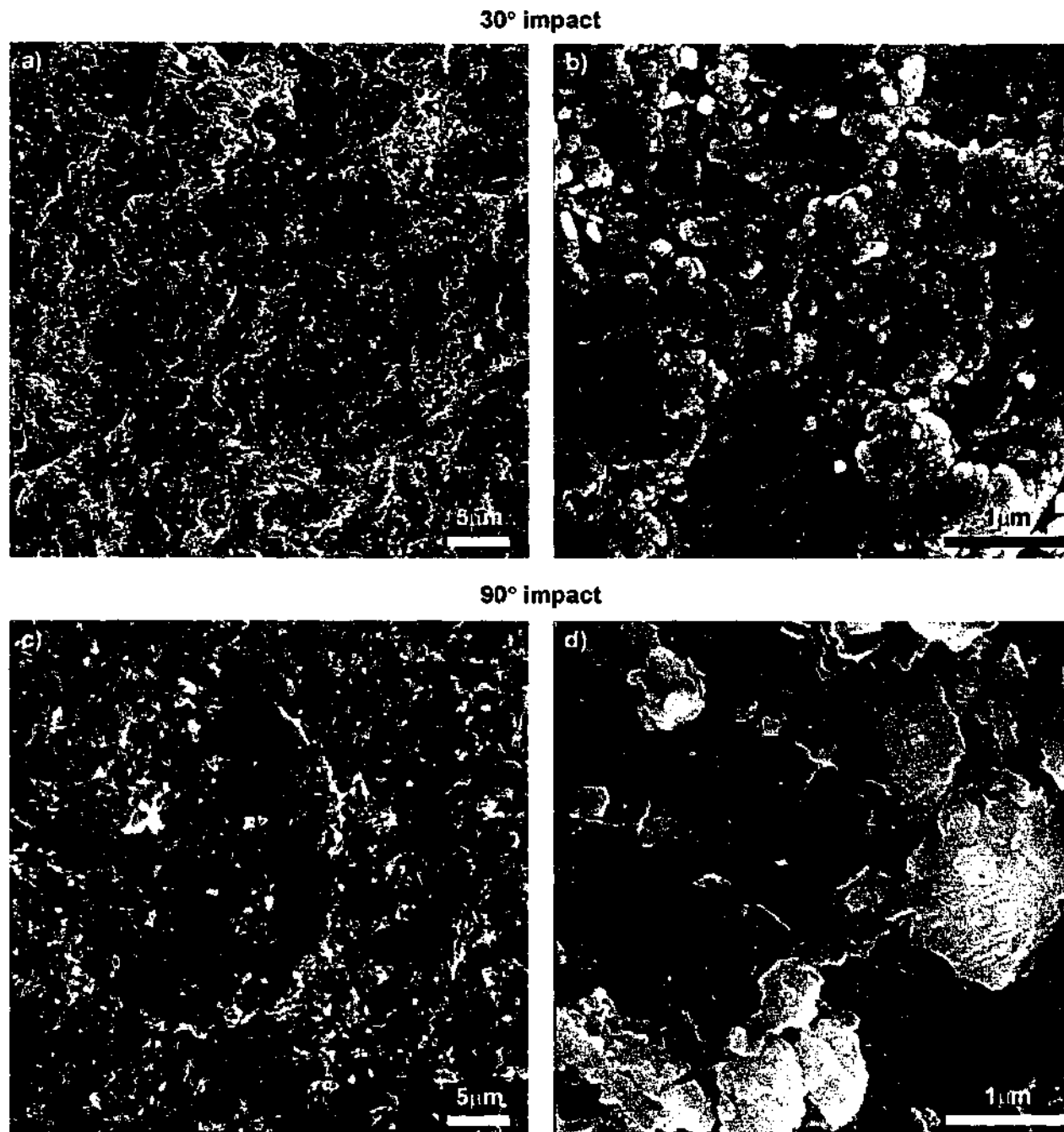


Figure 7.19 Eroded surfaces of the the K06 pellet: (a) & (b) 30° impact (the impact direction is from top to bottom in the images), (c) & (d) 90° impact.

7.4.3.4 P02

In terms of composition and microstructure, the P02 sample was most similar to K06, being fine-grained and predominantly α' . It displayed the greatest erosion resistance of all four materials, and the eroded surfaces are presented in Figure 7.20. The most noticeable feature of the surface of the P02 sample eroded at 30° (Figure 7.20a) is its smooth appearance compared to the other materials; very little flake formation is observed and there is little buildup of wear debris on the surface. The ploughmarks are considerably longer than in any of the other

- Iron and titanium impurities formed impurity phases FeSi' and TiN'. The FeSi phase tended to form as large blobs and was associated with microstructural heterogeneity, with probably having a detrimental effect on mechanical properties. Other impurities from the slag are generally taken up by the grain boundary glass.
- The ranking of materials in terms of decreasing hardness was P02, K06, P08, and K33. The two essentially single-phase α' had the highest hardness, indicating that the presence of secondary phases such as D' and E', and higher quantities of glass are detrimental to the hardness. The fracture toughness of the K06, P02, and P08 materials were all essentially the same, and the slight elongation of grains found in the K06 and P08 samples did not appear to provide any increase in toughness. The E'-phase in K33 is a soft phase with very poor mechanical properties.
- The erosion resistance of the four materials followed the rank order of hardness, with the best performing material being P02, which displayed an extremely high resistance to erosion at sliding impacts. Intergranular cracking followed by grain ejection was the dominant material removal mechanism in the equiaxed grained materials P02, K06, and P08. Brittle fracture and transgranular cracking dominated material removal in the coarse, plate K33 sample, and in areas of plate-like grains in P08.
- The mechanical properties of the P02 and K06 α' materials were generally comparable with those produced from high-glass containing Ca- α -sialon materials produced from laboratory-grade reagents. The erosion resistance of the slag-based CRN- α -sialons was comparable to, if not better than, hot-pressed Ca- α' materials fabricated from pure laboratory chemicals.

Chapter Eight

Conclusions and Suggestions for Future Work

8.1 Conclusions

This thesis has shown that inexpensive mixtures of waste steelmaking slag and clay can be successfully used to produce a highly value-added, α -sialon engineering ceramic. The process of carbothermal reduction-nitridation (CRN) can be controlled to produce predominantly α -sialon powders from various slag-containing compositions, and these powders can be densified into solid bodies that have good mechanical properties similar to those of conventional α -sialon ceramics produced from high-purity chemical reagents.

The standard conditions used for CRN in this investigation were a reaction temperature of 1450°C, a 12 hour reaction time, and N₂ gas flowing at 30ℓ/hr. α -Sialon was produced under these conditions from mixtures of slag and clay-K (kaolinite) combined in various ratios, with carbon comprising 25 wt% of the total batch weight and ~6 wt% α -Si₃N₄ seeds. Two compositions were found to produce predominantly α -sialon, with small amounts of AlN', α -Si₃N₄ or E'-phase (nominally CaAlSiN₃), and a grain boundary glass also produced. The α' grains produced from these compositions were solely stabilised by Ca with relatively high Ca-contents, had a generally equiaxed morphology, and were ~1µm in diameter.

Altering the composition by changing the slag content significantly altered the phase behaviour in these samples: compositions with a medium slag content produced gehlenite (nominally Ca₂Al₂SiO₇) as a secondary phase in equilibrium with α' , and further increasing the slag content produced an increasing proportion of E'. Most crystalline phases produced in this system were observed to be solid-solutions, including E', G' (gehlenite), AlN', and the FeSi' and TiN' formed from Fe and Ti impurities present in the raw materials. The grain boundary glass acted as a sink for many of the other impurities in the slag and clay, including Na, S, and most of the Mg.

The CRN reaction processes were studied and CRN was found to occur via three stages: 1) decomposition and phase transformations within the oxide reactants during heating to 1300°C; 2) melting of the oxide phases and early stage CRN between 1300 and 1400°C to produce the first oxynitride phases; and 3) final product formation and elimination of

intermediate phases with extended holding time at 1450°C. A low z-value β -sialon and M'-phase (nominally $\text{Ca}_2\text{AlSi}_3\text{O}_2\text{N}_5$) were the two main intermediate phases produced during CRN, which could be converted into α' via a series of CRN-induced solution-precipitation steps. The E'-phase product was also found to be a metastable phase that may be converted to α' under more favourable CRN conditions. In high-slag compositions the glass may devitrify upon cooling to produce gehlenite.

The kinetics of the CRN reactions were found to be a limiting factor in the ability of the system to produce the final, 'steady state' CRN phase assembly. The viscosity of the oxynitride liquid produced during CRN was found to control the diffusion of the solution-precipitation reactions that produce the final phases, thereby limiting the rate and extent of α' formation. α -Sialon production was enhanced via the formation of low viscosity liquids from compositions rich in slag, or from compositions with relatively low SiO_2 -contents. SiO_2 -rich clay-P (pyrophyllite) compositions experienced retarded α' formation compared to clay-K, requiring the longer reaction time of 18 hours to produce α' . D'-phase (nominally $2\text{CaO}\cdot\text{Si}_3\text{N}_4$) was the main secondary phase in the slag+clay-P system. Further increasing the concentration of SiO_2 by replacing clay-K with sand further increased the viscosity and prevented α -sialon formation via CRN at 1450°C, even after reaction for 24 hours.

Penetration of N_2 into the samples was also observed to have a considerable influence on the CRN process. The gas stream plays a pivotal role in both delivering the reactant nitrogen to the sample and in removing the unwanted by-products of the reversible, equilibrium CRN reactions. Restricting N_2 access to the sample by compacting the powder into pellets retarded the extent of α' formation due to increasing difficulty of achieving gas diffusion into, and out of, the core. The surfaces of the pellets in direct contact with the flowing N_2 gas produced significantly higher quantities of α -sialon, as did the uncompact loose powder, which formed the highest extent of α' . Excessively high N_2 gas flowrates were found to remove the intermediate SiO(g) product from the sample, depleting the system in Si. This will be detrimental to CRN and α' formation, especially in high-slag, Si-poor compositions which cannot afford to be depleted in Si. The amount of α' formed in high-slag compositions was significantly boosted by using a flowrate lower than the standard of 30 ℓ /hr used in this study, however, this caused the reaction rate to be slower and required a longer reaction time for completion of CRN.

Self-seeding of the mixture by using CRN- α' powder particles in the batch mix to promote the nucleation of α -sialon was not effective. A greater effect on α' formation resulted from the

addition of α - Si_3N_4 particles to seed the samples, but only in uncompacted, loose powders. No seeding effect was observed in compacted pellets. It is likely that optimising other factors such as N_2 flowrate may produce a greater effect on α' formation than the use of the expensive α - Si_3N_4 seeding component.

The CRN reactions may proceed more effectively at temperatures $>1450^\circ\text{C}$, however nitride formation via CRN may be in competition with SiC formation at these temperatures, especially if sources of carbon are present. Heat-treating the CRN powders at a potential densification temperature of 1600°C showed that the α' phase is stable at high temperatures, as long as excessive SiC formation is prevented by removing any opportunity for reaction with carbon in the furnace atmosphere. It was also found that residual E' and D' secondary phases were converted to α' at elevated temperatures via small-scale CRN reactions using SiC already present within the sample as a reductant. This allows for some degree of purification of partially α' -containing CRN powders during sintering, such as those produced from high-slag compositions.

Pressureless sintering at 1800°C was not able to produce a highly densified material from this CRN powder. Near-theoretical density could be obtained by hot-pressing the powders at 1700°C for 1 hour, except for the predominantly E'-phase material, which had a very coarse grain structure and could not be highly densified. The purification effect of the E' $\rightarrow\alpha'$ and D' $\rightarrow\alpha'$ phase transformations were limited to the pellet surfaces due to a lack of N_2 diffusion through the pellet. Analysis of the microstructures of these pellets showed that some grain growth did occur during hot-pressing, with a slight elongation and orientation of the α' grains produced. Highly anisotropic α' grains were formed on the transformed surfaces of the pellets, especially on the E'-phase-rich pellet. The microstructures were not homogenous, and generally had an uneven distribution of porosity, grain sizes, and impurity phases such as FeSi'.

An evaluation of the fundamental mechanical properties of the bulk-materials formed from the CRN powder revealed that the highest hardness of 14-14.8 GPa was achieved from the highest α' -containing powders. These values are typical of the hardness obtained from high glass-containing Ca- α -sialons produced via the conventional reaction-sintering of pure laboratory chemicals. The slight elongation of the α' grains did not contribute to an increase in fracture toughness, which was $4.1\text{MPam}^{1/2}$ for the three compositions tested, comparable to conventional Ca- α' materials.

A relationship between material hardness (ie. α' content) and erosion resistance was found, with the higher hardness materials displaying the best resistance to erosion. The largely equiaxed morphology of the grains in these samples resulted in grain ejection being the dominant material removal mechanism, though the presence of plate-like E' and D' phases produced some transgranular fracture. The E'-phase is an extremely soft phase with poor mechanical properties, and should be removed from the products of CRN in clay-K based compositions. Comparison of these results to those obtained for pure, reaction-sintered Ca- α -sialons showed that their wear performance was similar if not better than that of the pure α' materials, which are in turn better than commonly used Al_2O_3 or SiC wear linings. Slag-derived α -sialons thus show good potential for use in wear-resistant applications.

CRN is clearly a viable alternative for the production of Ca- α -sialon materials, with good engineering properties, from inexpensive mixtures of slag and clay.

8.2 Suggestions for Future Work

This is the first study of the CRN reaction process as applied to the slag+clay system for the production of α -sialon, thus there are many areas that were unable to be covered in this investigation and warrant further work. The most important of these are outlined below:

- Optimisation of the CRN process to produce a single-phase α' product. The work in this thesis identified several important variables that influence α' formation via CRN, the most important being slag content, reaction temperature, reaction time, and N_2 flowrate. It was seen that these factors are inter-related and composition-dependent; eg. lowering the N_2 flowrate had a large improvement on the yield of α' in high-slag compositions, but also increased the time at 1450°C required to complete the reactions. The results of the work in this thesis have shown that optimisation of these parameters may allow the production of highly α' -bearing powders from higher slag-containing mixtures than investigated here, potentially even a mixture of just slag and carbon alone, without clay. This should be investigated. In addition, carbon content is an important parameter that was not studied in this thesis, and an investigation into the optimum carbon content is warranted.

For the purposes of the current study the products of CRN from several of the compositions were considered to be nearly single-phase α' , however, significant amounts of minor phases AlN' , FeSi' , and TiN' , and glass remained in the products.

Optimisation of the CRN process should also serve to minimise the production of these phases.

- Alternative green-body forming mechanisms. The powder form of the CRN- α' powder is unique and may be amenable to unconventional green-body forming processes such as gel-casting, slip-casting, or tape-casting. This may produce novel α' components with unique geometries unable to be produced via reaction sintering.
- Densification of the CRN- α' powder. Pressureless sintering of the as-fired CRN powders was shown to be inadequate for achieving full density in these materials, thus hot-pressing was used to overcome this difficulty. This is an expensive technique with many limitations on specimen geometry, hence a method to improve the densification of the CRN- α' powder using pressureless methods should be investigated. One method may be to add a sintering aid to the CRN powder that forms a liquid at the densification temperature. Slag additions may be a potentially useful sintering aid. In fact, it may be the case that a small amount of a secondary phase such as G' (gehlenite) or D' present in the powder after CRN will provide enhanced densification, in which case the optimised CRN- α' product may not, in fact, be a single-phase α' material. The effect of any increase in the amount of glass or secondary products on mechanical properties will also need to be examined.
- A more detailed study of the reaction process may be useful in achieving greater control over the CRN reactions. This may require the use of other analytical techniques such as NMR to investigate the amorphous phase and the small quantities of intermediate phases precipitated from it during CRN. The slag+clay system is very complex with many impurity components, thus it may be useful to investigate a simplified system of just the four main constituents CaO, SiO₂, MgO, and Al₂O₃. Such an experiment was attempted during this investigation, however the crystalline nature of the starting mixture behaved considerably differently to the amorphous, slag-based mixture. Thus the creation of an artificial slag by melting and quenching mixtures of the four components may be more appropriate. This may enable an investigation into the role of impurity elements such as Fe, Ti, Na, K etc. on the CRN reactions by the controlled addition of impurity elements to the artificial slag. The impurity levels in the slag may vary slightly from batch to batch, hence some understanding of the effects of varying the quantities of these impurities would be useful.

- Scaling up the production process to a commercial scale. For the large-scale production of commercial quantities of CRN- α' powder, static batch processing in a tube furnace is not necessarily the most efficient method of production. Scaling up of the CRN process will require significant work to optimise the process parameters to the different furnace geometry and sample size. This is particularly important in terms of achieving good N_2 penetration throughout the bulk of the sample to avoid inhomogeneous CRN. Other issues that must be addressed include initial reactant mixing and drying, post-firing carbon removal, and breaking up of the agglomerated α' powder.
- Understanding the E- and D-phases. Little is known about the pure E- and D-phases, or the E'- and D'-phase solid-solutions formed in this system. If these phases remain as major secondary phases in the CRN powders, it may be necessary to perform some further investigation into the structure and properties of these compounds. Fabrication of pure E-phase via the hot pressing of laboratory reagents was attempted as part of the current study, however this was initially unsuccessful and not pursued further. The solid-solution nature of the E'- and D'-phases produced here may not provide a reliable product for analysis, however it may be worthwhile to at least identify the crystal structure of D'-phase using TEM methods, for scientific interest.

List of Publications

1. Australian Provisional Patent Application No PQ4354/99 (1999) and PQ8198/00, (2000) Process for production of alpha sialon material. Inventors: Y.-B.Cheng, and M.R.Terner.
2. Terner, M.R., Swenser, S.P., and Cheng, Y.-B. (2001), Characterisation of Multi-Cation stabilised Alpha Sialon Materials, *Proceedings of the 7th International Symposium on Ceramic Materials and Components for Engines, Goslar, Germany 2000*, ed. J. G. Heinrich and F. Aldinger, Wiley-VCH, Weinheim pp. 447-451.
3. Terner, M.R., Cheng Y.-B. (2002), Fabrication of α sialons from Slag via Carbothermal Reduction-Nitridation, *Austceram*, Perth 2002, pp 247-248.
4. Hotta, M., Tatami, J., Zhang, C., Komeya, K., Meguro, T., Terner, M.R., Cheng, Y.-B. (2002), Formation Mechanism of Ca- α -SiAlON Hollow Balls by TEM analysis, *Austceram*, Perth 2002, pp 95-96.
5. Terner, M.R., Cheng Y.-B., Chen, W.-W., and Wang, P.-L. Slag-Derived α -sialon Ceramics and their Properties, *Proceedings of the European Ceramic Society Conference 2003* – Awaiting publication

References

- Antsiferov, V. N., Gilev, V. G., Bekker, V. Y. and Filimonova, I. V. (2000), A Study of Sialon Synthesis from Kaolin by Carbothermal Reduction and Simultaneous Nitriding, *Refractories and Industrial Ceramics*, 41(9-10), pp.338-44.
- Arik, H. (2003), Synthesis of Si_3N_4 by the Carbo-thermal Reduction and Nitridation of Diatomite, *J. Eur. Cer. Soc.*, 23(12), pp.2005-14.
- ASA (2003), Australasian Slag Association Website, www.asa-inc.org.au/gbfs.htm.
- Bakharev, T., Sanjayan, J. G. and Cheng, Y.-B. (1999), Alkali Activation of Australian Slag Cements, *Cement and Concrete Research*, 29, pp.113-20.
- Barris, G. C., Brown, I. W. M., Owers, W. R., Ryan, M. J. and White, G. V. (1994), Mixtures of β -Sialon and SiC Prepared by Carbothermal Reduction of Silica-Rich Clays, *International Ceramics Conference*, International Ceramics Monographs, pp.1025-30.
- Boccaccini, A., Petitmermet, M. and Wintermantel, E. (1997), Glass-Ceramics from Municipal Incinerator Fly Ash, *Am. Ceram. Soc. Bull.*, November.
- Boyer, S. M. and Moulson, A. J. (1978), A Mechanism for the Nitridation of Fe-Contaminated Silicon, *J. Mater. Sci.*, 13, pp.1637-46.
- Brandt, G. (1991), Ceramic Cutting Tools, in Encyclopedia of Materials Science and Engineering, ed. R. W. Cahn, Pergamon Press, 2, pp.761-5.
- Brindley, G. W. and Brown, G. (1984), Crystal Structures of Clay Minerals and their Identification, Spottiswoode Ballantyne, London.
- Cao, G. Z. and Metselaar, R. (1991), α' Sialon Ceramics: A Review, *Chem.Mater.*, 3(2), pp.243-52.
- Cardile, C. M. (1990), Carbothermal Synthesis of β' -Sialon From a By-Product of Alumina Refining, *Key Engineering Materials*, 48-50.

- Chen, W.-W., Sun, W. Y., Wang, P.-L., Li, Y. W., Cheng, Y.-B. and Yan, D. S. (2002), Control of Microstructures in α -SiAlON Ceramics, *J. Am. Cer. Soc.*, **85**(1), pp.276-78.
- Chen, W.-W., Wang, P.-L., Chen, D. Y., Zhang, B. L., Cheng, Y.-B. and Yan, D. S. (2002), Synthesis of (Ca, Mg)- α -sialon From Slag by Self-Propagating High-Temperature Synthesis, *J. Mater. Chem.*, **12**, pp.1199-202.
- Cho, Y. W. and Charles, J. A. (1991a), Synthesis of Nitrogen Ceramic Powders by Carbothermal Reduction and Nitridation. Part 1: Silicon Nitride, *Materials Science and Technology*, **7**(April), pp.289-98.
- Cho, Y. W. and Charles, J. A. (1991b), Synthesis of Nitrogen Ceramic Powders by Carbothermal Reduction and Nitridation. Part 2: Silicon Aluminium Oxynitride (sialon), *Materials Science and Technology*, **7**(May), pp.399-406.
- Coother, N. E. (1987), Sialon Ceramics - their Development and Engineering Applications, *Materials and Design*, **8**(1), pp.2-9.
- Das, B. P., Panneerselvam, M. and Rao, K. J. (2003), A Novel Microwave Route for the Preparation of ZrC-SiC Composites, *Journal of Solid State Chemistry*, **173**(1), pp.196-202.
- Das, S. and Curlee, T. R. (1992), The Cost of Silicon Nitride Powder and the Economic Viability of Advanced Ceramics, *Bull. Am. Ceram. Soc.*, **71**(7), pp.1103.
- Della, V. P., Kuhn, I. and Hotza, D. (2002), Rice husk Ash as an Alternate Source for Active Silica Production, *Mater. Let.*, **57**(4), pp.818-21.
- Dominguez, E. A. and Ullmann, R. (1996), 'Ecological Bricks' Made With Clays And Steel Dust Pollutants, *Appl. Clay. Sci.*, **11**, pp.237-49.
- Dumbaugh, W. H. and Danielson, P. S. (1986), Aluminosilicate Glasses, in Commercial Glasses, ed. D. C. Boyd and J. F. MacDowell, The American Ceramic Society, Ohio, **18**.
- Edrees, H. J. and Hendry, A. (1995), Influence of Atmosphere and Sintering Additives on Clay-Silicon Nitride Densification, *British Ceramic Transactions*, **94**(1), pp.15-20.
- Edrees, H. J., Holling, G. E. and Hendry, A. (1995), Sialon Bonding Systems for Silicon Carbide Composites, *British Ceramic Transactions*, **94**(2), pp.52-6.

- Ekstrom, T. (1993), Research and Engineering Applications of Silicon Nitride Based Ceramics, *Materials Forum*, **17**, pp.67-82.
- Ekstrom, T. (1996), Personal communication.
- Ekstrom, T. and Nygren, M. (1992), SiAlON Ceramics, *J. Am. Cer. Soc.*, **75**(2), pp.259-76.
- Ekstrom, T., Shen, Z.-J., MacKenzie, K. J. D., Brown, I. W. M. and White, G. V. (1998), α -Sialon Ceramics Synthesised From a Clay Precursor By Carbothermal Reduction and Nitridation, *J. Mater. Chem.*, **8**(4), pp.977-83.
- Evans, A. G. and Charles, E. A. (1976), Fracture Toughness Determinations by Indentation, *J. Am. Cer. Soc.*, **59**(7-8), pp.371-2.
- Evans, A. G., Gulden, M. E. and Rosenblatt, M. (1978), Impact Damage in Brittle Materials in the Elastic-Plastic Response Regime, *Proc. R. Soc. London, Ser. A*, **361**, pp.343-65.
- Fabbri, B. and Dondi, M. (1991), Clays and Other Raw Materials for the Production of Sialon Ceramic Powders, *Ind. Ceram.*, **11**, pp.75-81.
- Ferreira, C., Ribeiro, A. and Ottosen, L. (2003), Possible Applications for Municipal Solid Waste Fly Ash, *Journal of Hazardous Materials*, **B96**, pp.201-16.
- Ghosh, S., Das, M., Chakrabarti, S. and Ghatak, S. (2002), Development of Ceramic Tiles From Common Clay and Blast Furnace Slag, *Ceram. Int.*, **28**(4), pp.393-400.
- Gilbert, J. E. and Mosset, A. (1998), Preparation of β -SiAlON From Fly Ashes, *Mater. Res. Bull.*, **33**(1), pp.117-23.
- Grimshaw, R. E. (1971), The Chemistry and Physics of Clays, Ernest & Benn, London.
- Hampshire, S. (1994), Nitride Ceramics, in Structure and Properties of Ceramics, ed. M. V. Swain, VCH, **11**, pp.119-71.
- Hampshire, S., Lonergan, J., Redington, W., Schneider, N. and Mooney, C. (1999), Effect of Crucible Powder Bed Composition on Densification of Silicon Nitride, Third International Symposium on Synergy Ceramics, Osaka, Japan, 140-1.

- Hewett, C. L. (1998), The Fabrication and Characterisation of Calcium α -Sialon Ceramics, *PhD Thesis*, Department of Materials Engineering, Monash University, Clayton, Melbourne.
- Hewett, C. L., Cheng, Y.-B., Muddle, B. C. and Trigg, M. B. (1998), Thermal Stability of Calcium α -Sialon Ceramics, *J. Eur. Cer. Soc.*, **18**, pp.417-27.
- Higgins, I. and Hendry, A. (1986), Production of β' -Sialon by Carbothermal Reduction of Kaolinite, *British Ceramic Transactions*, **85**, pp.161-6.
- Higgins, I. and Hendry, A. (1987), The Mechanism of Formation of β' -Sialons from Oxides, *British Ceramics Proceedings*, **38**, pp.163-78.
- Hong, F., Lumby, R. J. and Lewis, M. H. (1993), TiN/Sialon Composites Via In-Situ Reaction Sintering, *J. Eur. Cer. Soc.*, **11**, pp.237-9.
- Hotta, M., Tatami, J., Zhang, C., Komeya, K., Meguro, T., Ternner, M. R. and Cheng, Y.-B. (2002), Formation Mechanism of Ca- α -SiAlON Hollow Balls by TEM Analysis, *Austceram 2002*, Perth, pp.95-6.
- Huang, Z.-K., Sun, W.-Y. and Yan, D.-S. (1985), Phase Relations of the Si₃N₄-AlN-CaO system, *Journal of Materials Science Letters*, **4**, pp.255-9.
- Hyde, B. G., Thompson, J. G. and Withers, R. L. (1994), Crystal Structures of Principal Ceramic Materials, in *Structure and Properties of Ceramics*, ed. M. V. Swain, VCH, **11**, pp.1-46.
- ICL (1999), Personal Communication (Independent Cement and Lime Pty.Ltd).
- Izhevskiy, V. A., Genova, L. A., Bressiani, J. C. and Aldinger, F. (2000), Progress in SiAlON Ceramics, *J. Eur. Cer. Soc.*, **20**, pp.2275-95.
- Jack, K. H. (1976), Review: Sialons and Related Nitrogen Ceramics, *J. Mater. Sci.*, **11**, pp.1135-58.
- Jack, K. H. (1978), The Relationship of Phase Diagrams to Research and Development of Sialons, in *Phase Diagrams: Materials Science and Technology*, ed. A. M. Alper, Academic Press, NY, pp.241-85.

- Jack, K. H. (1983), The Characterisation of α -Sialons and the α - β Relationships in Sialons and Silicon Nitrides, *Progress in Nitrogen Ceramics*, Martinus Nijhoff, pp.45-9.
- Jin, G.-Q. and Guo, X.-Y. (2003), Synthesis and Characterization of Mesoporous Silicon Carbide, *Microporous and Mesoporous Materials*, **60**(1-3), pp.207-12.
- Jones, J. T. and Berard, M. F. (1993), Ceramics: Industrial Processing and Testing, Iowa State University Press, Ames.
- Kall, P.-O. (1988), Quantitative Phase Analysis of Si_3N_4 -based Materials, *Chemica Scripta*, **28**, pp.439-46.
- Kang, I.-H., Komeya, K., Meguro, T., Naito, M. and Hayakawa, O. (1996), Effect of Silicon Nitride Seeds Addition on the Particle Size and the Crystal Form of Resulting Powder in Carbothermal Reduction-Nitridation of Silica, *Journal of the Ceramic Society of Japan*, **104**(6), pp.471-5.
- Kang, I.-H., Komeya, K., Meguro, T., Naito, M. and Hayakawa, O. (1998), Preparation of Si_3N_4 Powder from the System SiO_2 -C- N_2 with Si_3N_4 Seed, *Journal of the Ceramic Society of Japan*, **106**(1), pp.30-4.
- Katz, R. N. (1993), Commercial Applications of Silicon Nitride Based Ceramics, *Technology Review*, **8**, pp.142-8.
- Kingery, W. D., Bowen, H. K. and Uhlraann, D. R. (1976), Introduction to Ceramics, John Wiley & Sons, Sydney.
- Klocke, F., Schippers, C. and Schmidt, C. (2001), Green Machining of Ceramics, *7th International Symposium on Ceramic Materials and Components for Engines*, Goslar, Germany, 2000, Wiley-VCH, pp.371-6.
- Komeya, K. (1994), High Temperature Engineering Ceramics, in Structure and Properties of Ceramics, ed. M. V. Swain, VCH, **11**, pp.517-65.
- Kudyba, A., Almeida, M., Hintzen, H. T., van der Heijde, J. C. T., Laven, J. and Metselaar, R. (1997), Aqueous Processing of Carbothermally Prepared Ca- α -SiAlON and β -SiAlON Powders: Powder and Suspension Characterisation, *Key Engineering Materials*, **132-136**, pp.325-8.

- Kudyba-Jansen, A., Almeida, M., Laven, J., van der Heijde, J. C. T., Hintzen, H. T. and Metselaar, R. (1999), Aqueous processing of carbothermally prepared Ca- α -SiAlON and β -SiAlON powders: powder and suspension characterisation, *J. Eur. Cer. Soc.*, **19**, pp.2711-21.
- Kudyba-Jansen, A., Hintzen, H. T. and Metselaar, R. (2001), Ca- α / β -sialon Ceramics Synthesised From Fly Ash - Preparation, Characterization, and Properties, *Mater. Res. Bull.*, **36**, pp.1215-30.
- Kurama, S., Herrmann, M. and Mandal, H. (2002), The Effect of Processing Conditions, Amount of Additives and Composition on the Microstructures and Mechanical Properties of α -SiAlON Ceramics, *J. Eur. Cer. Soc.*, **22**, pp.109-19.
- Lee, F. and Bowman, K. J. (1992), Texture and Anisotropy in Silicon Nitride, *J. Am. Cer. Soc.*, **75**(7), pp.1748-55.
- Lee, J. G. and Cutler, I. B. (1979), Sinterable Sialon Powder by Reaction of Clay with Carbon and Nitrogen, *Ceramic Bulletin*, **58**(9), pp.869-71.
- Lee, W. E. and Raintorth, W. M. (1994), Ceramic Microstructures, Chapman & Hall, Melbourne.
- Ma, R. and Bando, Y. (2002), High Purity Single Crystalline Boron Carbide Nanowires, *Chem. Phys. Lett.*, **364**(3-4), pp.314-7.
- Mandal, H. (1999), New Developments in α -SiAlON ceramics, *J. Eur. Cer. Soc.*, **19**, pp.2349-57.
- Mandal, H. and Hoffmann, M. (2000), Hard and Tough α -Sialon Ceramics, *Materials Science Forum*, **325-326**, pp.219-24.
- Mandal, H. and Hoffmann, M. J. (1999), Preparation of Multiple-Cation α -SiAlON Ceramics Containing Lanthanum, *J. Am. Cer. Soc.*, **82**(1), pp.229-32.
- Mazzoni, A. D. and Aglietti, E. F. (1996), Study of Carbonitriding Reactions of Bentonites, *Appl. Clay. Sci.*, **11**, pp.143-54.

- Mazzoni, A. D. and Aglietti, E. F. (1998), Mechanism of the carbonitriding reactions of SiO₂-Al₂O₃ minerals in the Si-Al-O-N system, *Appl. Clay. Sci.*, **12**, pp.447-61.
- Mazzoni, A. D. and Aglietti, E. F. (2000), Aluminothermic Reduction and Nitriding of High Silica Materials Diatomite and Bentonite Minerals, *Appl. Clay. Sci.*, **17**, pp.127-40.
- Mazzoni, A. D., Aglietti, E. F. and Pereira, E. (1992a), Carbonitriding Reaction of Clay. Involved Phases and Mechanism, *Mater. Chem. Phys.*, **31**, pp.325-31.
- Mazzoni, A. D., Aglietti, E. F. and Pereira, E. (1992b), Phases and Kinetics of β' -sialon Formation From Clays, *Mater. Let.*, **14**, pp.37-42.
- Mazzoni, A. D., Aglietti, E. F. and Pereira, E. (1993a), β' -Sialon Preparation From Kaolinite Clays, *Appl. Clay. Sci.*, **7**, pp.407-20.
- Mazzoni, A. D., Aglietti, E. F. and Pereira, E. (1993b), Carbonitriding of Clay: Relation between the Weight Loss and Crystalline Phases during Reaction, *J. Am. Cer. Soc.*, **76**(9), pp.2337-40.
- MBDC (2003), Eco-Effectiveness: Nature's Design Patterns, http://www.mbdc.com/c2c_ee.htm.
- McColm, I. J. (1995), Special Ceramics for Modern Applications: Which? Why? How?, in Ceramic Processing, ed. R. A. Terpstra, et al., Chapman & Hall, London, pp.1-33.
- McDonough, W. and Braungart, M. (2002), Design for the Triple Top Line: New Tools for Sustainable Commerce, *Corporate Environmental Strategy*, **9**(3), pp.251-8.
- McTigue, P. T. (1982), Chemistry: Key to the Earth, Melbourne University Press, Clayton, Victoria.
- Metselaar, R., Exalto, D., van Mol, T. and Hintzen, H. T. (1996), The Synthesis of α - and β -Sialon from Fly Ash, *PacRim2*, Cairns, Australia, International Ceramic Monographs, **2**.
- Mitomo, M., Takeuchi, M. and Ohmasa, M. (1988), Preparation of α -Sialon Powders by Carbothermal Reduction and Nitridation, *Ceram. Int.*, **14**, pp.43-8.
- Morrison, F. C. R., Maher, P. P. and Hendry, A. (1989), In-situ Formation of Sialons in Refractories Containing Silicon Carbide, *British Ceramic Transactions*, **88**, pp.157-61.

- Mowat, D. (2002), The VanCity Difference - A Case for the Triple Bottom Line Approach to Business, *Corporate Environmental Strategy*, **9**(1), pp.24-9.
- Nilsen, K. J. and Weimer, A. W. (1997), Chemical Purification, in Carbide, Nitride and Boride Materials Synthesis and Processing, ed. A. W. Weimer, Chapman & Hall, London, pp.479-503.
- Nordberg, L.-O., Shen, Z., Nygren, M. and Ekstrom, T. C. (1997), On the Extension of the α -SiAlON Solid Solution Range and Anisotropic Grain Growth in Sm-Doped α -SiAlON Ceramics, *J. Eur. Cer. Soc.*, **17**, pp.575-80.
- Pelino, M. (2000), Recycling of Zinc-Hydrometallurgy Wastes in Glass and Glass Ceramic Materials, *Waste Management*, **20**, pp.561-8.
- Pilkington (1999), Personal Communicatin (Pilkington Pty.Ltd).
- Pioro, L. S. and Pioro, I. L. (2003), Reprocessing of Metallurgical Slag into Materials for the Building Industry, *Waste Management*, (In Press).
- Pollmann, W. (2000), Keynote Presentation, *7th International Symposium on Ceramic Materials and Components for Engines*, Goslar, Germany, 2000).
- Prasad, C. S., Maiti, K. N. and Venugopal, R. (2003), Effect of Substitution of Quartz by Rice Husk Ash and Silica Fume on the Properties of Whiteware Compositions, *Ceram. Int.*, (In Press).
- Qiu, J. Y., Tatami, J., Zhang, C., Komeya, K., Meguro, T. and Cheng, Y.-B. (2002), Influence of Starting Material Composition and Carbon Content on the Preparation of Mg- α -SiAlON Powders by Carbothermal Reduction - Nitridation, *J. Eur. Cer. Soc.*, **22**, pp.2989-96.
- Radwan, M. and Miyamoto, Y. (2003), Synthesis of $\text{Si}_2\text{N}_2\text{O}$ Powder from Desert Sand by Nitriding Combustion Method, *International Symposium on SiAlONs*, Chiba, Japan, Dec 2001, *Key Engineering Materials*, **237**, pp.111-6.
- Rafaniello, W. (1997), Critical Powder Characteristics, in Carbide, Nitride and Boride Materials Synthesis and Processing, ed. A. W. Weimer, Chapman and Hill, London, pp.43-68.
- Rahaman, M. N. (2003), Ceramic Processing and Sintering, 2nd ed., Marcel Dekker, Inc, NY.

- Rahman, I. A. and Saleh, M. I. (1995), The Formation of β -sialon in the Carbothermal Reduction of Digested Rice Husks, *Mater. Let.*, **23**(April), pp.157-61.
- Rojan (2002), Personal Communication (Rojan Advanced Ceramics).
- Rosenflanz, A. (1999), Silicon Nitride and Sialon Ceramics, *Current Opinion in Solid State and Materials Science*, **4**, pp.453-9.
- Roston, E. (2002), New War on Waste, *Time*, 26 August.
- Schafer, L. (2000), Personal communication.
- Scott, H. G. (1986), Cellsiz, CSIRO.
- Seeber, A. J. and Cheng, Y.-B. (2003), Thermal Stability of Mixed-Cation α -Sialon Ceramics, *Materials Science and Engineering A*, **339**, pp.115-23.
- Sheldon (1966), On The Ductile Behaviour of Nominally Brittle Materials During Erosive Cutting, *Trans. ASME*, **88B**, pp.387-93.
- Singh, M. and Salem, J. A. (2002), Mechanical Properties and Microstructure of Biomorphic Silicon Carbide Ceramics Fabricated From Wood Precursors, *J. Eur. Cer. Soc.*, **22**, pp.2709-17.
- Sorrell, C. C. (1983), Silicon Nitride and Related Nitrogen Ceramics: II. Phase Equilibria and Properties of Reaction Bonded and Hot Pressed Si-Al-O-N Systems, *J. Australasian Cer. Soc.*, **19**(2), pp.48-67.
- Srinivasan, M. and Rafaniello, W. (1997), Non-Oxide Materials: Applications and Engineering, in Carbide, Nitride and Boride Materials Synthesis and Processing, ed. A. W. Weimer, Chapman and Hill, London, pp.1-42.
- Suzuki, D. and Dressel, H. (2002), Good News For A Change - Hope For A Troubled Planet, Allen & Unwin, Australia.
- Tatami, J., Iguchi, M., Hotta, M., Zhang, C., Komeya, K., Meguro, T., Omori, M., Hirai, T., Brito, M. E. and Cheng, Y.-B. (2003), Fabrication and Evaluation of Ca- α -SiAlON Nano Ceramics, *International Symposium on SiAlONs*, Chiba, Japan, Dec 2001, *Key Engineering Materials*, **237**, pp.105-110.

- Thompson, A. and Hendry, A. (1991), Carbothermal Processing of Powders for Sialon Ceramic Matrix Composites, *Fine Ceramic Powders*, British Ceramic Proceedings, **47**, pp.95-105.
- Thompson, D. P. (1989), The Crystal Chemistry of Nitrogen Ceramics, *Materials Science Forum*, **47**, pp.21-42.
- Trigg, M. B. and McCartney, E. R. (1981), Comparison of the reaction systems $ZrO_2-Si_3N_4$ and $TiO_2-Si_3N_4$, *Communications of the American Ceramic Society*, pp.C-151.
- Tsukada, M., Naito, J., Masuda, T. and Horio, M. (1989), Submicron Ceramic Powder Synthesis by a Fluidized Bed of Microcontainer Particles, *Powder Engineering Proceedings (Buntai Kogaku Kaishi)*, **26(3)**, pp.15-20.
- Unimin (2003), Personal Communication (Unimin Australia).
- van Dijen, F. K. and Vogt, U. (1992), The Chemistry of the Carbothermal Synthesis of α - SiN_4 : Reaction Mechanism, Reaction Rate and Properties of the Product, *J. Eur. Cer. Soc.*, **10**, pp.273-82.
- van Rutten, J. W. T., Hintzen, H. T. and Metselaar, R. (1996), Phase formation of Ca- α -sialon by Reaction Sintering, *J. Eur. Cer. Soc.*, **16**, pp.995-9.
- van Rutten, J. W. T., Hintzen, H. T. and Metselaar, R. (2001), Densification Behaviour of Ca- α -sialons, *Ceram. Int.*, **27**, pp.461-6.
- van Rutten, J. W. T., Terpstra, R. A., van der Heijde, J. C. T., Hintzen, H. T. and Metselaar, R. (1995), Carbothermal Preparation and Characterisation of Ca- α -sialon, *J. Eur. Cer. Soc.*, **15**, pp.1-6.
- Wada, H., Wang, M.-J. and Tien, T.-Y. (1988), Stability of Phases in the Si-C-N-O System, *J. Am. Cer. Soc.*, **71(10)**, pp.837-40.
- Walker, D. (1997), The Production of SiAlON from Slag, *4th Year Undergraduate Project Report*, Department of Materials Engineering, Monash University, Clayton, Melbourne.
- Wang, H., Cheng, Y.-B., Muddle, B. C., Gao, L. and Yen, T. S. (1996), Preferred Orientation in Hot-Pressed Ca- α -SiAlON Ceramics, *Journal of Materials Science Letters*, **15**, pp.1447-9.

- Wang, P.-L. (2002), Personal communication.
- Wang, P.-L., Jia, Y. X. and Sun, W. Y. (1999), Fabrication of 15R AlN-polytypoid ceramics, *Mater. Let.*, **41**, pp.78-82.
- Wang, P.-L., Sun, W. Y. and Yan, D. S. (1999), Mechanical properties of AlN-polytypoids - 15R, 12H and 21R, *Mater. Sci. Eng. A*, **272**, pp.351-6.
- Wang, P.-L. and Werner, P.-E. (1997), Study on the structures of N-containing melilite $Y_2Si_3ON_4$ and $Nd_2Si_{2.5}Al_{0.5}N_{3.5}$, *J. Mater. Sci.*, **32**, pp.1925-9.
- Wang, P.-L., Zhang, C., Sun, W. Y. and Yan, D. S. (1999a), Characteristics of Ca- α -sialon - Phase Formation, Microstructure, and Mechanical Properties, *J. Eur. Cer. Soc.*, **19**, pp.553-60.
- Wang, P.-L., Zhang, C., Sun, W. Y. and Yan, D. S. (1999b), Formation Behaviour of Multi-Cation α -Sialons Containing Calcium and Magnesium, *Mater. Let.*, **38**, pp.178-85.
- Weimer, A., Eisman, G., Susnitzky, D., Beaman, D. and McCoy, J. (1997), Mechanism and Kinetics of the Carbothermal Nitridation Synthesis of α -Silicon Nitride, *J. Am. Cer. Soc.*, **80**(11), pp.2853-63.
- Weimer, A. W. (1997), Thermochemistry and Kinetics, in Carbide, Nitride and Boride Materials Synthesis and Processing, ed. A. W. Weimer, Chapman and Hill, London, pp.79-113.
- Wendlandt, W. W. M. (1986), Thermal Analysis, John Wiley & Sons, Brisbane.
- White, G. V., Ekstrom, T. C., Barris, G. C., Sheppard, C. M., Brown, I. W. M., Chen, C. Y. and Cooper, M. (1998), New Synthesis Routes for Sialon and Sialon Bonded Ceramics, *J. Australasian. Cer. Soc.*, **34**(2), pp.98-103.
- Wiederhorn, S. M. and Lawn, B. R. (1979), Strength Degradation of Glass Impacted with Sharp Particles: I, *J. Am. Cer. Soc.*, **62**(1-2), pp.66-70.
- Wild, S. (1975), A Preliminary Investigation of the Reaction of Alpha-Silicon Nitride with Metakaolin, *Special Ceramics 6*, Versailles, Brit. Cer. Res. Assoc., pp.309-20.

- Wood, C. A. (2001), *Microstructural Development and Control of Ceramics in the Ca-Si-Al-O-N System*, *PhD Thesis*, School of Physics and Materials Engineering, Monash University, Clayton, Melbourne.
- Wood, C. A. and Cheng, Y.-B. (2000), Phase Relationships and Microstructures of Ca and Al-Rich α -Sialon Ceramics, *J. Eur. Cer. Soc.*, **20**, pp.357-66.
- Wood, C. A., Zhao, H. and Cheng, Y.-B. (1998), In-Situ Toughening of α -SiAlON Ceramics, *Materials 98*, Institute of Materials Engineering, Australasia.
- Xie, Z.-H., Moon, R. J., Hoffmann, M., Munroe, P. and Cheng, Y.-B. (2003), Role of Microstructure in the Grinding and Polishing of α -Sialon Ceramics, *J. Eur. Cer. Soc.*, **23**, pp.2351-60.
- Zenotchkine, M. Y., Shuba, R. A., Kim, J. S. and Chen, I.-W. (2002), Effect of Seeding on the Microstructure and Mechanical Properties of α -SiAlON: 1 Y-SiAlON, *J. Am. Cer. Soc.*, **85**(5), pp.1245-59.
- Zhang, C., Komeya, K., Tatami, J., Meguro, T. and Cheng, Y.-B. (2000), Synthesis of Mg- α -SiAlON Powders from Talc and Halloysite Clay Minerals, *J. Eur. Cer. Soc.*, **20**, pp.1809-14.
- Zhang, Y. (2002), *Erosion Behaviour of Engineering Ceramics*, *PhD Thesis*, School of Physics and Materials Engineering, Monash University, Clayton, Melbourne.
- Zhang, Y., Cheng, Y.-B. and Lathabai, S. (2000), Erosion of Alumina Ceramics by Air- and Water-Suspended Garnet Particles, *Wear*, **240**, pp.40-51.
- Zhang, Y., Cheng, Y.-B. and Lathabai, S. (2001), Influence of Microstructure on the Erosive Wear Behaviour of Ca α -sialon Materials, *J. Eur. Cer. Soc.*, **21**, pp.2435-45.

- Wood, C. A. (2001), Microstructural Development and Control of Ceramics in the Ca-Si-Al-O-N System, *PbD Thesis*, School of Physics and Materials Engineering, Monash University, Clayton, Melbourne.
- Wood, C. A. and Cheng, Y.-B. (2000), Phase Relationships and Microstructures of Ca and Al-Rich α -Sialon Ceramics, *J. Eur. Cer. Soc.*, **20**, pp.357-66.
- Wood, C. A., Zhao, H. and Cheng, Y.-B. (1998), In-Situ Toughening of α -SiAlON Ceramics, *Materials 98*, Institute of Materials Engineering, Australasia.
- Xie, Z.-H., Moon, R. J., Hoffmann, M., Munroe, P. and Cheng, Y.-B. (2003), Role of Microstructure in the Grinding and Polishing of α -Sialon Ceramics, *J. Eur. Cer. Soc.*, **23**, pp.2351-60.
- Zenotchkine, M. Y., Shuba, R. A., Kim, J. S. and Chen, I.-W. (2002), Effect of Seeding on the Microstructure and Mechanical Properties of α -SiAlON: 1 Y-SiAlON, *J. Am. Cer. Soc.*, **85**(5), pp.1245-59.
- Zhang, C., Komeya, K., Tatami, J., Meguro, T. and Cheng, Y.-B. (2000), Synthesis of Mg- α -SiAlON Powders from Talc and Halloysite Clay Minerals, *J. Eur. Cer. Soc.*, **20**, pp.1809-14.
- Zhang, Y. (2002), Erosion Behaviour of Engineering Ceramics, *PbD Thesis*, School of Physics and Materials Engineering, Monash University, Clayton, Melbourne.
- Zhang, Y., Cheng, Y.-B. and Lathabai, S. (2000), Erosion of Alumina Ceramics by Air- and Water-Suspended Garnet Particles, *Wear*, **240**, pp.40-51.
- Zhang, Y., Cheng, Y.-B. and Lathabai, S. (2001), Influence of Microstructure on the Erosive Wear Behaviour of Ca α -sialon Materials, *J. Eur. Cer. Soc.*, **21**, pp.2435-45.